UNIVERSITY OF OKLAHOMA

GRADUATE COLLEGE

INTERWELL CONNECTIVITY TESTS IN WATERFLOOD SYSTEMS

A DISSERTATION

SUBMITTED TO THE GRADUATE FACULTY

in partial fulfillment of the requirements for the

Degree of

DOCTOR OF PHILOSOPHY

By

ANH VIET DINH
Norman, Oklahoma
2009

Downloaded from SHAREOK. Persistent Handle URL: https://hdl.handle.net/11244/319175

INTERWELL CONNECTIVITY TESTS IN WATERFLOOD SYSTEMS

A DISSERTATION APPROVED FOR THE
MEWBOURNE SCHOOL OF PETROLEUM AND GEOLOGICAL ENGINEERING

BY

Dr. Djebbar Tiab, Chair

Dr. Roy Knapp

Dr. Faruk Civan

Dr. Samuel Osisanya

Dr. John Pigott

© Copyright by ANH VIET DINH 2009
All Rights Reserved.

DEDICATION

To my wife, my family and my teachers

ACKNOWLEDGEMENTS

I wish to express my deepest gratitude to Dr. Djebbar Tiab, my academic advisor, for his financial support, guidance, patience and motivation through the course of this study. His wisdom and knowledge has been a great inspiration to this work. I would like to thank Dr. Roy Knapp, who served as a dissertation committee member, for bringing the topic of interwell connectivity to my initial attention. I would also like to thank other dissertation committee members, Dr. Faruk Civan, Dr. Samuel Osisanya and Dr. John Pigott for their valuable criticisms and suggestions.

Special thanks are due to Dr. Ben Shiau, the director of applied surfactant laboratory, for his financial support toward the end of this study. The time that he and the surfactant laboratory team provided in order for me to complete this work in a timely manner is much appreciated. I would also like to thank all other faculty members and the department staff, especially Mike Shaw, Shalli Young, Sonya Grant and Mona Troxell for their help and support during my study.

I am also grateful for the help, support and friendship of my colleagues in the research group, Jing Lu, Alpheus Igbokoyi and Dora Restrepo. Many thanks are due to my friends from the school, Mr. and Mrs. Flanagan, the members of the Society of Vietnamese Students for their support and the time they shared with me during my study in Norman.

Last but not least, I am especially grateful for the support, endurance and understanding of my wife, Hong Truong, and my family. They have been a great motivation for me to complete this study.

TABLE OF CONTENTS

ACKNOWLEDGEMENTS iv

TABLE OF CONTENTS v

LIST OF TABLES ix

LIST OF FIGURES xvi

ABSTRACT xxviii

CHAPTER 1 - INTRODUCTION 1
1.1. Objectives 1
1.2. Organization 4

CHAPTER 2 - BACKGROUND 6
2.1. Literature Review 6
2.2. Multivariate Linear Regression (MLR) 7
2.3. Least Squares Linear Regression (LSLR) 10

CHAPTER 3 – INFERRING INTERWELL CONNECTIVITY FROM BOTTOM HOLE PRESSURE FLUCTUATIONS 12
3.1. Overview 13
3.2. Procedure 14
3.2.1. Multivariate Linear Regression for Pressure data 15
3.3. Assumptions 17
3.4. Simulation Results 18
3.4.1. Application to 5x4 Field. 19
3.4.2. Application to 25x16 Field. 33
3.5. Sensitivity Analysis 36
3.5.1. Assumptions 37
3.5.2. Possible sources of error. 38
3.5.3. Properties of the interwell connectivity coefficients. 40
3.5.4. Testing scheme and data selection 40
3.6. Conclusions 44

CHAPTER 4 – ANALYTICAL MODEL 45
4.1. Introduction 46
4.2. Background 47
4.3. Analytical Approach 48
4.3.1. Analytical Model Application 49
4.3.2. Interpretation of interwell connectivity coefficients using bottom hole pressure data 52
4.4. Model Verification 56

4.4.1. 5x4 Synthetic Field 57
4.4.2. 25x16 Synthetic Field 62
4.5. Calculation Techniques for Interwell Connectivity Tests 63
4.5.1. Calculation Approaches 64
4.5.2. Average Pressure Change Calculation 65
4.5.3. Calculation Procedures 68
4.6. Simulation Results 69
4.6.1. 5x4 Synthetic Field 69
4.6.2. Different flowing conditions at the response and signal wells 81
4.7. Conclusions 85
CHAPTER 5 – APPLICATIONS OF THE INTERWELL CONNECTIVITY TEST TO NATURALLY FRACTURED RESERVOIRS 87
5.1. Literature Review 87
5.2. Analytical Model 89
5.3. Calculation Methods 90
5.3.1. Ozkan Calculation Method 90
5.3.2. Valko Calculation Method 91
5.3.3. Shape Factor Calculation 94
5.4. Simulation Results 97
5.4.1. General Model Descriptions 97
5.4.2. Isotropic Reservoir 98
5.4.3. Anisotropic Reservoir 100
5.4.4. Dual porosity reservoir with high permeability channel 102
5.4.5. Dual porosity reservoir with a partially sealing barrier 105
5.4.6. Dual porosity reservoir with a sealing barrier 108
5.4.7. 25x16 isotropic reservoir 111
5.5. Conclusions 116
CHAPTER 6 – APPLICATIONS OF THE INTERWELL CONNECTIVITY TEST TO HYDRAULICALLY FRACTURED WELLS 118
6.1. Literature Review 118
6.2. Analytical Model and Calculation Approach 119
6.3. Simulation Results 121
6.3.1. Model Descriptions 121
6.3.2. Homogeneous reservoir with hydraulic fractures 123
6.3.3. Homogeneous reservoir with hydraulic fractures of different fracture half lengths 125
6.3.4. Homogeneous reservoir with hydraulic fractures with different fracture half lengths for injectors and the same fracture half length for producers 130
6.3.5. Anisotropic Reservoir with hydraulic fractures 131
6.3.6. Reservoir with a high permeability channel 133
6.3.7. Reservoir with a partially sealing barrier 135

6.3.8. Reservoir with a sealing barrier 138
6.4. Conclusions 142

CHAPTER 7 – APPLICATIONS OF INTERWELL CONNECTIVITY TEST TO HORIZONTAL WELLS 143
7.1. Literature Review 143
7.2. Analytical Model and Calculation Methods 144
7.3. Simulation Results 148
7.3.1. Model Description 148
7.3.2. Homogeneous Reservoir 149
7.3.3. Homogeneous Reservoir with horizontal wells of different lengths 152
7.3.4. Homogeneous Reservoir with horizontal injectors of different lengths and producers with the same length 157
7.3.5. Homogeneous Reservoir with horizontal wells in both x – y directions 159
7.3.6. Anisotropic Reservoir with horizontal wells 161
7.3.7. Reservoir with high permeability channel 164
7.3.8. Reservoir with a partially sealing barrier 166
7.3.9. Reservoir with a sealing barrier 169
7.4. Conclusions 172

CHAPTER 8 – SIMULATION RESULTS FOR MIXED WELL-BORE CONDITIONS 173
8.1. Fully Penetrating Vertical Wells and Fully Penetrating Hydraulic Fractures 173
8.2. Mixed case of fully penetrating vertical wells and fully penetrating hydraulic fractures 175
8.3. Fully Penetrating Vertical producers and Horizontal injectors 178
8.4. Mixed case of fully penetrating vertical wells and horizontal wells 181
8.5. Reservoir with Vertical Wells, Hydraulically Fractured Wells and Horizontal Wells 185

CHAPTER 9 – ANALYSIS OF PRODUCTION DATA OF A WATERFLOOD UNDER THE STEADY STATE FLOW CONDITION 189
9.1. Overview 189
9.2. Analytical Model for Reservoir Flowing in Steady State with Injection Wells 190
9.2.1. MLR method 190
9.2.2. Analytical Model for Production Data 192
9.3. Simulation Results 194
9.3.1. Model Description 194

9.3.2. Homogeneous Reservoir 195
9.3.3. Anisotropic Reservoir 201
9.3.4. Reservoir with high permeability channel 203
9.3.5. Reservoir with a partially sealing barrier 205
9.3.6. Reservoir with a sealing barrier 207
9.3.7. 25x16 Synthetic Field 209
9.4. Conclusions 214
9.5. Recommended Application 215
CHAPTER 10 – CONCLUSIONS AND RECOMMENDATIONS 219
10.1. Summary and Conclusions 219
10.1.1. Summary 219
10.1.2. Conclusions 220
10.2. Recommendations for Future Studies 221
NOMENCLATURE 223
REFERENCES 228
APPENDIX A – DERIVATION OF PRESSURE DISTRIBUTION FOR A VERTICAL WELL IN A CLOSED RECTANGULAR RESERVOIR 233
APPENDIX B – DERIVATION OF THE PRESSURE DISTRIBUTION CAUSED BY AN INJECTOR OR A PRODUCER IN A WATERFLOOD 237
APPENDIX c – DERIVATION OF THE LATE TIME PRESSURE DISTRIBUTION FOR A WELL IN A NATURALLY FRACTURED RESERVOIR 240

LIST OF TABLES

Table 3.1: Results for the interwell connectivity coefficients β. 5x4 field, homogeneous reservoir. 21

Table 3.2: Results for the interwell connectivity coefficients β. 5x4 Synthetic field, Anisotropic reservoir (R^2 =1.00). 26

Table 3.3: Results for the interwell connectivity coefficients β. 5x4 Synthetic field with high permeability channel..... 27

Table 3.4: Results for the interwell connectivity coefficients β. 5x4 Synthetic field with partially sealing barrier. 28

Table 3.5: Results for the interwell connectivity coefficients β. 5x4 Synthetic field with sealing barrier. 29

Table 3.6 . Results for the interwell connectivity coefficients β for the Example. 5x4 field, homogeneous reservoir (A_s = 0.0109). 44

Table 4.1: Input data for homogeneous simulation models 57

Table 4.2: Interwell Connectivity Coefficient results from MLR for the 5x4 Synthetic field 59

Table 4.3: Interwell Connectivity Coefficient results from analytical solution with Δteq = 12.63 days for the 5x4 Synthetic field 59

Table 4.4: Relative Interwell Permeability results for the 5x4 Homogeneous Synthetic Field (k_{ref}=100mD, Δt_{eq} = 12.63 days)..... 71

Table 4.5: Relative interwell permeability results from pseudo-steady state equation for the 5x4 Anisotropic Synthetic Field (k_{ref}=316mD, Δt_{eq} = 4.0 days)..... 72

Table 4.6: Relative interwell permeability results from pseudo-steady state equation for the 5x4 Synthetic field-Reservoir with High Permeability Channel (k_{ref}=300mD, Δt_{eq}=12.15 days)..... 74

Table 4.7: Relative interwell permeability results from pseudo-steady state equation for the 5x4 Synthetic field-Reservoir with partially sealing barrier (k_{ref}=100mD, Δt_{eq} = 12.63 days) 76

Table 4.8: Change of Average Reservoir Pressure results for the 5x4 Synthetic field-Reservoir with Sealing Barrier (k_{ref}=100mD,Δt_{eq}=12.63 days)..... 78

Table 4.9: Interwell connectivity result summary for different test schemes for the 5x4 homogeneous synthetic field (k_{ref}=100mD, Δt_{eq}=12.63 days)..... 85
Table 4.10: Interwell connectivity result summary for different test schemes for the 25x16 homogeneous synthetic field (k_{ref} = 100 mD, Δt_{eq} = 5.87 days)..... 85
Table 5.1: Dimensionless Pressures or Influence functions of the well at the center of the 5x4 synthetic field calculated from different equations/methods..... 95
Table 5.2: Dimensionless coordinates of the wells in the 5x4 synthetic field..... 96
Table 5.3: Shape factors for the wells in the 5x4 synthetic field calculated from different equations/methods 96
Table 5.4: Interwell Connectivity Coefficient results from simulation data for the isotropic dual-porosity 5x4 Synthetic field (A_s = 0.005201)..... 99
Table 5.5: Relative interwell permeability results for the 5x4 Isotropic Dual-porosity Synthetic Field (k_{ref}=100mD, Δt_{eq} = 12.16 days) 99
Table 5.6: Interwell Connectivity Coefficient results from simulation data for the Anisotropic Dual-porosity 5x4 Synthetic field..... 100
Table 5.7: Relative interwell permeability results for the 5x4 Anisotropic Dual-porosity Synthetic Field (k_{ref}=316mD, Δt_{eq} = 12.16 days) 101
Table 5.8: Interwell Connectivity Coefficient results from simulation data for the 5x4 Dual-porosity Synthetic field with High permeability channel..... 103
Table 5.9: Relative interwell permeability results for the 5x4 Dual-porosity Synthetic Field with High permeability channel (k_{ref}=300mD, Δt_{eq} = 12.16 days)... 104
Table 5.10: Interwell Connectivity Coefficient results from simulation data for the 5x4 Dual-porosity Synthetic field with a Partially sealing barrier 106
Table 5.11: Relative interwell permeability results for the 5x4 Dual-porosity Synthetic Field with a Partially sealing barrier (k_{ref}=100mD, Δt_{eq} = 12.16 days)..... 106
Table 5.12: Interwell Connectivity Coefficient results from simulation data for the 5x4 Dual porosity Synthetic field with a Sealing barrier..... 109
Table 5.13: Relative interwell permeability results for the 5x4 Dual porosity Synthetic field with a Sealing barrier (k_{ref}=100mD, Δt_{eq} = 12.16 days)..... 109
Table 5.14: Average pressure change (ΔP_{ave}) after each time interval for different cases of 5x4 Dual-porosity Synthetic Field..... 111

Table 5.15: Interwell Connectivity Coefficient results from simulation data for the 25x16 isotropic dual-porosity Synthetic field (A_s = 0.00799)..... 114
Table 5.16: Relative interwell permeability results for the 25x16 Isotropic Dual-porosity Synthetic Field (k_{ref}=100mD, Δt_{eq} = 5.6 days) 115
Table 6.1: Dimensionless coordinates of the fractured wells in the 5x4 synthetic field 120
Table 6.2: Shape factors for the fractured wells in the 5x4 synthetic field calculated for different fracture types..... 120
Table 6.3: Interwell Connectivity Coefficient results from simulation data for the 5x4 Homogeneous Synthetic field with Hydraulic fractured wells (A_s = 0.0048) 124
Table 6.4: Relative interwell permeability results for the 5x4 Homogeneous Synthetic Field with Hydraulic fractured wells (k_{ref}=100mD, Δt_{eq} = 5.66 days)..... 124
Table 6.5: Fracture half lengths for different fractured wells in the 5x4 Homogeneous Synthetic field..... 125
Table 6.6: Interwell connectivity coefficient results from simulation data for the 5x4 Homogeneous Reservoir with Vertically Fractured wells of Different Half Lengths..... 126
Table 6.7: Relative interwell permeability results for the 5x4 Homogeneous Field with Fractured wells of Different fracture half lengths (k_{ref}=100mD, Δt_{eq} = 6.21 days)..... 128
Table 6.8: Interwell Connectivity Coefficient results from simulation data for the 5x4 Homogeneous Synthetic field – Different fracture half lengths at injectors 130
Table 6.9: Interwell Connectivity Coefficient results from simulation data for the 5x4 Anisotropic Synthetic field– Hydraulically fractured wells 131
Table 6.10: Relative interwell permeability results for the 5x4 Anisotropic Synthetic Field – Hydraulically fractured wells (k_{ref}=316 mD, Δt_{eq} = 5.66 days)..... 133
Table 6.11: Interwell Connectivity Coefficient results from simulation data for the 5x4 Synthetic Reservoir with a high permeability channel– Hydraulically fractured wells..... 134

Table 6.12: Relative interwell permeability results for the 5x4 Synthetic Reservoir with a high permeability channel– Hydraulically fractured wells. (k_{ref}=300mD, Δt_{eq} = 5.66 days) 134
Table 6.13: Interwell Connectivity Coefficient results from simulation data for the 5x4 Synthetic field with partially sealing barrier– Hydraulically fractured wells. 137
Table 6.14: Relative interwell permeability results for the 5x4 Synthetic field with partially sealing barrier– Hydraulically fractured wells (k_{ref}=100mD, Δt_{eq} = 5.66 days)..... 137
Table 6.15: Interwell Connectivity Coefficient results from simulation data for the 5x4 Synthetic field with a sealing barrier – Hydraulically fractured wells. 139
Table 6.16: Relative interwell permeability results for the 5x4 Synthetic Field with a sealing barrier – Hydraulically fractured wells (k_{ref}=100mD, Δt_{eq} = 5.66 days)..... 139
Table 6.17: Average pressure change (ΔP_{ave}) after each time interval for different cases of 5x4 Synthetic Field – Hydraulically fractured wells. 142
Table 7.1: Dimensionless coordinates of the horizontal wells in the 5x4 synthetic field147
Table 7.2: Shape factors for uniform flux and infinite conductivity horizontal wells in 5x4 Synthetic Reservoir..... 148
Table 7.3: Interwell Connectivity Coefficient results from simulation data for the Homogeneous 5x4 Synthetic field with Horizontal wells (A = 0.00445) . 150
Table 7.4: Relative interwell permeability results for the 5x4 Homogeneous Synthetic Field with Horizontal wells (k_{ref}=100mD, Δt_{eq} = 6.59 days)..... 150
Table 7.5: Horizontal well half-lengths for different horizontal wells in the 5x4 Homogeneous Synthetic field..... 152
Table 7.6: Interwell Connectivity Coefficient results from simulation data for the 5x4 Homogeneous Synthetic field – Horizontal wells of different lengths..... 154
Table 7.7: Relative interwell permeability results for the 5x4 Homogeneous Synthetic field – Horizontal wells of different lengths (k_{ref}=100mD, Δt_{eq} = 6.21 days) 154

Table 7.8: Interwell Connectivity Coefficient results from simulation data for the 5x4 Homogeneous Synthetic field – Different fracture half-lengths at injectors 158
Table 7.9: Interwell Connectivity Coefficient results from simulation data for the 5x4 Homogeneous Synthetic field – Different horizontal well directions (A_s = 0.00484) 160
Table 7.10: Interwell Connectivity Coefficient results from simulation data for the 5x4 Anisotropic Synthetic field– Horizontal wells..... 162
Table 7.11: Relative interwell permeability results for the 5x4 Anisotropic Synthetic Field – Horizontal wells (k_{ref}=316 mD, Δt_{eq} = 6.59 days) 162
Table 7.12: Interwell Connectivity Coefficient results from simulation data for the High permeability channel case of the 5x4 Synthetic field – Horizontal wells. 165
Table 7.13: Relative interwell permeability results for the high permeability channel case of the 5x4 Synthetic field – Horizontal wells (k_{ref}=300mD, Δt_{eq} = 6.59 days) 165
Table 7.14: Interwell Connectivity Coefficient results from simulation data for the 5x4 Synthetic field with partially sealing barrier– Horizontal wells. 167
Table 7.15: Relative interwell permeability results for the 5x4 Synthetic field with partially sealing barrier– Horizontal wells (k_{ref}=100mD, Δt_{eq} = 6.59 days) 167
Table 7.16: Interwell Connectivity Coefficient results from simulation data for the 5x4 Synthetic field with a sealing barrier – Horizontal wells..... 170
Table 7.17: Relative interwell permeability results for the 5x4 Synthetic Field with a sealing barrier – Horizontal wells (k_{ref}=100mD, Δt_{eq} = 6.59 days) 170
Table 7.18: Average pressure change (ΔP_{ave}) after each time interval for different cases of 5x4 Synthetic Field – Horizontal wells. 172
Table 8.1: Interwell Connectivity Coefficient results from simulation data for the 5x4 Homogeneous Synthetic field – Hydraulically fractured injectors and vertical producers..... 174

Table 8.2: Interwell Connectivity Coefficient results from simulation data for the 5x4 Homogeneous Synthetic field – Mixed Hydraulically fractured and vertical wells. 176
Table 8.3: Relative interwell permeability results for the 5x4 Homogeneous Synthetic Field– Mixed Hydraulically fractured and vertical wells (k_{ref}=100mD, Δt_{eq} = 7.33 days) 176
Table 8.4: Interwell Connectivity Coefficient results from simulation data for the 5x4 Homogeneous Synthetic field – Horizontal injectors and vertical producers. 180
Table 8.5: Interwell Connectivity Coefficient results from simulation data for the 5x4 Homogeneous Synthetic field – Mixed horizontal and vertical wells. 183
Table 8.6: Relative interwell permeability results for the 5x4 Homogeneous Synthetic Field– Mixed horizontal and vertical wells (k_{ref}=100mD, Δt_{eq} = 7.33 days) 183
Table 8.7: Interwell Connectivity Coefficient results from simulation data for the 5x4 Homogeneous Synthetic field – Mixed horizontal, hydraulically fractured and vertical wells. 187
Table 8.8: Relative interwell permeability results for the 5x4 Homogeneous Synthetic Field– Mixed horizontal, hydraulically fractured and vertical wells (k_{ref}=100mD, Δt_{eq} = 7.33 days) 187
Table 9.1: Interwell Connectivity Coefficient results from MLR for the 5x4 homogeneous synthetic field-Production data (A_s = 0.00734) 197
Table 9.2: Relative interwell permeability results for the 5x4 Homogeneous Synthetic Field– Production data (k_{ref}=100mD, Δt_{eq} = 7.57 days) 197
Table 9.3: Interwell Connectivity Coefficient results from simulation data for the 5x4 Anisotropic Synthetic field– Production data 201
Table 9.4: Relative interwell permeability results for the 5x4 Anisotropic Synthetic Field – Production data (k_{ref}=316 mD, Δt_{eq} = 7.57 days) 203
Table 9.5: Interwell Connectivity Coefficient results from simulation data for the 5x4 Synthetic field with high permeability channel – Production data. 203

Table 9.6: Relative interwell permeability results for the 5x4 Synthetic Field with high permeability channel – Production data (k_{ref}=1000mD, Δt_{eq} = 7.57 days) 203
Table 9.7: Interwell Connectivity Coefficient results from simulation data for the 5x4 Synthetic field with partially sealing barrier– Production data. 205
Table 9.8: Relative interwell permeability results for the 5x4 Synthetic field with partially sealing barrier– Production data (k_{ref}=100mD, Δt_{eq} = 7.57 days)..... 205
Table 9.9: Interwell Connectivity Coefficient results from simulation data for the 5x4 Synthetic field with a sealing barrier – Production data. 207
Table 9.10: Relative interwell permeability results for the 5x4 Synthetic Field with a sealing barrier – Production data (k_{ref}=100mD, Δt_{eq} = 5.66 days)..... 207
Table 9.11: Interwell Connectivity Coefficient results from simulation data for the isotropic dual-porosity 25x16 Synthetic field (A_s =0.00588)..... 212
Table 9.12: Relative interwell permeability results for the 25x16 Isotropic Dual-porosity Synthetic Field (k_{ref}=100mD, Δt_{eq} = 5.87 days) 213

LIST OF FIGURES

Figure 1.1. Flowchart for the application of the proposed interwell connectivity test. 2

Figure 3.1. Grid system for the simulation model (5x4 Synthetic field). 19

Figure 3.2 . Flow Rates for five injectors. The total field injection is constant at 2000 bbl/d. 20

Figure 3.3 . Representation of the interwell connectivity coefficients β, shown in Table 3.1. The lengths of the arrows are proportional to the values of the coefficients. 5x4 field, homogeneous reservoir (R^2 =1.00, A_s = 0.000902). 23

Figure 3.4 . Comparison between total modeled pressure using MLR and the total simulated pressure. 5x4 field, homogeneous reservoir. 24

Figure 3.5 . The resulted interwell connectivity coefficients β versus the distances of well pairs. 5x4 field, homogeneous reservoir. 24

Figure 3.6 . Representation of the interwell connectivity coefficients β for 5x4 field, anisotropic reservoir (k_x/k_y=10). 26

Figure 3.7 . Representation of the interwell connectivity coefficients β for 5x4 field, reservoir with high permeability channel. 27

Figure 3.8 . Representation of the interwell connectivity coefficients β. 5x4 Field, reservoir with a partially sealing barrier (diagonal blocks). 28

Figure 3.9 . Representation of the interwell connectivity coefficients β. 5x4 field, reservoir with a sealing barrier (diagonal blocks). 29

Figure 3.10 . Asymmetry coefficients (A_s) versus cases of different production rates for 5x4 field, homogeneous reservoir. 31

Figure 3.11 . Asymmetry coefficients (A_s) versus cases of different formation permeability for 5x4 field, homogeneous reservoir. 32

Figure 3.12 . Asymmetry coefficients (A_s) versus cases of different time interval between data points for 5x4 field, homogeneous reservoir. 32

Figure 3.13 . Interwell connectivity coefficients (β) versus cases of different time interval between data points for 5x4 field, homogeneous reservoir. 33

Figure 3.14 . Representation of the interwell connectivity coefficients (β) for 25x16 field, homogeneous reservoir (R^2 =1.00, A_s = 0.000902)..... 34
Figure 3.15 . The resulted interwell connectivity coefficients (β) versus the distances of well pairs. 25x16 field, homogeneous reservoir. 35
Figure 3.16 . Number of data points versus the overdetermination coefficients (O_d) for both 5x4 and 25x16 field, homogeneous reservoir. 35
Figure 3.17 . Asymmetry coefficients (A_s) versus the overdetermination coefficients (O_d) for both 5x4 and 25x16 field, homogeneous reservoir. 36
Figure 3.18 . Coefficient of determination (R^2) versus the overdetermination coefficients (O_d) for both 5x4 and 25x16 field, homogeneous reservoir. 36
Figure 3.19 . Percent errors of the interwell connectivity coefficients versus random percent errors of Injector 1 data for 5x4 field, homogeneous reservoir. 38
Figure 3.20 . Bottom Hole Pressure Data for the Example. 5x4 field, homogeneous reservoir. 10-day intervals. 43
Figure 4.1. Grid system for 5x4 Synthetic Field (73x73x5). 58
Figure 4.2. Grid system for 25x16 Synthetic Field (59x59x5). 58
Figure 4.3. Absolute Values of (P_{ave}-P_{wf}) from Eq.4.28 and from simulation results for Well P-1, 5x4 homogeneous field..... 60
Figure 4.4. P_{wf} Results from Eq.4.30 and from Simulation for Well P-1, 5x4 homogeneous field. 61
Figure 4.5. Plot of the term $\beta_{0j'} = \Delta p_{pr}(\Delta t_{eq})$ versus different time interval (Δt), 5x4 homogeneous field. 61
Figure 4.6. P_{wf} Results from Eq.4.30 and from Simulation for Well P-1, 25x16 Homogeneous Synthetic Field (Δt_{eq} = 5.87 days)..... 62
Figure 4.7. Absolute Values of (P_{ave}-P_{wf}) Calculated and Simulated with P_{ave} taken from simulation results for Well P-1, 25x16 Homogeneous Synthetic Field (Δt_{eq} = 5.87 days). 64
Figure 4.8. Equivalent time (Δt_{eq}) as a function of permeability-Homogeneous 5x4 and 25x16 Synthetic Fields..... 65
Figure 4.9. Top view of the simulation model for the 5x4 Synthetic Homogeneous Reservoir. 70

Figure 4.10. Representation of relative interwell permeability for the case of 5x4 Homogeneous Reservoir. 71
Figure 4.11. Representation of relative interwell permeability for the case of 5x4 Anisotropic Reservoir. 73
Figure 4.12. Top view of the simulation model showing the x-direction permeability distribution for the 5x4 Synthetic Reservoir with high permeability channel. 74
Figure 4.13. Representation of relative interwell permeability for the case of 5x4 Synthetic field with high permeability channel. 75
Figure 4.14. Top view of the simulation model showing the x-direction permeability distribution for the 5x4 Synthetic Reservoir with a partially sealing barrier. 76
Figure 4.15. Representation of relative interwell permeability for the case of 5x4 synthetic field with partially sealing barrier 77
Figure 4.16. Top view of the simulation model showing the x-direction permeability distribution for the 5x4 Synthetic Reservoir with a sealing barrier. 78
Figure 4.17. Representation of relative interwell permeability for the case of 5x4 synthetic field with a sealing barrier. 79
Figure 4.18. Plot of relative interwell permeability (k_{ir}) after cut-off ($\beta_{ij\text{-}cut\text{-}off} = 0.04$) for 25x16 homogeneous synthetic field (k_{ref} = 100 mD, Δt_{eq} = 5.87 days). 80
Figure 4.19. Representation of relative interwell permeability after cut-off ($\beta_{ij\text{-}cut\text{-}off}$ = 0.04) for the case of 25x16 homogeneous synthetic field (k_{ref} = 100 mD, Δt_{eq} = 5.87 days). 81
Figure 5.1:. Idealization of a naturally fractured system showing I. The actual reservoir, II. Warren-Root's "Sugar cube model" & III. Kazemi's Model (Source: Kazemi H., 1969). 89
Figure 5.2:. Dimensionless Pressures or Influence functions versus dimensionless time for a fully penetrating vertical well at the center of a closed rectangular reservoir calculated by different methods. 94
Figure 5.3. Representation of the interwell connectivity coefficients for the case of 5x4 Isotropic Dual-porosity Reservoir. 98

Figure 5.4. Comparison of interwell connectivity coefficient results for the case of 5x4 Isotropic Dual-porosity and Homogeneous single-porosity Reservoir..... 99
Figure 5.5. Representation of relative interwell permeability for the case of 5x4 Isotropic Dual-porosity Reservoir..... 100
Figure 5.6. Representation of the connectivity coefficients for the case of 5x4 Anisotropic Dual-porosity Reservoir..... 101
Figure 5.7. Representation of relative interwell permeability for the case of 5x4 Anisotropic Dual-porosity Reservoir..... 102
Figure 5.8. Top view of the simulation model showing the fracture permeability in x direction for the High permeability channel case of the 5x4 Dual porosity Synthetic field..... 103
Figure 5.9. Representation of the interwell connectivity coefficients for the 5x4 Dual-porosity Synthetic field with High permeability channel..... 104
Figure 5.10. Representation of relative interwell permeability the 5x4 Dual-porosity Synthetic field with High permeability channel..... 105
Figure 5.11. Top view of the simulation model showing the fracture permeability in x direction for the 5x4 Dual porosity Synthetic field with a Partially sealing barrier..... 106
Figure 5.12. Representation of the connectivity coefficients for the 5x4 Dual-porosity reservoir with a Partially sealing barrier..... 107
Figure 5.13. Representation of relative interwell permeabilities for the 5x4 Dual-porosity reservoir with a Partially sealing barrier..... 107
Figure 5.14. Top view of the simulation model showing the fracture permeability in x direction for the 5x4 Dual porosity Synthetic field with a Sealing barrier.108
Figure 5.15. Representation of the connectivity coefficients for the 5x4 Dual porosity Synthetic field with a Sealing barrier..... 110
Figure 5.16. Representation of relative interwell permeability for the 5x4 Dual porosity Synthetic field with a Sealing barrier..... 110
Figure 5.17. Top view of the grid system showing the fracture permeability in the x-direction for 25x16 Dual porosity Synthetic field..... 112

Figure 5.18. Representation of relative interwell permeability for the 25x16 Isotropic Dual-porosity Reservoir. 113
Figure 5.19. Relative interwell permeability results for the case of 25x16 Isotropic Dual-porosity Reservoir. 116
Figure 5.20. Representation of relative interwell permeability for the case of 25x16 Isotropic Dual-porosity Reservoir. 116
Figure 6.1. Top view of the simulation model showing the LGRs at the fractured wells in the homogeneous 5x4 synthetic field. 122
Figure 6.2. Cross sectional view showing three wells and the hydraulic fractures in the 5x4 homogeneous synthetic Reservoir. 122
Figure 6.3. A zoom-in view of a LGR showing a high permeability strip representing a hydraulic fracture - 5x4 homogeneous reservoir. 123
Figure 6.4. Representation of the interwell connectivity coefficients for the 5x4 Homogeneous Reservoir with Hydraulically fractured wells. 124
Figure 6.5. Representation of the relative interwell permeability for the 5x4 Homogeneous Reservoir with Hydraulically fractured wells. 125
Figure 6.6. Cross sectional view showing three fractured wells of different fracture half lengths in the 5x4 Homogeneous synthetic reservoir. 126
Figure 6.7. Representation of the interwell connectivity coefficients for the 5x4 Homogeneous Reservoir with Vertically Fractured wells of Different half lengths. 127
Figure 6.8. Comparison of simulated and calculated interwell connectivity coefficient results for 5x4 Homogeneous Reservoir with Fractured wells of Different fracture half lengths. 127
Figure 6.9. Representation of relative interwell permeability for the 5x4 Homogeneous Reservoir with Vertical fractures of Different half lengths. 129
Figure 6.10. Maximum values of interwell connectivity coefficients versus fracture half-lengths. 129
Figure 6.11. Comparison of the interwell connectivity coefficient results for the case of the same vs. different fracture half lengths at the fractured producers in 5x4 Homogeneous Synthetic Reservoir. 131

Figure 6.12. Representation of the connectivity coefficients for the case of 5x4 Anisotropic Reservoir – Hydraulically fractured wells. 132
Figure 6.13. Representation of relative interwell permeability for the case of 5x4 Synthetic Reservoir– Hydraulically fractured wells. 132
Figure 6.14. Top view of the simulation model showing the permeability in x direction for the high permeability channel case of the 5x4 Synthetic field with fractured wells..... 134
Figure 6.15. Representation of the connectivity coefficients for the case of 5x4 Synthetic Reservoir with a high permeability channel– Hydraulically fractured wells. 135
Figure 6.16. Representation of relative interwell permeability for the 5x4 Synthetic Reservoir with a high permeability channel– Hydraulically fractured wells. 135
Figure 6.17. Top view of the simulation model showing the permeability distribution in x direction for the case of 5x4 Synthetic field with a partially sealing barrier– Hydraulically fractured wells..... 136
Figure 6.18. Representation of the connectivity coefficients for the case of 5x4 Dual-porosity reservoir with a partially sealing barrier– Hydraulically fractured wells. 137
Figure 6.19. Representation of relative interwell permeability for the case of 5x4 dual-porosity reservoir with a partially sealing barrier– Hydraulically fractured wells. 138
Figure 6.20. Top view of the simulation model showing the permeability in x direction for the case of 5x4 Synthetic field with a sealing barrier – Hydraulically fractured wells 138
Figure 6.21. Representation of the connectivity coefficients for the 5x4 Synthetic Field with a sealing barrier – Hydraulically fractured wells..... 140
Figure 6.22. Representation of relative interwell permeability for the 5x4 Synthetic Field with a sealing barrier – Hydraulically fractured wells..... 141
Figure 7.1. Top view of the simulation model showing the horizontal wells of the homogeneous 5x4 Synthetic field. 149

Figure 7.2. Cross sectional view showing three horizontal wells and their completions in the homogeneous 5x4 Synthetic Reservoir. 149
Figure 7.3. Representation of the connectivity coefficients for the case of 5x4 Homogeneous Reservoir with Horizontal wells. 151
Figure 7.4. Representation of the relative interwell permeability for the case of 5x4 Homogeneous Reservoir with Horizontal wells. 151
Figure 7.5. Top view of the simulation model showing the horizontal wells of different lengths for the homogeneous 5x4 Synthetic field. 153
Figure 7.6. Cross sectional view showing three horizontal wells of different lengths in the homogeneous 5x4 Synthetic Reservoir. 153
Figure 7.7. Comparison of simulated and calculated interwell connectivity coefficient results for the 5x4 Homogeneous Synthetic field – Horizontal wells of different lengths. 154
Figure 7.8. Representation of the connectivity coefficients for the case of 5x4 Homogeneous Reservoir - Horizontal wells of different lengths. 155
Figure 7.9. Representation of relative interwell permeability for the case of 5x4 Homogeneous Reservoir- Horizontal wells of different lengths. 155
Figure 7.10. Maximum values of interwell connectivity coefficients versus horizontal well half-lengths. 156
Figure 7.11. Top view of the simulation model showing the horizontal wells in the 5x4 homogeneous Synthetic field-The same horizontal well half lengths for producers. 157
Figure 7.12. Comparison of the interwell connectivity coefficient results for the case of the same vs. different horizontal well half lengths for the producers in the 5x4 Homogeneous Synthetic Reservoir. 158
Figure 7.13. Top view of the simulation model showing the horizontal wells of the homogeneous 5x4 Synthetic field-Different horizontal well directions. ... 159
Figure 7.14. Representation of the connectivity coefficients for the case of 5x4 Homogeneous Reservoir - Horizontal wells of different directions. 160

Figure 7.15. Comparison of the interwell connectivity coefficient results for the case of different well directions vs. all wells in the x-direction in 5x4 Homogeneous Synthetic Reservoir. 161
Figure 7.16. Comparison of the relative interwell permeability results for the case of different well directions vs. all wells in the x-direction in 5x4 Homogeneous Synthetic Reservoir. 161
Figure 7.17. Representation of the interwell connectivity coefficients for the case of 5x4 Anisotropic Reservoir – Horizontal wells. 163
Figure 7.18. Representation of relative interwell permeability for the case of 5x4 Synthetic Reservoir – Horizontal wells. 163
Figure 7.19. Top view of the simulation model showing the permeability in x direction for the high permeability channel case of the 5x4 Synthetic field – Horizontal wells. 164
Figure 7.20. Representation of the connectivity coefficients for the high permeability channel case of the 5x4 Synthetic field – Horizontal wells. 165
Figure 7.21. Representation of relative interwell permeability for the high permeability channel case of the 5x4 Synthetic field – Horizontal wells. 166
Figure 7.22. Top view of the simulation model showing the permeability distribution in x direction for the 5x4 Synthetic field with partially sealing barrier– Horizontal wells.. 167
Figure 7.23. Representation of the connectivity coefficients for the case of 5x4 Dual-porosity reservoir with a partially sealing barrier– Horizontal wells. 168
Figure 7.24. Representation of relative interwell permeability for the case of 5x4 dual-porosity reservoir with a partially sealing barrier– Horizontal wells. 168
Figure 7.25. Top view of the simulation model showing the permeability in x direction for the case of 5x4 Synthetic field with a sealing barrier – Horizontal wells 169
Figure 7.26. Representation of the connectivity coefficients for the 5x4 Synthetic Field with a sealing barrier – Horizontal wells. 171
Figure 7.27. Representation of relative interwell permeability for the 5x4 Synthetic Field with a sealing barrier – Horizontal wells. 171

Figure 8.1. Top view of the simulation model showing the x direction permeability for the 5x4 Homogeneous Synthetic field– Hydraulically fractured injectors and vertical producers 173
Figure 8.2. Cross sectional view showing three wells of the 5x4 Homogeneous Synthetic field– Hydraulically fractured injectors and vertical producers 174
Figure 8.3. Comparison of the interwell connectivity coefficient results for the case Hydraulically fractured injectors and vertical producers vs. All fractured wells in 5x4 Homogeneous Synthetic Reservoir. 175
Figure 8.4. Top view of the simulation model showing the x direction permeability for the 5x4 Homogeneous Synthetic field– Mixed Hydraulically fractured and vertical wells 176
Figure 8.5. Representation of the connectivity coefficients for the 5x4 Homogeneous Synthetic field – Mixed Hydraulically fractured and vertical wells. 177
Figure 8.6. Representation of relative interwell permeability for the 5x4 Homogeneous Synthetic field – Mixed hydraulically fractured and vertical wells. 177
Figure 8.7. Comparison of the interwell connectivity coefficient results for the 5x4 Homogeneous Synthetic field – Mixed hydraulically fractured and vertical wells. 178
Figure 8.8. Top view of the simulation model showing the x direction permeability for the 5x4 Homogeneous Synthetic field– Horizontal injectors and vertical producers 179
Figure 8.9. Cross sectional view showing three wells of the 5x4 Homogeneous Synthetic field– Horizontal injectors and vertical producers 179
Figure 8.10. Comparison of the interwell connectivity coefficient results for the case Horizontal injectors and vertical producers vs. All horizontal wells in 5x4 Homogeneous Synthetic Reservoir. 180
Figure 8.11. Top view of the simulation model showing the x direction permeability for the 5x4 Homogeneous Synthetic field– Mixed horizontal and vertical wells 182
Figure 8.12. Cross sectional view showing three wells of the 5x4 Homogeneous Synthetic field– Mixed horizontal and vertical wells.. 182

Figure 8.13. Representation of the connectivity coefficients for the 5x4 Homogeneous Synthetic field – Mixed horizontal and vertical wells. 183
Figure 8.14. Representation of relative interwell permeability for the 5x4 Homogeneous Synthetic field – Mixed horizontal and vertical wells. 184
Figure 8.15. Comparison of the simulated and calculated interwell connectivity coefficient results for the 5x4 Homogeneous Synthetic field – Mixed horizontal and vertical wells. 184
Figure 8.16. Top view of the simulation model showing the x direction permeability for the 5x4 Homogeneous Synthetic field– Mixed horizontal, hydraulically fractured and vertical wells 185
Figure 8.17. Cross sectional view showing three wells of the 5x4 Homogeneous Synthetic field– Mixed horizontal, hydraulically fractured and vertical wells..... 186
Figure 8.18. Representation of the connectivity coefficients for the 5x4 Homogeneous Synthetic field – Mixed horizontal, hydraulically fractured and vertical wells. 187
Figure 8.19. Representation of relative interwell permeability for the 5x4 Homogeneous Synthetic field – Mixed horizontal, hydraulically fractured and vertical wells. 188
Figure 8.20. Comparison of the simulated and calculated interwell connectivity coefficient results for the 5x4 Homogeneous Synthetic field – Mixed horizontal, hydraulically fractured and vertical wells. 188
Figure 9.1. Input flow rate data for the injectors, 5x4 homogeneous synthetic field-Production data. 195
Figure 9.2. Water injection and production total for the 5x4 homogeneous synthetic field-Production data. 196
Figure 9.3. Water injection and production rates for the 5x4 homogeneous synthetic field-Production data. 197
Figure 9.4. Representation of the connectivity coefficients for the 5x4 Homogeneous Synthetic fields – Production data. 198
Figure 9.5. Representation of relative interwell permeability for the 5x4 Homogeneous Synthetic field – Production data. 198

Figure 9.6. Flow rate from Eq.9.9 (t_{eq}=7.57 days) and from simulation results for Well P-01, 5x4 homogeneous synthetic field. 199
Figure 9.7. Comparison of the simulated and calculated interwell connectivity coefficient results for the 5x4 Homogeneous Synthetic field – Production data..... 200
Figure 9.8. Comparison of the interwell connectivity coefficient results for the 5x4 Homogeneous Synthetic field obtained from simulation data using MLR technique with diffusivity filters in the Albertoni and Lake study and the results obtained from analytical model in this study – Production data. ... 201
Figure 9.9. Representation of the interwell connectivity coefficients for the case of 5x4 Anisotropic Reservoir – Production data..... 202
Figure 9.10. Representation of the relative interwell permeabilities for the case of 5x4 Synthetic Reservoir– Production data..... 202
Figure 9.11. Representation of the connectivity coefficients for the case of 5x4 Synthetic Reservoir with high permeability channel – Production data..... 204
Figure 9.12. Representation of relative interwell permeability for the case of 5x4 Synthetic Reservoir with high permeability channel – Production data.... 204
Figure 9.13. Representation of the connectivity coefficients for the case of 5x4 homogeneous reservoir with a partially sealing barrier– Production data. 206
Figure 9.14. Representation of relative interwell permeability for the case of 5x4 dual-porosity reservoir with a partially sealing barrier– Production data..... 206
Figure 9.15. Representation of the connectivity coefficients for the 5x4 Synthetic Field with a sealing barrier – Production data. 208
Figure 9.16. Representation of relative interwell permeability for the 5x4 Synthetic Field with a sealing barrier – Production data. 208
Figure 9.17. Cumulative total water injection and production rates for the 25x16 homogeneous synthetic field-Production data..... 209
Figure 9.18. Water injection and production rates for the 25x16 homogeneous synthetic field-Production data..... 210
Figure 9.19. Representation of relative interwell permeability for the case of 25x16 Homogeneous Reservoir- Production data. 211

Figure 9.20. Relative interwell permeability results for the case of 25x16 Homogeneous Reservoir- Production data. 214
Figure 9.21. Representation of relative interwell permeability for the case of 25x16 Homogeneous Reservoir - Production data. 214
Figure 9.22. Flowchart showing a recommended application for the analytical model for production data in a waterflood. 218

ABSTRACT

Well testing is a common and important tool of reservoir characterization. Many well testing methods have been developed in order to obtain different reservoir properties. Interference tests and pulse tests are used to quantify communication between wells. These methods are often applied to two or more wells with only one active well sending the signals (by changing flow rates) and the shut-in observation wells receiving them. However, for a large field such as a waterflood system, multiple wells are present and most of them are active at the same time. In this case, a pulse test or an interference test with only one active well is difficult to conduct since the signal can be distorted by other active wells in the reservoir.

Interwell connectivity represents the ability of fluid to flow from one well to the others. It is a function of distance and reservoir properties between wells. In waterfloods, information on interwell connectivity is essential in reservoir management, infill drilling and field development plan. This study presents a novel technique to quantify interwell connectivity in a waterflood system based on fluctuations of bottom-hole pressure of both injectors and producers. The interwell connectivity between active and observation wells were quantified by calculating *interwell connectivity coefficients.* An interwell connectivity coefficient is the fraction of pressure change at an observation well due to an active well of the total pressure change at the observation well due to all active wells. More details on the interwell connectivity coefficients are provided later in this report. Both active and observation wells could be active at the same time. The technique utilizes a constrained multivariate linear regression analysis to obtain information about permeability trends, channels and barriers. Analytical models for the

multi-well systems with water injection are derived based on the concept of regional reservoir pressure trend and the pseudo-steady state pressure behavior. Solutions are provided for fully penetrating vertical wells, fully penetrating hydraulic fractures and horizontal wells. Different common reservoir characteristics were investigated including: homogeneous reservoirs, anisotropic reservoirs, reservoirs with high permeability channels, partially sealing barriers and sealing barriers and naturally fractured reservoirs which exhibited dual porosity behavior.

An analytical model, which is based on pseudo-steady state solutions of different wellbore conditions in a closed rectangular reservoir, has been developed for the new technique. By applying the analytical model, a new parameter, called the *relative interwell permeability*, is introduced to quantify the interwell connectivity: This parameter does not depend on the distance between wells and the wellbore conditions (vertical, horizontal or hydraulically fractured wellbores). A technique utilizing the least squares regression analysis is used to estimate the average pressure change at each test time interval. Thus, reservoir pore volume, total average porosity and reservoir compartmentalization can be inferred from the results. In this study, a new analytical model was also developed for a technique published by Albertoni and Lake (2003) that used production data of a waterflood to infer interwell connectivity. The results showed excellent agreement for a reservoir flowing under a steady state condition.

Instrumented oil fields, where down-hole pressure sensors are installed at every well to monitor real-time data, are becoming very common. Hence, collecting bottom hole pressure data at every well at any given time is no longer an impossible task. This study provides a robust technique to utilize these data for reservoir characterization. The

results obtained from the technique are essential for field development plans, which aim to optimize oil production by changing and managing well patterns, well locations and infill drilling. The study also provides better understanding of the reservoir behaviors of a multi-well system in which both injectors and producers are present.

The main conclusions drawn from this study can be stated as follows:

1. The proposed technique using bottom hole pressure data is more robust than a similar technique that uses production data as it provides better results with less data points and without the need of subjective judgments. The interwell connectivity coefficients obtained can be used to identify reservoir anisotropy, high permeability channels and flow barriers. The validity of the results for different heterogeneous reservoirs containing different wells of different wellbore conditions such as fully penetrating vertical wells, fully penetrating hydraulic fractures and horizontal wells were verified using data from a commercial black oil simulator.

2. Pressure transient solutions of a well in a multiwell system are used to derive the mathematical model for the technique. Thus, this study introduced a new parameter called relative interwell permeability to quantify interwell connectivity. The relative interwell permeability does not depend on distance between wells or wellbore conditions.

3. The new procedure also allows the calculation of average pressure change for each test time interval. Using a material balance equation, the total pore volume can be calculated. Furthermore, based on these pressure results, reservoir compartments can be identified.

4. The test design is flexible. This study has shown that active wells could be either injectors or producers and observation wells could be injectors, producers or shut-

in wells. This is important for the field applications as the actual field situations may vary from one reservoir to another.

5. Under the pseudo-steady state condition, pressure solution for a well in a naturally fractured reservoir, which behaves like a dual-porosity system, is the same as the solution for a well in a homogeneous reservoir given that the effective permeability for the naturally fractured reservoir is equal to the permeability of the homogeneous reservoir. Thus, the technique introduced in this study to determine interwell connectivity is applicable to both a naturally fractured reservoir and homogeneous reservoir.

6. Different wellbore conditions such as vertically fractured wells and horizontal wells were considered in this study. The interwell connectivity information can also be obtained from different types of wellbore conditions. With the analytical model, the systems with different wellbore conditions can be analyzed and the resulting relative interwell permeabilities can be used to infer the formation properties between active and observation wells.

7. The analytical approach can be used to develop an analytical model for production data from a waterflood system flowing under steady state condition. The results obtained from analytical models fit well with those obtained from synthetic models in the Albertoni and Lake study. Thus, the analytical solution gives a better understanding to the techniques available in the literature that require the use of production data.

CHAPTER 1 - INTRODUCTION

1.1. Objectives

The interwell connectivity is an important factor in reservoir characterization especially for a mature field where decisions on infill drilling, well flow rates and well pattern are essential in cost reduction and production optimization of the reservoir. The traditional well test techniques to quantify the degree of interwell connectivity are interference tests and pulse tests. These methods are often applied to two or more wells as only one active well sending the signals (by changing flow rates) and one or more observation wells receiving them. However, in a large field that has produced for sometime, there are often multiple active wells. In this case, a pulse test or an interference test between an active well and one or multiple observation wells are difficult to conduct since the signal can be distorted by other active wells in the same field. Furthermore, the observation wells in pulse tests or interference tests are often shut-in causing production down time.

Recent studies have introduced techniques to infer interwell connectivity from production data of a waterflood. Even though these techniques contributed greatly to the development of the interwell connectivity study in a waterflood system, they still have their own limitations and restrictions. The limitations include the need of diffusivity filters, large number of data points and subjective judgment. Thus, the main objectives of this work are as follows:

- Develop a novel multiwell testing technique to infer interwell connectivity from bottom hole pressure fluctuations. The new technique should address the major drawbacks of the current techniques as mentioned above with minimized complexity and maximized applicability.

- Derive an analytical model for the new technique for better understanding as well as for further extension of the technique.
- Extend the technique to a naturally fractured reservoir representing a dual porosity system and to different wellbore conditions such as fully penetrating vertically fractured wells and horizontal wells besides fully penetrating vertical wells.
- Provide an analytical solution for the existing technique that uses production data of a waterflood.

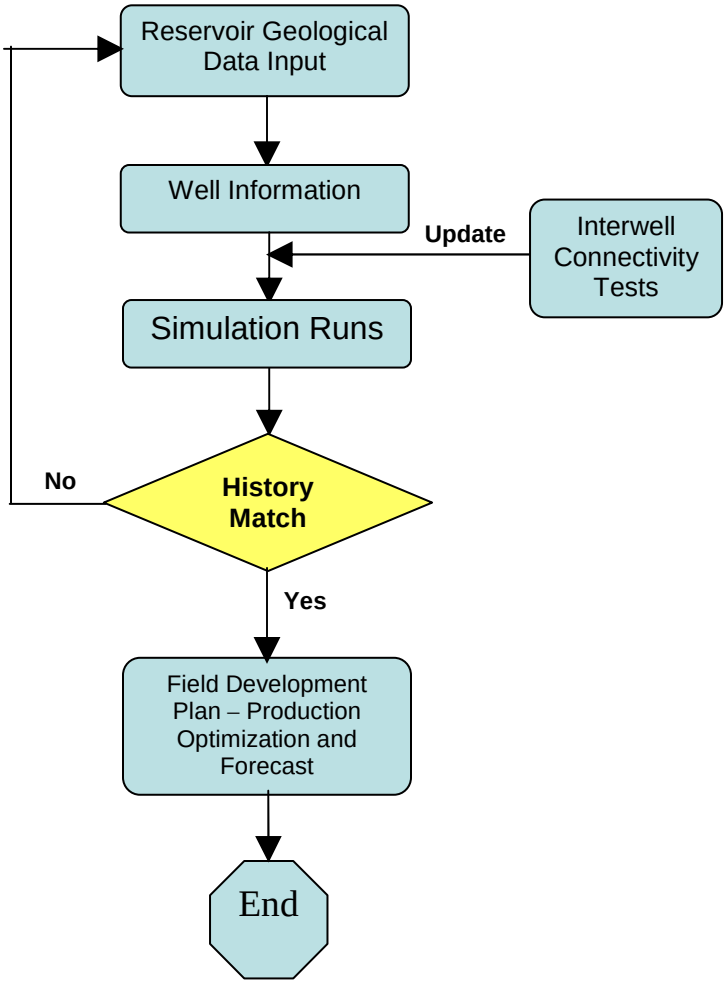


Figure 1.1. Flowchart for the application of the proposed interwell connectivity test.

Fig. 1.1 shows a flowchart of a possible application of the interwell connectivity test in a reservoir simulation study. Following is the step-by-step procedure for this application:

Step 1: Reservoir geological properties obtained from seismic, well log, core analysis and well test data are used to build the geological model of the reservoir. The model can contain reservoir boundaries and surfaces, fault structures, permeability and porosity maps.

Step 2: Well information is input into the model. The information includes well locations and trajectory. In this step, the data from an intewell connectivity test can be used to calculate the interwell connectivity coefficients. Details about the test are provided in the following chapters. Thus, the interwell connectivity between wells can be inferred and this information can be used to update the reservoir model and clarify uncertainties.

Step 3: In this step, simulation run is performed using injection and well control history.

Step 4: The resulted production from the simulation run is matched with the available production history. If a satisfactory match is obtained then the model can be used for production forecast and optimization. If the match is not satisfactory then the model should be revised or the steps 1 to 4 should be repeated.

Step 5: The future production forecast is performed in this step. Different production optimization strategies can be used to maximize the production using the simulation model.

All results in this study are verified using data generated from numerical simulation models using a commercial black oil reservoir simulator.

1.2. Organization

The following Chapter 2 provides a background on the development of techniques to infer interwell connectivities in a reservoir with water injection. Chapter 2 also includes important terms and definitions associated with the new technique and the statistical methods used in the technique.

Chapter 3 introduces the new technique to infer interwell connectivity from bottom hole pressure fluctuations in a waterflood. Simulation results for different cases of reservoir heterogeneity and detailed analysis of the results are also provided in this chapter.

Chapter 4 presents the analytical model for the technique which is derived from a transient pressure solution for a fully penetrating vertical well in a closed rectangular reservoir. In this chapter, new parameters such as the relative interwell permeability and the influence functions are introduced. The relative interwell permeability is then used along with the interwell connectivity coefficients to quantify the degree of connectivity between wells. The calculation of total reservoir pore volume is also presented in this chapter.

Chapter 5 presents the application of the technique to naturally fracture reservoir which represents a dual porosity system. Synthetic cases similar to the simulation cases in the previous chapters were run for the dual porosity system. The results were analyzed in details. A literature review and the important mathematical concepts are also provided.

Chapter 6 presents the application of the technique to fields with only hydraulically fractured wells. Only fully penetrating vertical fractures with different fracture half lengths were considered. Again, results for different synthetic cases were analyzed. The calculation method to calculate the influence function is also explained in detail.

Chapter 7 presents the application of the technique to fields with only horizontal wells. Only vertically centered horizontal wells were considered in the analysis. Results for different synthetic cases and calculation method for the influence function are provided.

Chapter 8 presents some simulation results obtained from different cases of mixed wellbore conditions. Fields with all vertical wells, hydraulically fractured wells and horizontal wells or fields with two of any of those well types were considered. The results were analyzed to validate the technique and assess the degree of errors.

Chapter 9 provides an analytical model for a system of vertical wells in a closed rectangular reservoir under steady state condition to work with production data. Thus the model was derived and the interwell connectivity results obtained were compared with the results from previous studies that used production data to infer interwell connectivity.

Chapter 10 provides the summary and conclusions of the study and recommendations for future work.

CHAPTER 2 - BACKGROUND

This chapter presents a literature review of studies directly related to the new technique and a mathematical review of the statistical techniques used in this work, the Multivariate Linear Regression (MLR) and the Least Squares Linear Regression (LSLR). Albertoni and Lake (2003) used the MLR technique to infer interwell connectivity from production data as described in section 2.2. The LSLR method is described in section 2.3.

2.1. Literature Review

Numerous studies on inferring interwell connectivity in a waterflood have been carried out. Some of the previous studies used statistical techniques that are very different from the approach used in this study. However, only MLR and LSLR techniques were used in this study.

Heffer et al. (1995) determined the connectivity between wells by calculating the Spearman rank correlation coefficients of nonparametric statistics and showed that these coefficients are somewhat related to the local orientation of horizontal earth stresses in waterfloods.

Refunjol (1996) also determined reservoir heterogeneities using the Spearman rank correlation coefficient and compared the results with gas tracer response. She correlated injection wells with their adjacent producers and calculated the maximum coefficient value by varying time lags. Refunjol (1996) also proposed for future work a linear model that related each production well to all the injectors and the other producers. DeSant'Anna Pizarro (1998) provided more insight into the Spearman rank correlation coefficient approach, as well as its advantages and limitations.

Albertoni and Lake (2003) developed a technique that calculates the fraction of flow caused by each of the injectors in a producer. This method uses a constrained multivariate linear regression model similar to the model proposed by Refunjol (1996). The model introduced by Albertoni & Lake, however, considered only the effect of injectors on producers, not producers on producers. Albertoni & Lake also introduced the concepts and uses of diffusivity filters to account for the time lag and attenuation that occurs between the stimulus (injection) and the response (production). The procedures were proven effective for synthetic reservoir models, as well as real water flood fields.

Yousef et al. (2006) introduced capacitance model in which a nonlinear signal processing model was used. Compared to Albertoni & Lake's model which was a steady-state (purely resistive), the capacitance model included both capacitance (compressibility) and resistivity (transmissibility) effects. The model used flow rate data and could include shut-in periods and bottom hole pressures (if available).

Recently, Dinh and Tiab (2007, 2008) used similar approach as Albertoni and Lake (2003), however, bottom hole pressure data were used instead of flow rate data. Some constraints were applied to the flow rates such as constant production rate at every producer and constant total injection rate. Some advantages of using bottom hole pressure data are no diffusivity filters needed, minimal of data required and flexible plan to collect data.

2.2. Multivariate Linear Regression (MLR)

A linear model is often used to predict the behavior of a dependent variable as a function of independent variables. A linear model can be expressed as follows:

$$y = \beta_0 + \sum_{k=1}^{K} \beta_k x_k + \varepsilon \tag{2.1}$$

where y is the dependent variable, x_k are the independent variables, ε is a random error, and β_0 and β_k are parameters to be adjusted or determined by regression. The error term ε is used to account for the imbalances in the model and measurement errors.

For example, considering flow rates data from a field with N producers and I injectors, the linear model for the j^{th} producer is (Albertoni and Lake, 2003):

$$\hat{q}_j(t) = \lambda_{0j} + \sum_{i=1}^{I} \lambda_{ij} i_i(t) \qquad (j = 1, 2, \ldots N) \tag{2.2}$$

This equation states that at any given time, the total production rate at well j has a linear relationship with the rates of every injector. The constant term λ_{0j} accounts for the possible imbalance in the field and the parameters λ_{ij} are called the interwell connectivity coefficients. Thus, the term λ_{0j} represents the liquid production not associated with injected water (primary production), and injection fluid losses. When $\sum_{j=1}^{N} \lambda_{0j}$ is significantly different from zero, the field is unbalanced and MLR must be used.

The model in Eq. 2.2 assumes steady state flow. So, changes in injection rate cause instant changes in production rate. However, most of the time in a waterflood, transient flow creates time lags and attenuation as fluid flows from injectors to producers. To account for the time lag and attenuation, diffusivity filters are used. The diffusivity filters partially correct these effects of transient flow. Further discussion of diffusivity filters is presented in section 2.4.

Given a set of observed data of production and injection rates, the variance of q_j

$$\sigma^2_{MLR,j} = Var(\hat{q}_j - q_j) = E\left[(\hat{q}_j - q_j)^2\right] \tag{2.3}$$

is a measure of the difference between the observed production rate and the modeled production rate calculated from the model for producer j. The interwell connectivity coefficients λ_{ij} and the constant term λ_{0j} can be determined by minimizing this variance. This minimization leads to the following system of linear equations:

$$\begin{bmatrix} \sigma^2_{11} & \sigma^2_{12} & & \sigma^2_{1I} \\ \sigma^2_{21} & \sigma^2_{22} & \cdots & \sigma^2_{2I} \\ \vdots & \vdots & \ddots & \vdots \\ \sigma^2_{I1} & \sigma^2_{I2} & \cdots & \sigma^2_{II} \end{bmatrix} \times \begin{bmatrix} \lambda_{1j} \\ \lambda_{2j} \\ \vdots \\ \lambda_{Ij} \end{bmatrix} = \begin{bmatrix} \sigma^2_{1j} \\ \sigma^2_{2j} \\ \vdots \\ \sigma^2_{Ij} \end{bmatrix} \tag{2.4}$$

The covariance between q_j and i_i is defined as

$$Cov(i_i, q_j) = \sigma^2_{ij} = E\left\{\left[i_i - E(i_i)\right] \times \left[q_j - E(q_j)\right]\right\} \tag{2.5}$$

Eq. 2.4 can be solved for the λ_{ij} s by conventional method such as Gauss Elimination.

The first term of Eq. 2.4, the σ^2_{ij} square matrix, is called injector-injector covariance matrix, and the vector on the right side of the equation is called injector-producer covariance column vector.

The constant term λ_{0j} is determined by

$$\lambda_{oj} = \bar{q}_j - \sum_{i=1}^{I} \lambda_{ij} \bar{i}_i \tag{2.6}$$

where the symbol $\bar{}$ indicates an average.

The MLR approach involves the determination process of the interwell connectivity coefficients λ_{ij} that relate a producer *j* to an injector *i*. Therefore, for each producer, a set of *I*+1 equations and *I*+1 unknowns must be solved (Eqs. 2.4 and 2.6).

The interwell connectivity coefficients λ_{ij} obtained from the solution of Eq. 2.4 provide a quantitative expression of the influence of each injector *i* on each producer *j*; the larger the magnitude of λ_{ij} is , the greater the influence. The constant term λ_{oj} represents amount of fluid produced at the producer j affected by the producers. Further discussion can be found in Chapter 9.

2.3. Least Squares Linear Regression (LSLR)

The LSLR method is well established in the literature and considered equivalent to the MLR method (Yousef et al., 2006). Considering the following model representing each data point:

$$Y = A_0 + C_1 A_1 + C_2 A_2 + \ldots + C_I A_I + \varepsilon \tag{2.7}$$

Where the response is Y. The regression model parameters are A_0 and A_i, the explanatory variables are C_i and ε is random error (Jensen et al., 2000, see also Chapra & Canale, 1988). With (L-1) data sets, (I+1) estimated model parameters, we have the following equation:

$$\begin{bmatrix} Y_1 \\ Y_2 \\ \vdots \\ Y_{L-1} \end{bmatrix} = \begin{bmatrix} 1 & C_1^{(1)} & C_2^{(1)} & \vdots & \vdots & C_I^{(1)} \\ 1 & C_1^{(2)} & C_2^{(2)} & \vdots & \vdots & C_I^{(2)} \\ \vdots & \vdots & \vdots & \vdots & \vdots & \vdots \\ 1 & C_1^{(L-1)} & C_2^{(L-1)} & \vdots & \vdots & C_I^{(L-1)} \end{bmatrix} \times \begin{bmatrix} A_0 \\ A_1 \\ \vdots \\ A_I \end{bmatrix} \tag{2.8}$$

The short form of Eq.2.8 is

$$Y = C \times A_v \tag{2.9}$$

By minimizing the sum of the squared differences between the observed responses and the predicted responses for each set of $C_i^{(l)}$, the least squares estimation of the parameter vector A_v is (Jensen et al., 2000 or Chapra & Canale, 1988):

$$A_v = \left[C^T C\right]^{-1} C^T Y \tag{2.10}$$

Where C^T is the transpose of C.

CHAPTER 3 – INFERRING INTERWELL CONNECTIVITY FROM BOTTOM HOLE PRESSURE FLUCTUATIONS

This chapter presents a new procedure to determine inter-well connectivity in a reservoir based on fluctuations of bottom hole pressure of both injectors and producers in a waterflood. The method uses the same constrained multivariate linear regression analysis as mentioned above to obtain information about permeability trends, channels and barriers.

Albertoni and Lake (2003) applied the same analysis to injection and production rates to infer connectivity between wells. However, in order to obtain good results, various diffusivity filters are applied to the flow rate data to account for the time lags and the attenuation. This process requires subjective judgments and is time consuming. Shut-in periods in the data, usually unavoidable when a large number of data points were used, created significant errors in the results and were often eliminated from the analysis.

This new method yielded better results compared to the results obtained when production data were used. Its advantages include: (1) No diffusivity filters needed for the analysis; (2) Minimal numbers of data points required to obtain good results; and (3) Flexible plan to collect data as all constraints can be controlled at the surface. The new procedure was tested using a numerical reservoir simulator. Thus, different cases were run on two fields, one with five injectors and four producers and the other with 25 injectors and 16 producers.

For a large waterflood system, multiple wells are present and most of them are active at the same time. In this case, pulse test or interference test between two wells are difficult to conduct since the signal can be distorted by other active wells in the reservoir.

In the proposed method, interwell connectivity can be obtained quantitatively from multi-well pressure fluctuations without running interference tests.

3.1. Overview

In this method, data can be obtained from multi-well pressure test that resemble interference test. Thus, we can have several wells sending signals and the others receiving the signals at the same time. However, the wells that are receiving the signal can either be shut-in or kept at constant producing rates. The pressures at all wells are recorded simultaneously within a constant time interval. The length of the test will depend on the length of the time interval and the number of data points. Results of this method can be used to optimize operations and economics and enhance oil recovery of existing waterfloods by changing well patterns, changing injection rates, recompletion of wells, and in-fill drilling.

This new technique is based on previous work conducted by Albertoni and Lake (2003) using injection and production rates. In their work, Albertoni and Lake developed and tested different approaches using constrained multivariate linear regression analysis with a numerical simulator and then applied to a waterflooded field in Argentina. Diffusivity filters are required to account for the time lag and attenuation of the data. Another drawback when production data were used includes the requirement of large number of data points. In his thesis, Dinh (2003) verified the method using different reservoir simulator and applied to a waterflood field in Nowata, Oklahoma. He also investigated the effect of shut-in periods and vertical distances on the results.

The main objectives of this chapter are to compare the results obtained from pressure data with results from flow rate data and to propose a new method to determine interwell connectivity.

Similar to the method that uses production rates, we will concentrate on waterflood system only. The reservoir is considered as a system that processes a stimulus (a well that is sending signals) and returns a response (a well that is receiving the signals). The effect of the reservoir on the input signal will depend on the location and the orientation of each stimulus-response pair. Since the total pressure changes at active and observation wells are not equal, only the Multivariate Linear Regression was used. The effect of diffusion was not significant, thus, the diffusivity filters were not used.

The method was applied to two synthetic fields, one with five injectors and four producers and the other with 25 injectors and 16 producers.

3.2. Procedure

The method uses the bottom hole flowing pressure or well shut-in pressure data of every well in a waterflood as input data. The pressure is obtained from pressure data measured simultaneously in every well. This analysis will only consider oil and water system, thus there is no gas involved. The multi-well pressure test can be conducted similarly to an interference test by changing flow rates at several active wells and records the pressure responses at the observation wells which are flowing at constant rates or have been shut-in. The test will require recording pressure data of every well simultaneously. In this analysis, we use injection wells as active wells and production wells as observation wells. Thus, the production rates are kept constant. All producers need to be able to flow at designated rates without any support from the surface

throughout the testing period. A well is considered shut in when its production rate is set to zero. The diffusivity filters were not used in this analysis because the effect of diffusion was not significant. Excellent results were obtained for the base case without diffusivity filters.

3.2.1. Multivariate Linear Regression for Pressure data

In a field with N producers and I injectors, the proposed model for the interwell connectivity test is expressed in Eq. 3.1. In this model, the estimated pressure at a producer *j* (observation well) is given by:

$$\hat{p}_j(t) = \beta_{0j} + \sum_{i=1}^{I} \beta_{ij}\, p_i(t) \quad (j = 1, 2, \ldots N) \tag{3.1}$$

where *N* is the total number of producers and *I* is the number of injectors. This equation states that at any time the total pressure at producer *j* is a linear combination of the pressure of every injector corresponding to that producer plus a constant term, β_{0j}. The factors β_{ij} are the weighting factors or the interwell connectivity coefficients and the constant term β_{0j} accounts for the unbalance. *Thus, the interwell connectivity coefficient, β_{ij}, represents the fraction of pressure change at the producer j due to the injector i of the total pressure change at the producer due to all injectors.* Since the total injection rates are kept constant in each time interval, the total pressure change at the producer *j* due to all injectors are expected to be constant once the reservoir reach pseudo-steady state at late time during each time interval. The pressure change at the producer due to the change in the reservoir pressure and the pressure drops at all the producers including the investigated producer *j* is accounted for in the constant term β_{0j}. Thus, the sum of interwell connectivity coefficients, β_{ij}, is equal to unity and the

coefficients vary from zero to unity. If the pressures in the injectors are known, the coefficients β_{ij} and the term β_{0j} need to be determined.

Jensen *et al.* (1997) present the solution for this multivariate linear regression problem. To solve this over-determined system the variance, $Var(\hat{p}_j - p_j)$, is minimized. This minimization leads to the following set of I linear equations:

$$\begin{pmatrix} \sigma_{11}^2 & \sigma_{12}^2 & \cdots & \sigma_{1I}^2 \\ \sigma_{21}^2 & \sigma_{22}^2 & \cdots & \sigma_{2I}^2 \\ \vdots & \vdots & \ddots & \vdots \\ \sigma_{I,1}^2 & \sigma_{I2}^2 & \cdots & \sigma_{II}^2 \end{pmatrix} \times \begin{pmatrix} \beta_{1j} \\ \beta_{2j} \\ \vdots \\ \beta_{Ij} \end{pmatrix} = \begin{pmatrix} \sigma_{1j}^2 \\ \sigma_{2j}^2 \\ \vdots \\ \sigma_{Ij}^2 \end{pmatrix} \qquad (3.2)$$

which can be solved by standard means. The constant term β_{0j} is given by:

$$\beta_{0j} = \bar{p}_j - \sum_{i=1}^{I} \beta_{ij} \bar{p}_i \qquad (3.3)$$

where σ^2_{ii} and σ^2_{ij} are injector-injector and injector-producer covariances respectively.

Thus, a set of I+1 equations and I+1 unknowns must be solved for each producer (Eqs. 3.2 and 3.3). The interwell connectivity coefficients β_{ij} obtained from the solution of the N systems of equations provide a quantitative expression of the influence of each injector i on each producer j; the larger the β_{ij}, the greater the influence.

Since all producers will be set to a constant rate, the total pressure change at all producers due to production will decrease linearly. However, since the total pressure loss at the producers is always lower than the total pressure increase caused by the injectors, pressure at all the wells will keep increasing. However, the analysis only considers the pressure change at the producers caused by pressure change at the injectors. If the increasing of pressure at all the wells is also changing, it will interfere in the analysis. Thus, in order for this analysis to work, the total pressure change at the injectors also

needs to be constant, or the total injection rate needs to be constant. In fact, β_{0j} terms account for the constant pressure increase due to higher total injection rate compared to total production rate.

The second term on the right hand side of Eq. 3.1, $\sum_{i=1}^{I} \beta_{ij} p_i(t)$, accounts for the increase of production pressure due to each individual injectors. Assuming the waterflood is a closed system, thus all increase in pressure at a producer is due to the injectors, we should have

$$\sum_{i=1}^{I} \beta_{ij} = 1 \qquad (j = 1, 2, \ldots N) \tag{3.4}$$

The larger is the term β_{0j} in equation 1, the smaller is the term $\sum_{i=1}^{I} \beta_{ij} p_i(t)$ and thus the interwell connectivity coefficient will be affected. In order for the coefficients to be comparable among producers, it is necessary to have the production rate constant and equal among producers.

3.3. Assumptions

This section describes assumptions for the techniques. In general, the technique assumes that all the parameters except injection and production rates (response and explanatory variables respectively) are constant. This includes constant injector and producer conditions and constant reservoir conditions. Possible sources of errors are discussed later in this chapter.

Two general assumptions for the methods are needed, constant injector and producer conditions and constant reservoir conditions. For the first general assumption to hold, no new wells should be drilled in the field over the analyzed period. New wells

result in a totally new set of coefficients for MLR and LSLR approaches and a completely new analysis must be done. Flow rates at the producers, given they are all operated under rate control, must be constant since the method assumes that changes in bottom hole pressures at the producers are due to the changes in injection rates, and the effects of the change in average reservoir pressure and bottom hole pressures at the producers on any producer are constant. The MLR method also assumes that the change of bottom hole pressure at the producers associated with all the producers and the field average pressure is constant over the entire analyzed period (β_{oj} is constant for each injector-producer pair). Finally, changes in well bore conditions at the injectors (active wells) will change the connectivity properties of those wells to the producers, so we assume the well bore conditions at the injectors are constant. Further discussion on wellbore conditions of the producers will follow in the next chapters.

The second general assumption, constant reservoir conditions, consists of assumption of constant main reservoir and fluid properties such as absolute permeability, porosity, layer thickness, fracture properties, fluid viscosity, constant total compressibility and constant relative permeability. In this study, we assume single phase flow. Some factors such as permeability trends, transmissibility barriers and fractures are to be determined from the results of the analysis and thus, their properties should be constant with time. The field is also assumed to be under pseudo steady state condition at the time the pressure data are recorded.

3.4. Simulation Results

The method was tested by applying it to two synthetic fields, one of four producers and five injectors (5x4 Field) and the other of 16 producers and 25 injectors

(25x16 Field). The results were verified with those obtained from application of the method to the flow rates data.

3.4.1. Application to 5x4 Field.

MLR approach as explained above was applied to a numerically simulated field with a five-spot injection pattern: 5 injectors and 4 producers. The oil is undersaturated oil. The injector-producer distance is 1000 ft. The oil-water mobility ratio is equal to one, and the oil, water, and rock compressibility are approximately $5x10^{-6}$, $1x10^{-6}$ and $1x10^{-6}$ psi^{-1} respectively. All wells are vertical wells.

Fig. 3.1 shows one layer of the grid system, the well locations and the field dimensions used in the model. Injection rate data was generated randomly ranging from 100 to 900 bbl/d, with total injection rates kept at 2000 bbl/d.

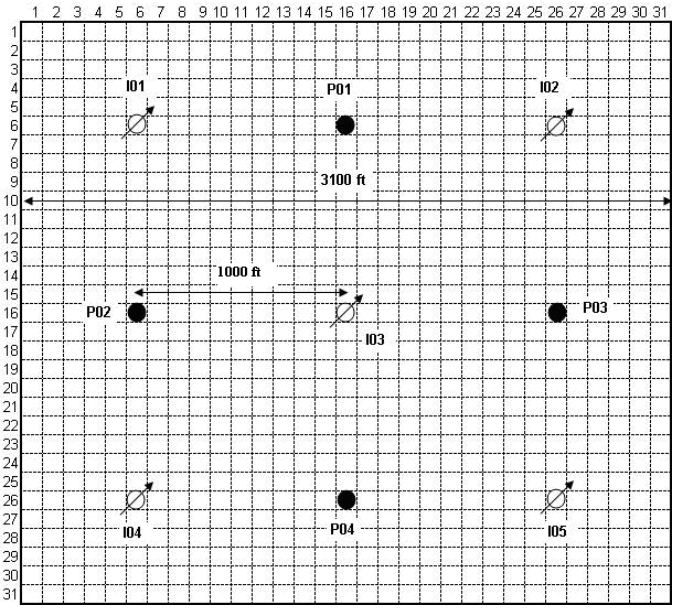


Figure 3.1. Grid system for the simulation model (5x4 Synthetic field).

Fig. 3.2 shows the injection rates for the five injectors in the field as well as the total field injection rates. The flow rate of each producer (observation well) was set to 300 bbl/d (Base case). The simulation was run for 50 months (1500 days approximately). This represented a history of 50 data points of injector and producer pressure. The numerical simulator used was Boast 98, a finite difference simulator that uses block centered calculations.

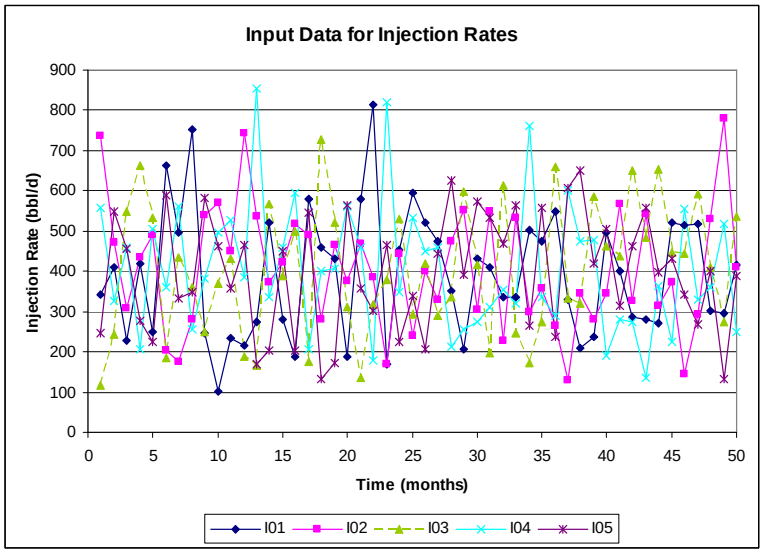


Figure 3.2 . Flow Rates for five injectors. The total field injection is constant at 2000 bbl/d.

Grid dimensions of the model is 31x31x1 (Fig. 3.1) and the grid block dimensions were 100 ft x 100 ft x 60 ft. The water-oil mobility ratio was set to one with constant oil and water viscosities. The pressure of the four producers and the five injectors obtained from the simulation process were analyzed using MLR method described previously. Several cases were analyzed for this field.

a. Homogeneous reservoir.

This is the simplest case of a single-layered homogeneous reservoir with an isotropic permeability of 100 mD. Different cases were run for this reservoir. The first case is also considered as the base case when the production rate at the observation wells was kept constant and equal to 300 bbl/d. Table 3.1 shows the numerical values of the interwell connectivity coefficients obtained from MLR.

Table 3.1: Results for the interwell connectivity coefficients β. 5x4 field, homogeneous reservoir.

	P1	P2	P3	P4	Sum
β_{0j} (psia)	-332.8	-332.8	-332.8	-332.8	-1331.19
I1	0.27	0.27	0.11	0.12	0.77
I2	0.27	0.12	0.27	0.12	0.79
I3	0.23	0.23	0.23	0.23	0.91
I4	0.12	0.27	0.12	0.27	0.77
I5	0.11	0.11	0.26	0.26	0.75
Sum	1.00	1.00	1.00	1.00	

Asymmetry coefficient (A_s): In order to compare the quality of the interwell connectivity coefficient results for homogeneous symmetric reservoirs, we use the asymmetry coefficient (A_s). Albertoni and Lake (2003) introduced the asymmetry coefficient (A_s) to measure the quality of the results in symmetric reservoirs. In the case of this 5x4 synthetic model, the reservoir has several planes of symmetry that define three groups of injector-producer pairs with similar relative locations. In a homogeneous and isotropic reservoir, the well pairs in each group should have the same or similar interwell connectivity coefficients. These groups are: (a) corner injectors with nearby producers I01-P01, I01-P02, I02-P01, I02-P03, I04-P02, I04-P04, I05-P03, and I05-P04; (b) corner injectors with farther producers I01-P03, I01-P04, I02-P02, I02-P04, I04-P01, I04-P03, I05-P01 and I05-P02; and (c) center injector with nearby producers I03-P01, I03-P02,

I03-P03 and I03-P04. According to Albertoni and Lake, "To quantify the symmetry shown by the interwell connectivity coefficients we define a term that describes their variability in each similar group. The asymmetry coefficient (A_s) is the square root of the sum of the variances of βs of the group, weighted by the number of well pairs in each group". For the case of 5x4 field, with 3 groups of weighing coefficients (or interwell connectivity coefficients) (a, b and c) shown above and a total of 20 β coefficients, the asymmetry coefficient (A_s) is defined as:

$$A_s = \sqrt{\frac{8\,\mathrm{var}_a(\beta) + 8\,\mathrm{var}_b(\beta) + 4\,\mathrm{var}_c(\beta)}{20}} \tag{3.5}$$

For a symmetric homogeneous and isotropic synthetic reservoir, good symmetry is expected from the interwell connectivity coefficient results. Since A_s indicates the asymmetry of the interwell connectivity coefficients, the smaller the asymmetry coefficient, the better the results. Thus, the closer A_s get to *zero*, the better are the results for the case of homogeneous symmetric synthetic reservoir.

Coefficient of Determination: Another way to determine the quality of the results is using the coefficient of determination, R^2. R^2 measures the quality of the correlation between observed and modeled response data.

$$R^2 = 1 - \frac{\sum_{m=1}^{M} (\hat{p}_j^{(m)} - p_j^{(m)})^2}{\sum_{m=1}^{M} (p_j^{m} - \overline{p}_j)^2} \tag{3.6}$$

However, the coefficient of determination provides only a poor description of the quality of the results. According to Jensen (1997), the coefficient of determination does not measure the appropriateness of the model. Thus, for a symmetric homogeneous and

isotropic synthetic reservoir, the asymmetry coefficient is a better tool to evaluate the quality of the results than R^2 and should be included in the analysis. However, in actual applications that involve heterogeneity and complication in the reservoirs, symmetry is not expected from the results and only R^2 can be used.

In the base case, with the production rates at the producers are kept constant at 300 bbl/d, the interwell connectivity coefficients results are shown in Table 3.1. Fig 3.3 presented the interwell connectivity coefficients for the base case by inverted arrows that start from the i^{th} injector and point to the j^{th} producer. The longer the arrow is and the larger the values of the coefficient are, the better is the connectivity between the two wells.

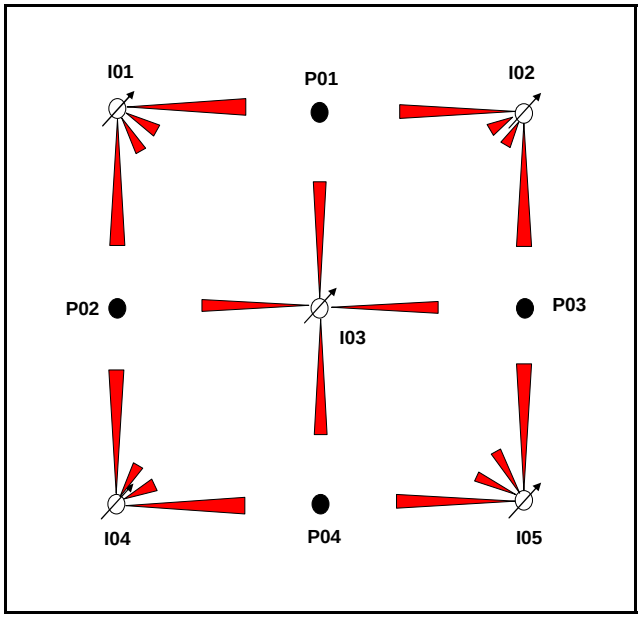


Figure 3.3 . Representation of the interwell connectivity coefficients β, shown in Table 3.1. The lengths of the arrows are proportional to the values of the coefficients. 5x4 field, homogeneous reservoir (R^2 =1.00, A_s = 0.000902).

The low asymmetry coefficient A_s (0.000902) and perfect R^2 (1.00) as shown in Fig. 3.4 represents excellent results. The above results are better than the results obtained

from the same field with flow rates data using MLR method without diffusivity filters (A_s = 0.01096 and R^2 = 0.970)^2. They are also better than results obtained by Albertoni and Lake (2003) using MLR without diffusivity filters (A_s = 0.00778 and R^2 = 0.977) or with diffusivity filters (A_s = 0.01160 and R^2 = 0.996).

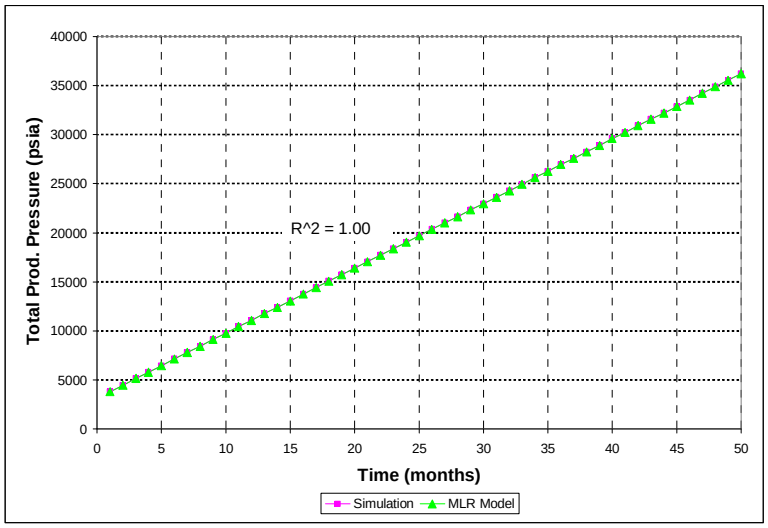


Figure 3.4 . Comparison between total modeled pressure using MLR and the total simulated pressure. 5x4 field, homogeneous reservoir.

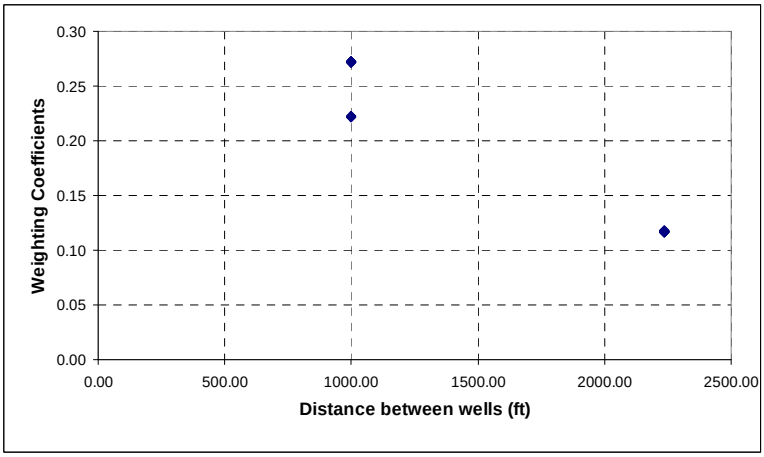


Figure 3.5 . The resulted interwell connectivity coefficients β versus the distances of well pairs. 5x4 field, homogeneous reservoir.

Fig**.** 3.5 shows the plot of the interwell connectivity coefficients versus distance between wells. The well pairs at the same position and in the same distance have almost exactly the same interwell connectivity coefficients. Summation of the coefficients of each producer was equal to one suggesting the previous mentioned condition is satisfied.

Since the injection rates are uncorrelated, the excellent symmetry shown by the calculated βs suggests that βs do not depend on injection rates. This was verified by using different sets of injection rates on the same field, the results are similar for all the cases. Thus, similar to the other approach where flow rates were used, the weighing coefficients, β, only depend on the reservoir properties and the relative location of the wells. With all the constraints stated before on production rates and total injection rates, the weighing coefficients are independent of injection rates at each producer.

Considering the case of production rate at observation wells equal 300 bbl/d as the base case, the obtained results were excellent (very low A_s and R^2 close to one). The diffusivity filters as applied when production data were used are not necessary for this method since the coefficient of determination was already equal to unity. This will help simplify the calculation and save time.

b. Anisotropic reservoir.

In this case, the permeability in the y direction was set to be $1/10^{th}$ of the permeability in the x direction. Results obtained from the MLR approach are presented in Fig**.** 3.6 and Table 3.2. As expected, larger interwell connectivity coefficients occurred in the x direction, indicating the obvious preferential permeability orientation.

Table 3.2: Results for the interwell connectivity coefficients β. 5x4 Synthetic field, Anisotropic reservoir (R^2 =1.00).

	P1	P2	P3	P4	Sum
β_{0j} (psia)	-269.5	-418.3	-418.2	-254.7	-1360.6
I1	0.40	0.10	0.10	0.05	0.65
I2	0.48	0.08	0.08	-0.02	0.63
I3	0.06	0.63	0.63	0.12	1.45
I4	0.05	0.09	0.09	0.41	0.64
I5	0.02	0.09	0.09	0.43	0.64
Sum	1.00	1.00	1.00	1.00	

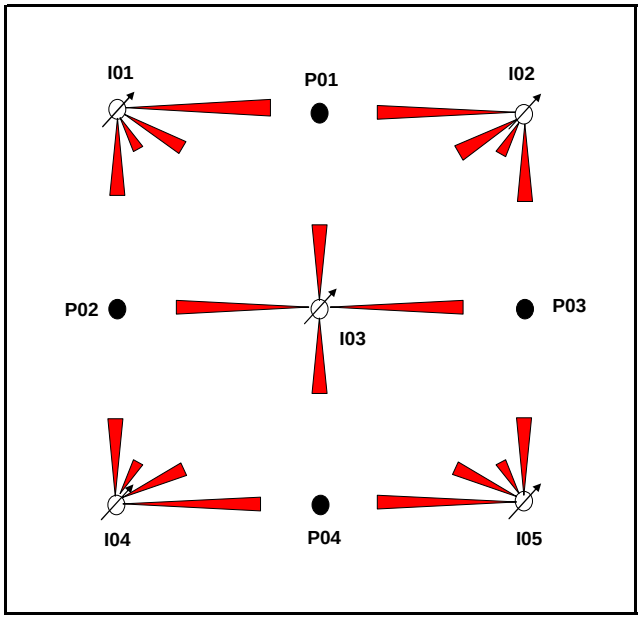


Figure 3.6 . Representation of the interwell connectivity coefficients β for 5x4 field, anisotropic reservoir (k_x/k_y=10).

c. Reservoir with high permeability channel.

To investigate the effect of spatial heterogeneity, a channel of high permeability was created in the original synthetic homogeneous one-layered reservoir. The results are presented in Fig. 3.7 and Table 3.3.

The shaded area in Fig**.** 3.7 represents a channel with a permeability of 1000 mD. Permeability for the rest of the reservoir was 100 mD. Vertical permeability was

constant at 10 mD. Within the same distance, the wells located in high permeability channel (I01 and P04) are better connected to other wells than those not in the channel.

Table 3.3: Results for the interwell connectivity coefficients β. 5x4 Synthetic field with high permeability channel.

	P1	P2	P3	P4	Sum
β_{0j} (psia)	-291.4	-242.9	-305.7	-213.8	-1053.8
I1	0.34	0.36	0.22	0.27	1.19
I2	0.21	0.10	0.24	0.10	0.64
I3	0.22	0.26	0.21	0.27	0.96
I4	0.12	0.17	0.11	0.18	0.57
I5	0.11	0.12	0.22	0.19	0.64
Sum	1.00	1.00	1.00	1.00	

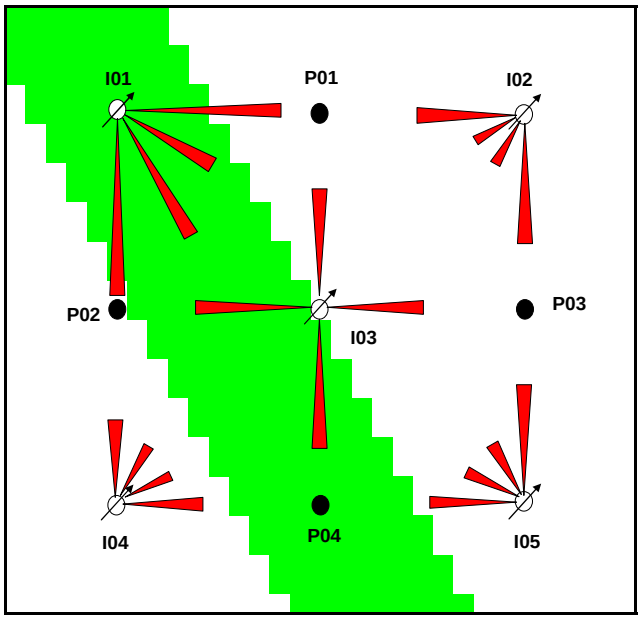


Figure 3.7 . Representation of the interwell connectivity coefficients β for 5x4 field, reservoir with high permeability channel.

d. Presence of a partially sealing barrier.

When the barrier is only partially sealing, the resulting coefficients are presented in Fig. 3.8 and Table 3.4. The presence of transmissibility barrier can also be inferred. Low connectivities are found for well pair on each side and close to the barrier.

From Fig. 3.8, we can see that connectivity between wells depends on the location of the well relative to the barrier. If two wells are on each side of the barrier, the closer they are to the open end of the barrier, the better they are connected.

Table 3.4: Results for the interwell connectivity coefficients β. 5x4 Synthetic field with partially sealing barrier.

	P1	P2	P3	P4	Sum
β_{0j} (psia)	-524.6	-293.5	-418.6	-329.8	-1566.4
I1	0.07	0.30	0.07	0.11	0.56
I2	0.60	0.07	0.41	0.11	1.19
I3	0.07	0.25	0.10	0.22	0.63
I4	0.06	0.29	0.09	0.28	0.72
I5	0.19	0.10	0.33	0.28	0.90
Sum	1.00	1.00	1.00	1.00	

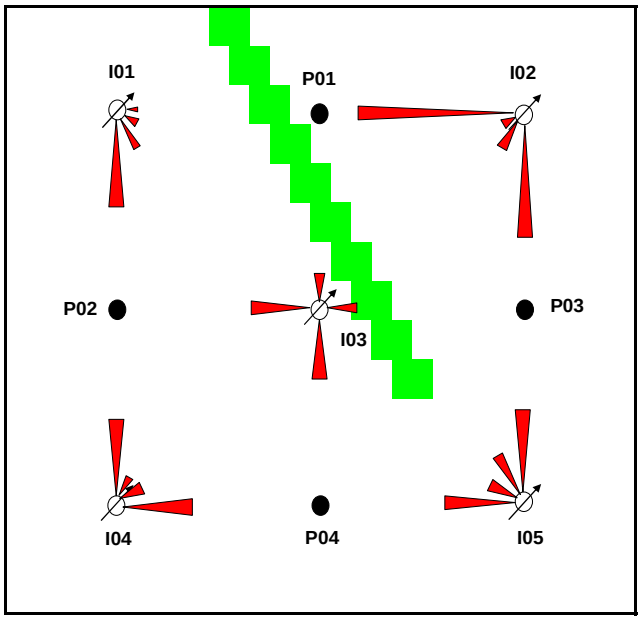


Figure 3.8 . Representation of the interwell connectivity coefficients β. 5x4 Field, reservoir with a partially sealing barrier (diagonal blocks).

e. Presence of a sealing barrier.

When a sealing barrier is introduced into the simulated reservoir and the MLR model is applied, results are presented in Fig**.** 3.9 and Table 3.5. The values of β corresponding to pairs of wells located on each side of the barrier such as β_{11}, β_{13}, β_{22}, β_{24}, are either zero or very close to zero. This indicates no communication between these wells based only on the analysis of the field pressure data.

Table 3.5: Results for the interwell connectivity coefficients β. 5x4 Synthetic field with sealing barrier.

	P1	P2	P3	P4	Sum
β_{0j} (psia)	-381.6	-379.0	-297.3	-443.3	-1501.2
I1	0.00	0.35	0.00	0.19	0.53
I2	0.70	0.02	0.53	0.03	1.27
I3	0.09	0.27	0.08	0.32	0.76
I4	-0.02	0.35	-0.02	0.44	0.76
I5	0.16	0.05	0.35	0.06	0.62
Sum	0.93	1.04	0.93	1.05	

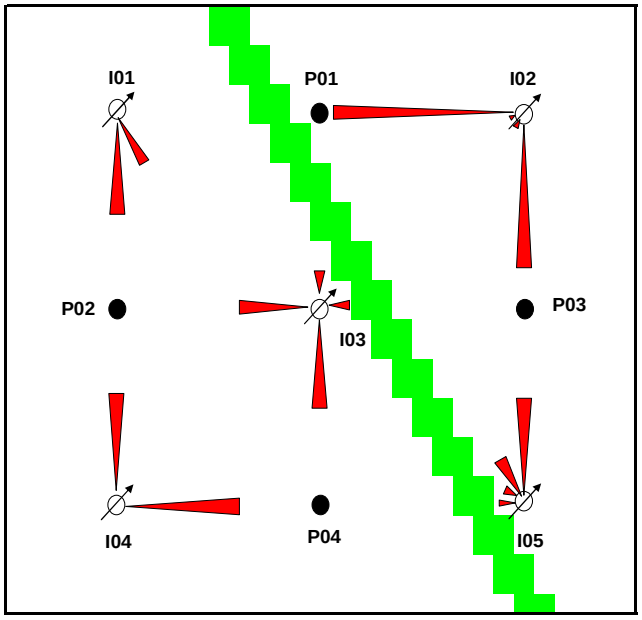


Figure 3.9 . Representation of the interwell connectivity coefficients β. 5x4 field, reservoir with a sealing barrier (diagonal blocks).

The coefficients for injectors close to the boundary and producers on the other side of the barrier such as β_{31}, β_{33}, β_{52}, β_{54} still show some connectivity. This is probably because of the boundary effect that creates error in the data. Some interwell connectivity coefficients, such as β_{41}, β_{43} are negative small numbers. These negative numbers are probably due to error in the calculation and can be translated as zeros for this case. Notice that for this case, the sealing barrier divides the reservoir into two compartments which could be considered as two separate reservoirs. Thus, the total injection rate is not constant in each of these reservoirs since one reservoir contains I02 and I05 and the other contains I01, I03 and I04. Thus, the changing total injection rate in each compartment would interfere in the analysis and caused errors. This is the reason sums of interwell connectivity coefficients for each producer are not equal to unity.

f. Other cases.

The base case of homogenous was run with different constant production rates. Producers were shut-in and put on production at 100, 200, 300, 400 and 500 bbl/d. Fig**.** 3.10 shows the asymmetry coefficients versus the production rates. When the total production rate was less than the injection rate (production rate at each producer is less than 500 bbl/d), asymmetry coefficients were about the same. However, when production rate was equal to 500 bbl/d at the producers, the asymmetry coefficient increased significantly indicating poor results. If the producers were on production at rate higher than 500 bbl/d or if the total production rate was higher than the total injection rate, the producers can not be maintained at the desired rate without other sources of pressure, then the analysis would be erroneous. Thus, the total production should be lower than total injection to avoid errors. More detail will be discussed later in this

chapter. Different cases of formation permeability of the homogeneous model were also run. Fig**.** 3.11 shows the graph of asymmetry coefficients versus formation permeability for the case of homogeneous reservoir. It is noticeable that the higher is the permeability, the lower is the asymmetry coefficient or the better are the results.

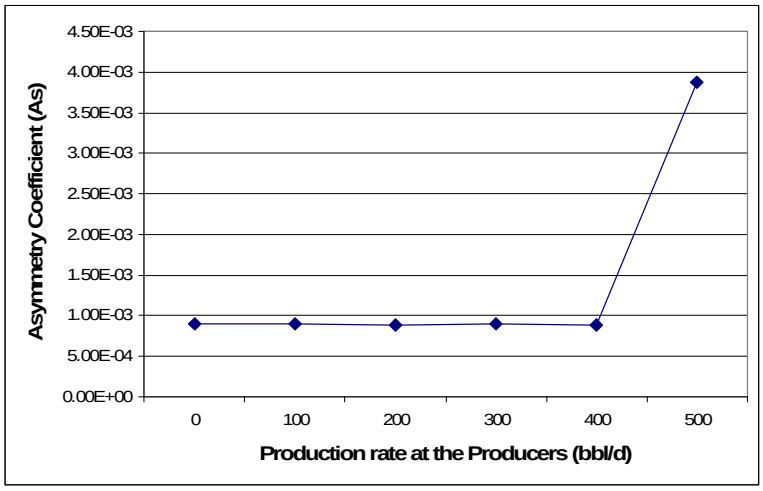


Figure 3.10 . Asymmetry coefficients (A_s) versus cases of different production rates for 5x4 field, homogeneous reservoir.

The time interval between data points for the base case is 30 days. However, different time intervals were also run for the base case. Figs. 3.12 and 3.13 show the relationship of the asymmetry coefficient and the interwell connectivity coefficient with the time interval respectively. From Fig. 3.12**,** it is clear that longer time interval between data points gives better results as the asymmetry coefficients are smaller.

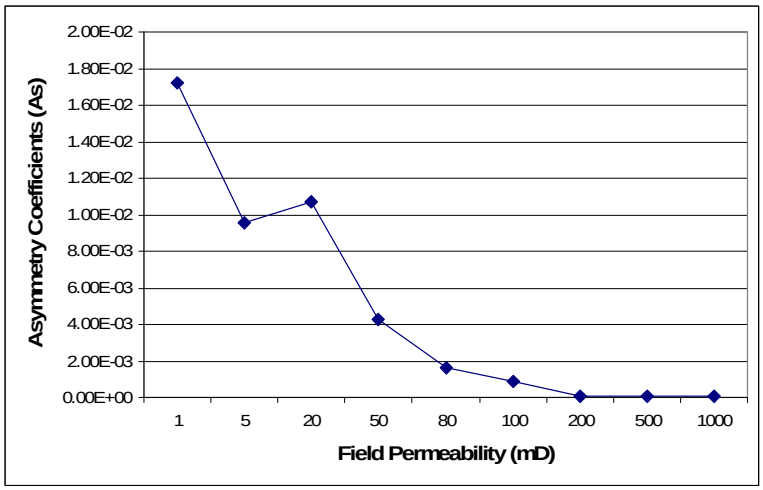


Figure 3.11 . Asymmetry coefficients (A_s) versus cases of different formation permeability for 5x4 field, homogeneous reservoir.

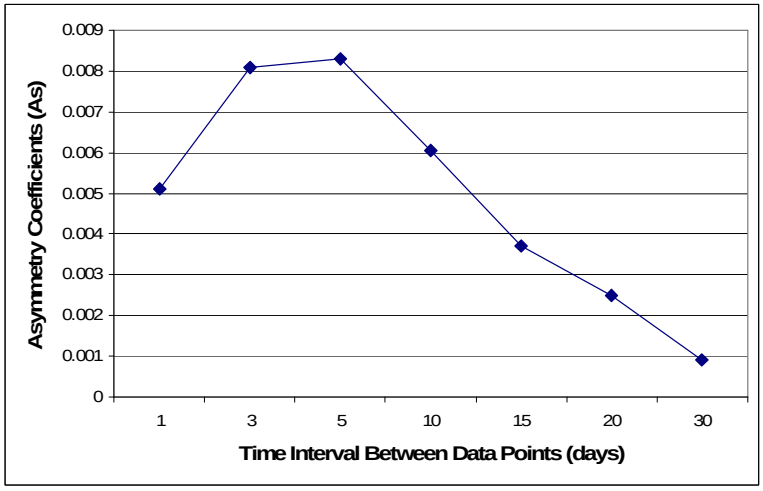


Figure 3.12 . Asymmetry coefficients (A_s) versus cases of different time interval between data points for 5x4 field, homogeneous reservoir.

Fig. 3.13 shows the maximum and the minimum interwell connectivity coefficients versus the time interval between data points for the homogeneous case. As the time interval gets smaller, the difference between the maximum and the minimum coefficients also gets smaller. This indicates the weakening of the signal from injectors to producers as the time interval between data points gets smaller. More details will be discussed later.

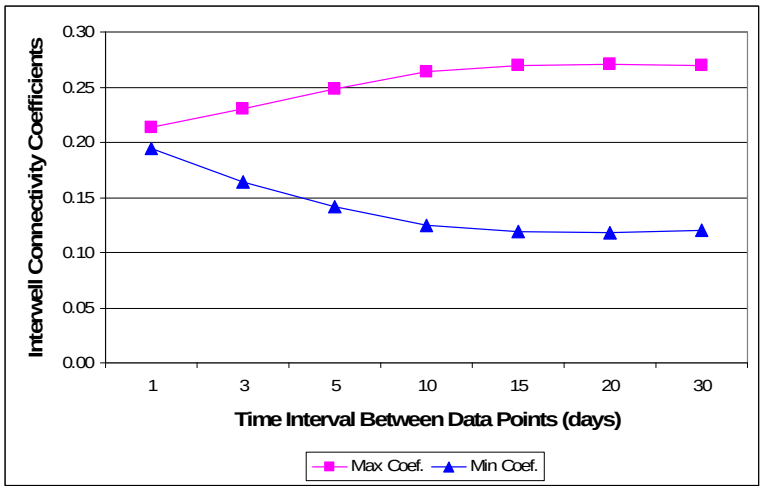


Figure 3.13 . Interwell connectivity coefficients (β) versus cases of different time interval between data points for 5x4 field, homogeneous reservoir.

3.4.2. Application to 25x16 Field.

MLR approach was again applied to a homogenous symmetric field with 25 injectors and 16 producers. Reservoir properties were kept the same as the homogenous 5x4 Field. The grid block dimensions were 100 ft x 100 ft x 60 ft. The distance between closest injector and producer was 848.5 ft. The injection rates at the injectors were randomly generated between 100 and 700 bbl/d. The total injection rates were kept constant at 10,000 bbl/d. The producers were kept at constant rate of 400 bbl/d. The simulation was run for 218 months (6540 days approximately). This represented a history of 218 data points of injector and producer pressure. Fig**.** 3.14 shows the resulted interwell connectivity coefficients for this field. Fig. 3.15 is the graph of distance between wells versus the interwell connectivity coefficients. The interwell connectivity coefficients are in great symmetry. The field has several planes of symmetry. There are 55 symmetric group of interwell connectivity coefficients over a total of 400 interwell connectivity coefficients. The small asymmetry coefficient (A_s) of 0.00416 indicates

excellent results. The results obtained were better than those by Albertoni and Lake (2003) (A_s = 0.00492) using 390 data points of flow rate data.

Overdetermination coefficient (O_d): Altertoni and Lake (2003) used the concept of Overdetermination coefficient to analyze the effect of the number of data points on the quality of the results. The Overdetermination coefficient is defined as:

$$O_d = \frac{M_e}{(I+1)} \tag{3.7}$$

Where M_e is the number of data points and I is the number of injector. In their analysis, where production data were used, the method yielded best results when O_d was larger than six. Fig. 3.16 shows a graph of number of data points versus O_d for both 5x4 Field and 25x16 Field.

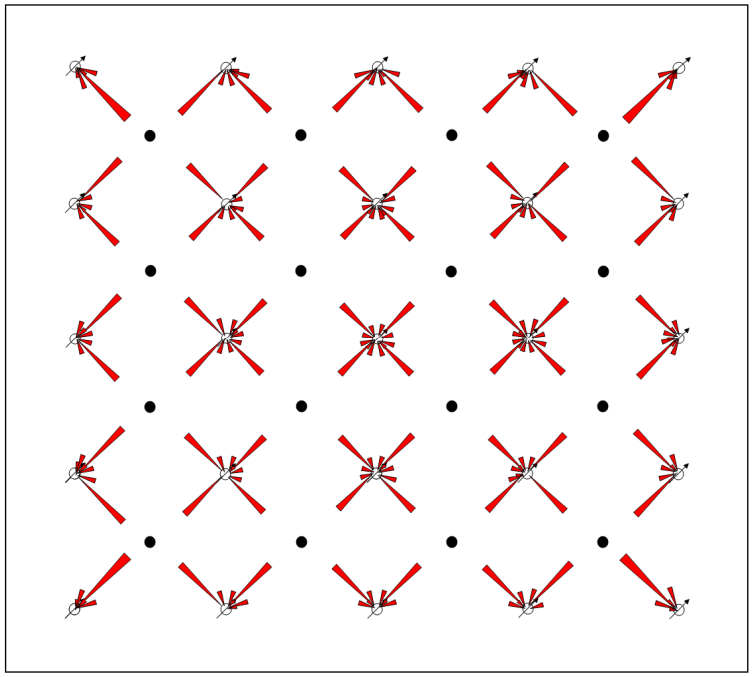


Figure 3.14 . Representation of the interwell connectivity coefficients (β) for 25x16 field, homogeneous reservoir (R^2 =1.00, A_s = 0.000902).

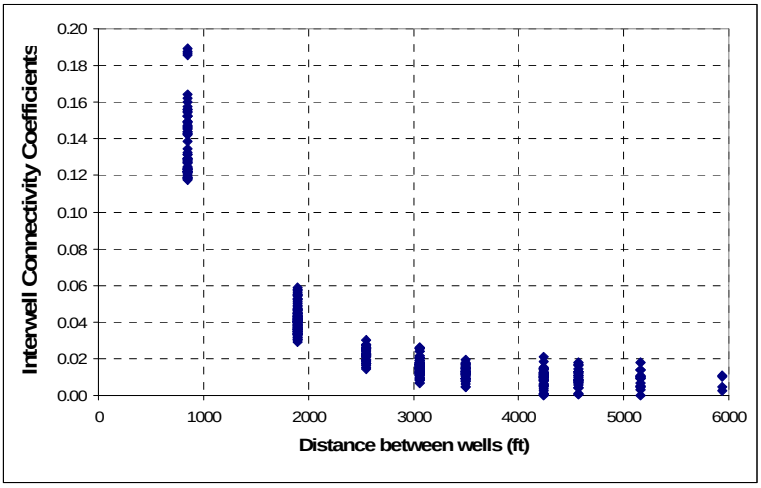


Figure 3.15 . The resulted interwell connectivity coefficients (β) versus the distances of well pairs. 25x16 field, homogeneous reservoir.

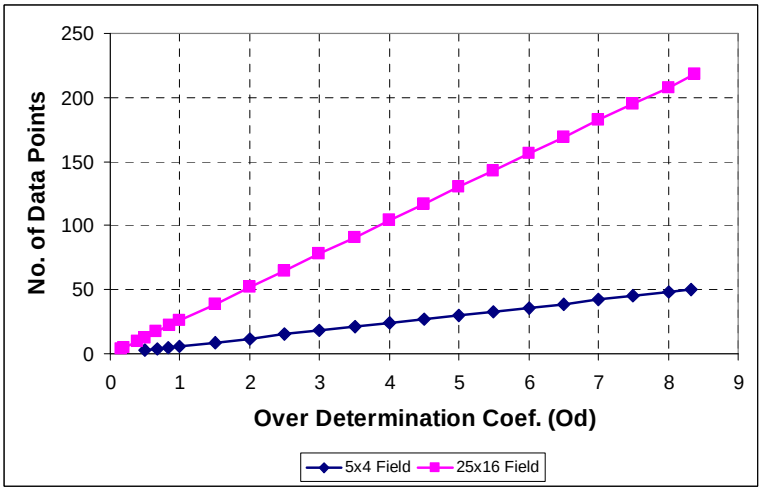


Figure 3.16 . Number of data points versus the overdetermination coefficients (O_d) for both 5x4 and 25x16 field, homogeneous reservoir.

Figs**.** 3.17 and 3.18 are the plots of the asymmetry coefficient (A_s) and the coefficient of determination (R^2) versus O_d respectively for both fields. According to the figures, the quality of the results significantly decreased as A_s increased and R^2 decreased when O_d was less than one. For O_d larger than one, A_s and R^2 remained almost the same. Thus, for this method, we can obtain very good results with O_d larger than one. So, with

a few more than six data points for 5x4 field and 26 data points for 25x16 field, we can obtain excellent result with the method. This means the method requires less time and measurements to obtain acceptable results.

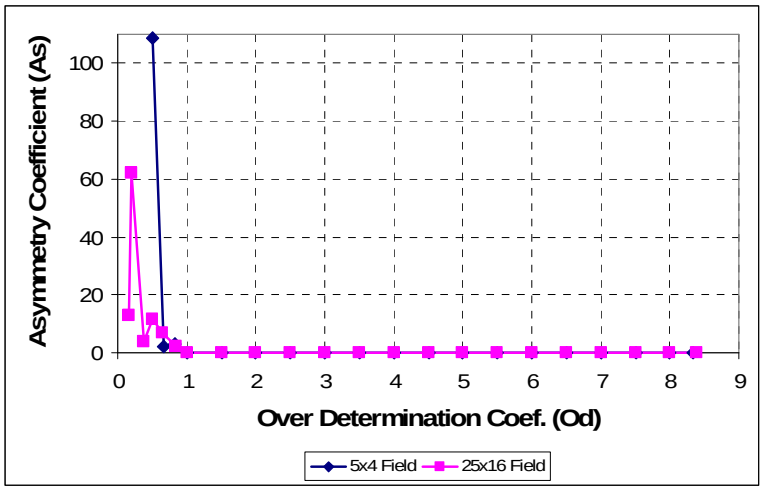


Figure 3.17 . Asymmetry coefficients (A_s) versus the overdetermination coefficients (O_d) for both 5x4 and 25x16 field, homogeneous reservoir.

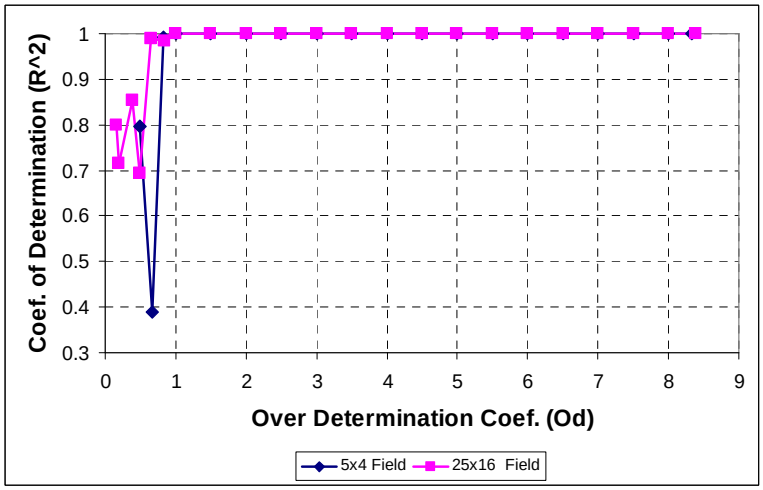


Figure 3.18 . Coefficient of determination (R^2) versus the overdetermination coefficients (O_d) for both 5x4 and 25x16 field, homogeneous reservoir.

3.5. Sensitivity Analysis

This section provides discussion on the assumptions, error analysis, properties of the interwell connectivity coefficients and discussion on selection of data points.

3.5.1. Assumptions.

As discussed above, the method uses some constraints. Thus, in order to obtain good results, the water flood system must satisfy several assumptions. Generally, the assumption for this method is that all the parameters in the field must be constant during the testing period, except the injection flow rates. Albertoni and Lake (2003) listed some assumptions when production data are used in details such as no new wells, constant well productivity, constant gas-oil ratio (GOR), and no new completion. These assumptions are also applied for this method. Other assumptions needed particularly for this analysis are shown below

Constant flow rates at observation wells: Changes in flow rates at the observation wells will produce pressure changes that are not caused by injectors resulting in erroneous results. Thus, all observation wells should be either kept at constant rate or shut-down. The method assumes that every change in the pressure at observation well is exclusively caused by changes in pressure at the active well and the pressure changes at a observation well due to its production rate is constant. As discussed above, flow rates of the production wells should also be equal in order for the interwell connectivity coefficients comparable among producers.

Constant total injection rate: As discussed above, the total injection rate needs to be constant. A variable total injection rate will cause changes of pressure that are not caused by individual injectors at the producers, and thus interfere in the analysis.

Flow rate at the observation wells is maintained by injection: All observation wells should flow at desired rate solely by the support of injectors. No outside supports such as artificial lift, surface pumping are allowed. If the injection is not enough to

support all producers flowing at a certain rate, we can either lower the production rate or increase the total injection rate.

3.5.2. Possible sources of error.

All the assumptions stated above must be applied to avoid any error in the results. Other possible sources of error are listed below:

Measurement Errors: Error analysis shows that the method is relatively sensitive to the quality of the data. Randomly generated errors within a certain range of negative and positive percent error of the first pressure data point were in turn added to the pressure data of Producer 1 and Injector 1. Fig**.** 3.19 show the percentage of resulted error in the interwell connectivity coefficients.

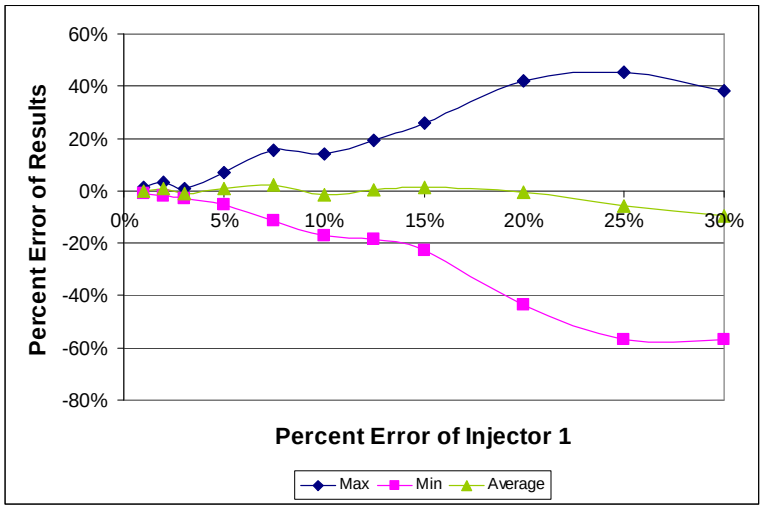


Figure 3.19 . Percent errors of the interwell connectivity coefficients versus random percent errors of Injector 1 data for 5x4 field, homogeneous reservoir.

It is clear that as the errors in the data increase, errors in the result also increase. We can also notice that the error in the results increases drastically as the data errors increase above 5%. Errors applied to producer 1 only affect interwell connectivity

coefficients of producer 1 while errors applied to injector 1 affect the interwell connectivity coefficients of all the wells.

When the same fraction of error was applied to every data point of producer 1, the same error fraction was observed at all the interwell connectivity coefficients of producer 1 and other interwell connectivity coefficients were not affected. When the error was applied to injector 1, only the coefficients of injector 1 were affected. In addition, the error fraction of the coefficients were the same for all coefficients and smaller than the fraction error of the input data.

Boundary effects: If a well is too close to a boundary, it is likely that the boundary effect will cause errors to the pressure data of the well.

Weak signal from injectors: When the permeability of the formation is too low or the time interval between data points is too short, the pressure signal from an injector to a producer will be weak. This causes inaccurate or uninterpretable results as in the case of 5x4 Field when the formation permeability equaled 1 mD or when the time interval was 1 day. The more fully the signals from injectors are received, the better is the quality of the interwell connectivity coefficients. However, it is necessary to notice that weak signals are also caused by poor connectivity between wells.

If the production rates at observation wells are greater than zero, they will have dampening effect on the signals from active wells. Thus, the larger are the production rates, the higher is the dampening effect and thus the less the producers can “feel” the pressure change at the injectors. Thus, too high production rates could lead to poor results. The best way to decide which production rate should be used is to operate the

field with different rates applied to the producers and make sure they are maintained at a constant total injection rates.

3.5.3. Properties of the interwell connectivity coefficients.

As discussed before, the interwell connectivity coefficients only depend on the relative location of the wells and the reservoir properties. From the results of both 5x4 field and 25x16 field cases, the sum of interwell connectivity coefficients for each observation well is equal to one.

$$\sum_{i=1}^{I} \beta_{ij} = 1 \qquad (j = 1, 2, \ldots N) \tag{3.8}$$

3.5.4. Testing scheme and data selection

Selection of a testing scheme includes choosing a time interval in which the flow rates at the active wells will be kept constant, a constant rate for observation wells and a constant total injection rate. As mentioned above, the constant rate at observation wells and the constant total injection rate should be based on actual performance of the waterflood on the field.

For the time interval between data points, an equation derived by Tiab[6] for interference test may apply. Considering an interference test between a constant rate active well and an observation well, the equation calculates the time (t_m) in hours to reach the maximum value of time rate of change of pressure (P_m') in psia at the observation well. In order to obtain a good response at the observation well, the time to run the constant rate at the active well should be well above t_m. The equation is

$$t_m = \frac{948 \times S_t \times r^2}{T_r} \tag{3.9}$$

Where r is the distance (ft) between active and observation wells. T_r is the transmissibility (mD-ft/cp) and S_t is the Storativity (ft/psi) which can be calculated as below:

$$S_t = \phi ch = 0.0274\left(\frac{qB}{P'_m}\right)\frac{1}{r^2} \tag{3.10}$$

$$T_r = \frac{kh}{\mu} \tag{3.11}$$

In reality, we can estimate T_r and S_t using data obtained from core data and well logs, then estimate t_m. Thus, the interval between data points should be well higher than t_m. For example, in the base case of homogenous 5x4 field, t_m was calculated to be 18.2 hours for the injector-producer pair with the longest distance (corner injectors with farther producers). Thus the time interval needs to be higher than 18.2 hours. P'_m could also be calculated to decide on sensitivity of the measuring device. However, since the reservoir boundaries need to be reached before pseudo-steady state flow is reached and the observation well may not be shut-down, observing the flooding performance is the best way to choose a time interval between data points for the analysis.

Since this method only requires O_d larger than 1 to obtain good results, the number of data points need to be larger than number of injectors plus one (six for 5x4 field and 26 for 25x16 field). This would make the test much shorter than when production rates were used (O_d larger than 6 to obtain best results).

Example

A synthetic field with grid dimensions of 31x31x1 was generated. The grid block dimensions were 100 ft x 100 ft x 60 ft. The field has five injectors and four producers. Similar to the Base Case, the reservoir was homogeneous with an isotropic permeability

of 100mD. Injection rate data was generated randomly ranging from 100 to 900 bbl/d with total injection rate kept at 2000 bbl/d. The step-by-step calculations are as followings:

Step 1 - Choosing a production rate for the test: Production rates at all producers need to be equal and kept constant throughout the test. Normally, the sum of the production rates should be lower than the sum of the injection rates to maintain a constant production rate at each producer. Trial-and-error method can be used to choose a suitable production rate by keeping the injection rates constant and adjusting the production. If a production rate can be maintained at every well with a constant total injection rate, the production rate can be used throughout the test. In our case, with total injection rate of 2000 bbl/d, any production rate below 400 bbl/d (total production rate of 1600 bbl/d) can be used. The production rate of 300 bbl/d was chosen for the example.

Step 2 – Choosing the time interval between data points. As shown before, the longer is the time interval between data points, the better are the results. Equation 7 can be used to estimate the time (t_m) to reach the maximum value of time rate of a change of pressure at the observation well as for an interference test (one active well and one observation well). In this case, t_m was estimated to be 18.2 hours for the most distanced injector-producer pair. However, we have multiple injectors and producers; thus rates of any well can be affected by those of other wells. Therefore, the time interval needs to be long enough so that the injection can reach the producers. This can be estimated as the time from the start of injection to the time when all producers start to produce at expected rates. In this example, we chose the interval to be 10 days (Fig. 3.20).

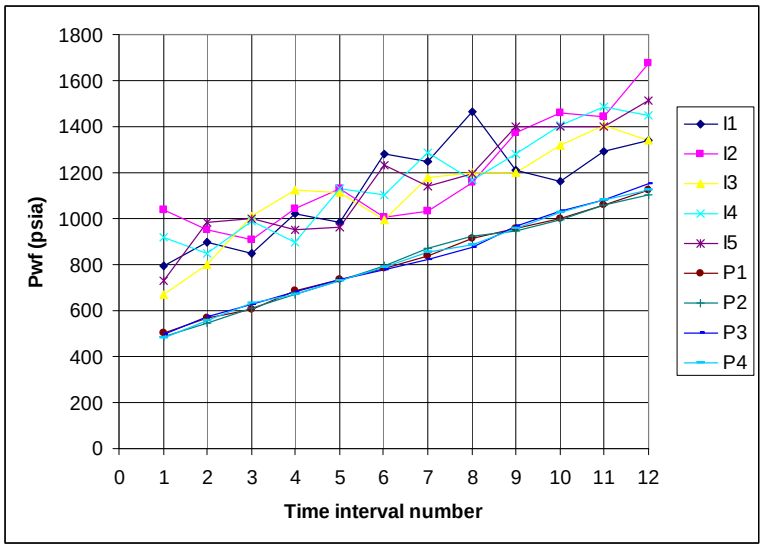


Figure 3.20 . Bottom Hole Pressure Data for the Example. 5x4 field, homogeneous reservoir. 10-day intervals.

Step 3 – Data collection. The number of data points needed should be more or equal to six (O_d is more or equal to one). However, the higher the number of data points are used, the better are the results. Thus, we run the test for 12 time intervals representing 12 data points with different injection rate sets. The data obtained are demonstrated in Fig. 3.20.

Step 4 – Interwell connectivity coefficients calculation. Injector-injector and injector-producer covariances were then calculated and plugged to Eqs. 3.2 and 3.3 to solve for the interwell connectivity coefficients.

Step 5 –The results for this example are shown in Table 3.6 . Notice that the results are similar to the results for the Base Case as shown in Table 3.1.

However, the Asymmetry Coefficient (A_s) is higher than that of the Base Case. This is due to shorter time interval and less data points. From the results, we can infer the relative connectivity among well pairs as well as formation properties.

Table 3.6 . Results for the interwell connectivity coefficients β for the Example. 5x4 field, homogeneous reservoir (A_s = 0.0109).

	P1	P2	P3	P4	Sum
I1	0.24	0.27	0.12	0.15	0.78
I2	0.25	0.14	0.25	0.14	0.78
I3	0.21	0.21	0.23	0.24	0.89
I4	0.14	0.25	0.14	0.24	0.78
I5	0.15	0.14	0.25	0.24	0.78
Sum	0.99	1.00	1.00	1.00	

3.6. Conclusions

Following are the conclusions for this chapter:

- Results from the proposed procedure are better than the results obtained from application of the method to production data presented in the literature in terms of asymmetry coefficient (A_s) and R^2.

- The fact that the new technique provides better results with an overdetermination coefficient Od larger than unity and no diffusivity filters are necessary indicates its advantage in saving time and computation.

- Pressure data used in the analysis can be obtained while all the producers in the field are still producing. Thus, different from regular interference test or pulse test, the producers do not need to be shut down.

CHAPTER 4 – ANALYTICAL MODEL

This chapter is an extension of the novel technique presented in the last chapter to determine interwell connectivity in a reservoir based on fluctuations of bottom hole pressure of both injectors and producers in a waterflood system. The technique uses a constrained multivariate linear regression analysis to obtain information about permeability trends, channel and barriers. Some of the advantages of this new technique are simplified one-step calculation of interwell connectivity coefficients (interwell connectivity coefficients), small number of data points and flexible testing plan. However, the previous chapter did not provide either in-depth understanding or any relationship between the interwell connectivity coefficients and other reservoir parameters.

This chapter presents a mathematical model for bottom hole pressure response of injectors and producers in a waterflood system. The model is based on available solution for fully penetrating vertical wells in a closed rectangular reservoir. It is then used to calculate relative interwell permeability, average reservoir pressure change and total reservoir pore volume using data from interwell connectivity test described in previous study. Reservoir compartmentalization can be inferred from the results. Cases of producers as signal wells, injectors as response wells and shut-in wells as response wells are also presented. Summary of results for these cases are provided. Reservoir behaviors and effect of skin factors are also discussed in this study.

Different synthetic reservoir models were analyzed including: homogeneous, anisotropic reservoirs, reservoirs with high permeability channel, partially sealing barrier and sealing barrier.

4.1. Introduction

Last chapter has introduced a new technique to infer interwell connectivity from bottom-hole pressure fluctuations in a waterflood system. The technique was proven to yield good results based on numerical simulation models of various cases of heterogeneity.

In this chapter, an analytical model for multi-well system with water injection was derived for the technique. The model is based on available solution for a fully penetrating vertical well in a closed rectangular multi-well system and uses the principle of superposition in space. Based on analytical analysis, a new technique to analyze data of interwell connectivity test was developed. This technique utilizes the least squares regression method to calculate the average pressure change. Thus, reservoir pore volume, average reservoir pressure and total average porosity can be estimated from available input data. The results were verified using a commercial black oil numerical simulator.

In this chapter, the interwell connectivity coefficients mentioned in the previous chapter will be referred to as interwell connectivity coefficients. The practical value of interwell connectivity coefficients was investigated. In order to derive the relationship between interwell connectivity coefficients with other reservoir parameters, a pseudo-steady state solution of the previously mentioned model was used. The wells were fully penetrating vertical wells flowing at constant rates. The investigation proves that the interwell coefficients between signal (active) and response (observation) wells are not only associated with the properties between the two wells but also the properties at the signal wells. In order to calculate relative interwell permeabilities, we assumed the properties at the signal wells are constant. Thus, by varying permeability between well

pairs to match the interwell connectivity coefficient calculated from analytical model and simulation results, the relative interwell permeabilities can be found. Different cases of heterogeneous synthetic fields were considered including anisotropy reservoir, reservoir with high permeability channel, partially sealing barrier and sealing barrier. In the sealing barrier case, the results indicated two groups of average reservoir pressure change corresponding to two reservoir compartments. Thus, reservoir compartmentalization can be detected.

The technique presented in the previous chapter requires several constraints including constant production rates and constant total injection rates. These constraints pose difficulties in applicability of the technique to a real field situation where production rates are hardly kept constant. For this chapter, the systems with constant injection rates and changing production rates were investigated. The obtained interwell connectivity coefficients were almost exactly the same as the results from the case of constant production rates and changing injection rates. The technique is also applicable for fields with only producers; where some producers are used as signal wells and others as response wells provided that all assumptions are valid. This suggests the technique is applicable to depletion field as well. Also, response wells can act as shut-in wells.

This new study provides a tool to analyze reservoir heterogeneity and better understanding of multiwell system with the presence of both injectors and producers.

4.2. Background

In 2002, Albertoni and Lake developed a technique that calculates the fraction of flow caused by each of the injectors in a producer. This method uses a constrained Multivariate Linear Regression (MLR) model.

Recently, Dinh and Tiab (2007, 2008) used similar approach as Albertoni and Lake (2003); however, bottom hole pressure data were used instead of flow rate data. Some constraints were applied to the flow rates such as constant production rate at every producer and constant total injection rate. Some advantages of using bottom hole pressure data are: (a) Diffusivity filters are not needed, (b) Only minimal number of data points are required and (c) The program for collecting data is flexible.

This chapter is to extend the work presented in Chapter 3 (see also Dinh and Tiab, 2008) on interwell connectivity calculation from bottom hole pressure in a multiwell system. The purpose of this chapter is to incorporate a pseudo-steady-state analytical solution for closed system to the problem. Thus, other reservoir parameters such as relative interwell permeability, reservoir pore volume can be quantified. This chapter also provides in-depth understanding of the method and its applications.

4.3. Analytical Approach

Numerous studies concerning multi-well systems have been carried out. Bourgeois and Couillens (1994) provided a technique to predict production from a well test analytical solution of a multi-well system. Umnuayponwiwat et al. (2000) investigated the pressure behavior of individual well in a multi-well closed system. Both vertical well and horizontal well pressure behaviors were considered. Valko et al. (2000) developed a solution for productivity index for multi-well system flowing at constant bottom hole pressure and under pseudo-steady state condition. Marhaendrajana et al. (1999 and 2001) introduced the solution for well flowing at constant rate in a multi-well system. The solution was used to analyze pressure build up test and to calculate average reservoir pressure using decline curve analysis. Lin et al. (2007) proposed an analytical

solution for the pressure behaviors in multi-well system with both injectors and producers based on the work by Marhaendrajana et al. (2001).

4.3.1. Analytical Model Application

Considering a multi-well system with producers or injectors and initial pressure p_i, the solution for pressure distribution due to a fully penetrated vertical well in a close rectangular reservoir is as follows (Marhaendrajana et al., 1999):

$$p_D(x_D, y_D, t_{DA}) = \sum_{i=1}^{n_{well}} q_{D,i} a_i \left(x_D, y_D, x_{wD,i}, y_{wD,i}, x_{eD}, y_{eD}, \left[t_{DA} - t_{sDA}\right]\right) \tag{4.1}$$

Where the dimensionless variables are defined in field units as follows:

$$x_D = \frac{x}{\sqrt{A}} \tag{4.2}$$

$$y_D = \frac{y}{\sqrt{A}} \tag{4.3}$$

$$p_D = \frac{kh}{141.2 q_{ref} B\mu}\left(p_{ini} - p(x, y, t)\right) \tag{4.4}$$

$$t_{DA} = 0.0002637 \frac{kt}{\phi c_t \mu A} \tag{4.5}$$

a_i is the influence function equivalent to the dimensionless pressure for the case of a single well in bounded reservoir produced at a constant rate. Assuming $t_{sDA}= 0$, the influence function is given as:

$$
\begin{aligned}
a_i\left(x_D, y_D, x_{wD,i}, y_{wD,i}, x_{eD}, y_{eD}, t_{DA}\right) = \frac{1}{2} \sum_{m=-\infty}^{\infty} \sum_{n=-\infty}^{\infty} & E_1\left[\frac{\left(x_D + x_{wD,i} + 2nx_{eD}\right)^2 + \left(y_D + y_{wD,i} + 2my_{eD}\right)^2}{4t_{DA}}\right] \\
& + E_1\left[\frac{\left(x_D - x_{wD,i} + 2nx_{eD}\right)^2 + \left(y_D + y_{wD,i} + 2my_{eD}\right)^2}{4t_{DA}}\right] \\
& + E_1\left[\frac{\left(x_D + x_{wD,i} + 2nx_{eD}\right)^2 + \left(y_D - y_{wD,i} + 2my_{eD}\right)^2}{4t_{DA}}\right] \\
& + E_1\left[\frac{\left(x_D - x_{wD,i} + 2nx_{eD}\right)^2 + \left(y_D - y_{wD,i} + 2my_{eD}\right)^2}{4t_{DA}}\right]
\end{aligned} \tag{4.6}
$$

Eq.4.1 is valid for all flow regimes and can be rewritten as below:

$$
p_{ini} - p(x,y) = \frac{141.2B\mu}{kh} \sum_{i=1}^{n_{well}} a_n\left[x_D, y_D, x_{wDn}, y_{wDn}, x_{eD}, y_{eD}, t_{AD}\right] q_n \tag{4.7}
$$

Eq. 4.7 is the pressure response at point (x_D, y_D) due to a well n at (x_{wDn}, y_{wDn}) in a homogeneous closed rectangular reservoir. The influence function (a_n) can be different for different wellbore conditions as well as flow regimes (horizontal well, partial penetrating vertical well, fractured vertical well…). This chapter only considered the case of fully penetrating vertical well in a closed rectangular reservoir, which is under pseudo-steady state condition. Summary of the derivation of Eq. 4.6 is presented in Appendix A.

Eq. 4.7 is applicable to a field where all the wells are either producing or injecting. Lin and Yang (2007) have extended the model to a field with both injectors and producers based on the model suggested by Eq. 4.7 as shown below:

$$
\begin{aligned}
p_{ini} - p(x,y) = \frac{141.2B\mu}{kh} \Bigg\{ & \sum_{j=1}^{n_{pr}} a_j\left[x_D, y_D, x_{wDj}, y_{wDj}\, x_{eD}, y_{eD}, t_{AD}\right] q_j \\
& - \sum_{i=1}^{n_{inj}} a_i\left[x_D, y_D, x_{wDi}, y_{wDi}, x_{eD}, y_{eD}, t_{AD}\right] q_i \Bigg\}
\end{aligned} \tag{4.8}
$$

Where i and j denote injectors and producers respectively. Eq. 4.8 is for a homogeneous reservoir with initial reservoir pressure (p_{ini}) equal everywhere. Applying Eq. 8 to each time interval of an interwell connectivity test, since the total injection and production are kept constant, the average reservoir pressure change is assumed to be constant for every time-interval. The first term in the bracket on the right hand side of Eq. 4.8 is constant due to constant rates at every producer throughout the test. Applying to each time interval in the interwell connectivity test, assuming the initial pressure at the beginning of each interval increases at the same rate as the average reservoir pressure (Δp_{ave}), Eq. 4.8 can be rewritten as:

$$p_{ave} - p(x,y) = \frac{141.2B\mu}{kh}\left\{-\sum_{i=1}^{n_{inj}} a_i\left[x_D, y_D, x_{wDi}, y_{wDi}, x_{eD}, y_{eD}, t_{AD}\right]q_i\right\} + \Delta p_{pr} \tag{4.9}$$

$$\text{Where} \quad \Delta p_{pr} = \frac{141.2B\mu}{kh}\sum_{j=1}^{n_{pr}} a_j\left[x_D, y_D, x_{wDj}, y_{wDj}\, x_{eD}, y_{eD}, t_{AD}\right]q_j + \Delta p_{ave} \tag{4.10}$$

$$p_{ave} = p_{ini} - \Delta p_{ave}$$

Both Δp_{pr} and Δp_{ave} are assumed to be constant. Applying Eq. 4.9 for a point at the circumference of the well bore of producer j' and taking into account the skin factor, we obtain:

$$p_{ave} - p_{wf,j'}\left(x_{wDj'}, y_{wDj'}\right) = \frac{141.2B\mu}{kh}\left\{-\sum_{i=1}^{n_{inj}} a_{ij'}\left[x_{wDj'}, y_{wDj'} + r_{wDj'}, x_{wDi}, y_{wDi}, y_{eD}\right]q_i + s_{j'}q_{j'}\right\} + \Delta p_{pr} \tag{4.11}$$

where the third term in the bracket accounts for the skin at well j'. For injector i', we have

$$p_{ave} - p_{wf,i'}(x_{wDi'}, y_{wDi'}) = \frac{141.2B\mu}{kh}\left\{-\sum_{i=1}^{n_{inj}} a_{ii'}\left[x_{wDi'}, y_{wDi'} + r_{wDj'}, x_{wDi}, y_{wDi}, y_{eD}\right]q_i + s_{i'}q_{i'}\right\} + \Delta p_{pr} \tag{4.12}$$

To simplify the problem, we assume all skin factors are equal to zeros. Eq. 4.11 & 4.12 can be rewritten for each time interval as

$$p_{ave} - p_{wf,j'} = -\frac{141.2B\mu}{kh}\left(\sum_{i=1}^{I} q_{ij'}a_{ij'}\right) + \Delta p_{pr} \quad \text{for j' = 1…J} \tag{4.13}$$

$$p_{ave} - p_{wf,i'} = -\frac{141.2B\mu}{kh}\left(\sum_{i=1}^{I} q_{ii'}a_{ii'}\right) + \Delta p_{pr} \quad \text{for i' = 1…I} \tag{4.14}$$

Where $q_{ij'} = q_{ii'} = q_i$ are the flow rates at injectors (signal wells).

4.3.2. Interpretation of interwell connectivity coefficients using bottom hole pressure data

Now, let us consider the interwell connectivity test. In order to obtain better results, the reservoir should reach pseudo-steady state before the test begins. Different testing schemes were also considered including (a) injectors as response wells, (b) producers as both response and signal wells and (c) shut-in wells as response wells. The response wells need to be directly effected by the signal wells. The case that total injection equals to total production is not considered for the test due to the reason stated in Chapter 3.

The interwell connectivity coefficients calculated using the bottom hole pressure data should satisfy the equation:

$$\hat{p}_j(\Delta t) = \beta_{0j} + \sum_{i=1}^{I} \beta_{ij}\, p_i(\Delta t) \quad \text{for j = 1…J} \tag{4.15}$$

Where $\hat{p}_j(\Delta t)$ is the bottom hole flowing pressure at producer j, β_{0j} is a constant and β_{ij} is the interwell connectivity coefficient accounting for the effect of bottom hole pressure at injector i (p_i) on producer j. Δt is the length of the time interval as the injection rates were changed after each time interval. Including the average reservoir pressure, p_{ave}, to Eq.4.15, we have

$$p_{ave} - p_{wf,j'}(\Delta t) = \beta_{0j'} + p_{ave} - \sum_{i=1}^{I} \beta_{ij'} p_{wf,i} \tag{4.16}$$

One of the properties of Eq.4.15 is

$$\sum_{i=1}^{I} \beta_{ij'} = 1 \tag{4.17}$$

Thus Eq.4.16 becomes

$$p_{ave} - p_{wf,j'} = \beta_{0j'} + \sum_{i=1}^{I} \beta_{ij'} \left(p_{ave} - p_{wf,i} \right) \tag{4.18}$$

Marhaendrajana et al. (1999) introduced the concept of interference effect as a regional pressure decline to analyze pressure build-up data at a production well. Lin and Yang (2007) extended the work to a field with both injectors and producers. Their solutions basically state that the pressure response of a well (injector or producer) in a multiwell system is affected by the flow rate at the well plus an interference effect due to other wells in the field flowing under pseudo-steady state. The solution for a producer (j') can be written as:

$$p_{ini} - p_{wf,j'}\left(x_{wDj'}, y_{wDj'}, t\right) = \frac{141.2B\mu}{kh}\left[q_{j'}\left(a_{j'j'} - 2\pi t_{DA}\right) + 2\pi \Delta q_{tot} t_{DA}\right] \tag{4.19}$$

For injector i', we have

$$p_{ini} - p_{wf,i'}(x_{wDi'}, y_{wDi'}, t) = \frac{141.2B\mu}{kh}\left[q_{i'}(a_{i'i'} + 2\pi t_{DA}) + 2\pi\Delta q_{tot} t_{DA}\right] \tag{4.20}$$

Where $\Delta q_{tot} = \sum_{j=1}^{n_{pr}} q_j - \sum_{i=1}^{n_{inj}} q_i$. Eqs. 4.19 and 4.20 state that the pressure change at a producer or injector is a combination of two terms as shown on the right hand sides of the two equations. The first term is proportional to the flow rate of the well itself and the second term account for the regional effect of the other wells. In our case, the second term in the brackets is constant for each time interval. Using material balance, we have

$$\frac{\Delta p_{ave}}{\Delta t} = \frac{0.23394B}{c_t V_p}\Delta q_{tot} \tag{4.21}$$

Where the constant 0.23394 is the conversion factor for field units and V_p is the reservoir pore volume in reservoir barrels. Applying the definition of t_{DA} (Eq.4.5) and Eq.4.21 to the second term in the right hand side bracket, Eq.4.20 becomes

$$p_{ini} - p_{wf,i'}(x_{wDi'}, y_{wDi'}, t) = \frac{141.2B\mu}{kh}\left[q_{i'}(a_{i'i'} + 2\pi t_{DA})\right] + \Delta p_{ave}(t) \tag{4.22}$$

Moving Δp_{ave} to the left-hand side, Eq. 4.22 can be rewritten for each time interval of the interwell connectivity test as

$$p_{ave}(t) - p_{wf,i'}(x_{wDi'}, y_{wDi'}, t) = \frac{141.2B\mu}{kh}\left[q_{i'}(a_{i'i'} + 2\pi t_{DA})\right] \tag{4.23}$$

or

$$q_{i'} = \frac{p_{ave}(t) - p_{wf,i'}(x_{wDi'}, y_{wDi'}, t)}{\frac{141.2B\mu}{kh}\left[(a_{i'i'} + 2\pi t_{DA})\right]} \tag{4.24}$$

Substitute $q_{i'}$ defined in Eq.4.24 into Eq.4.13, we have

$$p_{ave} - p_{wf,j'} = \sum_{i=1}^{I} \left[p_{ave} - p_{wf,i}(x_{wDi}, y_{wDi}) \right] \frac{a_{ij'}}{(a_{ii} + 2\pi t_{DA})} + \Delta p_{pr} \tag{4.25}$$

Eq.4.25 can only be applied to pseudo-steady state flow and equivalent to Eq.4.18 if the following condition satisfied:

$$\sum_{i=1}^{I} \beta_{ij'} = \sum_{i=1}^{I} \frac{a_{ij'}}{(a_{ii} + 2\pi t_{DA})} = 1 \tag{4.26}$$

Notice that Eq. 4.25 does not depend on production history and holds true for any time interval assuming pseudo-steady state flow. The sum $\sum_{i=1}^{I} \frac{a_{ij'}}{(a_{ii} + 2\pi t_{DA})}$ can be set to 1 by adjusting the time duration (Δt). The equivalent time duration (Δt_{eq}) obtained indicates the time of pseudo-steady state required so that Eq. 4.26 is satisfied at the response well. Thus, Eq.4.25 can be written as

$$p_{ave} - p_{wf,j'} = \sum_{i=1}^{I} \left[p_{ave} - p_{wf,i}(x_{wDi}, y_{wDi}) \right] \frac{a_{ij'}}{(a_{ii} + 2\pi t_{DA})} + \Delta p_{pr}(\Delta t_{eq}) \tag{4.27}$$

Where $\sum_{i=1}^{I} \frac{a_{ij'}}{(a_{ii} + 2\pi t_{DA})} = 1$ and $\Delta p_{pr}(\Delta t_{eq})$ is the pressure change defined by Eq. 4.10 corresponding to Δt_{eq}. $\Delta p_{pr}(\Delta t_{eq})$ depends on the pseudo-steady state initial pressure, the total field flow rate and the influence of producers and not on the actual time interval. Thus, with the same total field flow rate (Δq_{tot}), assuming pseudo-steady state has been reached, $\Delta p_{pr}(\Delta t_{eq})$ is constant with any test time interval (Δt). Eq. 4.27 is true for any p_{ave}. Since Equations 4.27 and 4.18 are now equivalent, we should have:

$$\beta_{ij'} = \frac{a_{ij'}}{(a_{ii} + 2\pi t_{DA})} \quad \text{with i = 1…I and j'=1…J} \tag{4.28}$$

$$\beta_{0j'} = \Delta p_{pr}(\Delta t_{eq}) \tag{4.29}$$

Eq.4.28 indicates that the interwell connectivity coefficient β_{ij} reflects the effect of both the flow rates at the signal wells and the influence of other wells on the signal wells. Since $\sum_{i=1}^{I} \frac{a_{ij'}}{(a_{ii} + 2\pi t_{DA})} = 1$, p_{ave} on both sides are canceled out and Eq. 4.27 can also be written as

$$p_{wf,j'} = \sum_{i=1}^{I} p_{wf,i}(x_{wDi}, y_{wDi}) \frac{a_{ij'}}{(a_{ii} + 2\pi t_{DA})} + \Delta p_{pr}(\Delta t_{eq}) \tag{4.30}$$

Even though $\sum_{i=1}^{I} \beta_{ij'}$ and $\sum_{i=1}^{I} \frac{a_{ij'}}{(a_{ii} + 2\pi t_{DA})}$ are both equal to 1, the meanings are different for each case. $\sum_{i=1}^{I} \beta_{ij'} = 1$ indicates the pressure fluctuation at the response wells are only due to signal wells while $\sum_{i=1}^{I} \frac{a_{ij'}}{(a_{ii} + 2\pi t_{DA})} = 1$ indicates a state of pressure distribution due to pseudo-steady state flow after the period Δt_{eq}.

Since the interwell connectivity coefficients were calculated without the knowledge of pressure history during each time interval, it is reasonable to apply the pseudo-steady state equation (Eq.4.25) with the flow duration of Δt_{eq} to each pressure data. Thus, the original test system is now set to an equivalent pseudo-steady state system with the time interval of Δt_{eq}. The model works with the assumption that the bottom hole pressures at the response wells reach pseudo-steady state before the rates at the signal wells are changed.

4.4. Model Verification

In order to verify the analytical model, two homogeneous synthetic fields were

used. One field has 5 injectors and 4 producers (5x4 Synthetic Field) and the other field has 25 injectors and 16 producers (25x16 Synthetic Field). The reservoir simulator used was ECLIPSE 100 Black Oil Simulator. Figs. 4.1 and 4.2 show the grid systems for the two models and the well locations with I and J indicating injector and producer respectively. The grid configuration for 5x4 Synthetic Field was 73x73x5 and for 25x16 Synthetic field was 59x59x5. The dimensions for the 5x4 Synthetic Field were 3100ft x 3100 ft x 60 ft and for 25x16 Synthetic Field were 5900 ft x 5900 ft x 60 ft. The initial static reservoir pressure was 650 psia.

Table 4.1: Input data for homogeneous simulation models

Horizontal Permeability	k_h = 100 mD	Water compressibility	c_w = 1E-6 psi^{-1}
Vertical Permeability	k_v = 10 mD	Oil compressibility	c_o = 5E-6 psi^{-1}
Porosity	φ = 0.3	Rock compressibility	c_r = 1E-6 psi^{-1}
Viscosity	μ = 2 cp	Total compressibility	c_t = 2.8E-6 psi^{-1}
Initial reservoir pressure	p_i = 650 psi	Formation volume factor	B = 1.03 bbl/STB
Water saturation	S_w = 0.8	Wellbore radius	r_w = 0.355 ft

Other reservoir properties for the homogeneous case are shown in Table 4.1. One phase flow of water was assumed. 5x4 Synthetic Field was run for 50 months representing 50 data points (time interval, Δt = 30 days), while 25x16 Synthetic Field was run for 130 months. However, only data after the second month were used to better satisfy the condition of over all pseudo-steady state.

4.4.1. 5x4 Synthetic Field

Both Eqs. 4.27 and 4.30 were used to verify the analytical model. The bottom hole pressure calculated from Eq. 4.15 and Eq. 4.30 were compared. The coefficients calculated from the influence function were also compared with those obtained from simulation data. Investigation on the effect of different t_{eq} on the interwell connectivity coefficients was also carried out.

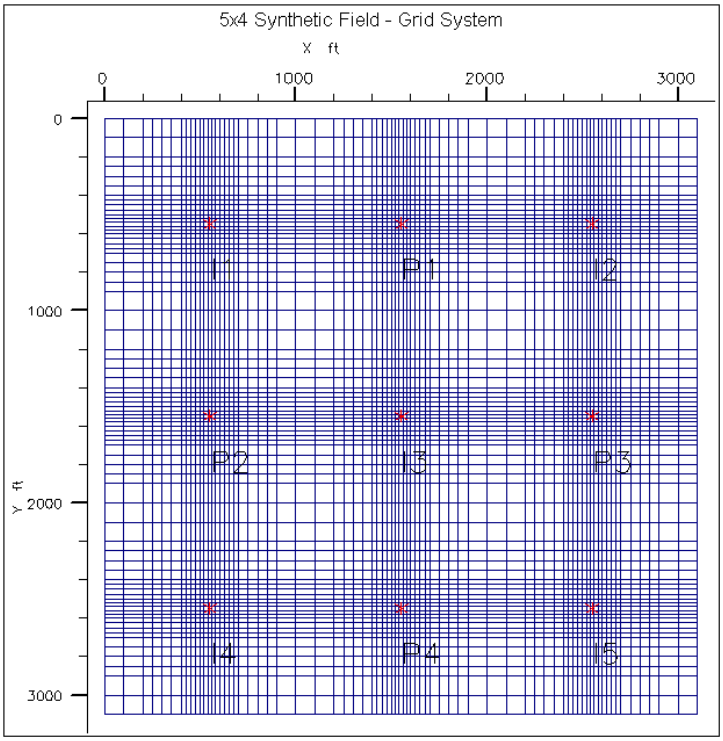


Figure 4.1. Grid system for 5x4 Synthetic Field (73x73x5).

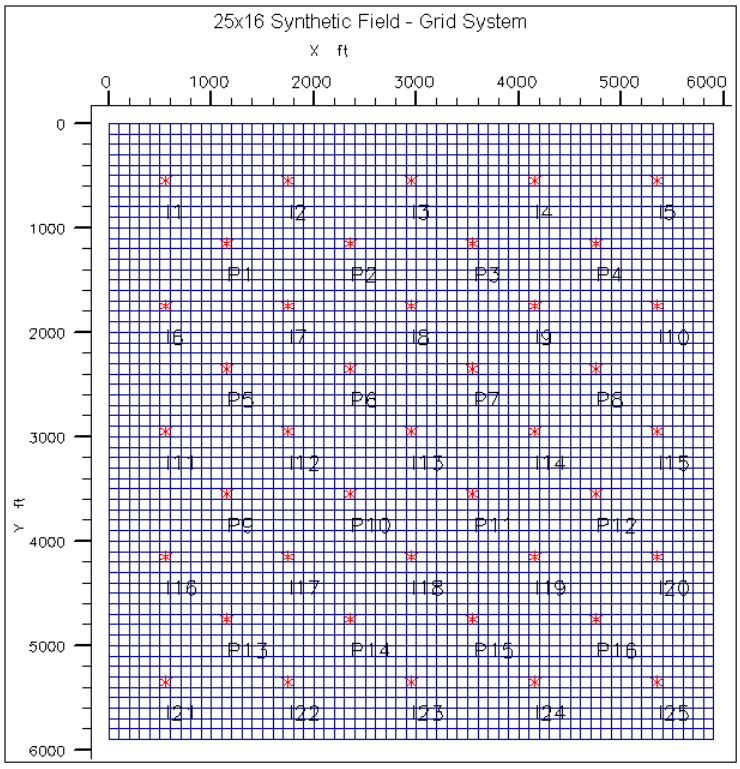


Figure 4.2. Grid system for 25x16 Synthetic Field (59x59x5).

Table 4.2: Interwell Connectivity Coefficient results from MLR for the 5x4 Synthetic field

	P1	P2	P3	P4	Sum
β_{0i} (psia)	-740.6	-740.3	-741.3	-741.0	-2963
I1	0.25	0.26	0.13	0.14	0.78
I2	0.25	0.14	0.26	0.14	0.78
I3	0.22	0.21	0.22	0.22	0.87
I4	0.14	0.25	0.14	0.25	0.78
I5	0.14	0.14	0.25	0.25	0.78
Sum	1.00	1.00	1.00	1.00	

Table 4.3: Interwell Connectivity Coefficient results from analytical solution with ⊿teq = 12.63 days for the 5x4 Synthetic field

	P1	P2	P3	P4	Sum
I1	0.24	0.24	0.15	0.15	0.77
I2	0.24	0.15	0.24	0.15	0.77
I3	0.23	0.23	0.23	0.23	0.91
I4	0.15	0.24	0.15	0.24	0.77
I5	0.15	0.15	0.24	0.24	0.77
Sum	1.00	1.00	1.00	1.00	

Table 4.2 and 4.3 show the interwell connectivity coefficients obtained from simulation data using MLR technique and calculated from analytical solution with equivalent time Δt_{eq} = 12.63 days. The coefficients for each well pair from both tables are close with the difference less than 10%. Notice that the interwell connectivity coefficients in Table 4.2 are different from those in Table 3.1 which were calculated using simulation data from different simulator (BOAST 98). These differences could be due to the way the data were input into the simulators. Different from ECLIPSE 100 where most input data can be entered directly, some input data for BOAST 98 are calculated from other inputs such as the fluid compressibilities. This leads to inconsistent input data of the same parameters for the two models, and thus produces slightly different interwell connectivity results.

Figs. 4.3 and 4.4 show the results obtained from Eqs. 4.27 and 4.30 with the simulation results respectively. The average pressures for analytical solution (Eqs. 4.27) were calculated using material balance equation (Eq. 4.21). The constant term $\Delta p_{pr}(\Delta t_{eq})$ was calculated using trial-and-error method by matching two representative equivalent points on both graphs. The coefficient of determination (R^2) does not depend on this constant term. Good match is observed on Fig. 4.3 with $R^2 = 0.95$. The error could be because the average reservoir pressure is not exactly constant due to the change in total compressibility. However, excellent match is observed in Fig. 4.4. The constant terms $\Delta p_{pr}(\Delta t_{eq})$ for both cases are close to β_{0j} calculated from simulation data using MLR technique (Table 4.2).

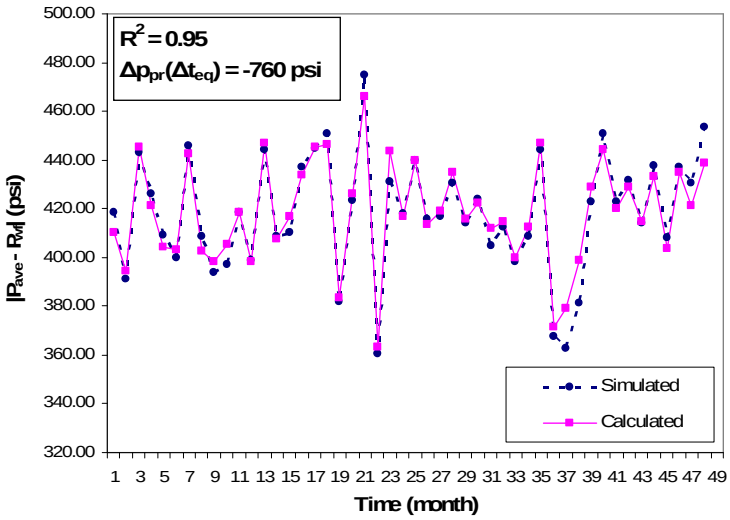


Figure 4.3. Absolute Values of (P_{ave}-P_{wf}) from Eq.4.28 and from simulation results for Well P-1, 5x4 homogeneous field.

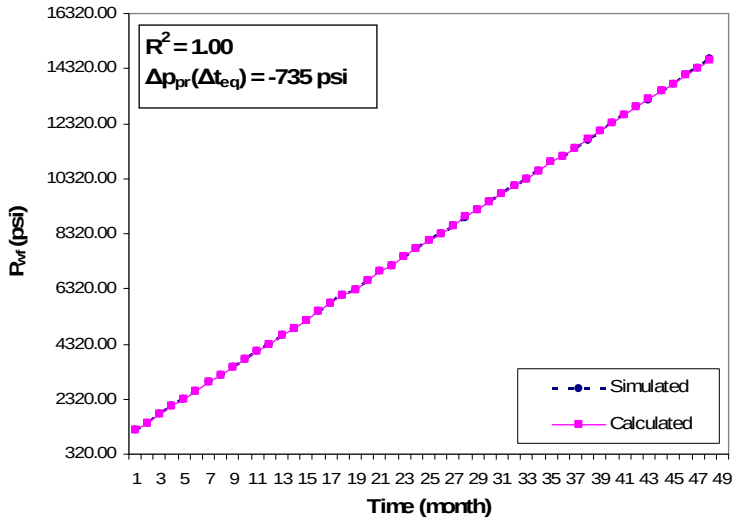


Figure 4.4. P_{wf} Results from Eq.4.30 and from Simulation for Well P-1, 5x4 homogeneous field.

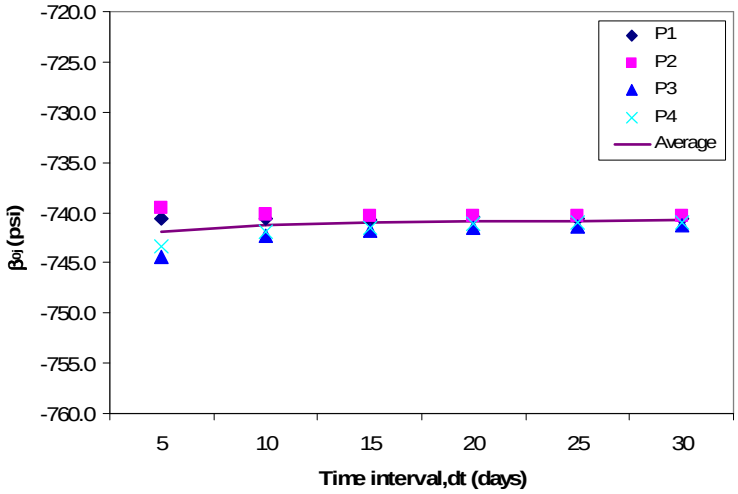


Figure 4.5. Plot of the term $\beta_{0j'} = \Delta p_{pr}(\Delta t_{eq})$ versus different time interval (Δt), 5x4 homogeneous field.

Similar results were obtained for other producers. Thus, the analytical approach works well for the 5x4 homogeneous reservoir. Fig. 4.5 shows a plot of the constant $\beta_{0j'}$ calculated from simulation results versus different length of the test time interval (Δt). $\beta_{0j'}$ for different Δt are almost the same with less than 1% difference. Hence, the results

agree with the analytical model that the term $\Delta p_{pr}(\Delta t_{eq}) = \beta_{0j'}$ does not depend on the test time interval.

4.4.2. 25x16 Synthetic Field

Similar procedure was used to verify the application of analytical model to 25x16 Synthetic Field. The equivalent time was found to be 5.87 days (Δt_{eq} = 5.87 days). Again, Fig. 4.6 shows the results obtained from Eq. 4.30 for Well P1.

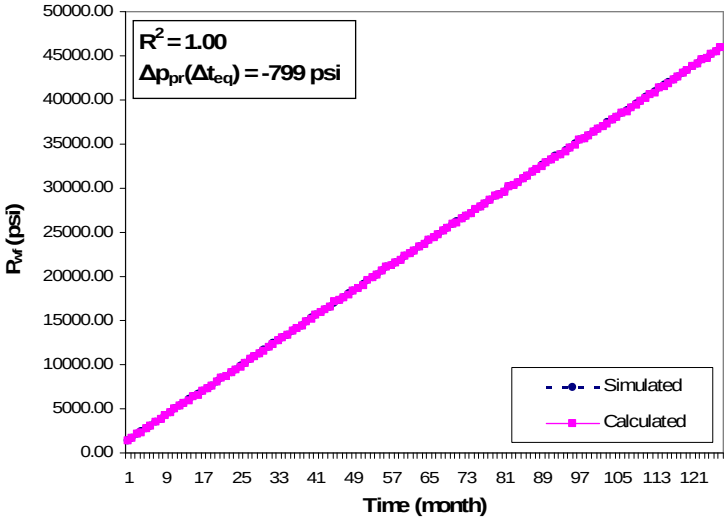


Figure 4.6. P_{wf} Results from Eq.4.30 and from Simulation for Well P-1, 25x16 Homogeneous Synthetic Field (Δt_{eq} = 5.87 days).

Again, a perfect match was obtained for bottom hole pressures calculated using Eq. 4.30 and from simulation results. However, the pressure difference plots display a good match only at early time. The poor match at late time resulted in low value of R^2 (0.42). At later time, as more water was pumped in, the change of water saturation became more significant. Since water and oil compressibility were different, the change in water saturation would lead to a change in total compressibility. Thus, the assumption of a constant average reservoir pressure change was violated. P_{ave} used in Eq. 4.27,

which was calculated from material balance, was no longer accurate with changing total compressibility. When the actual average field pressure from simulation results were used for Eq. 4.27, we obtained much better match as shown in Fig. 4.7 ($R^2 = 0.92$). Since excellent match was again obtained for bottom hole pressure results even at late time (Fig.4.6), it was confirmed that once the well reaches pseudo-steady state, the bottom hole pressure is independent from production history (Valko et al., 2000).

Different values of permeability were applied to the same reservoirs (5x4 and 25x16 Synthetic Fields) to investigate the behavior of the equivalent time (Δt_{eq}). Plots of permeability of both 5x4 and 25x16 synthetic fields vs. the equivalent time are shown on Fig.4.8. It is clear that as the permeability increases, Δt_{eq} decreases. The fact that Δt_{eq} of 25x16 field was higher than that of 5x4 field indicated that with the designed flow rates, 25x16 field reached pseudo-steady state quicker than 5x4 field.

4.5. Calculation Techniques for Interwell Connectivity Tests

Albertoni and Lake introduced the Multivariate Linear Regression (MLR) technique to solve a system of linear equations for interwell connectivity coefficients using flow rate data. Dinh and Tiab (2008) used the same technique to calculate interwell connectivity coefficients from bottom hole pressure data. Least Squares Linear Regression (LSLR) is another technique to solve a system of linear equations by least square fitting (Jensen et al., 2000, see also Chapra & Canale, 1988). According to Yousef et al. (2006), MLR technique is equivalent to Least Squares Linear Regression (LSLR). Thus, using either MLR or LSLR is an option based on convenience. In this study, both the MLR and the LSLR techniques were used.

4.5.1. Calculation Approaches

Consider a system of J producers and I injectors where injectors are the signal wells and producers are response wells. All wells are fully penetrating vertical wells. The reservoir is assumed to be homogeneous with constant rock properties. The fluid saturations are assumed to be constant. Single phase flow of a slightly compressible fluid of constant viscosity is also assumed. In an interwell connectivity test as described in Chapter 3, the injection rates were changed after a constant time interval (Δt) while the production rates were kept constant and equal throughout the test. The total injection and production rates were also kept constant. The reservoir was assumed to have reached pseudo-steady state at the end of each time interval.

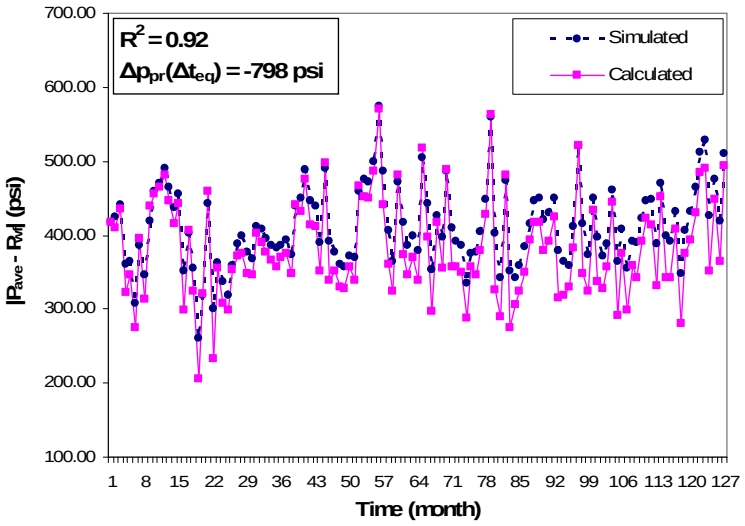


Figure 4.7. Absolute Values of (P_{ave}-P_{wf}) Calculated and Simulated with P_{ave} taken from simulation results for Well P-1, 25x16 Homogeneous Synthetic Field (Δt_{eq} = 5.87 days).

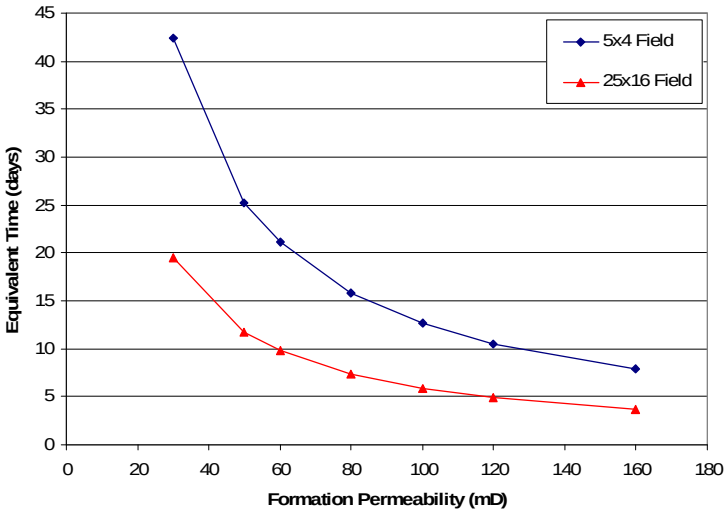


Figure 4.8. Equivalent time (Δt_{eq}) as a function of permeability-Homogeneous 5x4 and 25x16 Synthetic Fields.

Eqs. 4.18 and 4.19 were used as models for the interwell connectivity test. Thus the equations were applied to each time interval during the test. Since the total field-wise flow rate and the time interval are constant, the average reservoir pressure change is constant for every time interval. Let the superscript l be the order of the data points used for the test, we obtain a system of equations for L data points for producer j' as follows:

$$\begin{cases} \dfrac{141.2B\mu}{kh}\left(\sum_{i=1}^{I} q_{ij'}^{(1)} a_{ij'}\right) + \Delta p_{pr} = p_{ave}^{(1)} - p_{wf,j'}^{(1)} \\ \dfrac{141.2B\mu}{kh}\left(\sum_{i=1}^{I} q_{ij'}^{(2)} a_{ij'}\right) + \Delta p_{pr} = p_{ave}^{(2)} - p_{wf,j'}^{(2)} \\ \vdots \\ \dfrac{141.2B\mu}{kh}\left(\sum_{i=1}^{I} q_{ij'}^{(L)} a_{ij'}\right) + \Delta p_{pr} = p_{ave}^{(L)} - p_{wf,j'}^{(L)} \end{cases} \tag{4.31}$$

4.5.2. Average Pressure Change Calculation

Now, assuming constant B, μ, c_t and Δp_{ave}, we can subtract the previous equation in the system of Eq.4.31 from the next equation taking into account that Δp_{pr} stay constant. Thus, we have

$$\begin{cases} \sum_{i=1}^{I}\left(q_{ij'}^{(2)}-q_{ij'}^{(1)}\right)M_{ij'}-\Delta p_{ave}=-\left(p_{wf,j'}^{(2)}-p_{wf,j'}^{(1)}\right) \\ \sum_{i=1}^{I}\left(q_{ij'}^{(3)}-q_{ij'}^{(2)}\right)M_{ij'}-\Delta p_{ave}=-\left(p_{wf,j'}^{(3)}-p_{wf,j'}^{(2)}\right) \\ \vdots \\ \sum_{i=1}^{I}\left(q_{ij'}^{(L)}-q_{ij'}^{(L-1)}\right)M_{ij'}-\Delta p_{ave}=-\left(p_{wf,j'}^{(L)}-p_{wf,j'}^{(L-1)}\right) \end{cases} \tag{4.32}$$

Where $M_{ij'}$ are coefficients account for the state of the well regardless of production history. Since the total injection rate was kept constant, when one equation was subtracted from the other, the sum of the rate differences was equal to zero. The sum of the resulted coefficients ($M_{ij'}$) was also equal to zeros indicating that if the flow rates are kept constant and equal, the change of bottom hole pressure is equal to the change of average pressure. However, since $M_{ij'}$ were calculated without the information of production rates, they do not reflect the actual state and are not used in the analysis.

Eq.4.32 can be solved using either LSLR or MLR technique. In this study, LSLR was used to calculate Δp_{ave}. Δp_{ave} is positive when the average pressure increases and negative when it decreases. Assuming constant total compressibility and porosity, the reservoir pore volume (V_p) can be estimated using Eq.4.21. Knowing the initial static pressure, the average pressure after each time interval can be estimated by adding the total pressure change (Δp_{ave}). With the known total reservoir volume (V_b), total porosity can also be calculated:

$$\phi_{tot}=\frac{V_p}{V_b} \tag{4.33}$$

Relative Interwell Permeability Calculation from Interwell Connectivity Coefficients using Bottom Hole Pressures

A direct relationship between interwell connectivity coefficients and the influence functions (a_{ij}) is presented in Eq.4.28, in which $a_{ij'}$ represents the connectivity between two wells i and j' and the term $\left(a_{ii}+2\pi t_{DA}\right)$ is associated with the injector i. Thus, the permeability value in $a_{ij'}$ reflects the permeability between wells i and j' relative to the permeability given to injector i in the term $\left(a_{ii}+2\pi t_{DA}\right)$. If the permeability values given for every injector are equal, then the permeabilities in $a_{ij'}$ are relative to one another among injector-producer pairs and the permeability at the injectors. The equivalent time Δt_{eq} was calculated using trial-and-error technique with an assigned homogeneous permeability system to the injectors so that $\sum_{i=1}^{I}\frac{a_{ij'}}{\left(a_{ii}+2\pi t_{DA}\right)}=1$. Thus, by varying permeability between each well pair so that $\frac{a_{ij'}}{\left(a_{ii}+2\pi t_{DA}\right)}=\beta_{ij'}$, relative permeability among wells can be estimated.

The reference reservoir is a homogeneous reservoir with permeability equal to permeability given to the signal wells (injectors). We call the permeability assumed for the signal wells reference permeability (k_{ref}) and the permeability accounting for the flow property between signal and response wells relative interwell permeability (k_{ir}). The matching process can be carried out using trial-and-error method by varying relative interwell permeabilities until the total difference between interwell connectivity coefficients from analytical model and simulation results for each response well equal zero. Different from the interwell connectivity coefficients, the relative interwell permeabilities do not depend on the distance between wells and the position of the wells.

4.5.3. Calculation Procedures

Step 1: Obtain both flow rate and pressure data from the interwell connectivity test. The number of data points should be more than I+1 to obtain good results (Dinh & Tiab, 2007). The time interval should be long enough for every well to reach pseudo-steady state. However, if the reservoir is already in pseudo-steady state, the time required for each well to reach pseudo-steady state after each rate change will be much shorter than the time required for the reservoir to reach pseudo-steady state from a static initial pressure (Umnuayponwiwat et al., 2000). The interwell connectivity coefficients can then be calculated using MLR method as described in Chapter 3.

Step 2: Calculate the average reservoir pressure change corresponding to each producer, Δp_{ave}, using Eq.4.32. Δp_{ave} for every producer should be close if all producers are connected to the same reservoir pore volume. The bulk volume (V_b) of the reservoir can also be calculated knowing the reservoir geometry. The pore volume and the total average porosity can then be calculated using Eqs. 4.21 and 4.33.

Step 3: Define a homogeneous pseudo-steady-state reference reservoir by assuming a reference permeability (k_{ref}). k_{ref} should be representative of the entire reservoir. Further details about the characteristics of k_{ref} will be discussed later. The equivalent time interval (Δt_{eq}) corresponding to the reference reservoir can be calculated using trial-and-error method as described before.

Step 4: Using k_{ref} and Δt_{eq} from step 3, match the interwell connectivity coefficients from analytical equation (Eq.4.28) with those calculated from the bottom hole pressure data. The denominator in Eq. 4.28, $\left(a_{ii} + 2\pi t_{DA}\right)$, is associated with the injector i and is calculated using k_{ref}. The nominator is calculated using the relative

interwell permeability (k_{ir}). Thus, k_{ir} is varied to obtain the match while k_{ref} is kept constant. The match is obtained when the percent error between interwell connectivity coefficients calculated from analytical equation and simulation is 0%. The results include a value of k_{ir} for each injector-producer pair. These k_{ir} are relative interwell permeability corresponding to assumed reference permeability.

Step 5: The results obtained are used to analyze the reservoir properties including high permeability channel, permeability barrier and reservoir compartmentalization. More details are discussed in the next section.

4.6. Simulation Results

The calculation approaches presented in the last section were applied to data from two synthetic fields, one with 5 injectors and 4 producer (5x4 Synthetic Field) and the other with 25 injectors and 16 producers (25x16 Synthetic Field). These synthetic fields are already described in the previous sections. Both homogeneous reservoir and reservoirs with heterogeneity were considered.

4.6.1. 5x4 Synthetic Field

Consider a waterflood system of 5 injectors and 4 producers as shown in Fig. 4.1, where production and injection rates were kept constant during a constant time intervals. Injection rates were changed after each time interval but production rates and total injection rate stayed constant (q_{tot} = constant) as described in Chapter 3. The system was assumed to be in pseudo-steady state so Eqs. 4.18 and 4.19 apply.

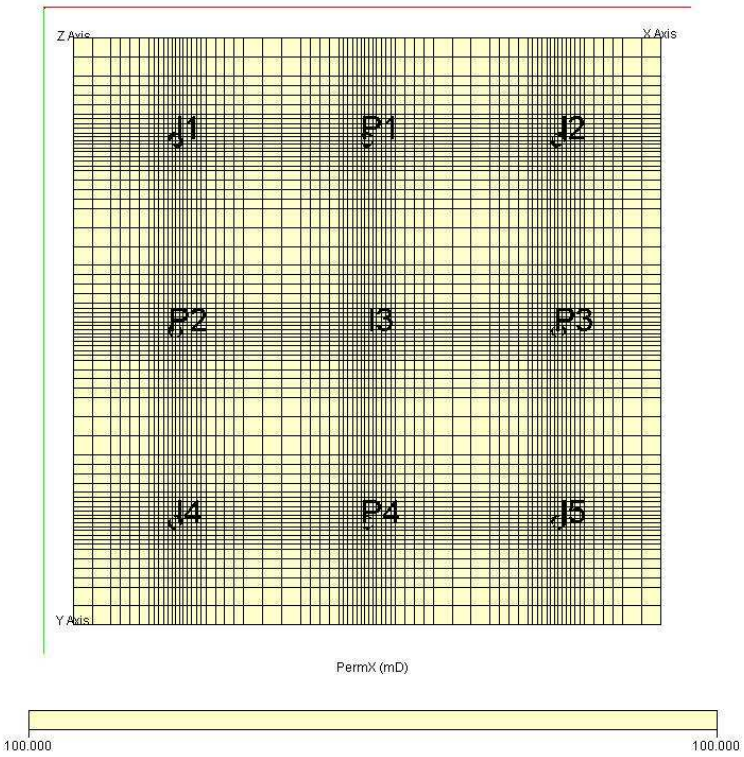


Figure 4.9. Top view of the simulation model for the 5x4 Synthetic Homogeneous Reservoir.

a. Homogeneous Reservoir

The permeability distribution for the simulation model for this case is shown in Fig. 4.9. The reservoir is homogeneous with formation permeability of 100 mD.

The interwell connectivity coefficients calculated from simulation data and analytical model were presented in the previous section. LSLR technique was used to calculate the average pressure change as described before. ΔP_{ave} is in perfect match with result obtained from material balance and the resulted porosity was 0.301. By keeping the permeabilities associated with injectors constant at 100 mD, the interwell coefficient in Table 4.3 can be matched with those in Table 4.2 by adjusting the permeability between injector/producer pairs or the influence function a_{ij}. The resulted relative

interwell permeabilities are shown in Table 4.4. Fig. 4.10 shows the representation of the permeabilities in Table 4.4 in form of inverse arrows. The lengths of the arrows are proportional to the permeability between injectors and producers. The relative interwell permeabilities are very close to each other and to the input formation permeability.

Table 4.4: Relative Interwell Permeability results for the 5x4 Homogeneous Synthetic Field (k_{ref}=100mD, Δt_{eq} = 12.63 days)

	P1	P2	P3	P4	Ave.
I1	105	109	93	98	101
I2	104	95	108	98	101
I3	95	94	97	95	95
I4	99	106	97	104	101
I5	97	97	105	106	101
Ave.	100	100	100	100	

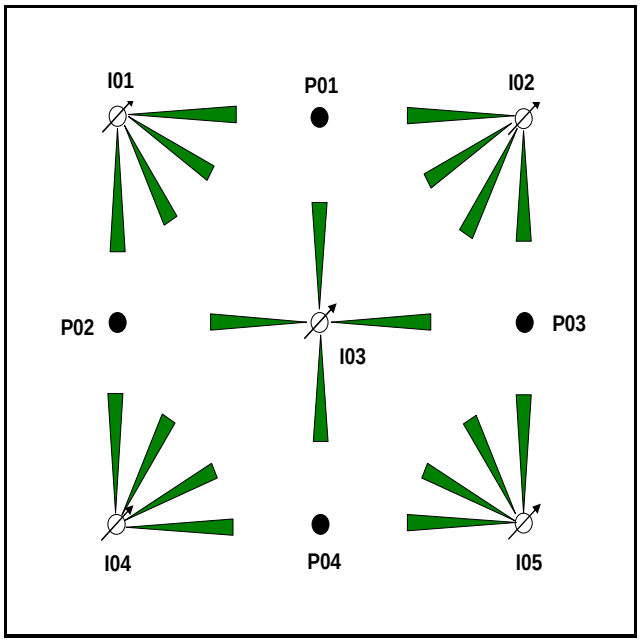


Figure 4.10. Representation of relative interwell permeability for the case of 5x4 Homogeneous Reservoir.

b. Anisotropic Reservoir

In this case, the permeability in x direction (1000 mD) is ten-fold the permeability in y direction (100 mD). The results for relative interwell permeability are shown in Table 4.5. The permeability at the injectors was set to the geometric average of the maximum and minimum permeability which equals 316 mD. The equivalent time (Δt_{eq}) was found to be 4.00 days.

Fig. 4.11 shows the representation of the relative interwell permeabilities. The results agree with the actual permeability of the field with high permeability in x direction and low permeability in y direction. The results indicate that the relative permeability is not directional permeability between well pairs but rather be the average permeability of the effective area between the two wells. The interwell connectivity for some well pairs such as I1P2 and I2P3 are larger than the others such as I2P2 and I1P3. However the permeabilities between I2P2 and I1P3 are larger than those of I1P2 and I2P3 even though the distance between the former pairs are less than the latter pairs. Thus, the relative interwell permeabilities are independent on the distance between wells or the position of the wells. Results for the change of average reservoir pressure for this case are almost the same as the previous case, thus, the average pressure change does not depend on permeability.

Table 4.5: Relative interwell permeability results from pseudo-steady state equation for the 5x4 Anisotropic Synthetic Field (k_{ref}=316mD, Δt_{eq} = 4.0 days)

	P1	P2	P3	P4	Ave.
I1	309	134	168	90	176
I2	307	170	136	92	176
I3	138	317	318	138	228
I4	95	134	168	305	175
I5	87	170	136	312	176
Ave.	187	185	185	187	

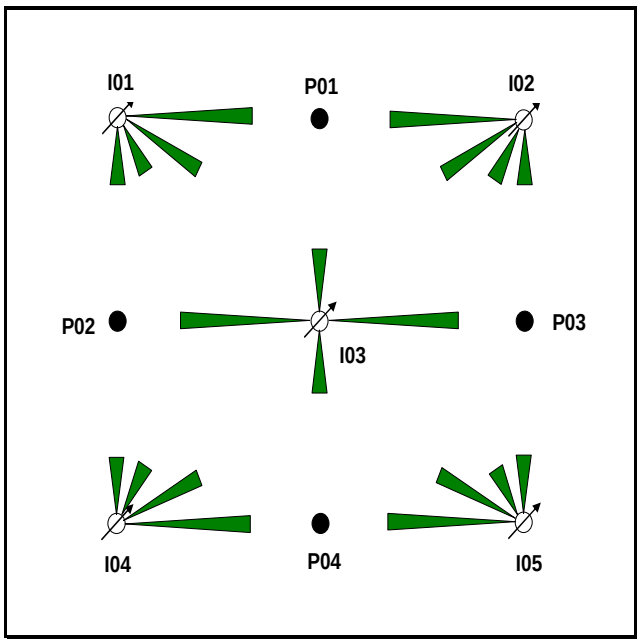


Figure 4.11. Representation of relative interwell permeability for the case of 5x4 Anisotropic Reservoir.

c. Reservoir with High Permeability Channel

In this case, a high permeability channel was present as shown on Fig.4.12. The red shaded area is the high permeability channels with permeability of 1000 mD which is ten-fold the permeability in other area of the reservoir (100 mD).

For this case, permeability at the injectors was set to 100 mD. Again, the relative interwell permeability between well pairs were calculated by matching the values of interwell connectivity coefficients calculated from analytical model with the values obtained from MLR technique using simulation results. Some resulted permeabilities were lower than reservoir permeability which was unreasonable. It was because well I1 was actually located in the high permeability zone and thus, assuming permeability of well I1 (k_{ref}) was the same as formation permeability would lead to unrealistic results. Thus, in order to address this problem, an approximate average reservoir permeability of

300 mD was assumed for well I1. The same permeability was applied to other injectors to guarantee comparable relative permeability. A new set of relative interwell permeabilities were found as shown in Table 4.6.

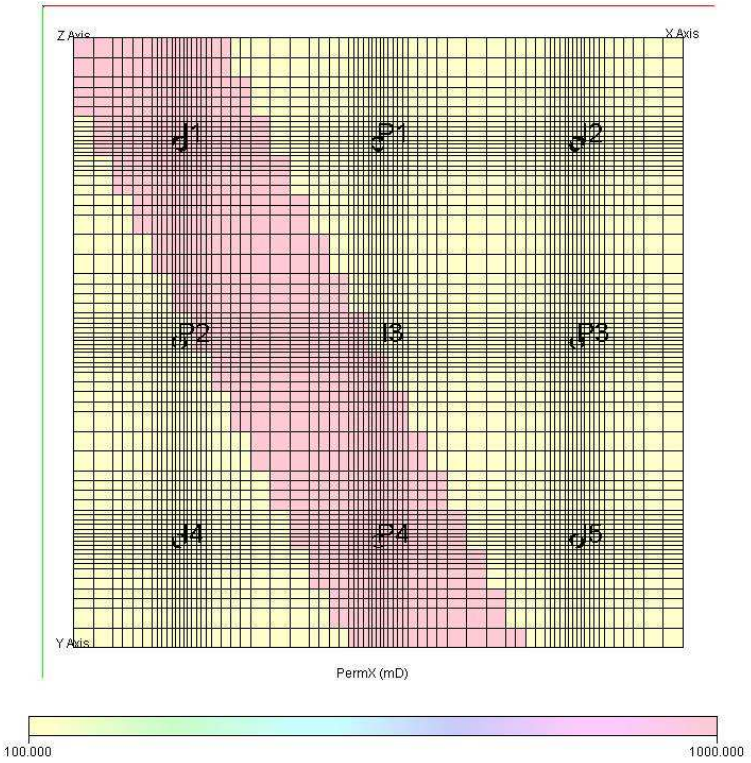


Figure 4.12. Top view of the simulation model showing the x-direction permeability distribution for the 5x4 Synthetic Reservoir with high permeability channel.

Table 4.6: Relative interwell permeability results from pseudo-steady state equation for the 5x4 Synthetic field-Reservoir with High Permeability Channel (k_{ref}=300mD, Δt_{eq}=12.15 days)

	P1	P2	P3	P4	Ave.
I1	529	568	424	508	507
I2	113	79	148	91	108
I3	87	102	107	124	105
I4	86	65	101	84	84
I5	92	94	127	98	103
Ave.	182	182	181	181	

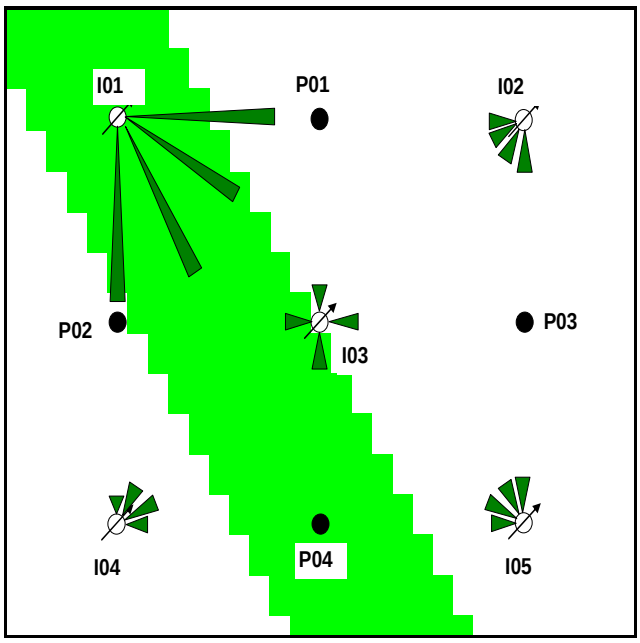


Figure 4.13. Representation of relative interwell permeability for the case of 5x4 Synthetic field with high permeability channel.

Representation of the relative interwell permeabilities is shown in Fig. 4.13. A clear trend of the high permeability channel can be observed by looking at the relative interwell permeabilities on Fig. 4.13. The flow in the channel seems to affect the relative interwell permeability between wells on each side of the channel. For example, k_{ir} for the pair I03-P02 is lower than k_{ir} for the pair I03-P03 even though the permeability between I03-P02 is higher. Thus, flow interference may affect the relative interwell permeability.

d. Reservoir with Partially Sealing Barrier

In this case, a reservoir with partially sealing barrier similar to the case discussed in Chapter 3 was investigated. The partially sealing barrier is indicated by the white shaded strip as shown on Fig. 4.14. The barrier was set to zero porosity and permeability. Permeability at injectors was equal to formation permeability of 100 mD.

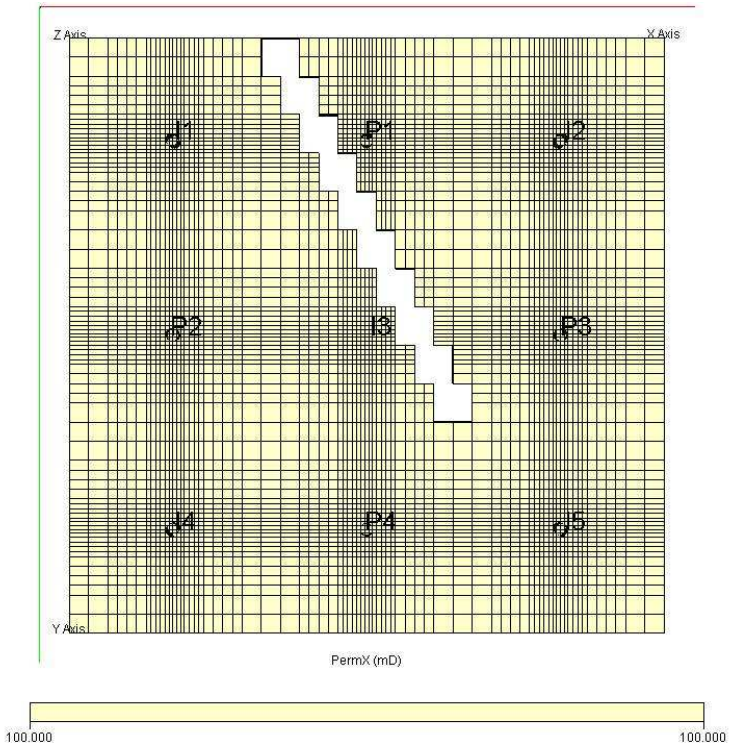


Figure 4.14. Top view of the simulation model showing the x-direction permeability distribution for the 5x4 Synthetic Reservoir with a partially sealing barrier.

Table 4.7: Relative interwell permeability results from pseudo-steady state equation for the 5x4 Synthetic field-Reservoir with partially sealing barrier (k_{ref}=100mD, Δt_{eq} = 12.63 days)

	P1	P2	P3	P4	Ave.
I1	20	129	62	98	77
I2	249	65	174	95	146
I3	52	99	60	94	76
I4	79	111	87	106	96
I5	116	95	120	108	110
Ave.	103	100	101	100	

The relative interwell permeability results are shown in Table 4.7. Fig. 4.15 shows the representation of the relative interwell permeabilities in form of reverse arrows. It is clear that the permeabilities of well pairs with wells on different side of the barrier are small. Unlike the homogeneous case, the constant β_{0j} calculated for each

producer were different indicating each producer was under different influence by the other producers.

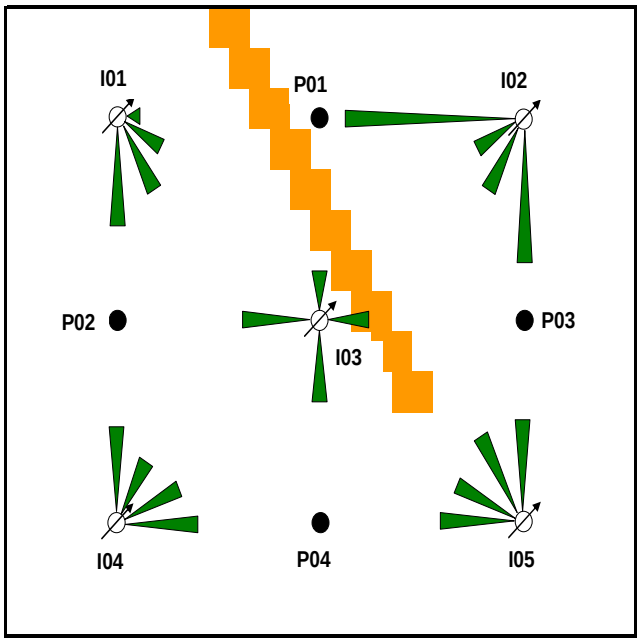


Figure 4.15. Representation of relative interwell permeability for the case of 5x4 synthetic field with partially sealing barrier

The average pressure change for this case is higher than that of previous case indicating a decrease in pore volume. This is because the barrier was set to zero porosity causing a decrease in overall pore volume. The calculated total porosity was 0.29 which is slightly lower than assigned formation porosity (0.30).

e. Reservoir with Sealing Barrier

This case is similar to the partially sealing barrier; however, the barrier seals completely as shown in Fig.4.16. Thus, the reservoir is actually divided into two compartments. The results for interwell connectivity coefficients were similar to those presented in the previous chapter. Some coefficients are significantly small compared to the others for the same producers. To simplify the calculation, a cut-off value was set at

0.1. Thus, any coefficients less than 0.1 were set to zeros. Since the relative interwell permeabilities do not exist at zero interwell coefficients, they were also set to zero.

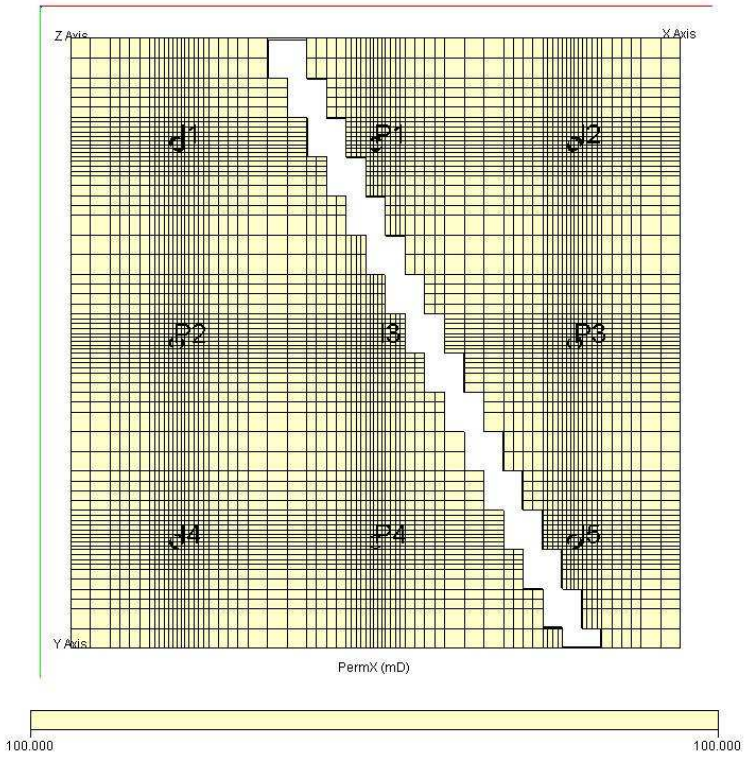


Figure 4.16. Top view of the simulation model showing the x-direction permeability distribution for the 5x4 Synthetic Reservoir with a sealing barrier.

Table 4.8: Change of Average Reservoir Pressure results for the 5x4 Synthetic field-Reservoir with Sealing Barrier (k_{ref}=100mD,Δt_{eq}=12.63 days)

	P1	P2	P3	P4	Ave
Δp_{ave} (psia)	181.0	390.3	180.8	390.2	285.6
I1	-0.13	0.14	-0.18	-0.01	-0.18
I2	0.42	-0.24	0.30	-0.20	0.28
I3	-0.21	0.16	-0.23	0.19	-0.08
I4	-0.09	0.07	-0.12	0.12	-0.02
I5	0.00	-0.13	0.23	-0.11	0.00
Sum	0.00	0.00	0.00	0.00	

The representation of relative interwell permeability results is presented in Fig.4.17. The resulted average pressure change along with coefficients M_{ij} are shown in

Table 4.8. It is obvious that there are two set of average pressure changes (181 psi and 390 psi) corresponding to two groups of producers (P1,P3) and (P2,P4) suggesting two different reservoir pore volumes. From the relative interwell permeability results, we can identify the wells connected to the same pore volumes by analyzing both relative interwell permeabilities and average pressure changes. The results indicate two groups of wells. One group of wells connected to the same pore volume includes well P1, P3, I2 and I5. The other group includes P2, P4, I1, I2 and I4. This agrees with the actual reservoir model setup. Thus, the new technique can be used to detect reservoir compartmentalization and identify the wells that are in the same compartment.

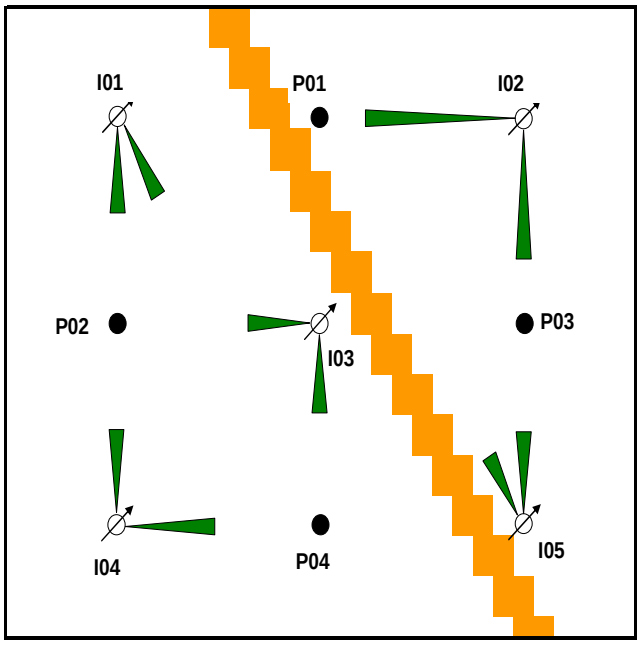


Figure 4.17. Representation of relative interwell permeability for the case of 5x4 synthetic field with a sealing barrier.

f. 25x16 Synthetic Field

Only the homogeneous case was considered for this field. As mentioned before, 128 data points were obtained to calculate interwell connectivity coefficients using MLR

technique. Similar results to the results presented in Chapter 3 were obtained. The interwell connectivity coefficients are very low for the well pairs that are too far apart. Since the percentage errors as mentioned in Step 4 were magnified for low interwell coefficients, a cut-off value of 0.04 was applied. Thus, the percentage errors of any coefficients lower than the cut-off value were set to zero, and the corresponding relative interwell permeability were considered as undetermined. Only relative interwell permeability corresponding to the connectivity coefficients higher than or equal to the cut-off values were calculated. The results are shown in Fig.4.18 and 4.19.

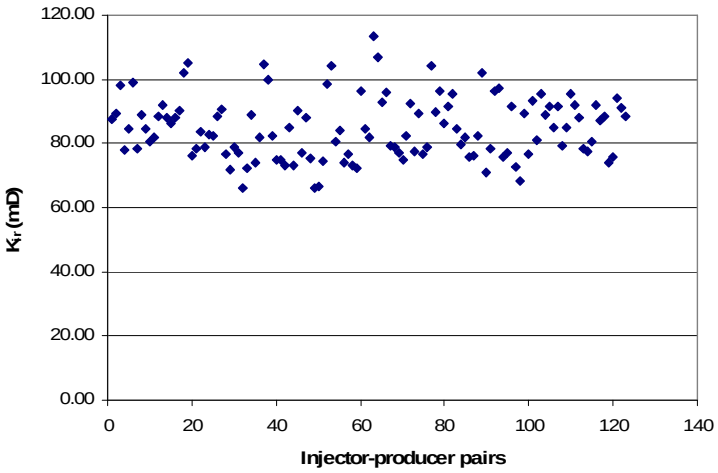


Figure 4.18. Plot of relative interwell permeability (k_{ir}) after cut-off ($\beta_{ij\text{-}cut\text{-}off}$ = 0.04) for 25x16 homogeneous synthetic field (k_{ref} = 100 mD, Δt_{eq} = 5.87 days).

The relative interwell permeability results are close to one another. However, the average value for k_{ir} is slightly lower than the input permeability of 100 mD as shown in Fig. 4.18. This could be due to cross flow effect among wells. As shown in Fig. 4.19, only k_{ir} between well pairs that did not have any other well between them could be determined. The relative interwell permeabilities of well pairs with farther distances

were slightly higher than those with closer distances. This agreed with a conclusion drawn by Umnuayponwiwat et al. (2000) that "the interference effects are not always dominated by the nearby wells. Under certain conditions, farther wells may play more important roles on the well performance."

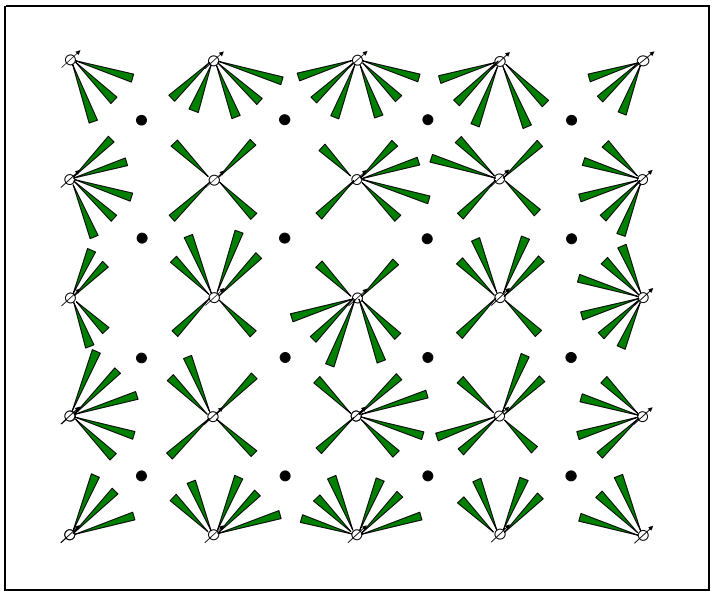


Figure 4.19. Representation of relative interwell permeability after cut-off ($\beta_{ij\text{-}cut\text{-}off}$ = 0.04) for the case of 25x16 homogeneous synthetic field (k_{ref} = 100 mD, Δt_{eq} = 5.87 days).

4.6.2. Different flowing conditions at the response and signal wells

The previous chapter considered injectors as signal wells (changing rates) and producers as response wells (constant rates). However, in real field situation, it is not always possible to keep the production rates constant. Thus, different test designs should be considered. The characteristics of the analytical model discussed in the previous section indicate that either injector or producer can be used as response wells or signal wells. Hence, the technique should not be restricted to the case injectors as signal wells and producers as response wells. In this section, we obtained simulation results from

several other case scenarios to verify this theory. Resulted interwell connectivity and discussion on any necessary modification to the analytical solutions are also presented.

Table 4.9 and 4.10 summarize the results for all the cases discussed in this section. The second column shows the average percent error of interwell connectivity coefficients comparing to the Base Case (constant production rate and changing injection rate in homogeneous reservoir). The third column presents the asymmetry coefficients (A_s). The fourth column is the total field flow rates. The fifth and sixth column shows the ΔP_{ave} results and their percent error comparing to the material balance solution respectively. The last column is the calculated porosities with input porosity of 0.3 for all the cases.

a. Constant injection rates and changing production rates

For this case (Constant Injection), the injectors of 5x4 homogeneous synthetic field described before were converted to producers and the producers were converted to injectors. Thus, the 5x4 synthetic field now have 5 producers and 4 injectors. Flow rates of the new producers are the same as of the original injectors except they are now producing flow rates. The new injectors were maintained at constant rates (850 STB/day) so that the difference between total injection and total production was the same as the Base case. The results are shown in Table 4.9.

Determination coefficients of R^2=1 and the low asymmetry coefficient A_s = 0.004482 indicate good results. The coefficients and average pressure change are almost exactly the same as for the case of constant production rates and changing injection rates (Table 4.9).

Similar results were obtained for 25x16 synthetic field with asymmetry coefficient A_s = 0.0059. Almost the same Δp_{ave} was also obtained. Table 4.10 summarizes the results.

A few changes are required for the analytical model in this case. The negative sign in front of the first terms on the right hand side of both Eqs.4.13 and 4.14 become positive and the Δp_{pr} becomes:

$$\Delta p_{pr} = -\frac{141.2B\mu}{kh}\sum_{j=1}^{n_{inj}} a_j \left[x_D, y_D, x_{wDj}, y_{wDj} x_{eD}, y_{eD}, t_{AD}\right] q_j + \Delta p_{ave} \tag{4.34}$$

j and i is now standing for injectors and producers respectively. Eq.4.19 should be used instead of Eq. 4.20 to derive the flow rates for active wells (producers).

b. All production wells with constant rates at response wells

In this case (All producers), for 5x4 homogeneous field, the injectors in the Base case were converted to producers and acted as signal wells. Thus, all wells in the system were producers. The response wells were set to constant production rate of 100 BPD. The results are shown in Table 4.9. Poorer result was obtained for ΔP_{ave} with the percentage error compared to the material balance result of 8.3% (Table 4.9). This was because as all wells were producing, the water saturation decreased leading to changing total compressibility or deviation from original assumption. Thus, ΔP_{ave} was actually different for each time interval.

Similar approach was applied to the 25x16 homogeneous synthetic field. However, with the original flow rates, when all well producing, it was impossible to maintain the production rates as scheduled due to quick depletion of the reservoir. Thus,

no results were obtained for 25x16 synthetic field in this case. Therefore, the challenge to carry out the interwell connectivity test when all wells are producing is to maintain the scheduled production rates and make adjustment to the change in total compressibility.

c. Shut-in Wells as Response Wells

In this case, all response wells in previous cases were shut-in (shut-in producers and shut-in injectors). The results obtained were also similar for both changing injection rates and changing production rates. Both cases of shut-in producers for the constant production rate and changing injection rate case and shut-in injectors for constant injection rates and changing production rates case for 5x4 homogeneous synthetic field were investigated. Results for the shut-in injector case (A_s = 0.0431) were not as good as the results for the shut-in producers (A_s = 0.0035) as shown in Table 4.9. The reason could be more significant change in total compressibility in the case of shut-in injectors.

The same approach was applied to 25x16 homogeneous synthetic field. The case of all producers with shut-in wells as response wells could be simulated for this field. Good results were obtained for the case of shut-in producer and changing injection rates (Table 4.10). However, poor results with an average percent error of β_{ij} = 420.85% were obtained for shut-in injectors and active producers even after a cut-off value of 0.04 was applied to the interwell connectivity coefficients as shown in Table 4.10. Again, these errors were due to the significant change in total compressibility as water was drawn from the reservoir and the decreasing reservoir pressure leading to weak signals from active producers.

As seen in the Tables 4.9 and 4.10, with negative total field flow rate (total injection is higher than total production), the calculated ΔP_{ave} are positive indicating an

increase in reservoir pressure and vice versa. The results for the Base case and the constant injection case are very close indicating the roles of injectors and producers can be switched without significantly affecting the interwell connectivity results.

Table 4.9: Interwell connectivity result summary for different test schemes for the 5x4 homogeneous synthetic field (k_{ref}=100mD, Δt_{eq}=12.63 days)

Cases	Ave. % Error for β_{ij}	A_s	Δq_{tot} (STB/day)	Ave. ΔP_{ave} (psi)	% Error for ΔP_{ave}	Porosity
Base Case	0.00%	0.0035	-800	286.0	0.01%	0.301
Constant Injection	2.28%	0.0045	-800	285.6	0.12%	0.301
All producers	2.27%	0.0044	2400	-930.3	8.30%	0.277
Shut-in Producers	0.04%	0.0035	-2000	711.5	0.63%	0.302
Shut-in Injectors	2.35%	0.0431	2000	-683.2	4.58%	0.315

Table 4.10: Interwell connectivity result summary for different test schemes for the 25x16 homogeneous synthetic field (k_{ref} = 100 mD, Δt_{eq} = 5.87 days)

Cases	Ave. % Error for β_{ij}	A_s	Δq_{tot} (STB/day)	Ave. ΔP_{ave} (psi)	% Error for ΔP_{ave}	Porosity
Base Case	0.00%	0.0059	-3600	353.0	0.58%	0.303
Constant Injection	0.70%	0.0059	-3600	352.5	0.70%	0.303
Shut-in Producers	1.37%	0.0072	-10000	964.6	2.45%	0.308
Shut-in Injectors	420.85%	0.1307	10000	-970.6	1.74%	0.306

4.7. Conclusions

Some conclusions drawn from this chapter are as follows:

- The analytical model presented in this study works well with the interwell connectivity tests with the assumption that the pseudo-steady state of the field has been reached at the end of each time interval. The model provides in-depth understanding of the multi-well system with water injection in the presence of heterogeneity

- Tests that are longer than required (more data points) may create errors because of deviation from the constant total compressibility assumption due to the change of total reservoir saturation. Thus, an adequate number of data points should give better results.

- The relative interwell permeability does not depend on the position and the distance between wells. Thus, it provides an additional parameter to evaluate interwell connectivity.

- The average reservoir pressure change with the interwell connectivity information can be used to identify reservoir compartmentalization as well as the wells connected to each compartment.

- Results from this study have shown that the signal wells could be either producers or injectors so are the response wells. The response well could also be either flowing or shut-in. Thus, this study provides the flexibility in design of interwell connectivity test to fit a field situation.

CHAPTER 5 – APPLICATIONS OF THE INTERWELL CONNECTIVITY TEST TO NATURALLY FRACTURED RESERVOIRS

This chapter extends the technique to naturally fractured reservoirs represented by dual porosity systems. A pseudo steady state solution for a fully penetrating vertical well in a dual-porosity closed rectangular reservoir was used to calculate the influence functions between active and observation wells. Similar to the procedure described in the previous chapter, the model was then used to calculate relative interwell permeability, change of average reservoir pressure and total pore volume with interwell connectivity coefficients obtained from simulation results.

Different dual porosity reservoir simulation models from a commercial reservoir simulator were run to verify the technique. Comparisons between the results obtained from single porosity systems and double porosity systems are explained in detail.

5.1. Literature Review

Naturally fractured reservoirs are often associated with carbonate rocks which contribute to more than half of the world oil reserve. A naturally fractured reservoir often consists of two system, the matrix system and the fracture system. Nelson classified the naturally fractured reservoirs into four types based on engineering criteria (Tiab and Donaldson, 2004):

- Type 1: Reservoir fractures provide both storage capacity and permeability while the matrix provides negligible or no storativity or permeability.
- Type 2: The fractures provide most or all of the flow capacity and the matrix contributes to most or all the storage capacity. This type is the most common type

among naturally fractured reservoirs and is often referred to as a dual porosity system.

- Type 3: Both fracture and matrix systems contribute to the permeability of the reservoir. This type of naturally fractured reservoirs is often referred to as a dual permeability system.
- Type 4: Fractures are filled with minerals and thus, become barriers to fluid flow. This reservoir type is often uneconomic to develop.

In this study, only naturally fractured reservoirs exhibiting dual porosity behaviors were considered (Type 2). There has been a number of studies on the behavior of dual porosity systems. Warren and Root (1963) provide a model for a dual porosity often referred to as "sugar cube model". In their model, Warren and Root divided the reservoir into a system of blocks that represent the matrix system and the space between the blocks represents the fracture system as shown in Fig. 5.1. The assumptions for Warren and Root's model are that the fluid flow from the matrix to the fracture system is under pseudo-steady state flow condition and only the fractures feed the wellbore. Two key parameters to characterize the dual porosity system were introduced, the storage capacity ratio (ω) and the inter-porosity flow parameter (λ). Kazemi (1969) developed a model for a dual porosity system based on the Warren and Root model. However, Kazemi's model assumed the matrix and the fractures as a slab system as shown in Fig. 5.1. The results for this model were similar to the Warren and Root model. In this study, the simulation models for naturally fractured reservoir were based on the Kazemi model.

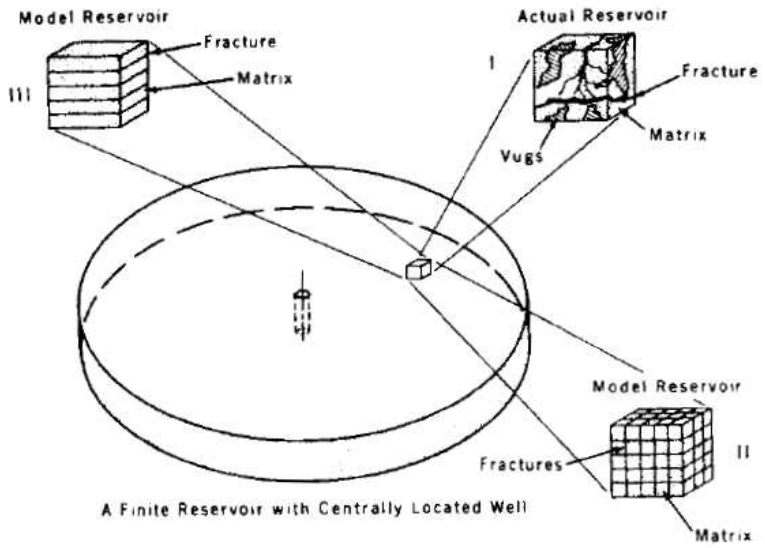


Figure 5.1:. Idealization of a naturally fractured system showing I. The actual reservoir, II. Warren-Root's "Sugar cube model" & III. Kazemi's Model (Source: Kazemi H., 1969).

De Swaan O, A (1976) provided analytical solutions for determining dual porosity system properties by well testing based on Kazemi's model. From the analytical solutions, different reservoir parameters could be calculated based on the transient pressure behavior of the reservoir. Engler and Tiab (1995) developed a transient pressure analysis technique to analyze natural fractured reservoirs based on pressure derivative curves.

5.2. Analytical Model

For simplicity, the pseudo-steady state solution for pressure distribution of a vertical well in a naturally fractured reservoir was used to calculate the influence function. Ozkan (1988) (also Raghavan (1993)) provided the late-time approximation for pressure distribution due to a fully penetrated vertical well in a closed rectangular dual porosity reservoir as follows:

$$p_{Dv} = a_v = 2\pi t_{DA} + 2\pi \frac{y_{eD}}{x_{eD}}\left(\frac{1}{3} - \frac{y_D}{y_{eD}} + \frac{y_D^2 + y_{wD}^2}{2y_{eD}^2}\right) +$$

$$+ 2\sum_{k=1}^{\infty} \frac{1}{k} \cos\left(k\pi \frac{x_D}{x_{eD}}\right) \cos\left(k\pi \frac{x_{wD}}{x_{eD}}\right) \frac{\cosh k\pi\left(\frac{y_{eD} - |y_D - y_{wD}|}{x_{eD}}\right) + \cosh k\pi\left(\frac{y_{eD} - (y_D + y_{wD})}{x_{eD}}\right)}{\sinh\left(k\pi \frac{y_{eD}}{x_{eD}}\right)} \quad (5.1)$$

Where t_{DA} is the dimensionless time based on drainage area $t_{DA} = \frac{t_D}{A_D} = \frac{t_D}{x_{eD} y_{eD}}$

The dimensionless variables are defined as follows:

$$x_D = \frac{x}{L} \quad (5.2)$$

$$y_D = \frac{y}{L} \quad (5.3)$$

$$p_D = \frac{kh}{141.2 q_{ref} B\mu}\left(p_{ini} - p(x, y, t)\right) \quad (5.4)$$

$$t_D = 0.0002637 \frac{kt}{\phi c_t \mu L^2} \quad (5.5)$$

Where $L = x_e$ for the vertical well case.

It is necessary to note that the dimensionless pressure in Eq. 5.1 is also the late time solution for a vertical well in a closed rectangular reservoir as described in Chapter 4. Eq. 5.1 does not depend on the dual porosity parameters and should be applicable to a homogenous medium as well. The derivation of Eq. 5.1 is described in the Appendix C.

5.3. Calculation Methods

5.3.1. Ozkan Calculation Method

Applying the formula given by Ozkan (1988, page 55), we have

$$\frac{\cosh\sqrt{b}\left(y_{eD}-\tilde{y}_D\right)}{\sinh\left(\sqrt{b}y_{eD}\right)}=\left\{\exp\left(-\sqrt{b}y_{eD}\right)+\exp\left[-\sqrt{b}\left(2y_{eD}-\tilde{y}_D\right)\right]\right\}\times\left[1+\sum_{m=1}^{\infty}\exp\left(-2m\sqrt{b}y_{eD}\right)\right] \tag{5.6}$$

Eq.5.1 and Eq.5.6 become

$$\begin{aligned} p_{Dv} &= 2\pi t_{DA}+2\pi\frac{y_{eD}}{x_{eD}}\left(\frac{1}{3}-\frac{y_D}{y_{eD}}+\frac{y_D^2+y_{wD}^2}{2y_{eD}^2}\right)+ \\ &\quad +2\sum_{k=1}^{\infty}\frac{1}{k}\cos\left(k\pi\frac{x_D}{x_{eD}}\right)\cos\left(k\pi\frac{x_{wD}}{x_{eD}}\right)G\left(x_{eD},y_{eD},y_{wD},y_D,k\right) \end{aligned} \tag{5.7}$$

Where

$$\begin{aligned} G\left(x_{eD},y_{eD},y_{wD},y_D,\sqrt{b}\right) &= \frac{\cosh\sqrt{b}\left(\frac{y_{eD}-\left|y_D-y_{wD}\right|}{x_{eD}}\right)+\cosh\sqrt{b}\left(\frac{y_{eD}-\left(y_D+y_{wD}\right)}{x_{eD}}\right)}{\sinh\left(\sqrt{b}\frac{y_{eD}}{x_{eD}}\right)} \\ &= \left\{\exp\left(-\sqrt{b}\frac{\left|y_D-y_{wD}\right|}{x_{eD}}\right)+\exp\left[-\sqrt{b}\left(\frac{2y_{eD}-\left|y_D-y_{wD}\right|}{x_{eD}}\right)\right]\right\}\times\left[1+\sum_{m=1}^{\infty}\exp\left(-2m\sqrt{b}\frac{y_{eD}}{x_{eD}}\right)\right]+ \\ &\quad +\left\{\exp\left(-\sqrt{b}\frac{\left(y_D+y_{wD}\right)}{x_{eD}}\right)+\exp\left[-\sqrt{b}\left(\frac{2y_{eD}-\left(y_D+y_{wD}\right)}{x_{eD}}\right)\right]\right\}\times\left[1+\sum_{m=1}^{\infty}\exp\left(-2m\sqrt{b}\frac{y_{eD}}{x_{eD}}\right)\right] \\ &= \left[1+\sum_{m=1}^{\infty}\exp\left(-2m\sqrt{b}\frac{y_{eD}}{x_{eD}}\right)\right]\left\{\begin{array}{l}\exp\left(-\sqrt{b}\frac{\left|y_D-y_{wD}\right|}{x_{eD}}\right)+\exp\left(-\sqrt{b}\frac{\left(y_D+y_{wD}\right)}{x_{eD}}\right)+ \\ +\exp\left[-\sqrt{b}\left(\frac{2y_{eD}-\left|y_D-y_{wD}\right|}{x_{eD}}\right)\right]+\exp\left[-\sqrt{b}\left(\frac{2y_{eD}-\left(y_D+y_{wD}\right)}{x_{eD}}\right)\right]\end{array}\right\} \end{aligned} \tag{5.8}$$

Where $b=(k\pi)^2$

5.3.2. Valko Calculation Method

Valko et al. (2000) proposed a different method to calculate the influence function using Ozkan's solution. The influence function presented in their study only considers the pseudo-steady state pressure distribution with respect to average reservoir pressure. Thus, the term $2\pi t_{DA}$ was not included in the equation of the influence function. In this study, however, the term $2\pi t_{DA}$ is necessary for the influence function to account for the time interval. The calculation procedure is summarized below.

Taking into account the symmetry:

$$a_{v1}[x_D, y_D, x_{wDn}, y_{wDn}, y_{eD}] = \\ = a^1[\max(x_D, x_{wDn}), \max(y_D, y_{wDn}), \min(x_D, x_{wDn}), \min(y_D, y_{wDn}), y_{eD}] \tag{5.9}$$

Where a is defined as (Valko et. al., 2000)

$$a_{v1}[x_D, y_D, x_{wDn}, y_{wDn}, y_{eD}] = 2\pi \frac{y_{eD}}{x_{eD}}\left(\frac{1}{3} - \frac{y_D}{y_{eD}} + \frac{y_D^2 + y_{wD}^2}{2y_{eD}^2}\right) + \\ + 2\sum_{m=1}^{\infty} \frac{1}{m} \cos(m\pi x_D)\cos(m\pi x_{wD}) \frac{\cosh m\pi\left(y_{eD} - |y_D - y_{wD}|\right) + \cosh m\pi\left(y_{eD} - |y_D + y_{wD}|\right)}{\sinh(m\pi y_{eD})} \tag{5.10}$$

-The a^1 term above can be calculated as follows:

$$a_{v1}^1[x_D, y_D, x_{wDn}, y_{wDn}, y_{eD}] = \begin{cases} a_{v1}^0[x_D, y_D, x_{wDn}, y_{wDn}, y_{eD}] & if\ |x_D - x_{wD}| > |y_D - y_{wD}| \\ a_{v1}^0[y_D, x_D, y_{wDn}, x_{wDn}, 1/y_{eD}] & otherwise \end{cases} \tag{5.11}$$

-The equation a^0 can be calculated as

$$a_{v1}[x_D, y_D, x_{wDn}, y_{wDn}, y_{eD}] = 2\pi \frac{y_{eD}}{x_{eD}}\left(\frac{1}{3} - \frac{y_D}{y_{eD}} + \frac{y_D^2 + y_{wD}^2}{2y_{eD}^2}\right) + S_T \tag{5.12}$$

Where

$$S_T = 2\sum_{m=1}^{\infty} \frac{t_m}{m} \cos m\pi \frac{x_D}{x_{eD}} \cos m\pi \frac{x_{wD}}{x_{eD}} \tag{5.13}$$

$$t_m = \frac{\cosh m\pi\left(\frac{y_{eD} - |y_D - y_{wD}|}{x_{eD}}\right) + \cosh m\pi\left(\frac{y_{eD} - |y_D + y_{wD}|}{x_{eD}}\right)}{\sinh m\pi\left(\frac{y_{eD}}{x_{eD}}\right)} \tag{5.14}$$

The infinite sum of equation above can be rewritten in finite approximation as follows (P Valko et. al., 2000):

$$S_T = S_1 + S_2 + S_3 \tag{5.15}$$

$$S_1 = 2\sum_{m=1}^{N} \frac{t_m}{m} \cos(m\pi x_D)\cos(m\pi x_{wD}) \tag{5.16}$$

$$\begin{aligned} S_2 = &-\frac{t_N}{2} \ln\left\{\left[1-\cos(\pi(x_D + x_{wD}))\right]^2 + \left[\sin(\pi(x_D + x_{wD}))\right]^2\right\} \\ &-\frac{t_N}{2} \ln\left\{\left[1-\cos(\pi(x_D - x_{wD}))\right]^2 + \left[\sin(\pi(x_D - x_{wD}))\right]^2\right\} \end{aligned} \tag{5.17}$$

$$S_3 = 2t_N \sum_{m=1}^{N} \frac{1}{m} \cos(m\pi x_D)\cos(m\pi x_{wD}) \tag{5.18}$$

N is the number of term in the summation.

Adding the term $2\pi t_{DA}$ to a_{v1}, we obtain the influence function for vertical well as

$$a_v[x_D, y_D, x_{wDn}, y_{wDn}, y_{eD}, t_{DA}] = 2\pi t_{DA} + a_{v1}[x_D, y_D, x_{wDn}, y_{wDn}, y_{eD}] \tag{5.19}$$

Fig. 5.2 shows the comparison of the influence function values calculated using different calculation methods and equations. The well is at the center of the closed rectangular reservoir and the dimensionless wellbore radius equals 0.000229. The results are in good agreement especially at late time. Since the calculation methods suggested by Ozkan and Valko et al. are for the late time solution, the results for the influence functions fit well into a straight line with a slope of 2π. The solution provided by Marhaendrajana et al. (1999), on the other hand, is good for both early and late time flow. Thus, at small dimensionless time (t_{DA} <0.3), the results by the Marhaendrajana et al. equation are different from those calculated using the Ozkan or Valko et al. equations. However, for this case at smaller dimensionless time (t_{DA} < 0.02), the Marhaendrajana et al. solution could not give a value for the influence function due to calculation errors. Solutions that are applicable for both early time and late time are recommended because

they better represent the actual pressure behavior at the wells. Further discussion on the different solutions is presented later in this report.

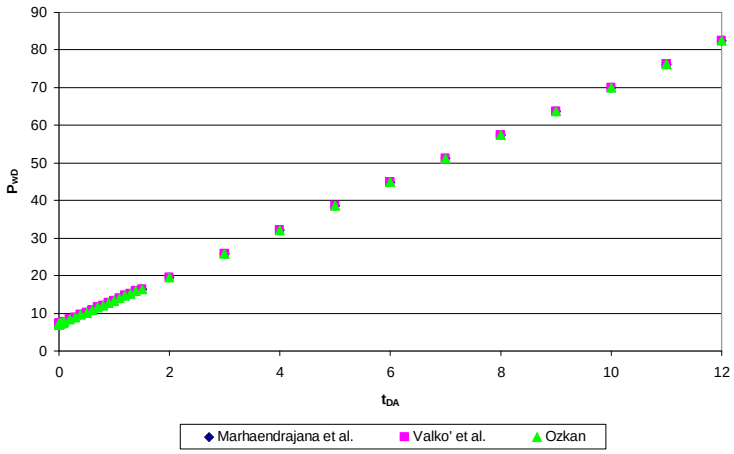


Figure 5.2:. Dimensionless Pressures or Influence functions versus dimensionless time for a fully penetrating vertical well at the center of a closed rectangular reservoir calculated by different methods.

Fig. 5.2 and Table 5.1 show the comparison of the influence function results calculated using the methods mentioned above. The method by Marhaendrajana et al. is good for both the early and late time. However, when the time became very small, this method could not provide any results (see Table 5.1). The results obtained from Ozkan and Valko et al. can fit into a straight line. However, at early time when transient flow is dominant, these results are not accurate as the equations are late time solutions.

5.3.3. Shape Factor Calculation

Shape factors are used to calculate pressure at wells at different locations in a reservoir of a certain shape. Letting C_A denote the shape factor, we have the well known shape factor equation (Dietz, 1965):

$$p_{wD} = 2\pi t_{DA} + 0.5 \ln \frac{4A}{e^{\gamma} C_A L^2} \tag{5.20}$$

with L = r_w, L_{xf} and $L_h/2$ for vertical well, vertically fractured well and horizontal well respectively and γ is Euler's constant ($\gamma = 0.5772\ldots$)

Table 5.1: Dimensionless Pressures or Influence functions of the well at the center of the 5x4 synthetic field calculated from different equations/methods

t_{DA}	Marhaendrajana et al.	Valko' et al.	Ozkan
1.00E-04	N/A	7.072	7.072
5.00E-04	N/A	7.074	7.074
1.00E-03	N/A	7.077	7.077
5.00E-03	N/A	7.103	7.102
1.00E-02	N/A	7.134	7.134
2.00E-02	6.830	7.197	7.197
3.00E-02	7.033	7.260	7.260
4.00E-02	7.177	7.322	7.322
5.00E-02	7.291	7.385	7.385
6.00E-02	7.386	7.448	7.448
7.00E-02	7.470	7.511	7.511
8.00E-02	7.546	7.574	7.574
9.00E-02	7.618	7.637	7.637
1.00E-01	7.687	7.699	7.699
2.00E-01	8.328	8.328	8.328
3.00E-01	8.956	8.956	8.956
4.00E-01	9.584	9.584	9.584
5.00E-01	10.213	10.213	10.213
6.00E-01	10.841	10.841	10.841
7.00E-01	11.469	11.469	11.469
8.00E-01	12.098	12.098	12.098
9.00E-01	12.726	12.726	12.726
1.00E+00	13.354	13.354	13.354
1.10E+00	13.983	13.983	13.983
1.20E+00	14.611	14.611	14.611
1.30E+00	15.239	15.239	15.239
1.40E+00	15.868	15.868	15.868
1.50E+00	16.496	16.496	16.496
2.00E+00	19.637	19.637	19.637
3.00E+00	25.921	25.921	25.921
4.00E+00	32.204	32.204	32.204
5.00E+00	38.487	38.487	38.487
6.00E+00	44.770	44.770	44.770
7.00E+00	51.053	51.053	51.053
8.00E+00	57.337	57.337	57.337
9.00E+00	63.620	63.620	63.620
1.00E+01	69.903	69.903	69.903

Thus, the shape factor can be calculated using the following equation

$$C_A = Exp\left[\left(4\pi t_{DA} - 2p_{wD}\right) + Log\frac{4A}{L^2 e^{\gamma}}\right] \tag{5.21}$$

Table 5.2 presents the dimensionless coordinates for all the wells in the 5x4 synthetic field. Other data includes $x_{eD} = y_{eD} = 1$ and $r_{wD} = 0.00029$. Table 5.3 shows the shape factors for all the wells in the 5x4 synthetic field calculated using P_{wD} results (influence functions) from the different calculation techniques and Eq. 5.21. As shown in Table 5.3, the shape factors are in good agreement. These shape factors can be used to calculate the influence functions using Eq. 5.20.

Table 5.2: Dimensionless coordinates of the wells in the 5x4 synthetic field

Wells	x_{wDv}	y_{wDv}
I01	0.1774	0.8226
I02	0.8226	0.8226
I03	0.5000	0.5000
I04	0.1774	0.1774
I05	0.8226	0.1774
P01	0.5000	0.8226
P02	0.1774	0.5000
P03	0.8226	0.5000
P04	0.5000	0.1774

Table 5.3: Shape factors for the wells in the 5x4 synthetic field calculated from different equations/methods

Wells	C_A		
	Marhaendrajana et al.	Valko et al.	Ozkan
I01	0.8456	0.8470	0.8457
I02	0.8436	0.8442	0.8437
I03	30.8823	30.8811	30.8848
I04	0.8476	0.8470	0.8477
I05	0.8456	0.8442	0.8457
P01	6.6951	6.7012	6.6959
P02	6.7072	6.7097	6.7080
P03	6.6951	6.6926	6.6959
P04	6.7072	6.7012	6.7080

5.4. Simulation Results

5.4.1. General Model Descriptions

A dual porosity simulation model was set up for this study in ECLIPSE 100 simulator (2006). The keyword DUALPORO was used for the dual porosity model. The grid system was kept the same as in the case of the single porosity reservoir presented in the previous chapter. Since the simulator defined half of the layers as matrix blocks and the other half as fracture blocks, the number of layers for the model needed to be an even number. In our case, the number of layers was increased to six and the thickness of each layer was changed to 10 ft so that the total thickness stayed the same at 60 ft. The Kazemi dual porosity model was used by the simulator. This model is similar to the Warren and Root model, however, instead of dividing the reservoir into sugar-cube blocks, the Kazemi model defined matrix blocks and fractures as slabs and was proved to be a more effective dual porosity model for numerical simulation (Kazemi, 1969).

The Dual Porosity Matrix-Fracture Coupling parameter (SIGMA keyword) was set to 0.12. The SIGMA keyword represents the interfacial contact between matrix and fracture blocks. Further details can be found in the ECLIPSE 100 manual (2006). The No Dual Porosity Permeability Multiplier (NODPPM keyword) option was chosen. Thus, as defined by the simulator, the effective permeabilities at different directions (x, y and z) can be entered directly. The effective permeabilities were set to be equal to those in the single porosity cases as described in chapter 4 for easy comparison. Thus these dual-porosity systems and the corresponding single-porosity systems as described in Chapter 4 are comparable.

5.4.2. Isotropic Reservoir

Similar to the homogeneous case of the single porosity 5x4 Synthetic field, the effective permeability for both x and y directions in this case was set to 100 mD. Table 5.4 and Fig. 5.3 present the interwell connectivity coefficient results for this case. The results are approximately equal to the results from the single porosity homogeneous reservoir as shown in Fig. 5.4 (also see Table 4.2). Table 5.5 and Fig. 5.5 show the corresponding relative interwell permeability results for this reservoir. The calculated relative interwell permeability is in good agreement with the input effective permeability of the model of 100 mD.

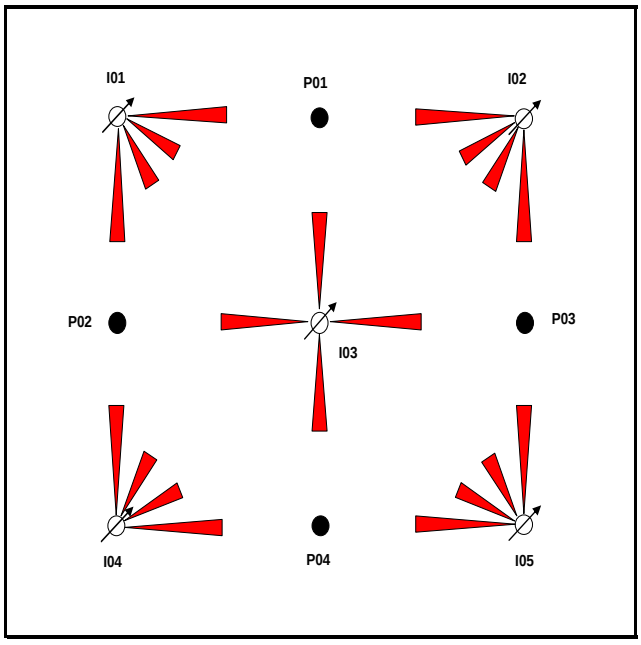


Figure 5.3. Representation of the interwell connectivity coefficients for the case of 5x4 Isotropic Dual-porosity Reservoir.

Table 5.4: Interwell Connectivity Coefficient results from simulation data for the isotropic dual-porosity 5x4 Synthetic field (A_s = 0.005201)

	P1	P2	P3	P4	Sum
β_{0j} (psia)	-1481.8	-1481.0	-1483.9	-1483.1	-5930
I1	0.24	0.25	0.14	0.15	0.79
I2	0.24	0.14	0.25	0.15	0.79
I3	0.22	0.21	0.22	0.22	0.86
I4	0.15	0.24	0.15	0.24	0.78
I5	0.15	0.15	0.24	0.24	0.79
Sum	1.00	1.00	1.00	1.00	

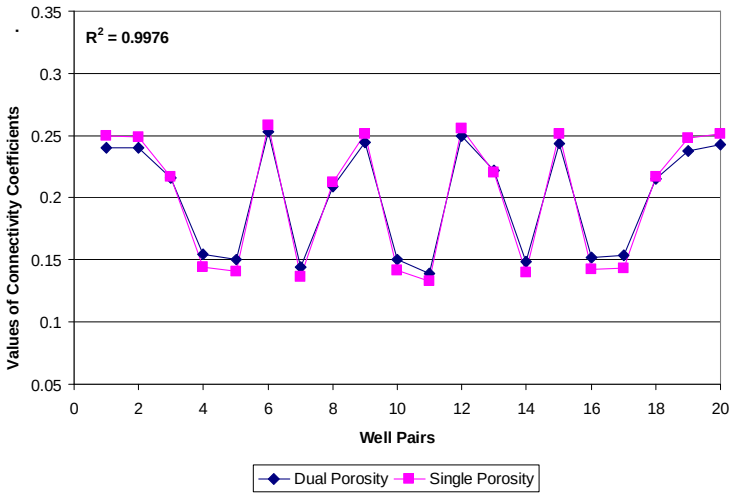


Figure 5.4. Comparison of interwell connectivity coefficient results for the case of 5x4 Isotropic Dual-porosity and Homogeneous single-porosity Reservoir.

Table 5.5: Relative interwell permeability results for the 5x4 Isotropic Dual-porosity Synthetic Field (k_{ref}=100mD, Δt_{eq} = 12.16 days)

	P1	P2	P3	P4	Ave.
I1	99	106	98	104	102
I2	99	100	104	105	102
I3	94	92	97	94	94
I4	106	101	102	98	102
I5	103	103	101	101	102
Ave.	100	100	100	100	

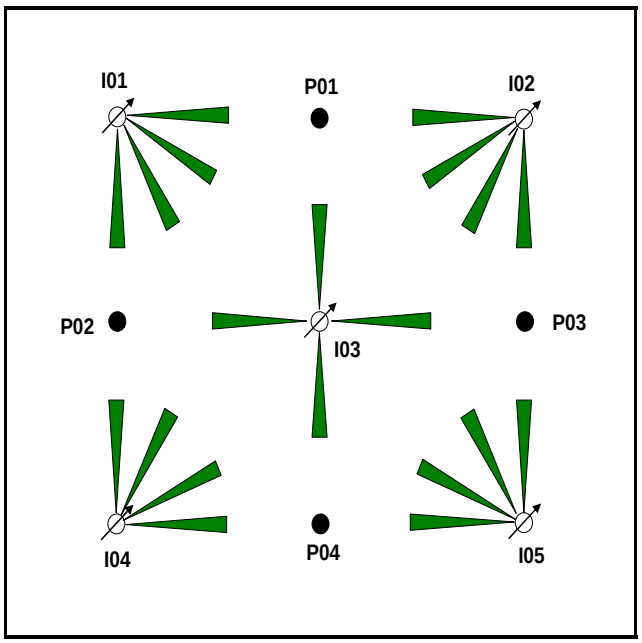


Figure 5.5. Representation of relative interwell permeability for the case of 5x4 Isotropic Dual-porosity Reservoir.

5.4.3. Anisotropic Reservoir

The effective permeability in the x direction (k_x = 100 mD) for the 5x4 dual porosity reservoir was tenfold the effective permeability in the y direction (k_y = 1000 mD). Table 5.6 and Fig. 5.6 show the results for the interwell connectivity coefficients. As expected, the results are very close to the results obtained in the single porosity homogeneous reservoir.

Table 5.6: Interwell Connectivity Coefficient results from simulation data for the Anisotropic Dual-porosity 5x4 Synthetic field

	P1	P2	P3	P4	Sum
β_{0j} (psia)	-414.6	-492.2	-492.2	-415.2	-1814
I1	0.34	0.17	0.15	0.08	0.74
I2	0.34	0.16	0.17	0.08	0.74
I3	0.16	0.36	0.36	0.16	1.03
I4	0.09	0.16	0.15	0.34	0.74
I5	0.07	0.16	0.17	0.35	0.74
Sum	1.00	1.00	1.00	1.00	

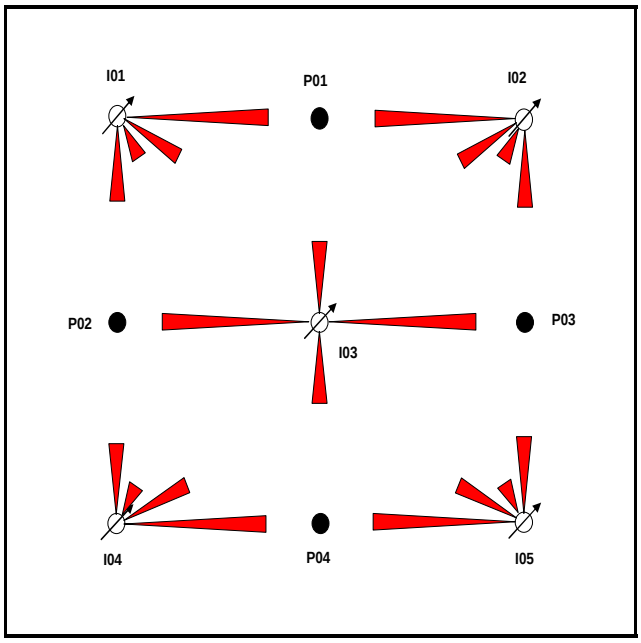


Figure 5.6. Representation of the connectivity coefficients for the case of 5x4 Anisotropic Dual-porosity Reservoir.

Table 5.7 and Fig. 5.7 present the corresponding relative interwell permeabilities with the equivalent time of 12.16 days, and the reference permeability of 316 mD. As shown on both figures, the inverted arrows clearly show the anisotropy of the reservoir with high connectivity (high relative interwell permeability) in the x direction and lower connectivity in the y direction.

Table 5.7: Relative interwell permeability results for the 5x4 Anisotropic Dual-porosity Synthetic Field (k_{ref}=316mD, Δt_{eq} = 12.16 days)

	P1	P2	P3	P4	Ave.
I1	297	135	170	102	176
I2	296	173	137	102	177
I3	139	311	311	139	225
I4	109	133	170	291	176
I5	96	174	137	302	177
Ave.	187	185	185	187	

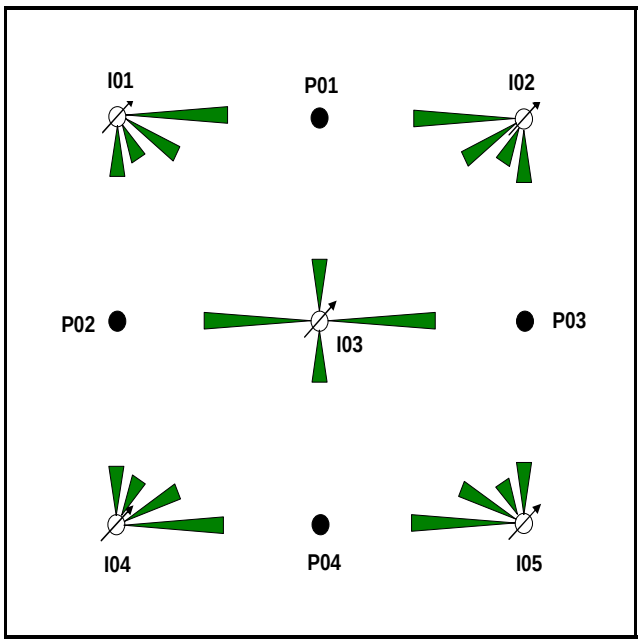


Figure 5.7. Representation of relative interwell permeability for the case of 5x4 Anisotropic Dual-porosity Reservoir.

5.4.4. Dual porosity reservoir with high permeability channel

Fig. 5.8 shows the top view of the fracture permeability distribution for this case. The cells in red color indicate high permeability in both x and y directions. Similar to the high permeability channel case in chapter 4, the permeability of the channel was ten-fold (1000 mD) of that in other areas of the reservoir.

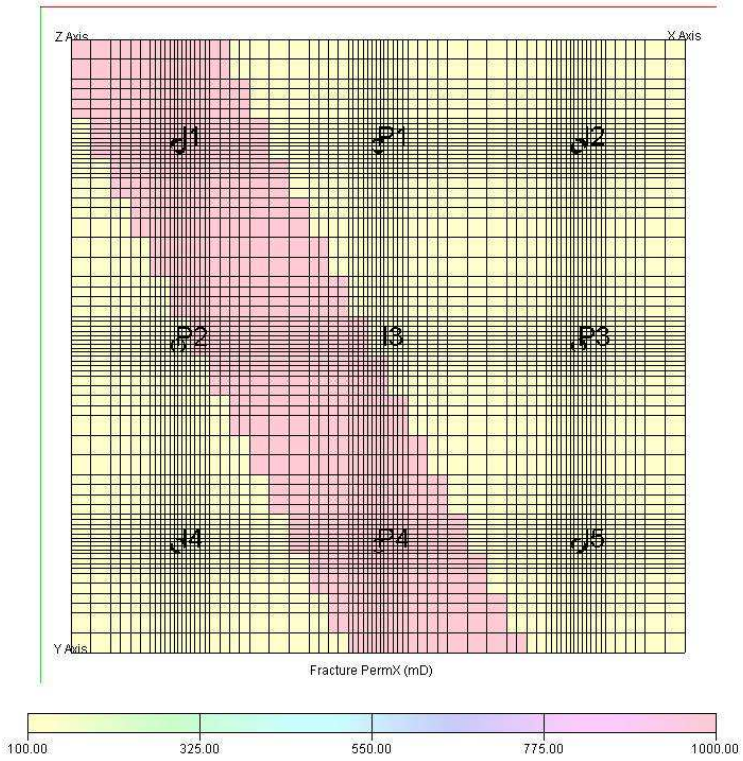


Figure 5.8. Top view of the simulation model showing the fracture permeability in x direction for the High permeability channel case of the 5x4 Dual porosity Synthetic field.

Table 5.8 and Fig. 5.9 show the results for the interwell connectivity coefficients. Similar to previous cases, the results are in good agreement with the results obtained in the single porosity reservoir with high permeability channel. The high permeability channel is indicated by the high connectivity of well I01, which is located in the channel, with other producers.

Table 5.8: Interwell Connectivity Coefficient results from simulation data for the 5x4 Dual-porosity Synthetic field with High permeability channel

	P1	P2	P3	P4	Sum
β_{0j} (psia)	-1078.9	-914.6	-1199.2	-578.1	-3771
I1	0.55	0.59	0.39	0.46	2.00
I2	0.15	0.07	0.19	0.09	0.50
I3	0.12	0.14	0.15	0.17	0.58
I4	0.08	0.11	0.10	0.13	0.42
I5	0.09	0.09	0.17	0.15	0.50
Sum	1.00	1.00	1.00	1.00	

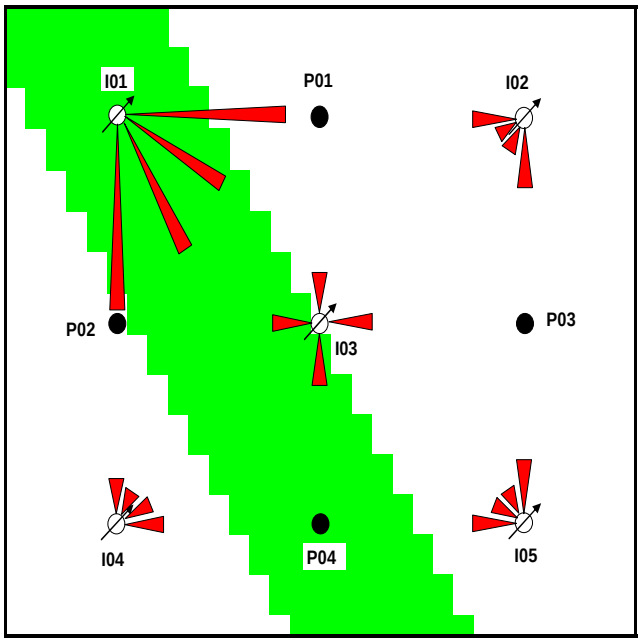


Figure 5.9. Representation of the interwell connectivity coefficients for the 5x4 Dual-porosity Synthetic field with High permeability channel.

Table 5.9 and Fig. 5.10 present the corresponding relative interwell permeabilities with the equivalent time of 12.16 days, and the reference permeability of 300 mD. The magnitude of the relative interwell permeabilities reflects the formation permeability of 100 mD and the channel permeability of 1000 mD.

Table 5.9: Relative interwell permeability results for the 5x4 Dual-porosity Synthetic Field with High permeability channel (k_{ref}=300mD, Δt_{eq} = 12.16 days)

	P1	P2	P3	P4	Ave.
I1	476	509	379	442	452
I2	119	93	151	107	117
I3	104	117	125	139	121
I4	102	79	117	100	99
I5	105	107	135	116	116
Ave.	181	181	181	181	

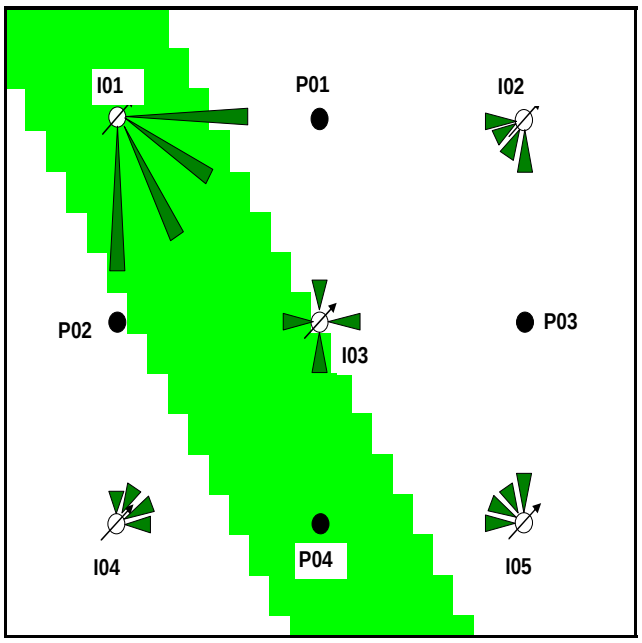


Figure 5.10. Representation of relative interwell permeability the 5x4 Dual-porosity Synthetic field with High permeability channel.

5.4.5. Dual porosity reservoir with a partially sealing barrier

Fig. 5.11 below shows the top view of the fracture permeability distribution for this case. The cells in white color were set to inactive and thus, served as a partially sealing barrier. Table 5.10 and Fig. 5.12 show the results for the interwell connectivity coefficients. Similar to previous cases, the results are close to the results obtained in the single porosity homogeneous reservoir. Table 5.11 and Fig. 5.13 present the corresponding relative interwell permeabilities with the equivalent time of 12.16 days, and the reference permeability of 100 mD.

Similar to results of the single porosity reservoir, the partially sealing barrier can be inferred from the interwell connectivity and the relative interwell permeability.

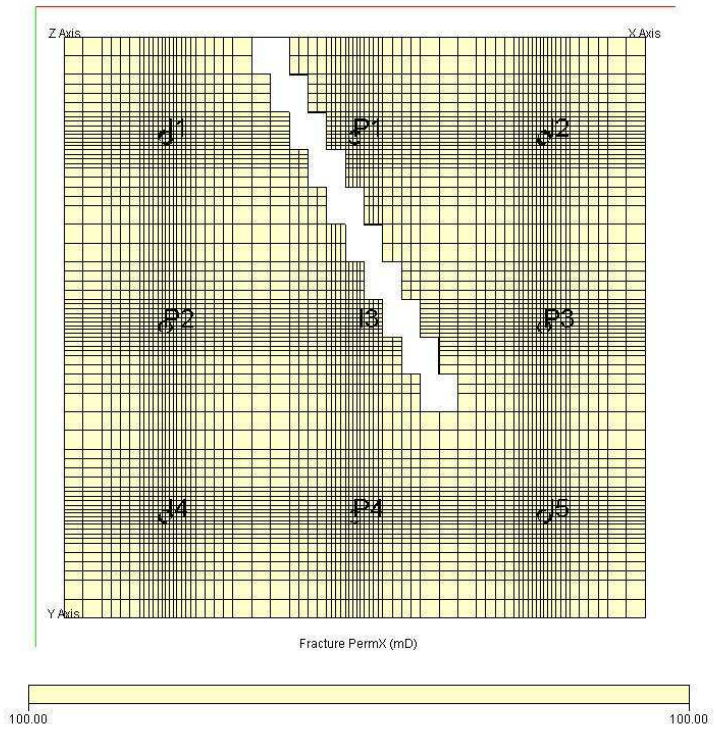


Figure 5.11. Top view of the simulation model showing the fracture permeability in x direction for the 5x4 Dual porosity Synthetic field with a Partially sealing barrier.

Table 5.10: Interwell Connectivity Coefficient results from simulation data for the 5x4 Dual-porosity Synthetic field with a Partially sealing barrier

	P1	P2	P3	P4	Sum
β_{0j} (psia)	-2179.0	-1321.2	-1807.8	-1462.9	-6771
I1	0.08	0.28	0.09	0.15	0.61
I2	0.48	0.10	0.36	0.15	1.08
I3	0.14	0.21	0.16	0.21	0.72
I4	0.12	0.26	0.13	0.24	0.75
I5	0.17	0.15	0.27	0.25	0.84
Sum	0.99	1.01	0.99	1.00	

Table 5.11: Relative interwell permeability results for the 5x4 Dual-porosity Synthetic Field with a Partially sealing barrier (k_{ref}=100mD, Δt_{eq} = 12.16 days)

	P1	P2	P3	P4	Ave.
I1	19	121	73	104	79
I2	216	79	156	104	139
I3	63	93	68	92	79
I4	86	108	93	100	97
I5	115	103	112	104	108
Ave.	100	101	100	101	

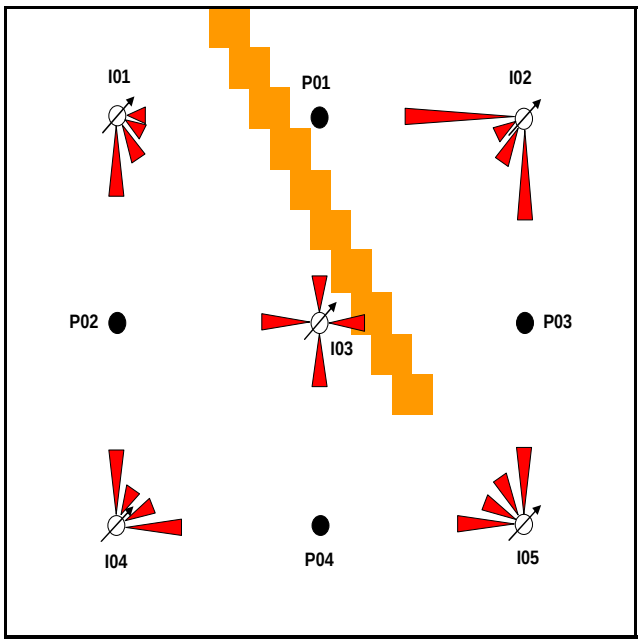


Figure 5.12. Representation of the connectivity coefficients for the 5x4 Dual-porosity reservoir with a Partially sealing barrier.

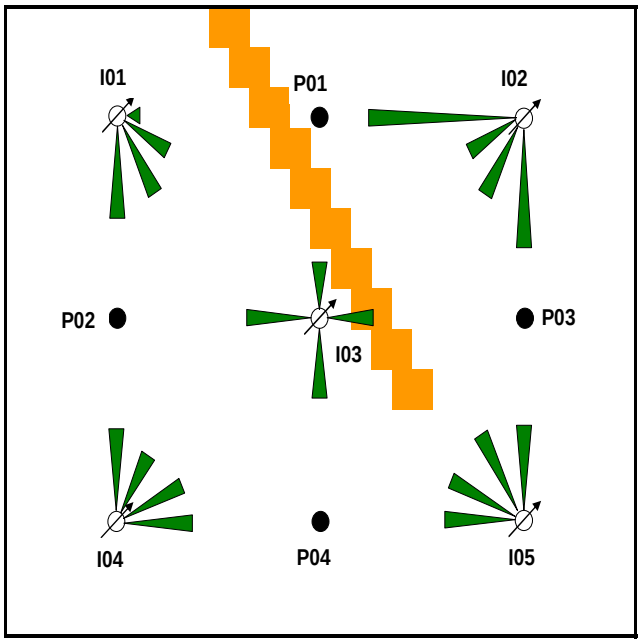


Figure 5.13. Representation of relative interwell permeabilities for the 5x4 Dual-porosity reservoir with a Partially sealing barrier.

5.4.6. Dual porosity reservoir with a sealing barrier

Fig. 5.14 is the top view of the fracture permeability distribution for the dual porosity reservoir with a sealing barrier case. Again, the cells in white color were set to inactive and thus, served as a sealing barrier. As seen on the figure, the barrier completely seals the reservoir and divides it into two compartments. Based on the change in average reservoir pressure calculated from each producer, the compartmentalization can be inferred.

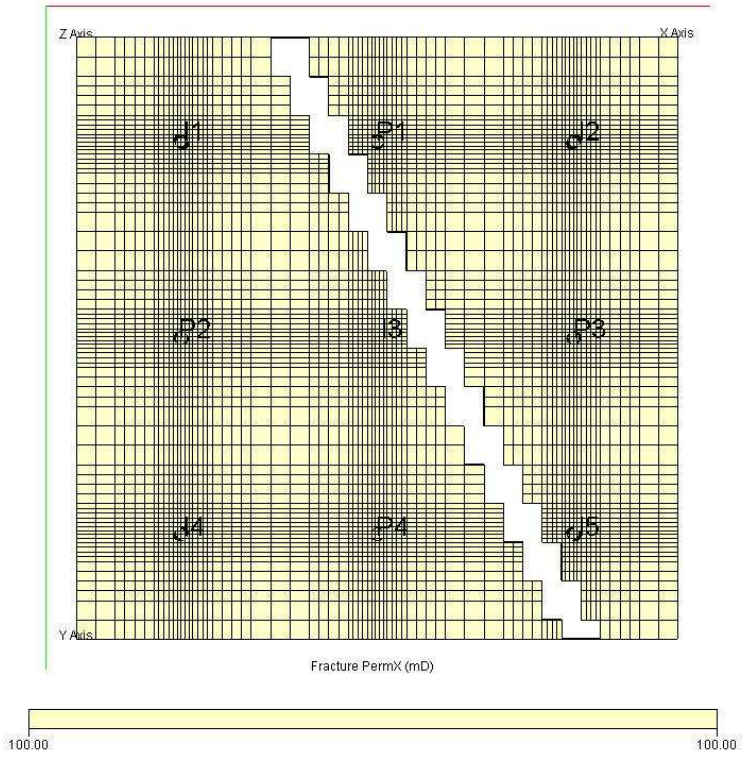


Figure 5.14. Top view of the simulation model showing the fracture permeability in x direction for the 5x4 Dual porosity Synthetic field with a Sealing barrier.

Table 5.12 and Fig. 5.15 show the results for the interwell connectivity coefficients. Similar to previous cases, the results are very close to the results obtained in the single porosity reservoir. Small connectivity coefficients are still observed for

injectors and producers on different sides of the barrier. This could be due to noises in the data as well as numerical errors.

Table 5.12: Interwell Connectivity Coefficient results from simulation data for the 5x4 Dual porosity Synthetic field with a Sealing barrier

	P1	P2	P3	P4	Sum
β_{0j} (psia)	-1460.0	-1780.1	-1149.5	-2033.2	-6423
I1	0.03	0.33	0.02	0.24	0.63
I2	0.49	0.09	0.39	0.12	1.10
I3	0.08	0.26	0.09	0.29	0.72
I4	0.06	0.31	0.06	0.35	0.78
I5	0.13	0.12	0.26	0.13	0.65
Sum	0.80	1.11	0.82	1.13	

Table 5.13 and Fig. 5.16 present the corresponding relative interwell permeabilities with the equivalent time of 12.16 days, and the reference permeability of 100 mD. A cut-off coefficient of 0.13 was applied to eliminate the low connectivity coefficients. Thus, the relative interwell permeabilities corresponding to the coefficients lower than 0.13 were set to zeros. The resulting relative interwell permeabilities show a clear presence of the sealing barrier.

Table 5.13: Relative interwell permeability results for the 5x4 Dual porosity Synthetic field with a Sealing barrier (k_{ref}=100mD, Δt_{eq} = 12.16 days)

	P1	P2	P3	P4	Ave.
I1	0.00	143.44	0.00	148.71	73.04
I2	224.68	0.00	173.82	0.00	99.63
I3	0.00	114.15	0.00	127.18	60.33
I4	0.00	134.08	0.00	152.29	71.59
I5	0.00	0.00	110.82	0.00	27.71
Ave.	45	78	57	86	

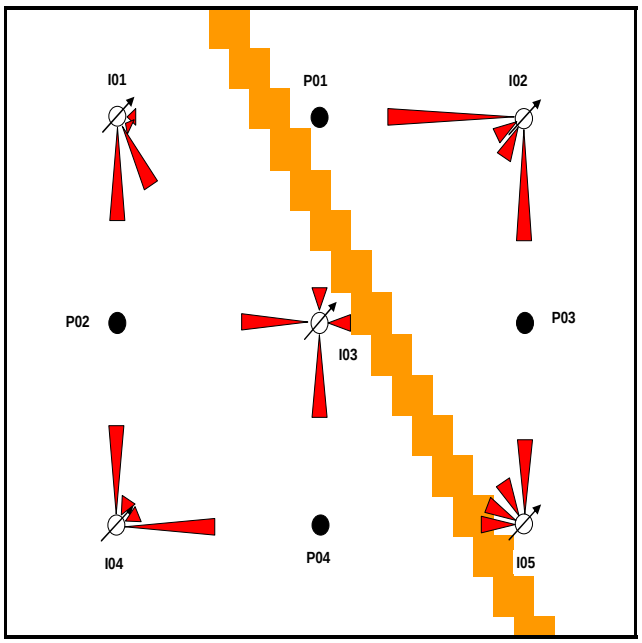


Figure 5.15. Representation of the connectivity coefficients for the 5x4 Dual porosity Synthetic field with a Sealing barrier.

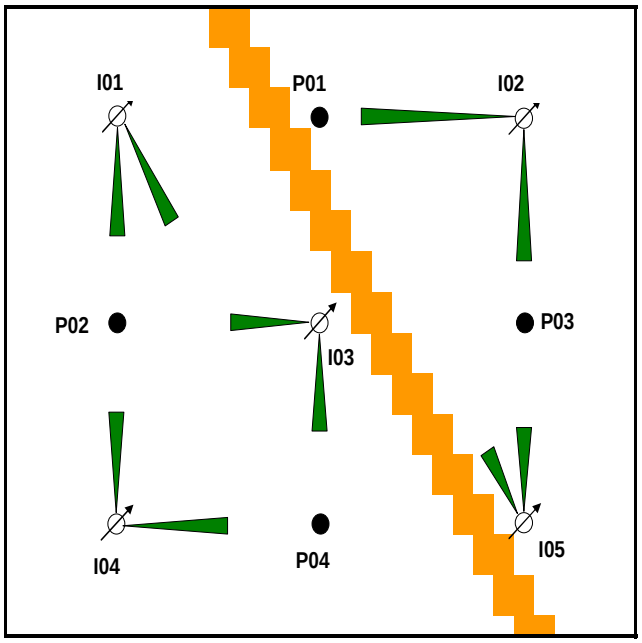


Figure 5.16. Representation of relative interwell permeability for the 5x4 Dual porosity Synthetic field with a Sealing barrier.

Table 5.14 presents the results for the average reservoir pressure change as described in Chapter 4 for all producers in each case of the 5x4 synthetic field. Except for the case with the presence of the sealing barrier, the changes in average reservoir pressure for all the cases are consistent and close to the corresponding values for single porosity reservoirs. For the case with the presence of sealing barrier, the resulting pressure change for wells P01 and P03 (about 181 psi) is different from those for wells P02 and P04 (390 psi) indicating two different reservoir compartments (see Chapter 4).

Table 5.14: Average pressure change (ΔP_{ave}) after each time interval for different cases of 5x4 Dual-porosity Synthetic Field

Cases	P1	P2	P3	P4
Isotropic Reservoir	286.36	286.51	285.67	285.82
Anisotropic Reservoir	286.13	286.05	286.04	285.57
Channel	286.08	286.27	285.77	286.02
Partially Sealing Barrier	288.03	305.29	291.57	300.53
Sealing Barrier	181.24	390.59	180.94	390.07

5.4.7. 25x16 isotropic reservoir

Fig. 5.17 shows the top view of the fracture permeability distribution for the dual porosity 25x16 synthetic field. As seen on the figure, the permeability was set to 100 mD.

Table 5.15 presents the results for the interwell connectivity coefficients. Similar to the case of 25x16 homogeneous single porosity field, good results were obtained for the connectivity coefficients with the asymmetry coefficient (A_s) of 0.00799. Table 5.16 and Fig. 5.18 present the corresponding relative interwell permeabilities with the equivalent time of 5.6 days, and the reference permeability of 100 mD. A cut-off coefficient of 0.07 was applied to eliminate the low connectivity coefficients. Thus, the

relative interwell permeabilities corresponding to the coefficients lower than 0.07 were set to zeros.

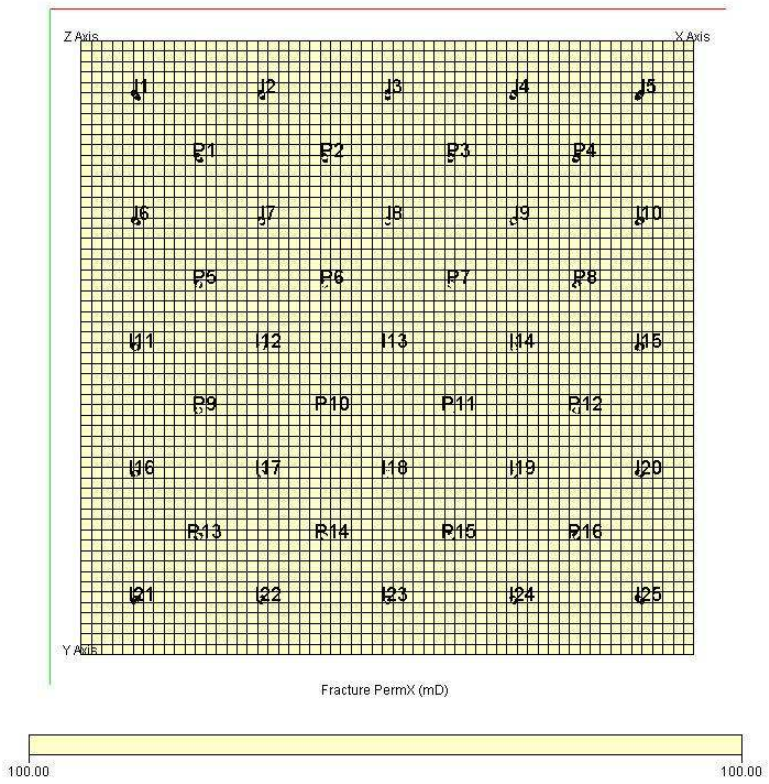


Figure 5.17. Top view of the grid system showing the fracture permeability in the x-direction for 25x16 Dual porosity Synthetic field.

Fig. 5.19 shows the plot of all relative interwell permeability values. The results show two groups of permeabilities. One group for the pairs of wells close to each other has value close to the input value of 100 mD. The other group for pairs with wells that are far away from each other has a permeability value of about 50 mD which is lower than the input value. This is different from the homogeneous single porosity case. However, if we compare the interwell connectivity coefficients as shown in Fig. 5.20, it is clear that the interwell connectivity coefficients for both cases are the same. Thus, the difference is due to the equation used to calculate the influence functions. In this case,

the late time solution was used, so when the interwell connectivity coefficients became very small, they were translated to very small values of time and the influence functions were not accurate any more. On the other hand, when influence functions are calculated from a solution which is good for both early time and late time, they are able to give relative interwell permeability closer to the actual input permeability. Thus, for a field with many low interwell connectivity coefficients, the influence function should be calculated from a solution applicable for both early time and late time.

The average reservoir pressure changes for the producers are about the same at 353 psi. Based on the material balance, this pressure change is equivalent to the pore volume of the reservoir or a porosity of 0.302, which is in agreement with the input porosity of 0.3.

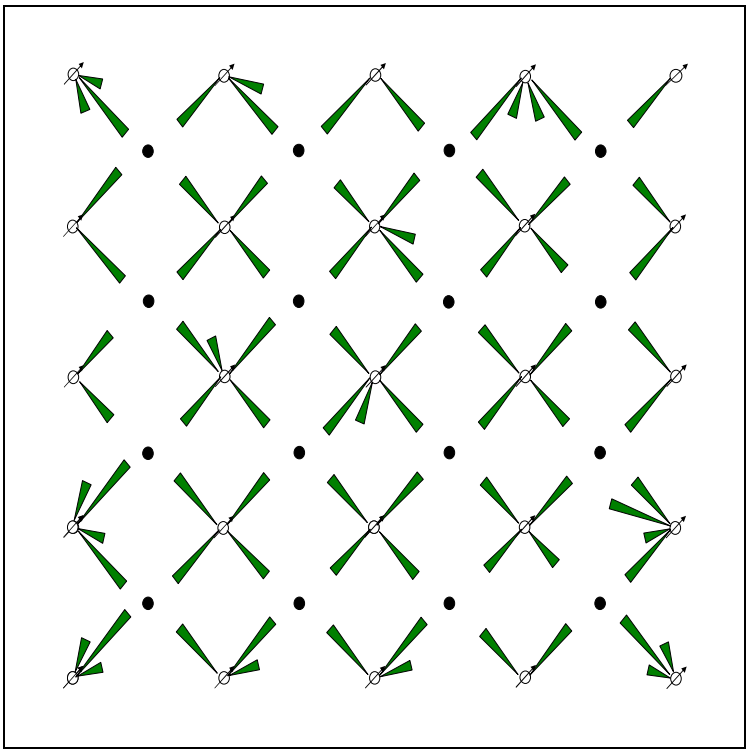


Figure 5.18. Representation of relative interwell permeability for the 25x16 Isotropic Dual-porosity Reservoir.

Table 5.15: Interwell Connectivity Coefficient results from simulation data for the 25x16 isotropic dual-porosity Synthetic field (A_s = 0.00799)

	P1	P2	P3	P4	P5	P6	P7	P8	P9	P10	P11	P12	P13	P14	P15	P16	Sum
I1	0.15	0.05	0.02	0.00	0.06	0.04	0.02	0.00	0.04	0.03	0.02	0.00	0.03	0.03	0.02	0.01	0.52
I2	0.12	0.12	0.06	0.04	0.03	0.04	0.03	0.03	0.01	0.02	0.02	0.02	0.00	0.01	0.02	0.02	0.60
I3	0.05	0.12	0.12	0.05	0.03	0.04	0.04	0.02	0.03	0.02	0.02	0.01	0.03	0.02	0.02	0.00	0.62
I4	0.02	0.04	0.13	0.14	0.01	0.03	0.05	0.06	0.00	0.01	0.03	0.04	0.00	0.01	0.02	0.03	0.60
I5	0.02	0.02	0.04	0.13	0.03	0.02	0.02	0.04	0.03	0.02	0.02	0.02	0.03	0.02	0.02	0.02	0.50
I6	0.13	0.04	0.01	0.00	0.12	0.04	0.02	0.02	0.05	0.03	0.02	0.02	0.03	0.02	0.02	0.02	0.60
I7	0.11	0.09	0.03	0.01	0.10	0.10	0.03	0.02	0.04	0.04	0.03	0.03	0.02	0.02	0.03	0.04	0.72
I8	0.03	0.09	0.10	0.05	0.03	0.09	0.10	0.05	0.03	0.04	0.04	0.04	0.02	0.01	0.02	0.03	0.76
I9	0.03	0.05	0.11	0.11	0.02	0.03	0.09	0.10	0.01	0.02	0.03	0.04	0.01	0.02	0.03	0.03	0.71
I10	0.02	0.03	0.04	0.11	0.02	0.03	0.04	0.11	0.01	0.02	0.03	0.05	0.01	0.02	0.03	0.03	0.61
I11	0.04	0.04	0.04	0.04	0.10	0.03	0.03	0.03	0.10	0.03	0.02	0.02	0.04	0.02	0.01	0.01	0.61
I12	0.05	0.05	0.04	0.03	0.10	0.10	0.04	0.02	0.10	0.09	0.03	0.01	0.03	0.03	0.02	0.01	0.76
I13	0.01	0.03	0.03	0.02	0.03	0.09	0.09	0.03	0.04	0.10	0.10	0.04	0.04	0.05	0.05	0.03	0.79
I14	0.02	0.02	0.04	0.05	0.02	0.04	0.10	0.10	0.02	0.04	0.10	0.10	0.02	0.03	0.03	0.03	0.75
I15	0.02	0.02	0.03	0.04	0.03	0.03	0.04	0.11	0.02	0.03	0.04	0.11	0.01	0.02	0.02	0.04	0.64
I16	0.04	0.03	0.02	0.00	0.06	0.03	0.02	0.00	0.13	0.05	0.02	0.00	0.14	0.05	0.02	0.00	0.60
I17	0.02	0.02	0.02	0.02	0.04	0.04	0.02	0.02	0.11	0.10	0.03	0.02	0.12	0.10	0.03	0.01	0.72
I18	0.01	0.01	0.02	0.03	0.02	0.03	0.04	0.04	0.04	0.10	0.10	0.05	0.03	0.09	0.10	0.05	0.76
I19	0.01	0.02	0.03	0.03	0.01	0.02	0.04	0.05	0.02	0.03	0.09	0.10	0.03	0.04	0.09	0.09	0.72
I20	0.02	0.02	0.02	0.02	0.02	0.02	0.02	0.03	0.02	0.03	0.04	0.11	0.03	0.03	0.05	0.13	0.59
I21	0.02	0.02	0.01	0.01	0.03	0.02	0.01	0.01	0.06	0.04	0.02	0.01	0.15	0.06	0.02	0.01	0.51
I22	0.01	0.02	0.02	0.02	0.02	0.02	0.02	0.02	0.04	0.04	0.03	0.02	0.12	0.12	0.05	0.03	0.60
I23	0.02	0.02	0.01	0.01	0.02	0.03	0.02	0.01	0.03	0.04	0.04	0.03	0.04	0.11	0.12	0.06	0.62
I24	0.02	0.02	0.02	0.03	0.02	0.02	0.03	0.03	0.02	0.02	0.04	0.05	0.01	0.03	0.11	0.12	0.60
I25	0.01	0.02	0.02	0.02	0.01	0.02	0.03	0.03	0.01	0.02	0.04	0.06	0.01	0.02	0.05	0.15	0.53
Sum	1.00	1.00	1.00	1.00	1.00	1.00	1.00	1.00	1.00	1.00	1.00	1.00	1.00	1.00	1.00	1.00	

Table 5.16: Relative interwell permeability results for the 25x16 Isotropic Dual-porosity Synthetic Field (k_{ref}=100mD, Δt_{eq} = 5.6 days)

	P01	P02	P03	P04	P05	P06	P07	P08	P09	P10	P11	P12	P13	P14	P15	P16
I01	111	37	0	0	49	0	0	0	0	0	0	0	0	0	0	0
I02	86	100	55	0	0	0	0	0	0	0	0	0	0	0	0	0
I03	0	99	99	0	0	0	0	0	0	0	0	0	0	0	0	0
I04	0	0	106	112	0	0	51	55	0	0	0	0	0	0	0	0
I05	0	0	0	86	0	0	0	0	0	0	0	0	0	0	0	0
I06	94	0	0	0	99	0	0	0	0	0	0	0	0	0	0	0
I07	85	78	0	0	88	87	0	0	0	0	0	0	0	0	0	0
I08	0	77	86	0	0	87	96	56	0	0	0	0	0	0	0	0
I09	0	0	95	83	0	0	83	82	0	0	0	0	0	0	0	0
I10	0	0	0	81	0	0	0	90	0	0	0	0	0	0	0	0
I11	0	0	0	0	73	0	0	0	75	0	0	0	0	0	0	0
I12	49	0	0	0	93	97	0	0	83	89	0	0	0	0	0	0
I13	0	0	0	0	0	86	86	0	0	98	96	0	0	61	0	0
I14	0	0	0	0	0	0	91	89	0	0	91	86	0	0	0	0
I15	0	0	0	0	0	0	0	93	0	0	0	93	0	0	0	0
I16	0	0	0	0	58	0	0	0	110	0	0	0	109	43	0	0
I17	0	0	0	0	0	0	0	0	96	90	0	0	95	84	0	0
I18	0	0	0	0	0	0	0	0	0	90	94	0	0	80	89	0
I19	0	0	0	0	0	0	0	0	0	0	83	86	0	0	76	65
I20	0	0	0	0	0	0	0	0	0	0	0	83	0	0	41	94
I21	0	0	0	0	0	0	0	0	50	0	0	0	117	40	0	0
I22	0	0	0	0	0	0	0	0	0	0	0	0	91	101	48	0
I23	0	0	0	0	0	0	0	0	0	0	0	0	0	92	101	52
I24	0	0	0	0	0	0	0	0	0	0	0	0	0	0	84	88
I25	0	0	0	0	0	0	0	0	0	0	0	43	0	0	37	112

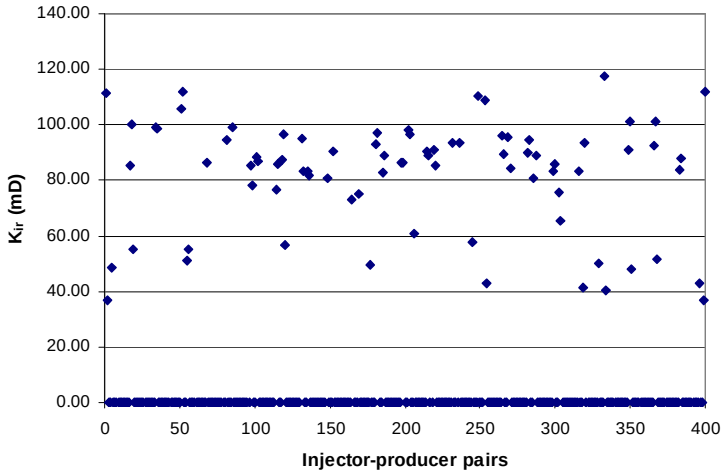


Figure 5.19. Relative interwell permeability results for the case of 25x16 Isotropic Dual-porosity Reservoir.

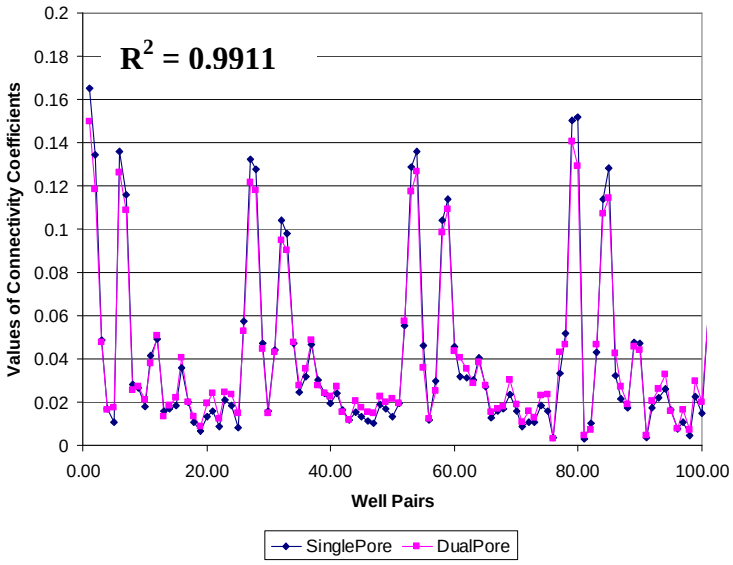


Figure 5.20. Representation of relative interwell permeability for the case of 25x16 Isotropic Dual-porosity Reservoir.

5.5. Conclusions

Some of the conclusions drawn from this chapter are:

- The technique can be applied to dual-porosity systems to infer interwell connectivity as it is applied to single porosity systems;

- Since the late time analytical solution for single porosity and dual porosity reservoirs are identical, the results from simulation data obtained from a dual porosity system are close to the results from its single porosity counterpart given the same effective permeability;

- For the cases where many interwell connectivity coefficients are small, the use of pseudo-steady state solutions to calculate the influence functions may lead to errors because the small coefficients can be translated to the early time effects. Thus, the solutions good for both transient and late-time periods should be used to calculate influence functions for more accurate results.

.

CHAPTER 6 – APPLICATIONS OF THE INTERWELL CONNECTIVITY TEST TO HYDRAULICALLY FRACTURED WELLS

Bottom hole pressure fluctuations were used to determine the interwell connectivity in a waterflood where all the vertical wells are hydraulically fractured. The previous chapters only considered reservoirs with vertical wells without any hydraulic fractures.

A late time solution for a well with a fully penetrating vertical fracture in a closed rectangular reservoir was used to calculate the influence functions and the relative interwell permeabilities. The results were then used to obtain information on reservoir anisotropy, high permeability channels and transmissibility barriers.

Different synthetic reservoir models were analyzed including: homogeneous, anisotropic reservoirs, reservoirs with high permeability channel, partially sealing barrier and sealing barrier. The case where the fractures are of different fracture half lengths is also considered.

6.1. Literature Review

Hydraulic fracturing is an important well stimulation technique that has been widely used in the oil and gas industry. Gringarten et al. (1974) provided a solution for a fully penetrating vertically fractured well in an infinite horizontal reservoir. Gringarten obtained the solution for the pressure distribution of the fracture by Green's function and the product solution method using source functions (Gringarten and Ramey, 1973). Tiab (1994) provided a technique to analyze transient pressure data of fractured wells using both pressure and pressure derivative. His technique has been applied successfully to pressure analysis of vertically fractured well in closed systems for both uniform flux and infinite conductivity vertical fracture cases with wellbore storage and mechanical skin

factor. The technique was also applied to finite conductivity hydraulic vertical fracture (Tiab, 2005). Several other studies were focused on the type curve matching technique to obtain a quick approximation of reservoir parameters from a fractured well pressure response. The technique provides best results when used simultaneously with a specific analysis method for each flow regime (Cinco-Ley et al.,1981 & Tiab et al., 1987). Ozkan (1999) provided pressure distribution solutions for both uniform flux and infinite conductivity fractures in a closed rectangular reservoir in Laplace space.

6.2. Analytical Model and Calculation Approach

For a hydraulically fractured well, for simplicity, the late time solution for a uniform flux fracture in a closed rectangular reservoir provided by Ozkan was used (Ozkan, 1988):

$$p_{Df} = a_f = 2\pi t_{DA} + 2\pi \frac{y_{eD}}{x_{eD}}\left(\frac{1}{3} - \frac{y_D}{y_{eD}} + \frac{y_D^2 + y_{wD}^2}{2y_{eD}^2}\right) + \\ + \frac{2x_{eD}}{\pi}\sum_{k=1}^{\infty}\frac{1}{k^2}\sin\left(k\pi\frac{1}{x_{eD}}\right)\cos\left(k\pi\frac{x_{wD}}{x_{eD}}\right)\cos\left(k\pi\frac{x_D}{x_{eD}}\right)\frac{\cosh k\pi\left(\frac{y_{eD} - |y_D - y_{wD}|}{x_{eD}}\right) + \cosh k\pi\left(\frac{y_{eD} - (y_D + y_{wD})}{x_{eD}}\right)}{\sinh\left(k\pi\frac{y_{eD}}{x_{eD}}\right)} \quad (6.1)$$

Where the L term in the definitions of dimensionless quantities is $L = L_{xf}$ which is the fracture half length. For the case of infinite conductivity fractures, the dimensionless pressure can be obtained by evaluating the above equation at $x_D = 0.732$ (Gringarten et al., 1974). In term of the G equation as described in the last section, Eq. 6.1 can be written as:

$$p_{Df} = 2\pi t_{DA} + 2\pi \frac{y_{eD}}{x_{eD}}\left(\frac{1}{3} - \frac{y_D}{y_{eD}} + \frac{y_D^2 + y_{wD}^2}{2y_{eD}^2}\right) + \\ + \frac{2x_{eD}}{\pi}\sum_{k=1}^{\infty}\frac{1}{k^2}\sin\left(k\pi\frac{1}{x_{eD}}\right)\cos\left(k\pi\frac{x_{wD}}{x_{eD}}\right)\cos\left(k\pi\frac{x_D}{x_{eD}}\right)G\left(x_{eD}, y_{eD}, y_{wD}, y_D, k\right) \quad (6.2)$$

Table 6.1 presents the dimensionless coordinates for all the vertically fractured wells in the 5x4 Synthetic field given the same fracture half length of 145 ft. Other data include $x_{eD} = y_{eD} = 21.38$ and $r_{wD} = 0.0049$.

Table 6.1: Dimensionless coordinates of the fractured wells in the 5x4 synthetic field

Wells	x_{wDf}	y_{wDf}
I01	3.7931	17.5862
I02	17.5862	17.5862
I03	10.6897	10.6897
I04	3.7931	3.7931
I05	17.5862	3.7931
P01	10.6897	17.5862
P02	3.7931	10.6897
P03	17.5862	10.6897
P04	10.6897	3.7931

Table 6.2 shows the shape factors for all the wells in the 5x4 synthetic field calculated using P_{wD} results (influence functions) from the different calculation techniques and Eq. 5.21. As shown in Table 6.2, the shape factors are in good agreement. These shape factors can be used to calculate the influence functions using Eq. 5.20.

Table 6.2: Shape factors for the fractured wells in the 5x4 synthetic field calculated for different fracture types

Wells	C_{Af}	
	Uniform Flux	Infinite Conductivity
I01	0.1144	0.2665
I02	0.1140	0.1606
I03	4.1698	7.5580
I04	0.1144	0.2665
I05	0.1140	0.1606
P01	0.9083	1.6560
P02	0.9026	1.9678
P03	0.9003	1.3396
P04	0.9083	1.6560

6.3. Simulation Results

6.3.1. Model Descriptions

The grids in the small areas containing the wells were refined using the Local Grid Refinement (LGR) options. Thus, there are nine LGRs in this model. Fig. 6.1 shows the top view of the permeability distribution for this case. The LGRs can be seen at each well. Fig. 6.2 is a permeability distribution plot showing the cross sectional through three wells. The hydraulic fractures are represented in red indicating high permeability. The LGR areas are 300ft x 20ft each with a global grid configuration of 13 x 1 which is refined to a grid configuration of 65 x 25. No refinement in the vertical direction was applied. Thus, the number of layers in the LGRs stayed at five layers. Fig. 6.3 presents a zoom-in top view of a LGR containing a high permeability strip representing a hydraulic fracture. Notice that the permeability of the cell at the tips of the fracture was set to zero following the assumption that there was no flow through the tips of the fracture. The permeability of the fractures was set to 8000 Darcys. The width of the fractures was 0.8 ft and the fracture half-lengths were the same at 145 ft. Thus, the dimensionless fracture conductivity for every fracture, which is the product of fracture permeability and fracture width divided by the product of formation permeability and fracture half-length, is equal to 441. Thus, according to previous studies (Tiab, 1994 and Cinco-Ley and Samaniego, 1981), the fractures can be considered as infinite conductivity fractures (dimensionless fracture conductivity is larger than 300). The porosity of the fracture was input as 0.6 which is higher than the porosity of the formation of 0.3.

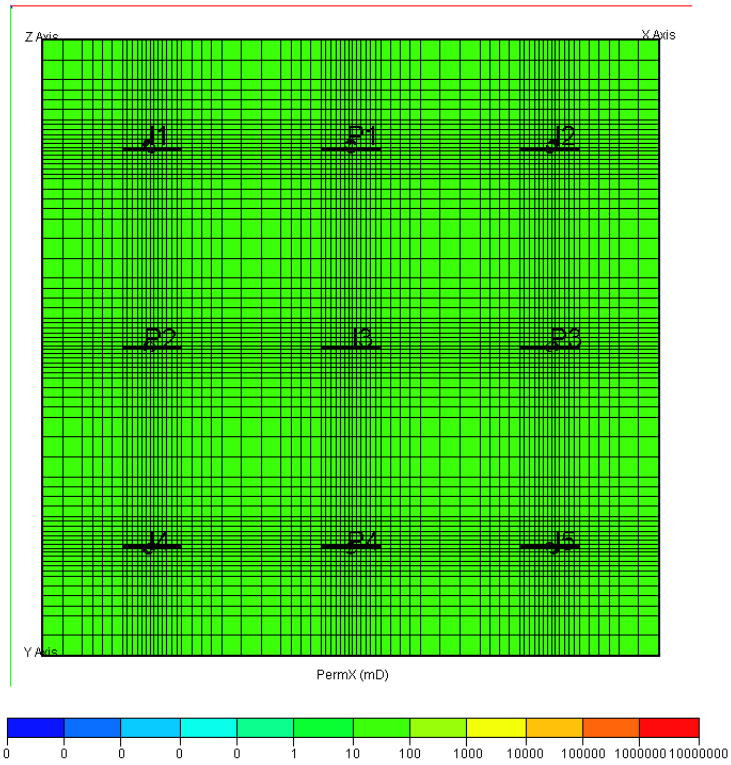


Figure 6.1. Top view of the simulation model showing the LGRs at the fractured wells in the homogeneous 5x4 synthetic field.

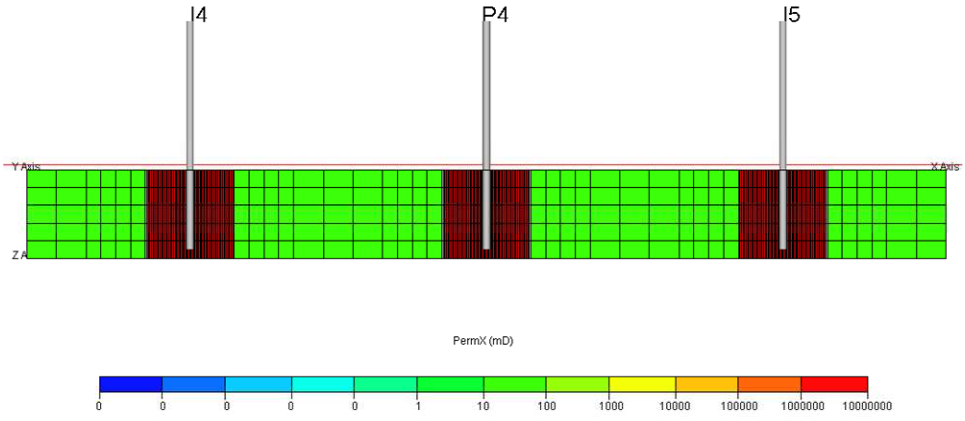


Figure 6.2. Cross sectional view showing three wells and the hydraulic fractures in the 5x4 homogeneous synthetic Reservoir.

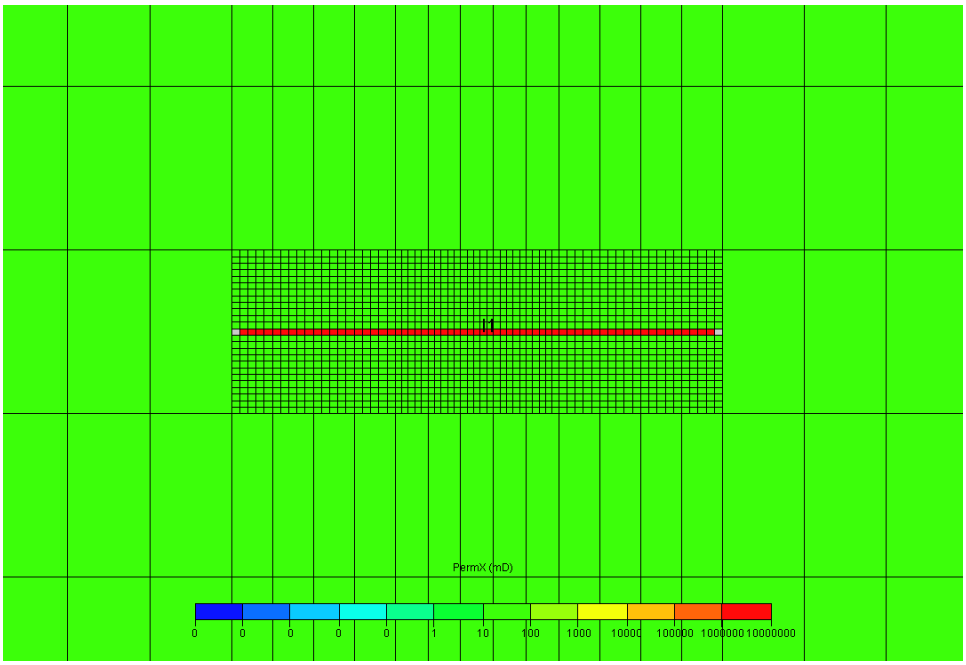


Figure 6.3. A zoom-in view of a LGR showing a high permeability strip representing a hydraulic fracture - 5x4 homogeneous reservoir.

6.3.2. Homogeneous reservoir with hydraulic fractures

Table 6.3 and Fig. 6.4 show the results for the interwell connectivity coefficients. Similar to previous cases, the results are as good as the results obtained in the case of homogeneous reservoir with vertical wells only with asymmetry coefficient of 0.0048. Table 6.4 and Fig. 6.5 present the corresponding relative interwell permeabilities with the equivalent time of 5.66 days, and the reference permeability of 100 mD. The difference between the high and low interwell connectivity coefficients is more significant than in the case of vertical wells suggesting an observation well is less affected by a far away active fractured well than by a vertical unfractured well of the same distance away. This is reasonable because with the same flow rate, the pressure drop in a fractured well is less than its unfractured counterpart.

Table 6.3: Interwell Connectivity Coefficient results from simulation data for the 5x4 Homogeneous Synthetic field with Hydraulic fractured wells (A_s = 0.0048)

	P1	P2	P3	P4	Sum
β_{0j} (psia)	-223.6	-226.1	-225.7	-223.6	-899
I1	0.32	0.31	0.06	0.06	0.75
I2	0.32	0.06	0.31	0.06	0.75
I3	0.24	0.25	0.26	0.25	1.01
I4	0.06	0.31	0.06	0.32	0.75
I5	0.06	0.06	0.31	0.32	0.75
Sum	1.00	1.00	1.00	1.00	

Table 6.4: Relative interwell permeability results for the 5x4 Homogeneous Synthetic Field with Hydraulic fractured wells (k_{ref}=100mD, Δt_{eq} = 5.66 days)

	P1	P2	P3	P4	Ave.
I1	114	112	90	91	102
I2	114	91	111	91	102
I3	92	96	99	93	95
I4	92	111	91	114	102
I5	91	92	113	117	103
Ave.	101	101	101	101	

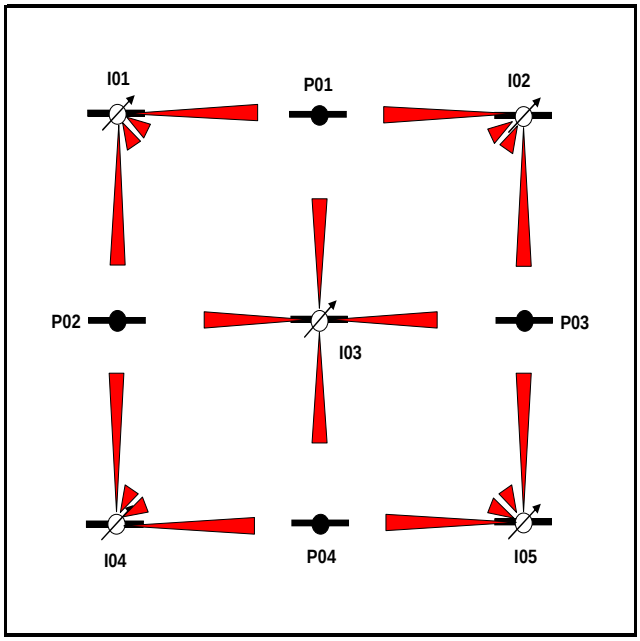


Figure 6.4. Representation of the interwell connectivity coefficients for the 5x4 Homogeneous Reservoir with Hydraulically fractured wells.

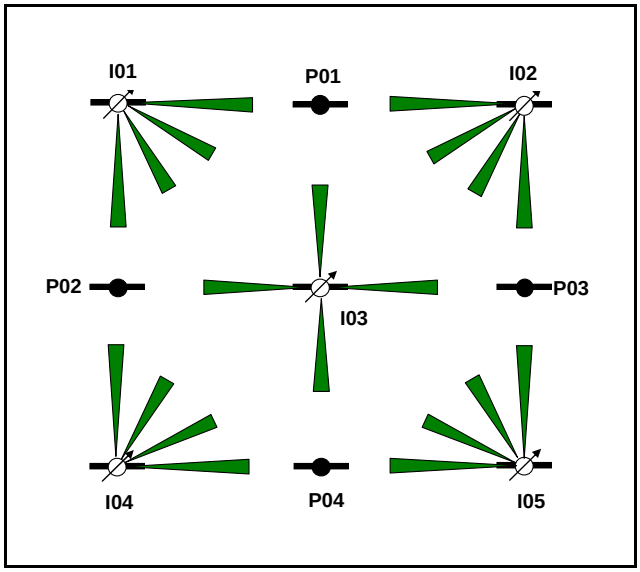


Figure 6.5. Representation of the relative interwell permeability for the 5x4 Homogeneous Reservoir with Hydraulically fractured wells.

6.3.3. Homogeneous reservoir with hydraulic fractures of different fracture half lengths

In this case, the fracture half length can be different for each well. The fracture half length values are presented in Table 6.5. Fig. 6.6 shows the cross section through wells I4, P4 and I5. The fracture cells are shown in red clearly indicating different half lengths (Table 6.5).

Table 6.5: Fracture half lengths for different fractured wells in the 5x4 Homogeneous Synthetic field

Wells	L_{xf} (ft)
I1	76.15
I2	126.93
I3	99.25
I4	76.15
I5	145.40
P1	145.40
P2	99.25
P3	126.93
P4	53.08

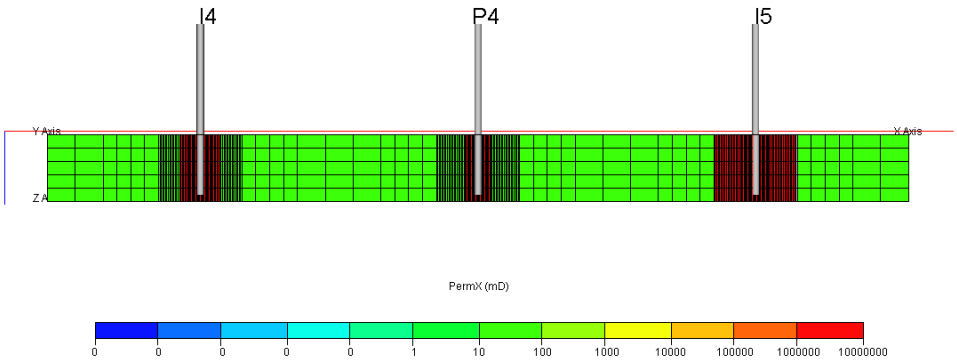


Figure 6.6. Cross sectional view showing three fractured wells of different fracture half lengths in the 5x4 Homogeneous synthetic reservoir.

Table 6.6 and Fig. 6.7 present the interwell connectivity coefficient results for this case. Fig. 6.8 shows the comparison between the interwell connectivity coefficient results obtained from simulation data and calculated using the influence functions. The coefficients are in good agreement with $R^2 = 0.9834$. Table 6.7 and Fig. 6.9 show the corresponding relative interwell permeability results for this reservoir. The calculated relative interwell permeabilities are in good agreement with the input permeability of the model of 100 mD.

Table 6.6: Interwell connectivity coefficient results from simulation data for the 5x4 Homogeneous Reservoir with Vertically Fractured wells of Different Half Lengths

	P1	P2	P3	P4	Sum
β_{0j} (psia)	-246.4	-273.0	-245.4	-293.8	-1059
I1	0.29	0.30	0.06	0.07	0.72
I2	0.33	0.08	0.32	0.07	0.79
I3	0.24	0.25	0.24	0.24	0.98
I4	0.07	0.29	0.06	0.29	0.71
I5	0.07	0.08	0.32	0.34	0.81
Sum	1.00	1.00	1.00	1.00	

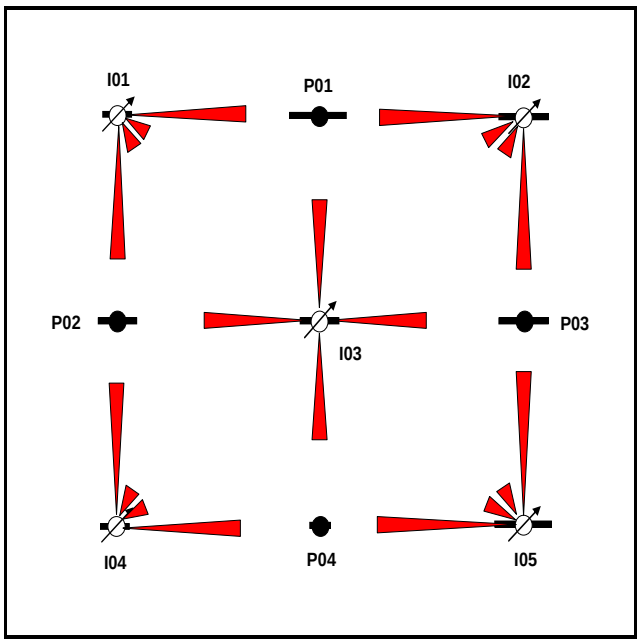


Figure 6.7. Representation of the interwell connectivity coefficients for the 5x4 Homogeneous Reservoir with Vertically Fractured wells of Different half lengths.

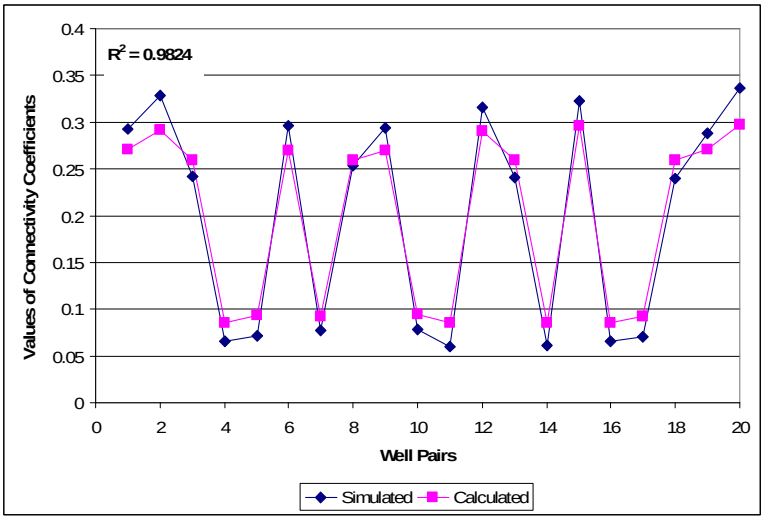


Figure 6.8. Comparison of simulated and calculated interwell connectivity coefficient results for 5x4 Homogeneous Reservoir with Fractured wells of Different fracture half lengths.

Table 6.7: Relative interwell permeability results for the 5x4 Homogeneous Field with Fractured wells of Different fracture half lengths (k_{ref}=100mD, Δt_{eq} = 6.21 days)

	P1	P2	P3	P4	Ave.
I1	111	114	87	90	101
I2	118	93	112	89	103
I3	94	98	93	93	94
I4	90	112	87	109	100
I5	90	93	115	120	105
Ave.	101	102	99	100	

In order to investigate the effect of fracture half lengths on the interwell connectivity coefficients, a graph of the maximum values of the coefficients for every injectors versus their fracture half lengths was plotted as shown on Fig. 6.10. Except for well I03, which is at the center of the reservoir, other wells positions can be considered as equivalent to each other due to the symmetry of the reservoir. A clear trend is shown on Fig. 6.10. The higher the fracture half-lengths are, the larger the maximum coefficient values become. Well I01 and I04 have the same fracture half length and thus, the maximum coefficients for those two wells are the same. Thus, the longer the fracture half length of an active fractured well is, the more influence the well has on nearby observation wells and the less influence it has on far-away wells.

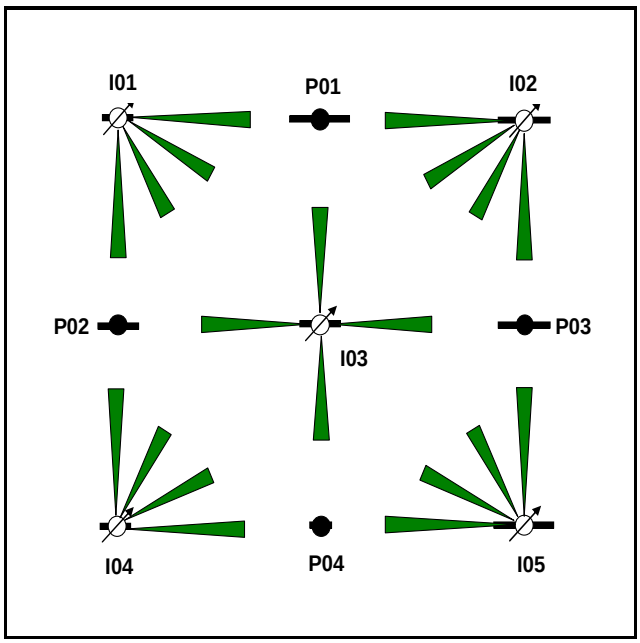


Figure 6.9. Representation of relative interwell permeability for the 5x4 Homogeneous Reservoir with Vertical fractures of Different half lengths.

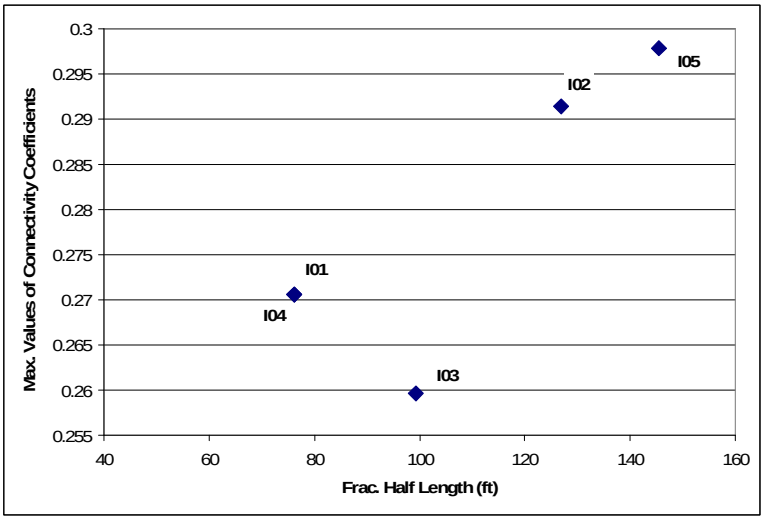


Figure 6.10. Maximum values of interwell connectivity coefficients versus fracture half-lengths.

6.3.4. Homogeneous reservoir with hydraulic fractures with different fracture half lengths for injectors and the same fracture half length for producers

To investigate the effect of fracture half lengths of the producers or the response wells on the interwell connectivity coefficients, the same simulation model as in the previous case was run with an exception that the fracture half lengths of the producers were the same at 145 ft. The fracture half lengths for the injectors are different as indicated in Table 6.5. The results of the interwell connectivity coefficients are presented in Table 6.8.

Table 6.8: Interwell Connectivity Coefficient results from simulation data for the 5x4 Homogeneous Synthetic field – Different fracture half lengths at injectors

	P1	P2	P3	P4	Sum
β_{0j} (psia)	-246.4	-255.8	-239.7	-245.2	-987
I1	0.29	0.30	0.06	0.07	0.71
I2	0.33	0.08	0.32	0.07	0.79
I3	0.24	0.26	0.24	0.24	0.98
I4	0.07	0.29	0.06	0.29	0.71
I5	0.07	0.08	0.32	0.34	0.81
Sum	1.00	1.00	1.00	1.00	

Fig. 6.11 presents a comparison of the interwell connectivity coefficient results for the case of the same and different fracture half lengths at the vertically fractured producers. The results for both cases are identical indicating that the fracture half lengths at the producers or the response wells do not affect the interwell connectivity coefficients. This is also in excellent agreement with the analytical model because the wellbore conditions of the producers or response wells are not part of the equation to calculate interwell connectivity coefficients.

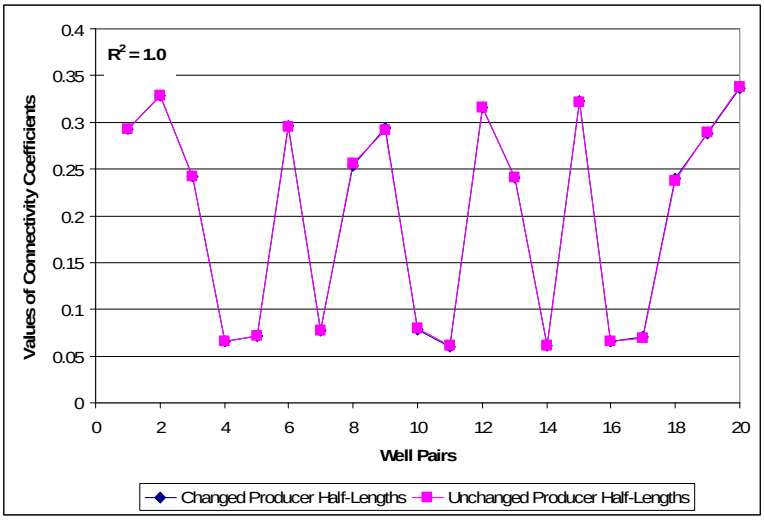


Figure 6.11. Comparison of the interwell connectivity coefficient results for the case of the same vs. different fracture half lengths at the fractured producers in 5x4 Homogeneous Synthetic Reservoir.

6.3.5. Anisotropic Reservoir with hydraulic fractures

Similar to the anisotropic case in the previous chapter, the effective permeability in the x direction is tenfold the fracture permeability in the y direction. Table 6.9 and Fig. 6.12 show the results for the interwell connectivity coefficients. As expected, the results are good indications of the anisotropy with large coefficients for well pairs in the direction of high permeability. Table 6.10 and Fig. 6.13 present the corresponding relative interwell permeabilities with the equivalent time of 5.66 days, and the reference permeability of 316 mD.

Table 6.9: Interwell Connectivity Coefficient results from simulation data for the 5x4 Anisotropic Synthetic field– Hydraulically fractured wells

	P1	P2	P3	P4	Sum
β_{0j} (psia)	-69.6	-96.5	-96.5	-69.6	-332
I1	0.43	0.13	0.10	0.02	0.67
I2	0.43	0.10	0.13	0.02	0.67
I3	0.11	0.55	0.55	0.11	1.32
I4	0.02	0.13	0.10	0.42	0.67
I5	0.02	0.10	0.13	0.43	0.67
Sum	1.00	1.00	1.00	1.00	

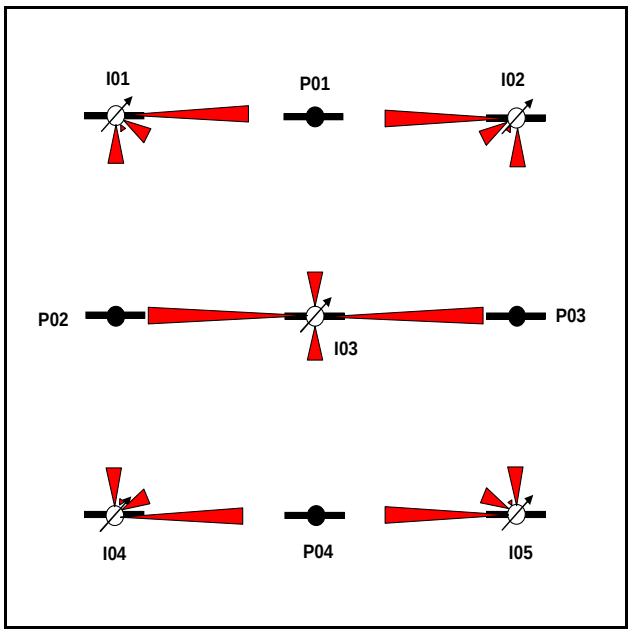


Figure 6.12. Representation of the connectivity coefficients for the case of 5x4 Anisotropic Reservoir – Hydraulically fractured wells.

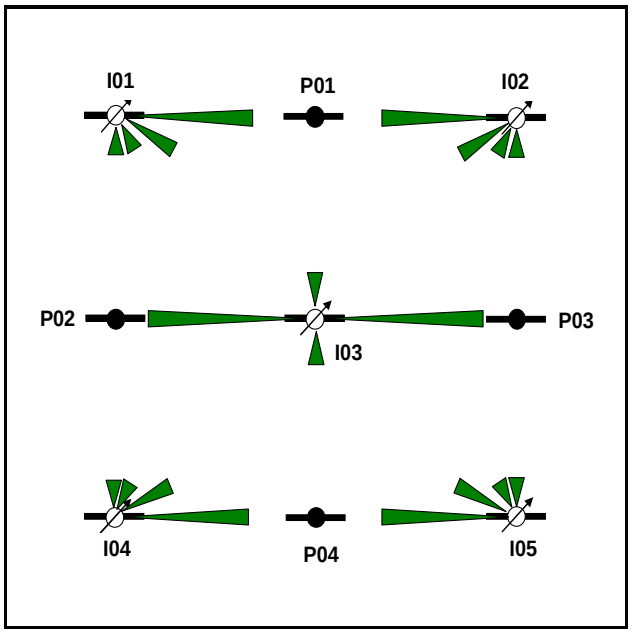


Figure 6.13. Representation of relative interwell permeability for the case of 5x4 Synthetic Reservoir– Hydraulically fractured wells.

Table 6.10: Relative interwell permeability results for the 5x4 Anisotropic Synthetic Field – Hydraulically fractured wells (k_{ref}=316 mD, Δt_{eq} = 5.66 days)

	P1	P2	P3	P4	Ave.
I1	353	75	152	78	164
I2	351	152	76	80	164
I3	90	444	444	90	267
I4	80	75	151	350	164
I5	77	153	77	357	166
Ave.	190	180	180	191	

6.3.6. Reservoir with a high permeability channel

Fig. 6.14 shows the top view of the permeability distribution for this case. The cells in yellow color have high permeability in both x and y direction. Similar to the high permeability channel cases in the previous chapters, the permeability of the channel was ten-fold (1000 mD) of that in the other areas of the reservoir (100 mD). There are nine vertically fractured wells with the same fracture half length of 145 ft.

Table 6.11 and Fig. 6.15 show the results for the interwell connectivity coefficients. Similar to previous cases of high permeability channel, the results reflect well the presence of the channel. Different from the previous cases, well I03 has much higher connectivity with producers P02 and P04. The reason for this is in the previous cases, well I03 was not connected to the high permeability channel while in this case, due the extension provided by the hydraulic fracture, it is directly connected to the channel and has better connectivity with the producers.

Table 6.12 and Fig. 6.16 present the corresponding relative interwell permeabilities with the equivalent time of 5.66 days, and the reference permeability of 300 mD.

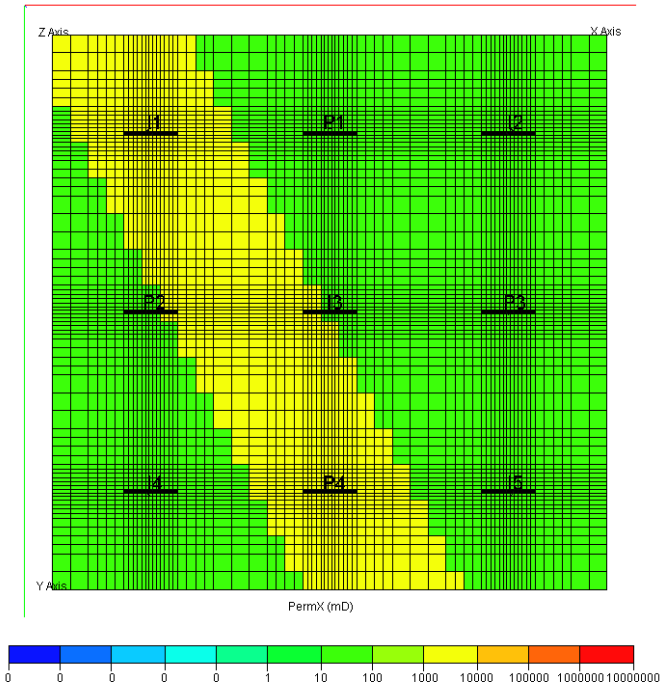


Figure 6.14. Top view of the simulation model showing the permeability in x direction for the high permeability channel case of the 5x4 Synthetic field with fractured wells.

Table 6.11: Interwell Connectivity Coefficient results from simulation data for the 5x4 Synthetic Reservoir with a high permeability channel– Hydraulically fractured wells

	P1	P2	P3	P4	Sum
β_{0j} (psia)	-153.5	-54.1	-194.2	-65.4	-467
I1	0.46	0.42	0.10	0.16	1.14
I2	0.23	0.02	0.28	0.02	0.55
I3	0.26	0.45	0.33	0.53	1.57
I4	0.02	0.07	0.03	0.13	0.25
I5	0.03	0.04	0.25	0.16	0.48
Sum	1.00	1.00	1.00	1.00	

Table 6.12: Relative interwell permeability results for the 5x4 Synthetic Reservoir with a high permeability channel– Hydraulically fractured wells. (k_{ref}=300mD, Δt_{eq} = 5.66 days)

	P1	P2	P3	P4	Ave.
I1	369	337	153	200	265
I2	162	77	210	84	133
I3	202	347	256	412	304
I4	79	24	92	69	66
I5	90	94	184	104	118
Ave.	180	176	179	174	

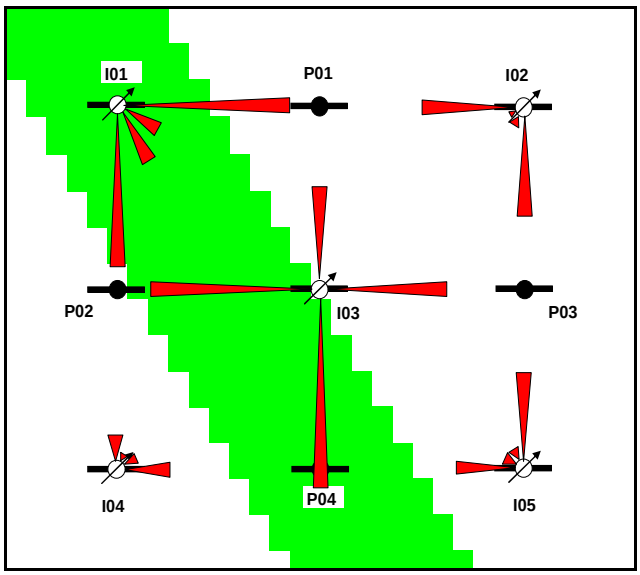


Figure 6.15. Representation of the connectivity coefficients for the case of 5x4 Synthetic Reservoir with a high permeability channel– Hydraulically fractured wells.

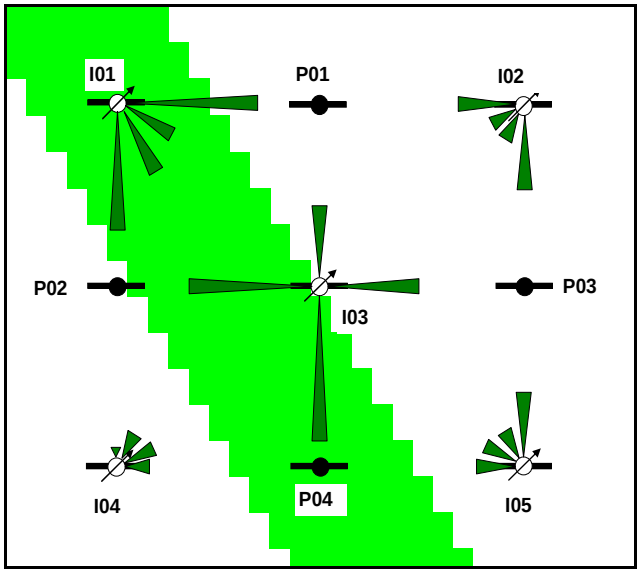


Figure 6.16. Representation of relative interwell permeability for the 5x4 Synthetic Reservoir with a high permeability channel– Hydraulically fractured wells.

6.3.7. Reservoir with a partially sealing barrier

Fig. 6.17 shows the top view of the x-direction permeability distribution for this case. The permeability for the cells in gray color were set to zero and thus, those cells served as a partially sealing barrier. The formation permeability was 100 mD.

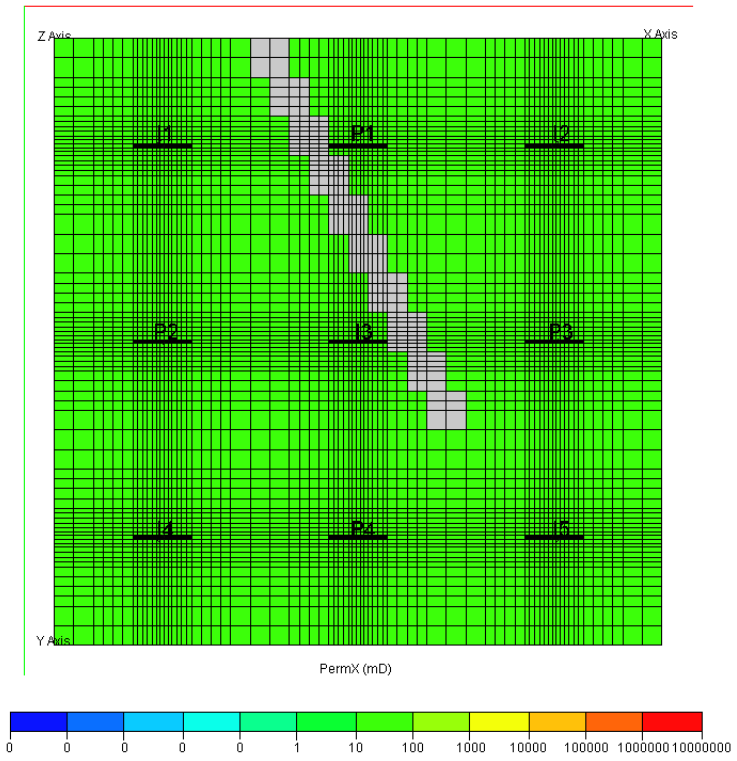


Figure 6.17. Top view of the simulation model showing the permeability distribution in x direction for the case of 5x4 Synthetic field with a partially sealing barrier– Hydraulically fractured wells..

Table 6.13 and Fig. 6.18 show the results for the interwell connectivity coefficients. The presence of the partially sealing barrier is well established by the results. Table 6.14 and Fig. 6.19 present the corresponding relative interwell permeabilities with the equivalent time of 5.66 days, and the reference permeability of 100 mD. The relative interwell permeability for well pair I01-P01 was negative because the influence function for the pair was calculated using the late time solution. When the interwell connectivity coefficients are small, they are translated to early time periods and thus the late time solution becomes inaccurate. Solutions that are good for both early time and late time should be used for better results.

Table 6.13: Interwell Connectivity Coefficient results from simulation data for the 5x4 Synthetic field with partially sealing barrier– Hydraulically fractured wells.

	P1	P2	P3	P4	Sum
β_{0j} (psia)	-440.1	-204.0	-306.9	-226.1	-1177
I1	0.01	0.34	0.01	0.06	0.42
I2	0.79	0.02	0.49	0.06	1.36
I3	0.06	0.25	0.08	0.22	0.61
I4	0.04	0.32	0.05	0.33	0.73
I5	0.11	0.07	0.37	0.33	0.87
Sum	1.00	1.00	1.00	1.00	

Table 6.14: Relative interwell permeability results for the 5x4 Synthetic field with partially sealing barrier– Hydraulically fractured wells (k_{ref}=100mD, Δt_{eq} = 5.66 days)

	P1	P2	P3	P4	Ave.
I1	-40	127	68	90	62
I2	347	71	199	92	177
I3	23	95	29	83	58
I4	80	114	88	119	100
I5	115	95	141	125	119
Ave.	105	101	105	102	

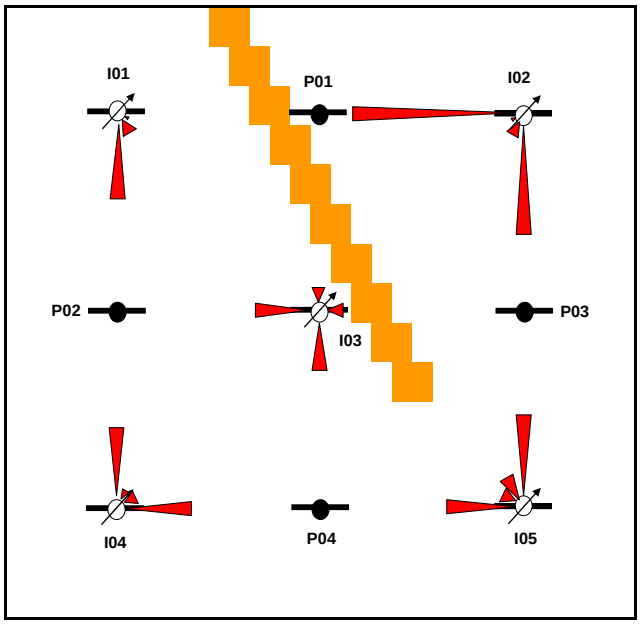


Figure 6.18. Representation of the connectivity coefficients for the case of 5x4 Dual-porosity reservoir with a partially sealing barrier– Hydraulically fractured wells.

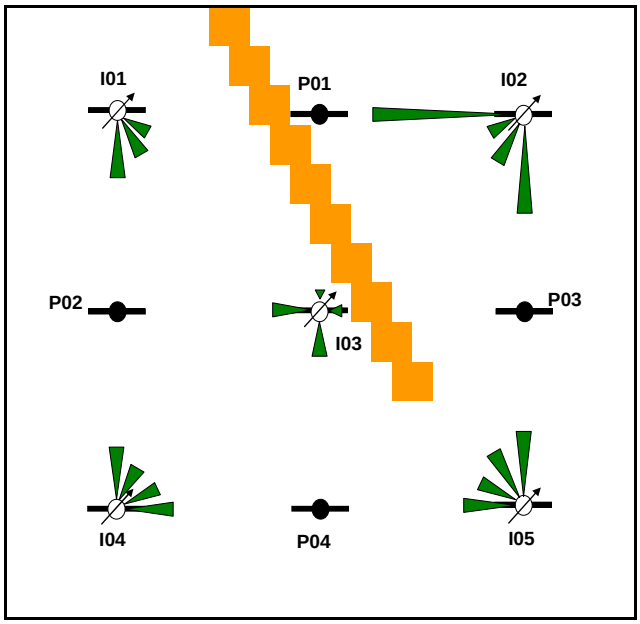


Figure 6.19. Representation of relative interwell permeability for the case of 5x4 dual-porosity reservoir with a partially sealing barrier– Hydraulically fractured wells.

6.3.8. Reservoir with a sealing barrier

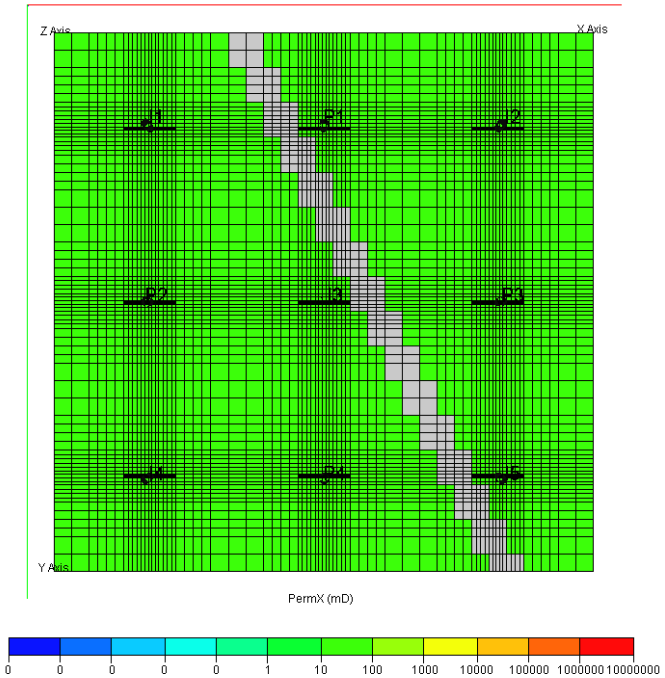


Figure 6.20. Top view of the simulation model showing the permeability in x direction for the case of 5x4 Synthetic field with a sealing barrier – Hydraulically fractured wells .

Fig. 6.20 shows the top view of the x-direction permeability distribution with a sealing barrier case. The permeability of the cells in grey color was set to zero and thus, those cells served as a sealing barrier. As seen on the figure, the barrier completely divides the reservoir into two compartments. Based on the change in average reservoir pressure calculated from each producer, this compartmentalization can be inferred.

Table 6.15: Interwell Connectivity Coefficient results from simulation data for the 5x4 Synthetic field with a sealing barrier – Hydraulically fractured wells.

	P1	P2	P3	P4	Sum
β_{0j} (psia)	-336.6	-266.0	-225.4	-365.7	-1194
I1	0.00	0.35	0.00	0.10	0.45
I2	0.87	-0.01	0.60	-0.01	1.44
I3	0.05	0.27	0.05	0.35	0.73
I4	-0.02	0.36	-0.02	0.53	0.84
I5	0.07	0.04	0.35	0.05	0.51
Sum	0.97	1.01	0.97	1.02	

Table 6.16: Relative interwell permeability results for the 5x4 Synthetic Field with a sealing barrier – Hydraulically fractured wells (k_{ref}=100mD, Δt_{eq} = 5.66 days)

	P1	P2	P3	P4	Ave.
I1	0.00	131.54	0.00	112.52	61.01
I2	385.61	0.00	253.13	0.00	159.69
I3	0.00	101.71	0.00	132.58	58.57
I4	0.00	137.43	0.00	216.59	88.51
I5	98.19	0.00	132.61	0.00	57.70
Ave.	97	74	77	92	

Table 6.15 and Fig. 6.21 show the results for the interwell connectivity coefficients. Similar to previous cases, the results clearly reflect the presence of the sealing barrier. Some connectivity coefficients are very small and even negative. They indicate poor connectivity or no connectivity at all. Small connectivities were still observed for some pairs of wells on different sides of the sealing barrier. As explained before, these non-zero connectivity coefficients are due to the noises in the data as the

injection rates were generated randomly. This problem can be resolved by increasing the number of data points. For this case, the interwell connectivity coefficients should be analyzed with the average reservoir pressure change results. If the pressure changes indicate reservoir compartmentalization, then the small interwell connectivity coefficients can be evaluated to decide whether the injectors and producers are on different side of the barrier. Table 6.16 and Fig. 6.22 present the corresponding relative interwell permeabilities with the equivalent time of 5.66 days, and the reference permeability of 100 mD. A cut-off coefficient of 0.06 was applied to eliminate the low connectivity coefficients. Thus, the relative interwell permeability corresponding to the coefficients lower than 0.06 were set to zeros. The resulted relative interwell permeabilities show a clear presence of the sealing barrier.

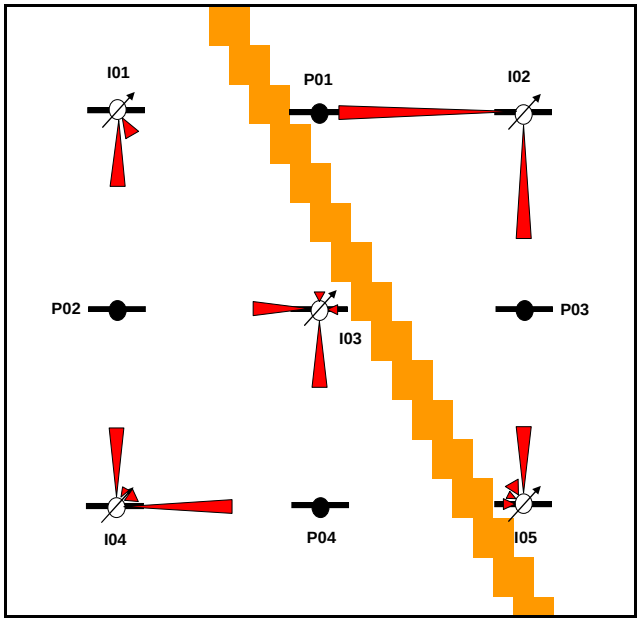


Figure 6.21. Representation of the connectivity coefficients for the 5x4 Synthetic Field with a sealing barrier – Hydraulically fractured wells.

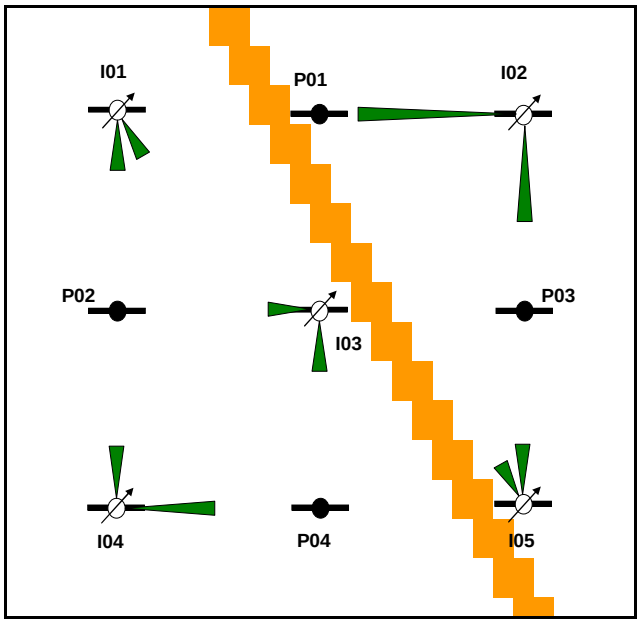


Figure 6.22. Representation of relative interwell permeability for the 5x4 Synthetic Field with a sealing barrier – Hydraulically fractured wells.

Table 6.17 shows the results for the average reservoir pressure change as described in Chapter 4 for all producers in each case described above. Similar to the results obtained from the previous chapters, except for the case of sealing barrier, the changes in average reservoir pressure for all the cases are consistent and close to the pressure changes obtained from the simulation results. For the case with the presence of sealing barrier, the calculated pressure changes for wells P01 and P03 (about 181 psi) are different from those for wells P02 and P04 (about 390 psi) indicating two different pore volumes and thus, two different reservoir compartments (see Chapter 4). The calculated values of reservoir pressure change are almost the same as the results obtained from the previous chapters showing the consistency of the calculation method.

Table 6.17: Average pressure change (ΔP_{ave}) after each time interval for different cases of 5x4 Synthetic Field – Hydraulically fractured wells.

Cases	P1	P2	P3	P4
Homogeneous Reservoir	285.93	285.93	285.74	285.74
Anisotropic Reservoir	285.83	285.82	285.82	285.77
Channel	285.82	285.82	285.81	285.82
Partially Sealing Barrier	295.33	300.01	296.38	298.84
Sealing Barrier	180.93	390.14	180.77	390.18

6.4. Conclusions

Some of the conclusions drawn from this chapter are:

- The interwell connectivity determination technique can be applied to reservoirs with presence of hydraulic fractures;

- The effect of a vertically fractured well on other wells at far distance is very close to the effect of its vertical well counterpart given the same flow rate. Thus, only the pressure drops at the wells themselves are different;

- Fracture half-lengths have effect on the magnitude of the interwell connectivities. The longer the fracture half-length of an active fractured well is, the more influence it has on the observation wells.

CHAPTER 7 – APPLICATIONS OF INTERWELL CONNECTIVITY TEST TO HORIZONTAL WELLS

In this chapter, reservoirs with only horizontal wells were considered. Similar to the previous chapters, MLR was used to determine the interwell connectivity coefficients from bottom hole pressure data. For simplicity, the late time solution for a horizontal well in a closed rectangular reservoir was used to calculate the influence functions and the relative interwell permeabilities. The results were then used to obtain information on the reservoir anisotropy and the presence of high permeability channels and transmissibility barriers. The cases in which the reservoir contains horizontal wells of different lengths and different directions were also considered. To investigate the effect of observation wells on the interwell connectivity coefficients, the case of different injector well lengths and unchanged producer well lengths was analyzed.

Different synthetic reservoir models were analyzed including: homogeneous, anisotropic reservoirs, reservoirs with high permeability channel, partially sealing barrier and sealing barrier. Results for different cases such as all wells are horizontal wells along x direction, along both x and y-directions and different horizontal well lengths are provided in this chapter.

7.1. Literature Review

Horizontal wells are widely used to increase productivity of the field. They are often used to overcome fluid flow problems such as high viscosity and high density reservoir fluids and to overcome heterogeneous reservoir characteristics. In naturally fractured reservoir, horizontal wells can intersect higher number of fractures and thus are much more effective than vertical wells. Horizontal wells are also a good choice for the

field development of a thin reservoir as they are able to drain a much larger area than their vertical well counterparts. As for gas reservoir, the use of horizontal wells can reduce the near well bore pressure drop and thus, avoid high gas velocity at the wellbore (Joshi, S. D., 1991).

There are numerous studies concerning the pressure behavior of a horizontal well covering a wide variety of topics on horizontal wells. A few relevant studies are mentioned in this section. Ozkan provided the pressure distribution solutions for the uniform flux and infinite conductivity horizontal wells at an arbitrary location in a closed rectangular reservoir (Ozkan 1988, Ozkan and Raghavan, 1988). Umnuayponwiwat and Ozkan (2000) investigated the inflow performance of multiple horizontal wells in closed systems based on the pseudo-steady state solution. Engler and Tiab (1996) analyzed transient pressure data of a horizontal well in an anisotropy reservoir based on both pressure and pressure derivative curves. Ozkan (1988) proposed a transient solution in Laplace space for a horizontal well at an arbitrary location in a closed rectangular reservoir. In this study, for simplicity, we only use the late time form of the solution provided by Ozkan (1988).

7.2. Analytical Model and Calculation Methods

The pressure distribution equation for a horizontal well in a closed rectangular reservoir is (Ozkan, 1988):

$$p_{Dh} = a_h = p_{Df} + F_1 \tag{7.1}$$

where

$$F_1 = \frac{2}{x_{eD} L_D} \sum_{n=1}^{\infty} \frac{1}{n} \cos(n\pi z_D) \cos(n\pi z_{wD}) \frac{\cosh n\pi \left(\frac{y_{eD} - |y_D - y_{wD}|}{x_{eD}} \right) + \cosh n\pi \left(\frac{y_{eD} - (y_D + y_{wD})}{x_{eD}} \right)}{\sinh\left(n\pi \frac{y_{eD}}{x_{eD}} \right)} +$$

$$+ 4 \sum_{n=1}^{\infty} \cos(n\pi z_D) \cos(n\pi z_{wD}) \sum_{k=1}^{\infty} \frac{1}{k} \frac{\sin\left(k\pi \frac{1}{x_{eD}} \right) \cos\left(k\pi \frac{x_{wD}}{x_{eD}} \right) \cos\left(k\pi \frac{x_D}{x_{eD}} \right)}{\sqrt{b}} \tag{7.2}$$

$$\frac{\cosh \sqrt{b}(y_{eD} - |y_D - y_{wD}|) + \cosh \sqrt{b}(y_{eD} - (y_D + y_{wD}))}{\sinh\left(\sqrt{b} y_{eD} \right)}$$

Where $b = n^2\pi^2 L_D^2 + k^2\pi^2 / x_{eD}^2$ and the L term in the dimensionless definition is the horizontal well half length L = L_h/2, $z_D = z/h$ and $L_D = 1/h_D = L/2h$. x_{wD} and y_{wD} are at the mid-point of the well length for the uniform flux horizontal well case. For the infinite conductivity horizontal well case, Ozkan (1988) showed that the point x_D = 0.732 used to calculate pressure distribution for a infinite conductivity fracture can also be used for a infinite conductivity horizontal well. The term F_1 can be rewritten as follows:

$$F_1 = \frac{2}{x_{eD} L_D} \sum_{n=1}^{\infty} \frac{1}{n} \cos(n\pi z_D) \cos(n\pi z_{wD}) G(x_{eD}, y_{eD}, y_{wD}, y_D, n\pi) +$$

$$+ 4 \sum_{n=1}^{\infty} \cos(n\pi z_D) \cos(n\pi z_{wD}) \sum_{k=1}^{\infty} \frac{1}{k} \sin\left(k\pi \frac{1}{x_{eD}} \right) \cos\left(k\pi \frac{x_{wD}}{x_{eD}} \right) \cos\left(k\pi \frac{x_D}{x_{eD}} \right) GH\left(y_{eD}, y_{wD}, y_D, \sqrt{b} \right) \tag{7.3}$$

Where $b = n^2\pi^2 L_D^2 + k^2\pi^2 / x_{eD}^2$, $GH\left(y_{eD}, y_{wD}, y_D, \sqrt{b} \right) = \frac{G\left(1, y_{eD}, y_{wD}, y_D, \sqrt{b} \right)}{\sqrt{b}}$

To calculate F_1 as suggested by Ozkan:

$$F_1 = F + F_{b1} + F_{b2} + F_{b3} \tag{7.4}$$

Where

$$F = \sum_{n=1}^{\infty} \cos(n\pi z_D) \cos(n\pi z_{wD}) \int_{-1}^{+1} K_0 \left[n\pi L_D \sqrt{(x_D - x_{wD} - \alpha)^2 + (y_D - y_{wD})^2} \right] d\alpha \tag{7.5}$$

$$F_{b1}=\frac{2}{x_{eD}L_D}\sum_{n=1}^{\infty}\frac{1}{n}\cos(n\pi z_D)\cos(n\pi z_{wD})\left\{\begin{array}{l}\left[e^{-n\pi L_D(y_D+y_{wD})}+e^{-n\pi L_D(2y_{eD}-|y_D-y_{wD}|)}+e^{-n\pi L_D(2y_{eD}-(y_D+y_{wD}))}\right]\\ \left[1+\sum_{m=1}^{\infty}e^{-2mn\pi L_D y_{eD}}\right]+e^{-n\pi L_D|y_D-y_{wD}|}\sum_{m=1}^{\infty}e^{-2mn\pi L_D y_{eD}}\end{array}\right\} \tag{7.6}$$

$$\begin{aligned}F_{b2}=4\sum_{n=1}^{\infty}\cos(n\pi z_D)\cos(n\pi z_{wD})\sum_{k=1}^{\infty}\frac{1}{k}\frac{\sin\left(k\pi\frac{1}{x_{eD}}\right)\cos\left(k\pi\frac{x_D}{x_{eD}}\right)\cos\left(k\pi\frac{x_{wD}}{x_{eD}}\right)}{\sqrt{n^2\pi^2L_D+\frac{k^2\pi^2}{x_{eD}^2}}}\times\\ \times\left\{\left[e^{-\sqrt{n^2\pi^2L_D^2+\frac{k^2\pi^2}{x_{eD}^2}}(y_D+y_{wD})}+e^{-\sqrt{n^2\pi^2L_D^2+\frac{k^2\pi^2}{x_{eD}^2}}(2y_{eD}-(y_D+y_{wD}))}+e^{-\sqrt{n^2\pi^2L_D^2+\frac{k^2\pi^2}{x_{eD}^2}}(2y_{eD}-|y_D-y_{wD}|)}\right]\times\right.\\ \left.\times\left[1+\sum_{m=1}^{\infty}e^{-2m\sqrt{n^2\pi^2L_D^2+\frac{k^2\pi^2}{x_{eD}^2}}y_{eD}}\right]+e^{-\sqrt{n^2\pi^2L_D^2+\frac{k^2\pi^2}{x_{eD}^2}}|y_D-y_{wD}|}\sum_{m=1}^{\infty}e^{-2m\sqrt{n^2\pi^2L_D^2+\frac{k^2\pi^2}{x_{eD}^2}}y_{eD}}\right\}\end{aligned} \tag{7.7}$$

$$F_{b3}=\sum_{n=1}^{\infty}\cos(n\pi z_D)\cos(n\pi z_{wD})\left\{\begin{array}{l}\int_{-1}^{+1}K_0\left[n\pi L_D\sqrt{(x_D+x_{wD}-\alpha)^2+(y_D-y_{wD})^2}\right]d\alpha+\\ +\sum_{k=1}^{\infty}\int_{-1}^{+1}\left\{\begin{array}{l}K_0\left[n\pi L_D\sqrt{(x_D-x_{wD}-2kx_{eD}-\alpha)^2+(y_D-y_{wD})^2}\right]+\\ +K_0\left[n\pi L_D\sqrt{(x_D+x_{wD}-2kx_{eD}-\alpha)^2+(y_D-y_{wD})^2}\right]+\\ +K_0\left[n\pi L_D\sqrt{(x_D-x_{wD}+2kx_{eD}-\alpha)^2+(y_D-y_{wD})^2}\right]+\\ +K_0\left[n\pi L_D\sqrt{(x_D+x_{wD}+2kx_{eD}-\alpha)^2+(y_D-y_{wD})^2}\right]\end{array}\right\}d\alpha\end{array}\right\} \tag{7.8}$$

For the case of $y_D = y_{wD}$, if $|X|\le a$ then

$$\int_{-a}^{+a}K_0\left[b\sqrt{(X-\alpha)^2}\right]d\alpha=\frac{1}{b}\left[\int_0^{b(a+X)}K_0(u)du+\int_0^{b(a-X)}K_0(u)du\right] \tag{7.9}$$

If $|X| \geq a$ then

$$\int_{-a}^{+a} K_0\left[b\sqrt{(X-\alpha)^2}\right]d\alpha = \frac{1}{b}\left[\int_0^{b(|X|+a)} K_0(u)du - \int_0^{b(|X|-a)} K_0(u)du\right] \tag{7.10}$$

If $|X| = a$ then

$$\int_{-a}^{+a} K_0\left[b\sqrt{(X-\alpha)^2}\right]d\alpha = \frac{1}{b}\int_0^{2ab} K_0(u)du \tag{7.11}$$

Where a = 1, b = $n\pi L_D$

Table 7.1 presents the dimensionless coordinates for all the wells in the 5x4 Homogeneous Synthetic field. Other data include $x_{eD} = y_{eD} = 20.67$ and $r_{wD} = 0.004733$. Table 7.2 shows the shape factors for the horizontal wells in the 5x4 synthetic field calculated using P_{wD} results (influence functions) from Eq.7.1 and Eq. 5.21. These shape factors can be used to calculate the influence functions by applying Eq. 5.20.

Table 7.1: Dimensionless coordinates of the horizontal wells in the 5x4 synthetic field

Wells	x_{wDh}	y_{wDh}
I01	3.6667	17.0000
I02	17.0000	17.0000
I03	10.3333	10.3333
I04	3.6667	3.6667
I05	17.0000	3.6667
P01	10.3333	17.0000
P02	3.6667	10.3333
P03	17.0000	10.3333
P04	10.3333	3.6667

Table 7.2: Shape factors for uniform flux and infinite conductivity horizontal wells in 5x4 Synthetic Reservoir

Wells	C_{Ah}	
	Uniform Flux	Infinite Conductivity
I01	0.0404	0.0950
I02	0.0403	0.0563
I03	1.4741	2.6713
I04	0.0404	0.0950
I05	0.0403	0.0563
P01	0.3212	0.5857
P02	0.3190	0.6997
P03	0.3182	0.4699
P04	0.3212	0.5857

7.3. Simulation Results

7.3.1. Model Description

Fig. 7.1 shows the top view of the permeability distribution of the 5x4 homogeneous synthetic field with horizontal wells. All the wells were horizontal wells with their centers at the cell where the vertical wells were completed in the previous chapters(see Table 7.1). Fig. 7.2 shows the permeability distribution cross section cutting through three representative horizontal wells. Thus, all the wells were completed in the center layer of the reservoir so that their distances to the top and bottom boundaries of the reservoir were equal. The formation permeability was set to 100 mD in the x, y and z directions. All wells are at the same length of 300 ft and completed along the x direction. The wells were assumed to be infinite conductivity horizontal wells. Thus, the influence functions were calculated using the pressure distribution equation (Eq.7.1) evaluated at the point $x_D = 0.732$ and $y_D = y_{wD}$.

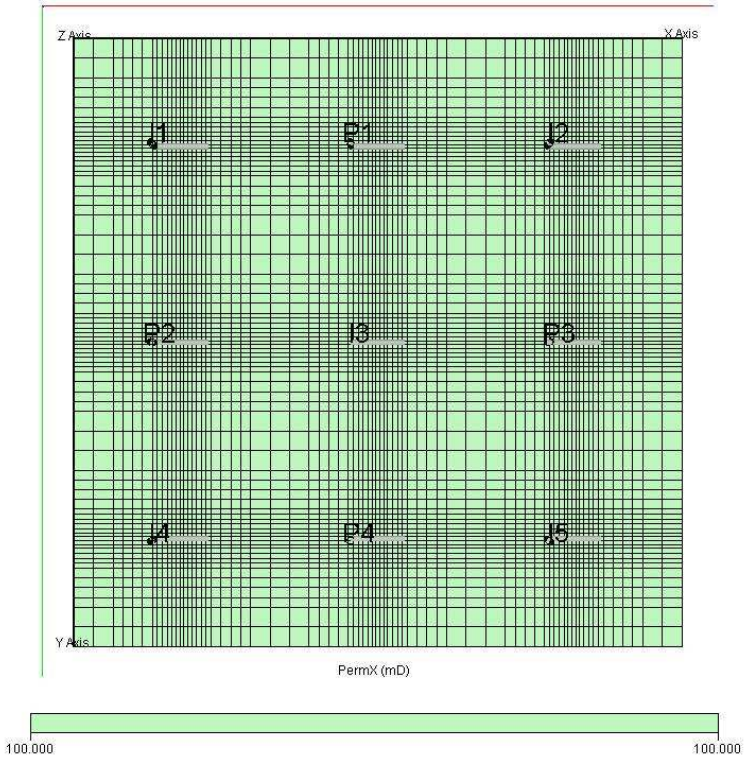


Figure 7.1. Top view of the simulation model showing the horizontal wells of the homogeneous 5x4 Synthetic field.

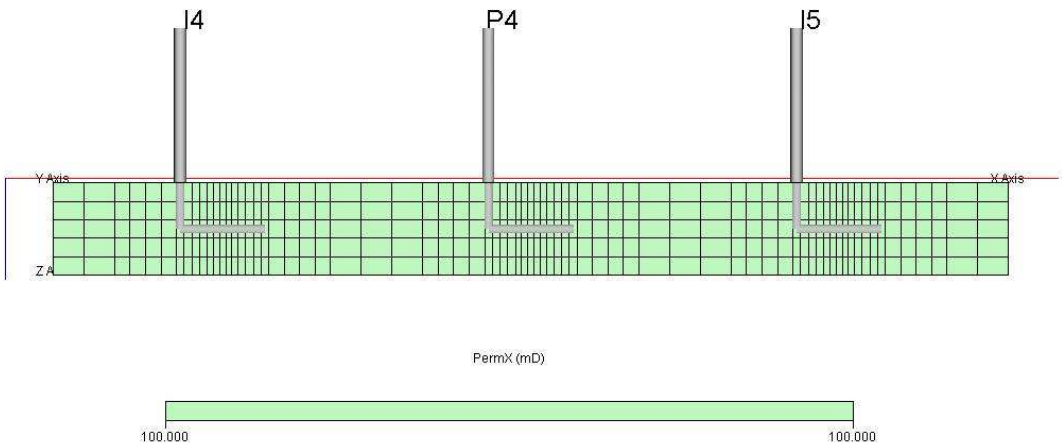


Figure 7.2. Cross sectional view showing three horizontal wells and their completions in the homogeneous 5x4 Synthetic Reservoir.

7.3.2. Homogeneous Reservoir

Table 7.3 and Fig. 7.3 show the results for the interwell connectivity coefficients obtained from the simulation data for this case. Similar to the same cases in the previous

chapters, the results are very close to the results obtained for the homogeneous reservoir with vertical wells. Small value of the asymmetry coefficient for this case (A_s = 0.00445) indicates good results for the interwell connectivity coefficients. Table 7.4 and Fig. 7.4 present the corresponding relative interwell permeabilities with the equivalent time of 6.59 days, and the reference permeability of 100 mD. Notice that the differences between the high and low interwell connectivity coefficients are less significant than in the case of vertically fractured wells of similar half length suggesting the observation wells are less affected by the nearby active horizontal wells than as in the vertically fractured well case. This is reasonable because for the same flow rate, the pressure drop in a fractured well is less than in a horizontal well considering the fracture half-length is approximately equal to the horizontal well half-length.

Table 7.3: Interwell Connectivity Coefficient results from simulation data for the Homogeneous 5x4 Synthetic field with Horizontal wells (A = 0.00445)

	P1	P2	P3	P4	Sum
β_{0j} (psia)	-291.9	-293.7	-294.0	-292.1	-1172
I1	0.29	0.30	0.08	0.09	0.76
I2	0.29	0.08	0.30	0.09	0.76
I3	0.24	0.24	0.25	0.23	0.96
I4	0.09	0.29	0.09	0.29	0.76
I5	0.09	0.09	0.29	0.30	0.76
Sum	1.00	1.00	1.00	1.00	

Table 7.4: Relative interwell permeability results for the 5x4 Homogeneous Synthetic Field with Horizontal wells (k_{ref}=100mD, Δt_{eq} = 6.59 days)

	P1	P2	P3	P4	Ave.
I1	108	112	92	97	102
I2	107	94	109	97	102
I3	93	93	98	93	94
I4	98	107	96	106	102
I5	96	97	106	109	102
Ave.	100	101	100	100	

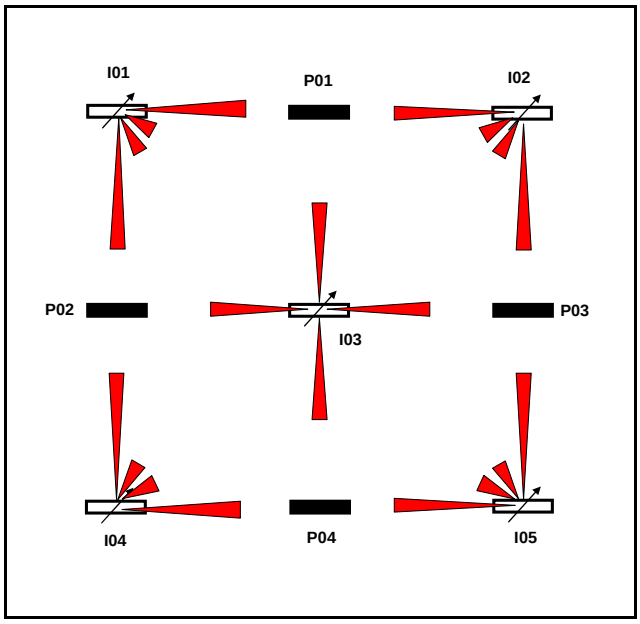


Figure 7.3. Representation of the connectivity coefficients for the case of 5x4 Homogeneous Reservoir with Horizontal wells.

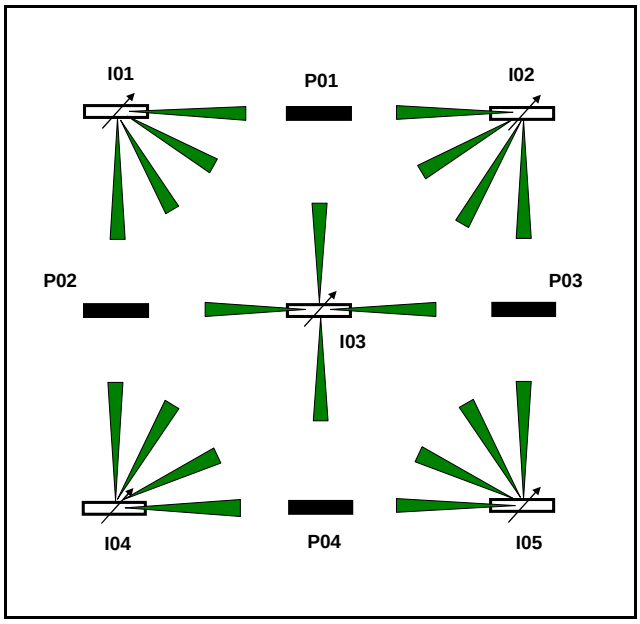


Figure 7.4. Representation of the relative interwell permeability for the case of 5x4 Homogeneous Reservoir with Horizontal wells.

7.3.3. Homogeneous Reservoir with horizontal wells of different lengths

In this case, the horizontal well half-lengths are different. The half-length values are presented in Table 7.5. Fig. 7.5 shows the top view of the permeability distribution of the reservoir. In Fig. 7.5, the lengths of the horizontal wells corresponding to the data given in Table 7.5 are also observed. Figure 7.6 shows the cross section through wells I04, P04 and I05. Again, the wells are completed in the middle layer.

Table 7.5: Horizontal well half-lengths for different horizontal wells in the 5x4 Homogeneous Synthetic field

Wells	L/2 (ft)
I1	75.00
I2	125.00
I3	100.00
I4	75.00
I5	200.00
P1	150.00
P2	100.00
P3	125.00
P4	50.00

Table 7.6 and Fig. 7.8 present the interwell connectivity coefficient results for this case. Fig. 7.7 shows the comparison of the interwell connectivity coefficients results obtained from simulation data and by calculation using influence functions. The coefficients are in good agreement with $R^2 = 0.9607$. Table 7.7 and Fig. 7.9 show the corresponding relative interwell permeability results for this reservoir. The calculated relative interwell permeabilities are in good agreement with the simulation model input permeability of 100 mD.

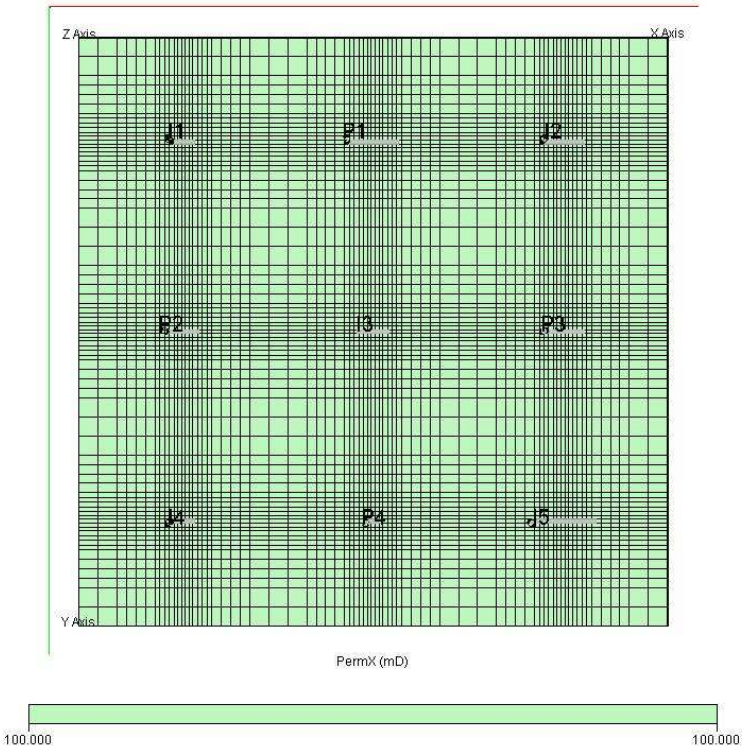


Figure 7.5. Top view of the simulation model showing the horizontal wells of different lengths for the homogeneous 5x4 Synthetic field.

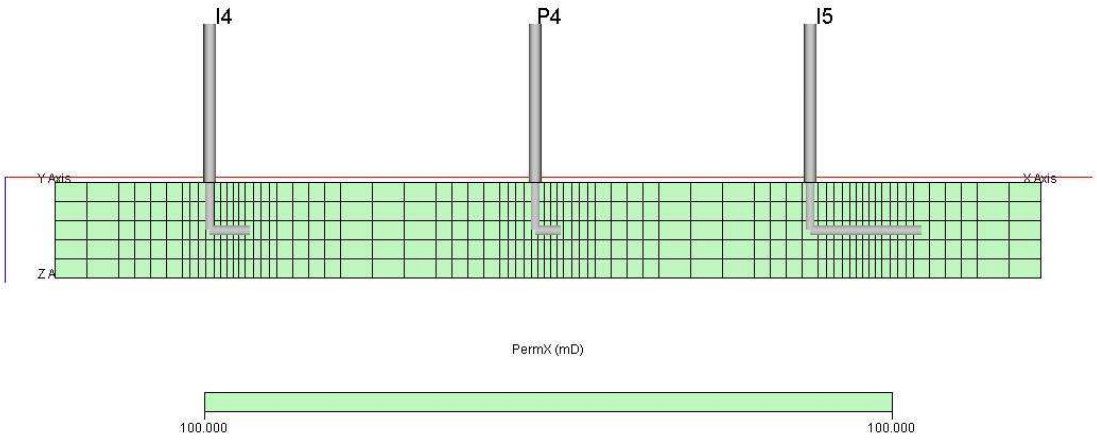


Figure 7.6. Cross sectional view showing three horizontal wells of different lengths in the homogeneous 5x4 Synthetic Reservoir.

Table 7.6: Interwell Connectivity Coefficient results from simulation data for the 5x4 Homogeneous Synthetic field – Horizontal wells of different lengths

	P1	P2	P3	P4	Sum
β_{0j} (psia)	-330.5	-371.6	-325.9	-420.8	-1449
I1	0.25	0.27	0.08	0.09	0.69
I2	0.30	0.11	0.29	0.10	0.80
I3	0.23	0.23	0.22	0.22	0.89
I4	0.10	0.26	0.08	0.24	0.68
I5	0.12	0.13	0.33	0.35	0.94
Sum	1.00	1.00	1.00	1.00	

Table 7.7: Relative interwell permeability results for the 5x4 Homogeneous Synthetic field – Horizontal wells of different lengths (k_{ref}=100mD, Δt_{eq} = 6.21 days)

	P1	P2	P3	P4	Ave.
I1	101	109	87	95	98
I2	111	98	107	95	102
I3	92	94	88	88	91
I4	97	103	89	94	96
I5	100	105	113	119	109
Ave.	100	102	97	98	

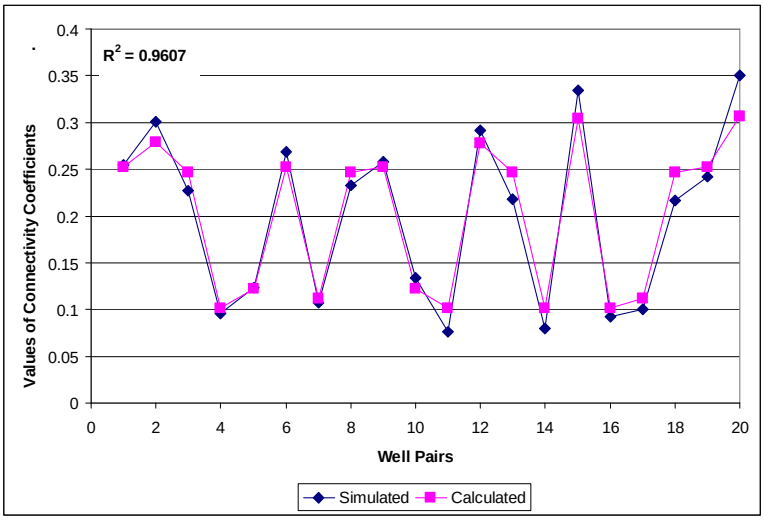


Figure 7.7. Comparison of simulated and calculated interwell connectivity coefficient results for the 5x4 Homogeneous Synthetic field – Horizontal wells of different lengths.

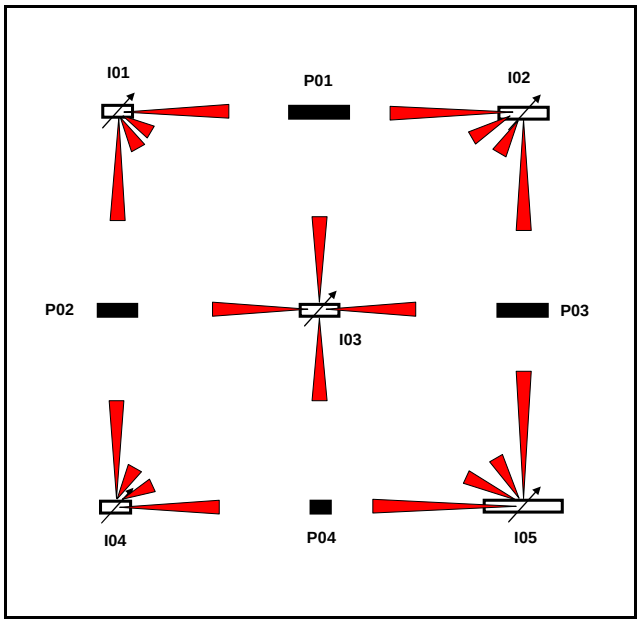


Figure 7.8. Representation of the connectivity coefficients for the case of 5x4 Homogeneous Reservoir - Horizontal wells of different lengths.

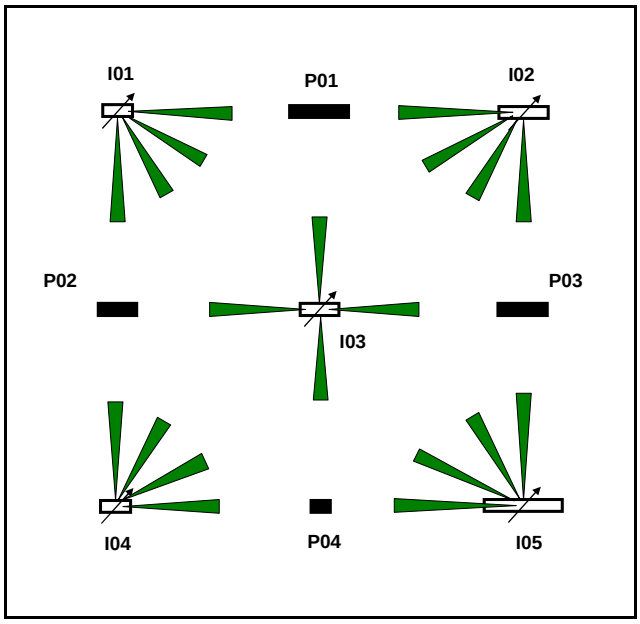


Figure 7.9. Representation of relative interwell permeability for the case of 5x4 Homogeneous Reservoir- Horizontal wells of different lengths.

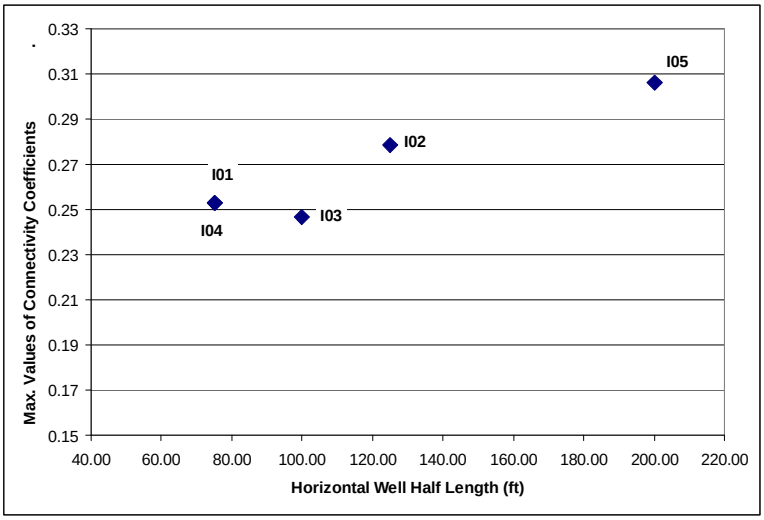


Figure 7.10. Maximum values of interwell connectivity coefficients versus horizontal well half-lengths.

Similar to the case of vertically fractured wells, in order to investigate the effect of horizontal well half-lengths on the interwell connectivity coefficients, a graph of maximum values of the interwell connectivity coefficients for every injector versus their horizontal well half-lengths was plotted as shown on Fig. 7.10. Except for well I03, which is at the center of the reservoir, the positions of the other wells can be considered as equivalent to each other due to the symmetry of the reservoir. A clear trend is shown on Fig. 7.10. The higher the horizontal well half-lengths, the larger the maximum coefficient values. Well I01 and I04 have the same horizontal well half-length and, consequently, the maximum coefficients for those two wells are the same. Thus, the longer the horizontal well half-lengths are, the more influence the wells have on nearby wells and the less influence they have on far away wells.

7.3.4. Homogeneous Reservoir with horizontal injectors of different lengths and producers with the same length

Again, to investigate the effect of horizontal well half lengths of the producers or response wells on the interwell connectivity coefficients, the same simulation model as in previous case was run with the exception that the horizontal well half lengths of the producers were the same at 150 ft. The fracture half-lengths of the injectors are shown in Table 7.5. Fig. 7.11 shows the top view of the reservoir permeability distribution. From Fig. 7.11, the lengths of the horizontal injectors corresponding to the data given in Table 7.5 are also observed. However, the lengths of the horizontal producers are the same.

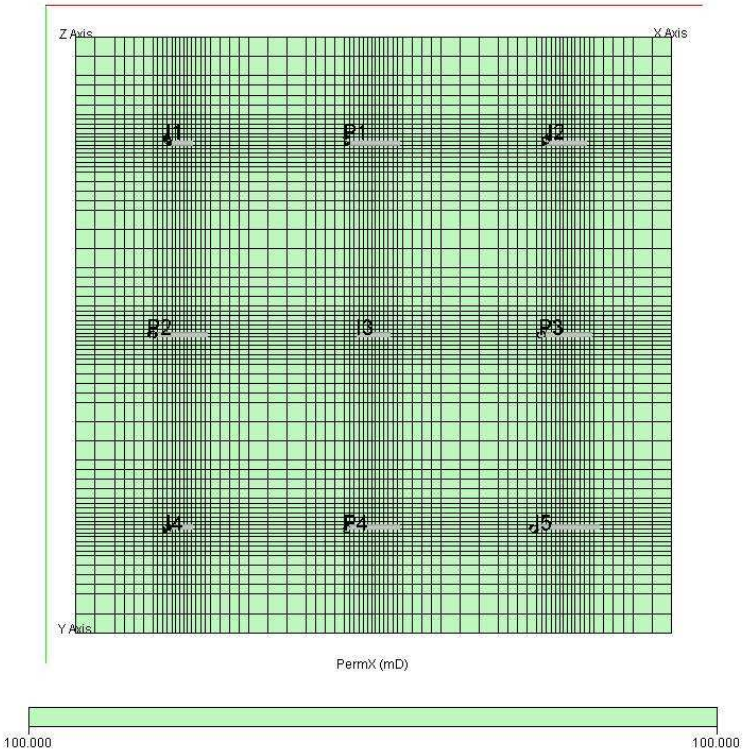


Figure 7.11. Top view of the simulation model showing the horizontal wells in the 5x4 homogeneous Synthetic field-The same horizontal well half lengths for producers.

The results of the interwell connectivity coefficients are presented in Table 7.8. Fig. 7.12 presents a comparison of the interwell connectivity coefficients for the case of the same and different horizontal well half lengths at the producers. The results for both cases are identical indicating that the horizontal well lengths for the producers do not affect the interwell connectivity coefficients. This is also in excellent agreement with the analytical model because the wellbore conditions of the producers or observation wells are not part of the equation to calculate interwell connectivity coefficients.

Table 7.8: Interwell Connectivity Coefficient results from simulation data for the 5x4 Homogeneous Synthetic field – Different fracture half-lengths at injectors

	P1	P2	P3	P4	Sum
β_{0j} (psia)	-330.4	-340.9	-313.0	-319.3	-1304
I1	0.25	0.27	0.08	0.09	0.69
I2	0.30	0.11	0.29	0.10	0.80
I3	0.23	0.23	0.22	0.22	0.89
I4	0.10	0.26	0.08	0.24	0.67
I5	0.12	0.13	0.33	0.35	0.94
Sum	1.00	1.00	1.00	1.00	

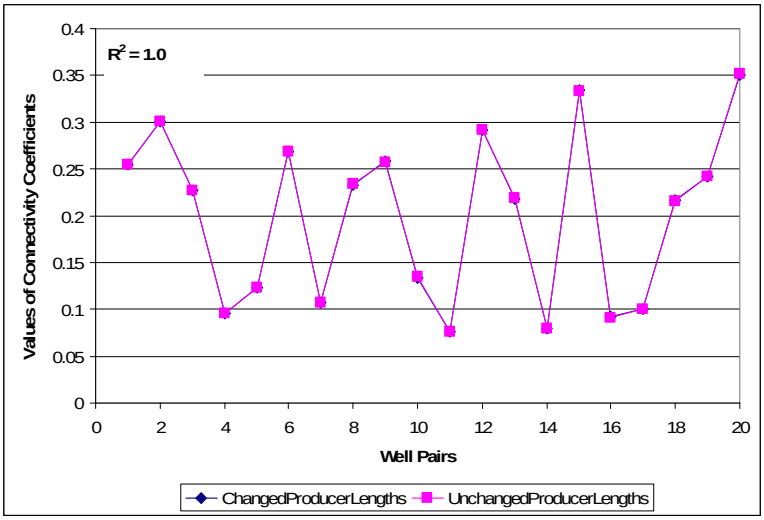


Figure 7.12. Comparison of the interwell connectivity coefficient results for the case of the same vs. different horizontal well half lengths for the producers in the 5x4 Homogeneous Synthetic Reservoir.

7.3.5. Homogeneous Reservoir with horizontal wells in both x – y directions

To investigate the effect of horizontal well directions on the interwell connectivity coefficients, the 5x4 simulation model with horizontal wells of different directions (x and y directions) was run. Fig. 7.13 shows the top view of the reservoir permeability distribution and the horizontal well directions. As shown on Fig. 7.13, wells I02, I03, P03 and I04 are in y-direction while the other wells are in the x-direction. The centers of the wells however are at the same positions as in the previous cases.

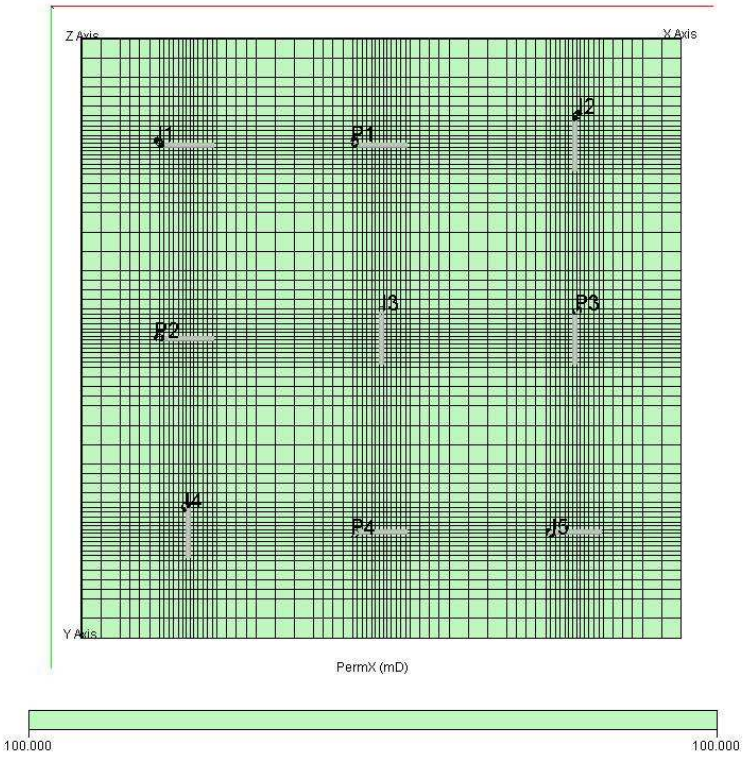


Figure 7.13. Top view of the simulation model showing the horizontal wells of the homogeneous 5x4 Synthetic field-Different horizontal well directions.

The results of the interwell connectivity coefficients are presented in Table 7.9 and Fig. 7.14. Figs. 7.15 and 7.16 present a comparison of the interwell connectivity coefficient results of this case with the case where all wells are in the x-direction. The

results for both cases are almost identical indicating that the horizontal well directions do not affect the interwell connectivity coefficient results given the same well locations.

Table 7.9: Interwell Connectivity Coefficient results from simulation data for the 5x4 Homogeneous Synthetic field – Different horizontal well directions (A_s = 0.00484)

	P1	P2	P3	P4	Sum
β_{0j} (psia)	-292.0	-293.5	-292.9	-292.2	-1171
I1	0.29	0.30	0.08	0.09	0.76
I2	0.29	0.08	0.30	0.09	0.76
I3	0.24	0.23	0.24	0.24	0.95
I4	0.09	0.29	0.09	0.29	0.76
I5	0.09	0.09	0.29	0.30	0.76
Sum	1.00	1.00	1.00	1.00	

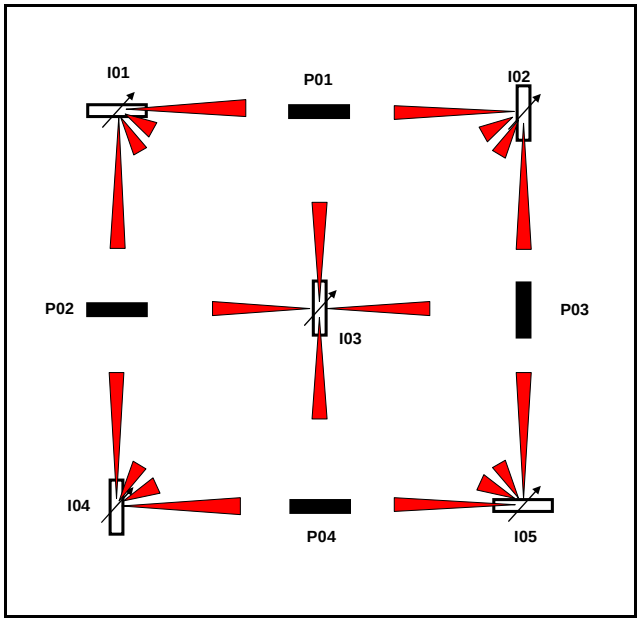


Figure 7.14. Representation of the connectivity coefficients for the case of 5x4 Homogeneous Reservoir - Horizontal wells of different directions.

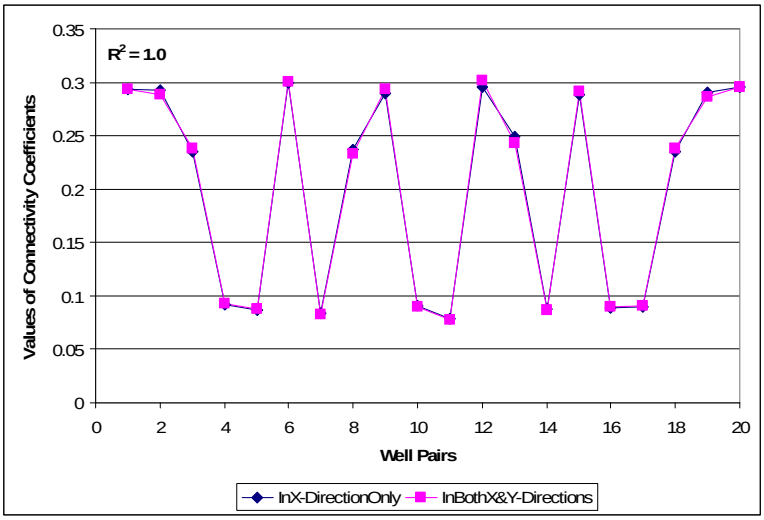


Figure 7.15. Comparison of the interwell connectivity coefficient results for the case of different well directions vs. all wells in the x-direction in 5x4 Homogeneous Synthetic Reservoir.

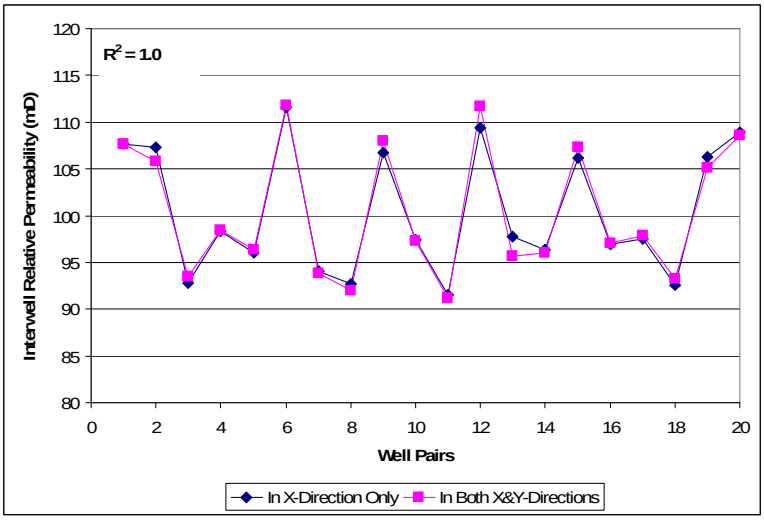


Figure 7.16. Comparison of the relative interwell permeability results for the case of different well directions vs. all wells in the x-direction in 5x4 Homogeneous Synthetic Reservoir.

7.3.6. Anisotropic Reservoir with horizontal wells

In this case, the effective permeability in the x direction (1000 mD) is tenfold the permeability in the y direction (100 mD). Similar to the homogeneous base case, all wells have the same horizontal half-lengths. Table 7.10 and Fig. 7.17 show the results

for the interwell connectivity coefficients. As expected, the results are good indications of the reservoir anisotropy with large coefficients for well pairs in the direction of high permeability. Table 7.11 and Fig. 7.18 present the corresponding relative interwell permeabilities with the equivalent time of 6.59 days, and the reference permeability of 316 mD.

Table 7.10: Interwell Connectivity Coefficient results from simulation data for the 5x4 Anisotropic Synthetic field– Horizontal wells

	P1	P2	P3	P4	Sum
β_{0j} (psia)	-131.3	-165.7	-165.7	-131.5	-594
I1	0.38	0.15	0.13	0.05	0.71
I2	0.38	0.13	0.15	0.05	0.72
I3	0.14	0.43	0.43	0.14	1.14
I4	0.05	0.15	0.13	0.38	0.71
I5	0.04	0.13	0.15	0.39	0.72
Sum	1.00	1.00	1.00	1.00	

Table 7.11: Relative interwell permeability results for the 5x4 Anisotropic Synthetic Field – Horizontal wells (k_{ref}=316 mD, Δt_{eq} = 6.59 days)

	P1	P2	P3	P4	Ave.
I1	319	104	175	95	173
I2	317	177	105	96	174
I3	117	354	355	117	236
I4	100	103	174	314	173
I5	91	177	105	321	174
Ave.	189	183	183	189	

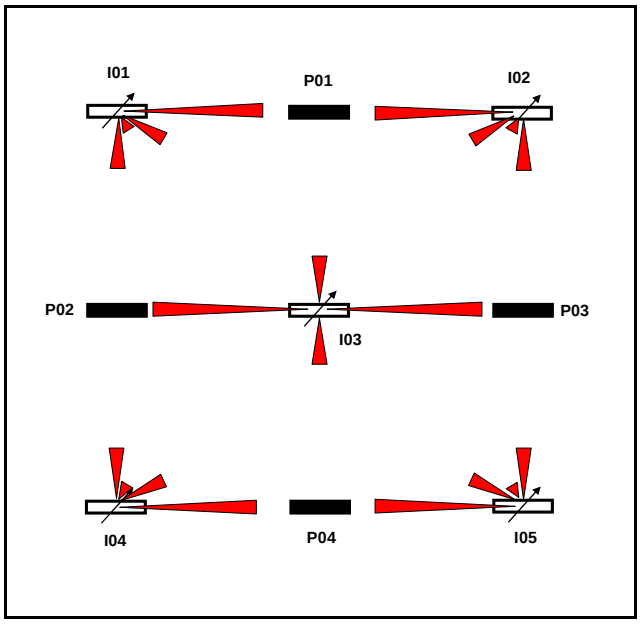


Figure 7.17. Representation of the interwell connectivity coefficients for the case of 5x4 Anisotropic Reservoir – Horizontal wells.

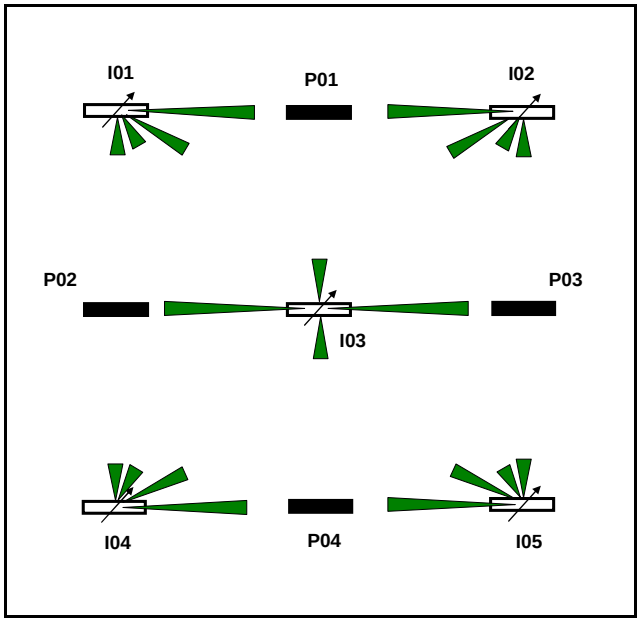


Figure 7.18. Representation of relative interwell permeability for the case of 5x4 Synthetic Reservoir – Horizontal wells.

7.3.7. Reservoir with high permeability channel

Fig. 7.19 shows the top view of the permeability distribution for this case. The cells in red color indicate high permeability in both x and y directions. Similar to the high permeability channel cases in the previous chapters, the permeability of the channel was ten-fold (1000 mD) of that in the other areas the reservoir (100 mD). There are nine horizontal wells with the same horizontal well half-length of 150 ft.

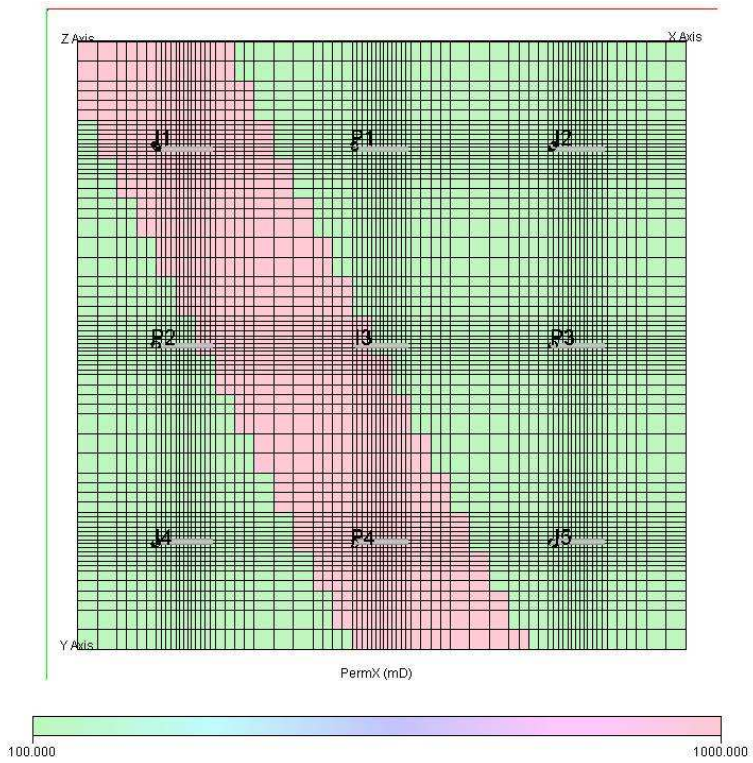


Figure 7.19. Top view of the simulation model showing the permeability in x direction for the high permeability channel case of the 5x4 Synthetic field – Horizontal wells.

Table 7.12 and Fig. 7.20 show the results for the interwell connectivity coefficients. Similar to the fractured well case of a reservoir with high permeability channel, the results reflect accurately the presence of the channel. Table 7.13 and Fig. 7.21 present the corresponding relative interwell permeabilities with the equivalent time of 6.59 days, and the reference permeability of 300 mD.

Table 7.12: Interwell Connectivity Coefficient results from simulation data for the High permeability channel case of the 5x4 Synthetic field – Horizontal wells

	P1	P2	P3	P4	Sum
β_{0j} (psia)	-197.5	-73.2	-241.7	-83.5	-596
I1	0.46	0.45	0.14	0.22	1.27
I2	0.20	0.03	0.25	0.04	0.51
I3	0.26	0.41	0.34	0.48	1.50
I4	0.03	0.07	0.05	0.12	0.27
I5	0.04	0.04	0.21	0.15	0.45
Sum	1.00	1.00	1.00	1.00	

Table 7.13: Relative interwell permeability results for the high permeability channel case of the 5x4 Synthetic field – Horizontal wells (k_{ref}=300mD, Δt_{eq} = 6.59 days)

	P1	P2	P3	P4	Ave.
I1	374	368	179	245	292
I2	142	76	188	86	123
I3	209	321	271	384	296
I4	83	29	97	66	69
I5	91	92	155	95	108
Ave.	180	177	178	175	

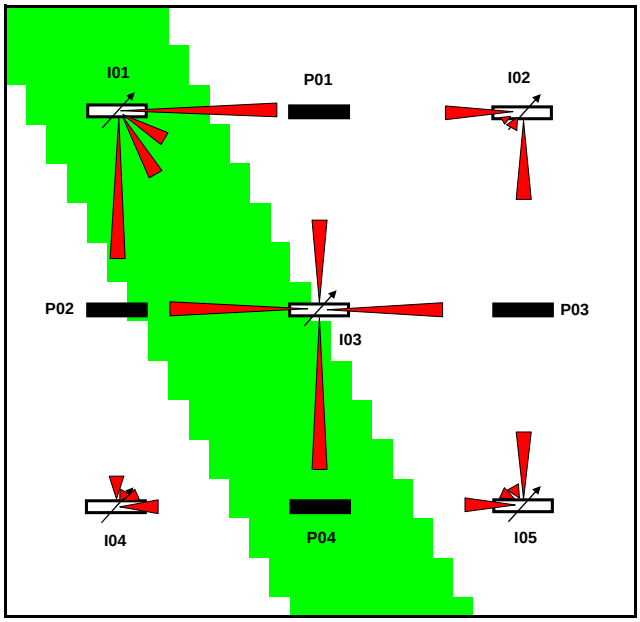


Figure 7.20. Representation of the connectivity coefficients for the high permeability channel case of the 5x4 Synthetic field – Horizontal wells.

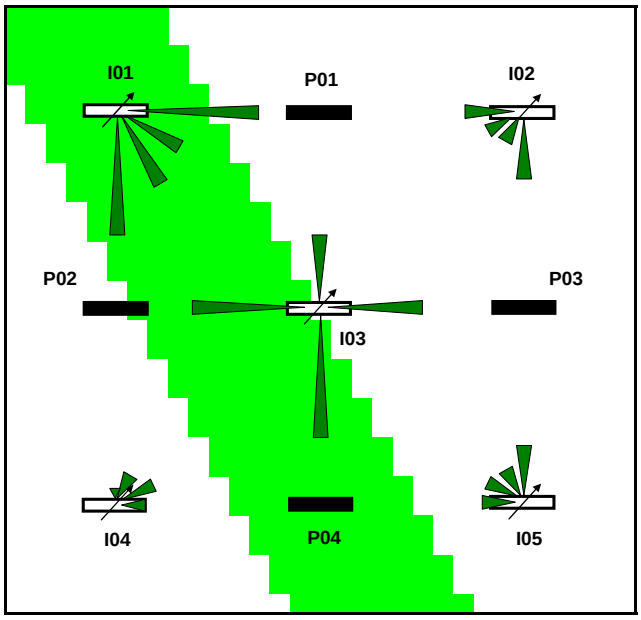


Figure 7.21. Representation of relative interwell permeability for the high permeability channel case of the 5x4 Synthetic field – Horizontal wells.

7.3.8. Reservoir with a partially sealing barrier

Fig. 7.22 below shows the top view of the x-direction permeability distribution for this case. The cells in white color were inactive and thus, served as a partially sealing barrier. The formation permeability was 100 mD.

Table 7.14 and Fig. 7.22 show the results for the interwell connectivity coefficients. The presence of the partially sealing barrier is well established based on the results. Table 7.15 and Fig. 7.24 present the corresponding relative interwell permeabilities with the equivalent time of 6.59 days, and the reference permeability of 100 mD. Similar to the same case for fractured wells, the relative interwell permeability for well pair I01-P01 was negative because the influence function for the pair was calculated using the late time solution. When the interwell connectivity coefficients are small, they are translated to early time-periods and, thus, the late time solution becomes inaccurate. Thus, the negative value was set to zero due to small connectivity coefficient.

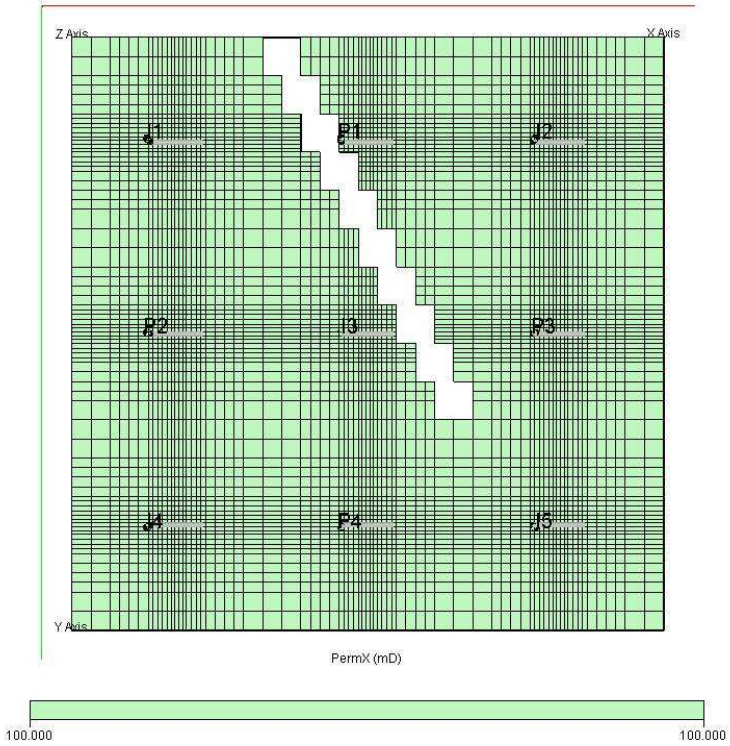


Figure 7.22. Top view of the simulation model showing the permeability distribution in x direction for the 5x4 Synthetic field with partially sealing barrier– Horizontal wells..

Table 7.14: Interwell Connectivity Coefficient results from simulation data for the 5x4 Synthetic field with partially sealing barrier– Horizontal wells.

	P1	P2	P3	P4	Sum
β_{0j} (psia)	-540.6	-260.1	-391.4	-291.3	-1483
I1	0.01	0.34	0.02	0.09	0.46
I2	0.73	0.03	0.47	0.09	1.31
I3	0.07	0.24	0.10	0.22	0.63
I4	0.05	0.30	0.07	0.30	0.73
I5	0.13	0.09	0.34	0.31	0.87
Sum	1.00	1.00	1.00	1.00	

Table 7.15: Relative interwell permeability results for the 5x4 Synthetic field with partially sealing barrier– Horizontal wells (k_{ref}=100mD, Δt_{eq} = 6.59 days)

	P1	P2	P3	P4	Ave.
I1	-32	130	64	97	65
I2	321	67	195	96	170
I3	30	93	38	85	62
I4	80	114	89	111	98
I5	119	98	130	115	116
Ave.	104	101	103	101	

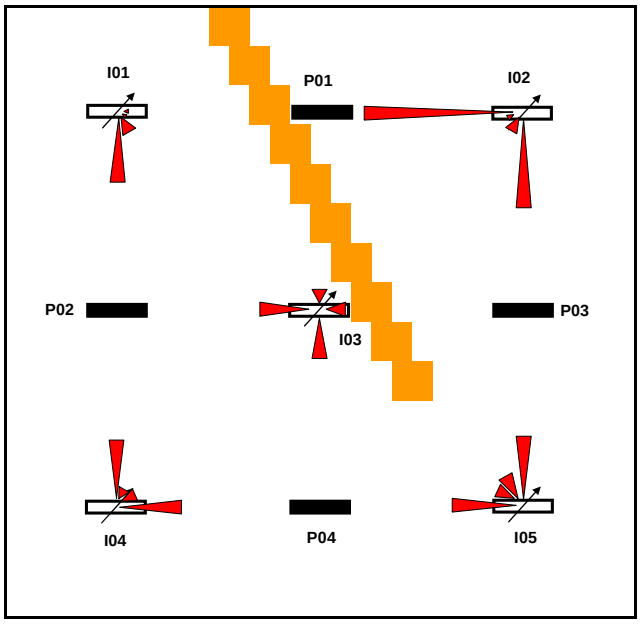


Figure 7.23. Representation of the connectivity coefficients for the case of 5x4 Dual-porosity reservoir with a partially sealing barrier– Horizontal wells.

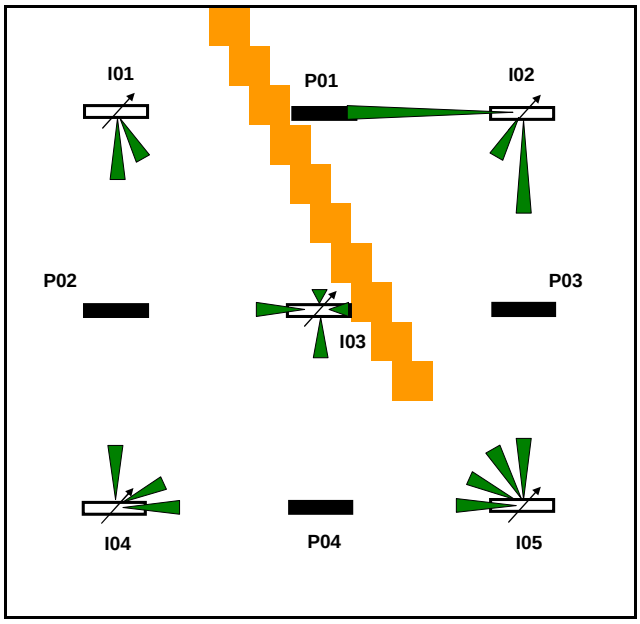


Figure 7.24. Representation of relative interwell permeability for the case of 5x4 dual-porosity reservoir with a partially sealing barrier– Horizontal wells.

7.3.9. Reservoir with a sealing barrier

Fig. 7.25 shows the top view of the x-direction permeability distribution for the sealing barrier case. The cells in white color were inactive and thus, served as a sealing barrier. As seen on the figure, the barrier completely divides reservoir into two compartments. Based on the change in average reservoir pressure calculated from each producer, the compartmentalization can be inferred.

Table 7.16 and Fig. 7.26 show the results for the interwell connectivity coefficients. Similar to the previous cases, the results clearly reflect the presence of the sealing barrier. Some connectivity coefficients are very small and even negative. They indicate poor connectivity or no connectivity at all.

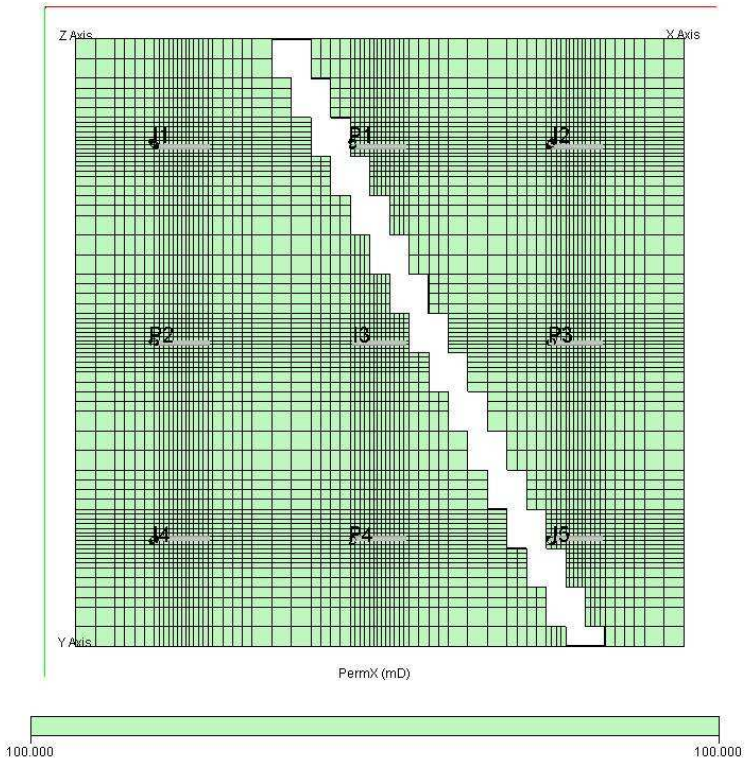


Figure 7.25. Top view of the simulation model showing the permeability in x direction for the case of 5x4 Synthetic field with a sealing barrier – Horizontal wells .

Table 7.17 and Fig. 7.27 present the corresponding relative interwell permeabilities with the equivalent time of 6.59 days, and the reference permeability of 100 mD. A cut-off coefficient of 0.06 was applied to eliminate the low connectivity coefficients. Thus, the relative interwell permeability corresponding to the coefficients lower than 0.06 were set to zeros. The resulted relative interwell permeabilities show a clear presence of the sealing barrier (Fig. 7.27).

Table 7.16: Interwell Connectivity Coefficient results from simulation data for the 5x4 Synthetic field with a sealing barrier – Horizontal wells.

	P1	P2	P3	P4	Sum
β_{0j} (psia)	-336.6	-266.0	-225.4	-365.7	-1194
I1	0.00	0.35	0.00	0.10	0.45
I2	0.87	-0.01	0.60	-0.01	1.44
I3	0.05	0.27	0.05	0.35	0.73
I4	-0.02	0.36	-0.02	0.53	0.84
I5	0.07	0.04	0.35	0.05	0.51
Sum	0.97	1.01	0.97	1.02	

Table 7.17: Relative interwell permeability results for the 5x4 Synthetic Field with a sealing barrier – Horizontal wells (k_{ref}=100mD, Δt_{eq} = 6.59 days)

	P1	P2	P3	P4	Ave.
I1	0	137	0	104	60
I2	391	0	259	0	163
I3	0	106	0	138	61
I4	0	143	0	222	91
I5	89	0	135	0	56
Ave.	96	77	79	93	

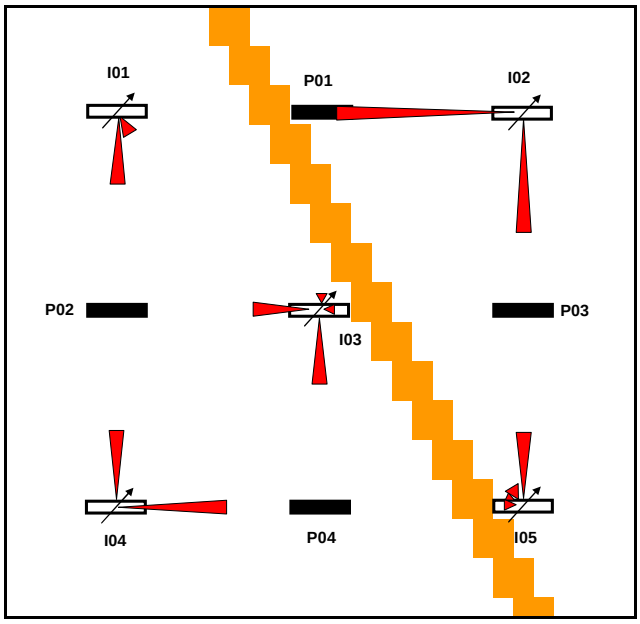


Figure 7.26. Representation of the connectivity coefficients for the 5x4 Synthetic Field with a sealing barrier – Horizontal wells.

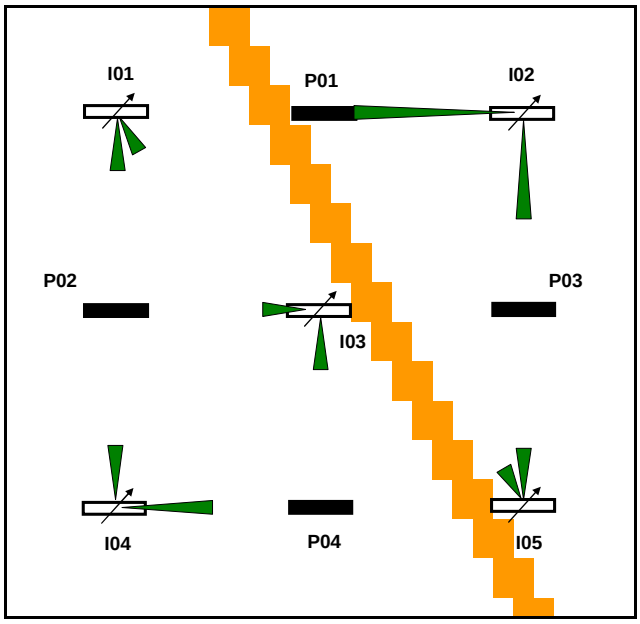


Figure 7.27. Representation of relative interwell permeability for the 5x4 Synthetic Field with a sealing barrier – Horizontal wells.

Table 7.18 shows the results for the average reservoir pressure change for all producers in each representative case described in this chapter. Similar to previous

chapters, the changes in average reservoir pressure for all the cases are about the same and close to the simulated pressure changes. For the case with the presence of a sealing barrier, the resulted pressure changes for wells P01 and P03 (about 181 psi) are different from those for wells P02 and P04 (390 psi) indicating two different reservoir compartments (see Chapter 4 and 5). Thus, the reservoir pressure change results are consistent.

Table 7.18: Average pressure change (ΔP_{ave}) after each time interval for different cases of 5x4 Synthetic Field – Horizontal wells.

Cases	P1	P2	P3	P4
Homogeneous Reservoir	285.98	286.04	285.79	285.84
Anisotropic Reservoir	285.93	285.92	285.92	285.79
Channel	285.90	285.94	285.82	285.91
Partially Sealing Barrier	294.99	300.45	296.10	298.96
Sealing Barrier	180.93	390.14	180.77	390.18

7.4. Conclusions

Some of the conclusions drawn from this chapter are:

- The interwell connectivity determination technique can be applied to reservoirs containing horizontal wells;

- The well length at the observations wells or the well directions do not affect the interwell connectivity results;

- The complication of pressure distribution caused by a horizontal well can be captured using the analytical model and thus its connectivities with other wells can be interpreted.

- Given the same well position (position of the mid-point of a horizontal well), the directions of the horizontal wells do not have significant effect on the interwell connectivity coefficients.

CHAPTER 8 – SIMULATION RESULTS FOR MIXED WELL-BORE CONDITIONS

This chapter provides the results for different cases where mixed wellbore conditions are present. The 5x4 synthetic reservoirs containing hydraulic fractures and vertical wells, horizontal and vertical wells or all three types of wellbore conditions are considered.

8.1. Fully Penetrating Vertical Wells and Fully Penetrating Hydraulic Fractures

In this section we investigate the effect of well bore conditions of the hydraulically fractured injector and vertical producers on the interwell connectivity coefficients. Fig. 8.1 shows the top view of the permeability distribution for this case. Thus, we have all the injectors as hydraulically fractured wells and all producers as vertical wells.

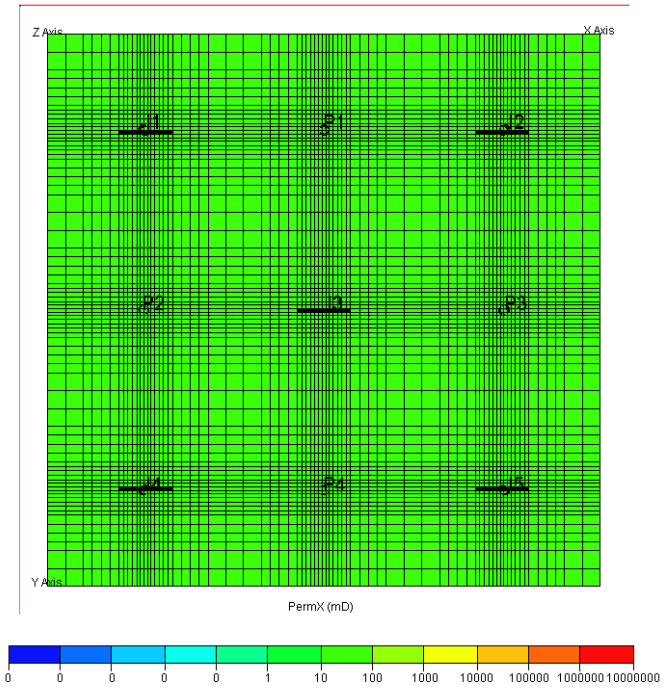


Figure 8.1. Top view of the simulation model showing the x direction permeability for the 5x4 Homogeneous Synthetic field– Hydraulically fractured injectors and vertical producers .

Fig. 8.2 shows the cross section through wells I04, P04 and I05. The fractures are shown in red, which indicates high permeability. Well P04 is a vertical well and does not intersect any hydraulic fractures. More model descriptions for the fractures can be found in section 6.3.1. The results of the interwell connectivity coefficients for this case are presented in Table 8.1.

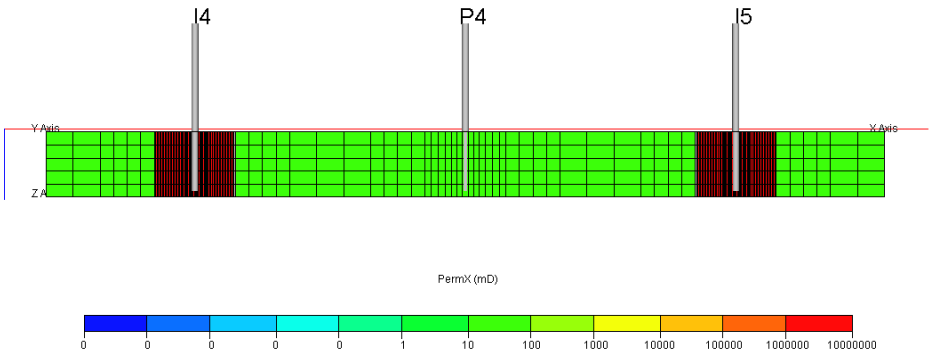


Figure 8.2. Cross sectional view showing three wells of the 5x4 Homogeneous Synthetic field– Hydraulically fractured injectors and vertical producers .

Table 8.1: Interwell Connectivity Coefficient results from simulation data for the 5x4 Homogeneous Synthetic field – Hydraulically fractured injectors and vertical producers.

	P1	P2	P3	P4	Sum
β_{0j} (psia)	-444.6	-446.2	-445.8	-444.6	-1781
I1	0.32	0.32	0.06	0.06	0.75
I2	0.32	0.06	0.31	0.06	0.75
I3	0.25	0.25	0.26	0.25	1.01
I4	0.06	0.31	0.06	0.32	0.75
I5	0.06	0.06	0.31	0.32	0.75
Sum	1.00	1.00	1.00	1.00	

Fig. 8.3 shows a comparison of the interwell connectivity coefficient results for the case of all fractured wells versus the case of hydraulically fractured injectors and vertical producers. The results for both cases are identical, again indicating that the wellbore conditions at the producers do not affect the interwell connectivity coefficients. This is also in excellent agreement with the analytical model because the wellbore

conditions of the producers or observation wells are not part of the equation to calculate interwell connectivity coefficients.

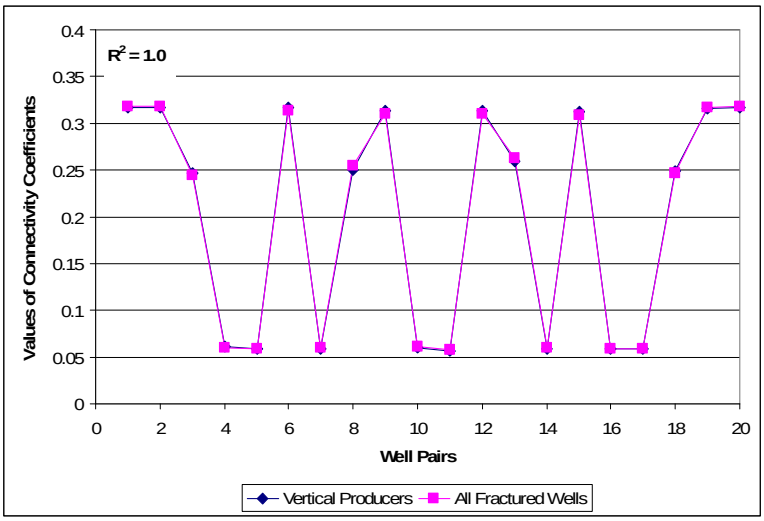


Figure 8.3. Comparison of the interwell connectivity coefficient results for the case Hydraulically fractured injectors and vertical producers vs. All fractured wells in 5x4 Homogeneous Synthetic Reservoir.

8.2. Mixed case of fully penetrating vertical wells and fully penetrating hydraulic fractures

Fig. 8.4 shows the top view of the permeability distribution for this case. As shown on the figure, wells I01, P01, I03, P03 and I05 are hydraulically fractured wells and all the other wells are fully penetrating vertical wells.

Table 8.2 and Fig. 8.5 present the interwell connectivity coefficient results for this case. It is obvious that hydraulically fractured injectors have better connectivity with the producers than the vertical injectors. Table 8.3 and Fig. 8.6 show the corresponding relative interwell permeability results for this reservoir. The relative permeabilities for the well pairs of vertical injectors are slightly lower than those of hydraulic fractures. However, the calculated relative interwell permeability is in good agreement with the input permeability for the model of 100 mD.

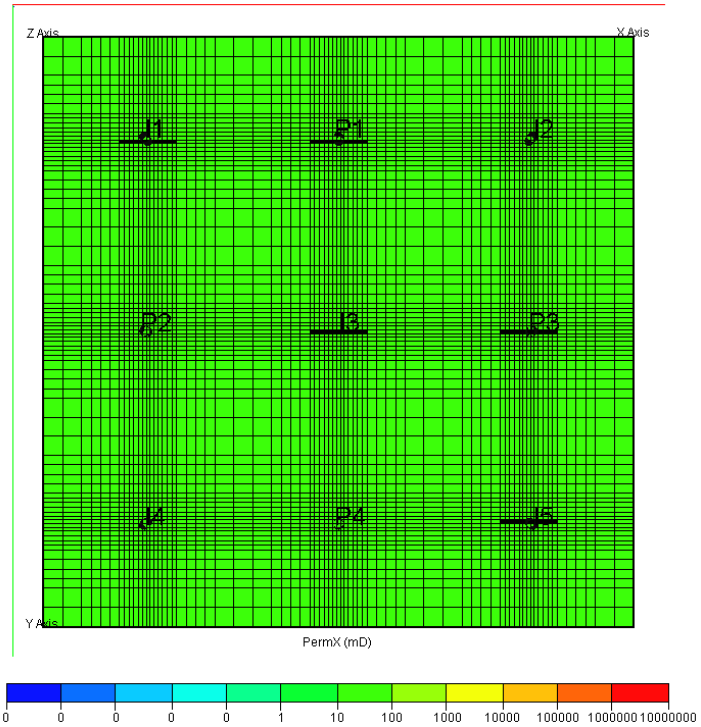


Figure 8.4. Top view of the simulation model showing the x direction permeability for the 5x4 Homogeneous Synthetic field– Mixed Hydraulically fractured and vertical wells .

Table 8.2: Interwell Connectivity Coefficient results from simulation data for the 5x4 Homogeneous Synthetic field – Mixed Hydraulically fractured and vertical wells.

	P1	P2	P3	P4	Sum
β_{0j} (psia)	-281.1	-502.1	-282.1	-501.9	-1567
I1	0.37	0.36	0.10	0.11	0.94
I2	0.16	0.04	0.16	0.04	0.41
I3	0.32	0.33	0.34	0.33	1.32
I4	0.04	0.16	0.04	0.16	0.41
I5	0.11	0.11	0.35	0.36	0.93
Sum	1.00	1.00	1.00	1.00	

Table 8.3: Relative interwell permeability results for the 5x4 Homogeneous Synthetic Field– Mixed Hydraulically fractured and vertical wells (k_{ref}=100mD, Δt_{eq} = 7.33 days)

	P1	P2	P3	P4	Ave.
I1	123	122	92	93	108
I2	81	74	80	74	77
I3	109	110	114	110	111
I4	75	81	74	80	78
I5	93	94	121	125	108
Ave.	96	96	96	97	

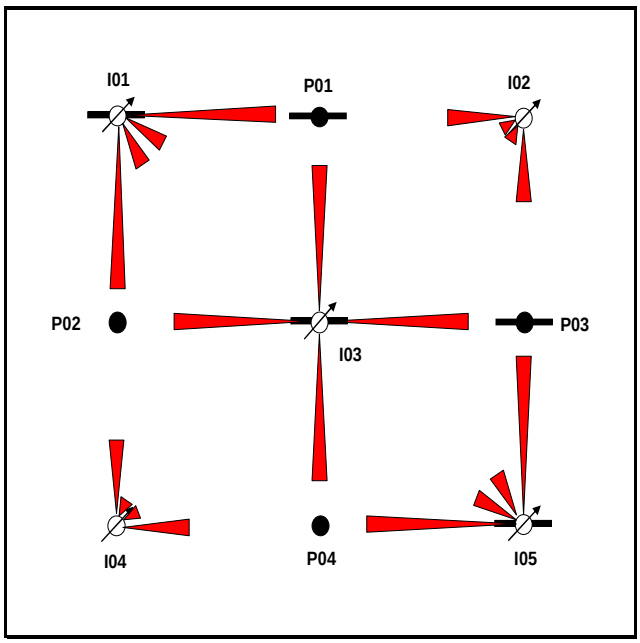


Figure 8.5. Representation of the connectivity coefficients for the 5x4 Homogeneous Synthetic field – Mixed Hydraulically fractured and vertical wells.

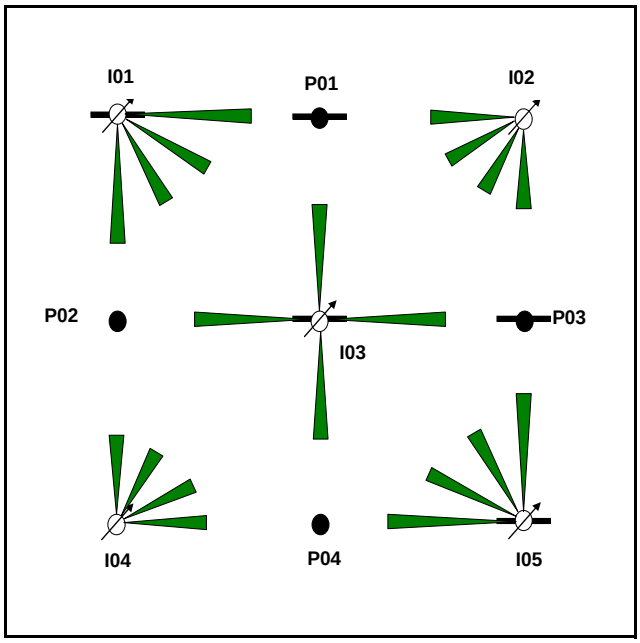


Figure 8.6. Representation of relative interwell permeability for the 5x4 Homogeneous Synthetic field – Mixed hydraulically fractured and vertical wells.

Fig. 8.7 shows the comparison of the interwell connectivity coefficients results obtained from simulation data and calculations using influence functions. The coefficients are in good agreement with $R^2 = 0.9875$.

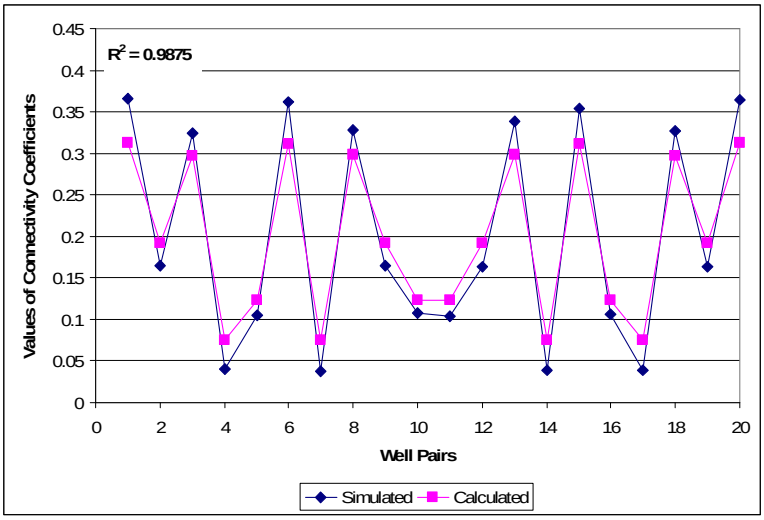


Figure 8.7. Comparison of the interwell connectivity coefficient results for the 5x4 Homogeneous Synthetic field – Mixed hydraulically fractured and vertical wells.

8.3. Fully Penetrating Vertical producers and Horizontal injectors

In this section, the effect of well bore conditions is investigated in a homogeneous reservoir with horizontal injectors and vertical producers on the interwell connectivity coefficients. Fig. 8.8 shows the top view of the permeability distribution for this case. As shown on the figure, all the injectors are horizontal wells and all the producers are vertical wells. Fig. 8.9 shows the cross section through wells I04, P04 and I05. Wells I04 and I05 are horizontal wells completed in the center layer. Well P04 is a vertical well penetrating all five layers. More description on the horizontal well models can be found in section 7.3.1.

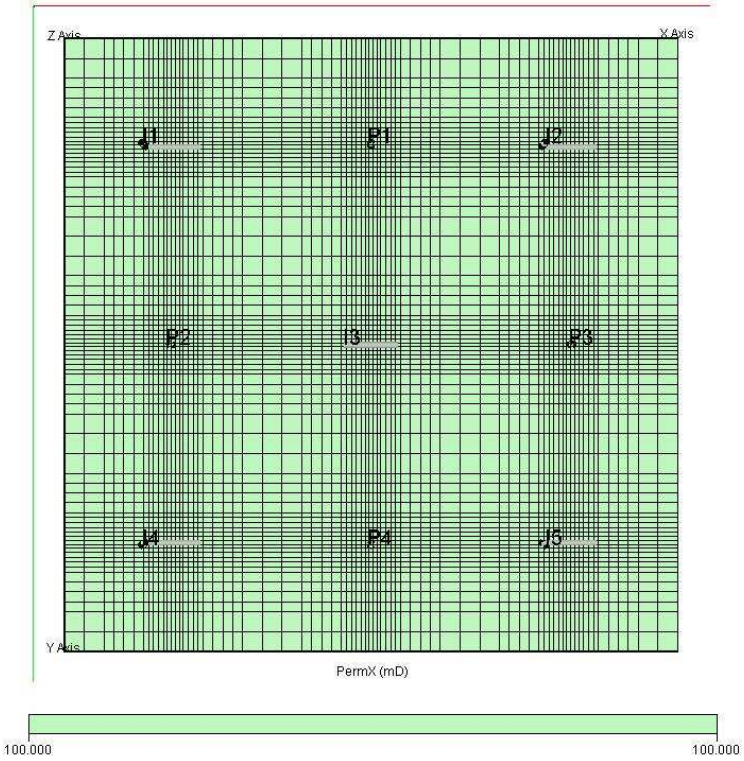


Figure 8.8. Top view of the simulation model showing the x direction permeability for the 5x4 Homogeneous Synthetic field– Horizontal injectors and vertical producers .

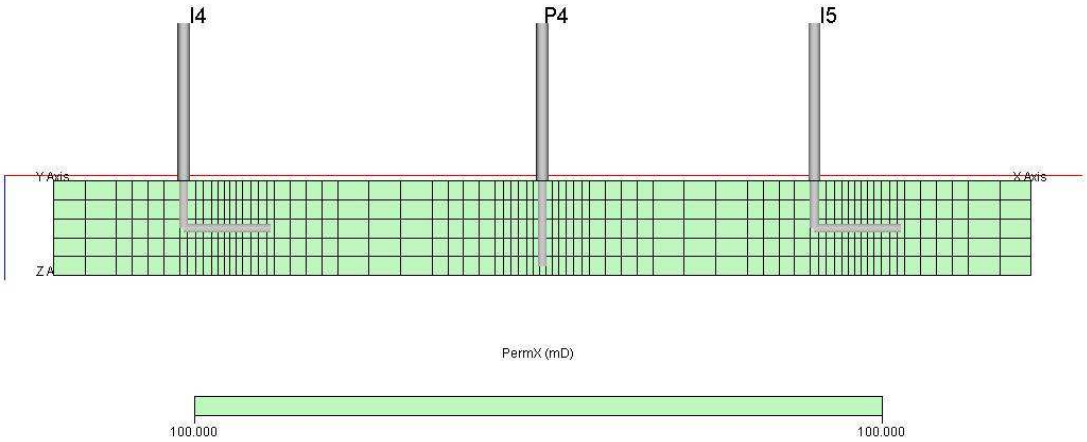


Figure 8.9. Cross sectional view showing three wells of the 5x4 Homogeneous Synthetic field– Horizontal injectors and vertical producers ..

The results of the interwell connectivity coefficients for this case are presented in

Table 8.4. Fig. 8.10 shows a comparison of the interwell connectivity coefficient results

for the case of all horizontal wells versus the case of horizontal injectors and vertical producers. The results for both cases are identical again indicating that the wellbore conditions at the producers do not affect the interwell connectivity coefficients. Again, this is also in excellent agreement with the analytical model because the wellbore conditions of the producers or observation wells are not part of the equation to calculate interwell connectivity coefficients.

Table 8.4: Interwell Connectivity Coefficient results from simulation data for the 5x4 Homogeneous Synthetic field – Horizontal injectors and vertical producers.

	P1	P2	P3	P4	Sum
β_{0j} (psia)	-484.0	-484.8	-485.2	-484.2	-1938
I1	0.29	0.30	0.08	0.09	0.76
I2	0.29	0.08	0.30	0.09	0.76
I3	0.24	0.23	0.25	0.24	0.96
I4	0.09	0.29	0.09	0.29	0.76
I5	0.09	0.09	0.29	0.29	0.76
Sum	1.00	1.00	1.00	1.00	

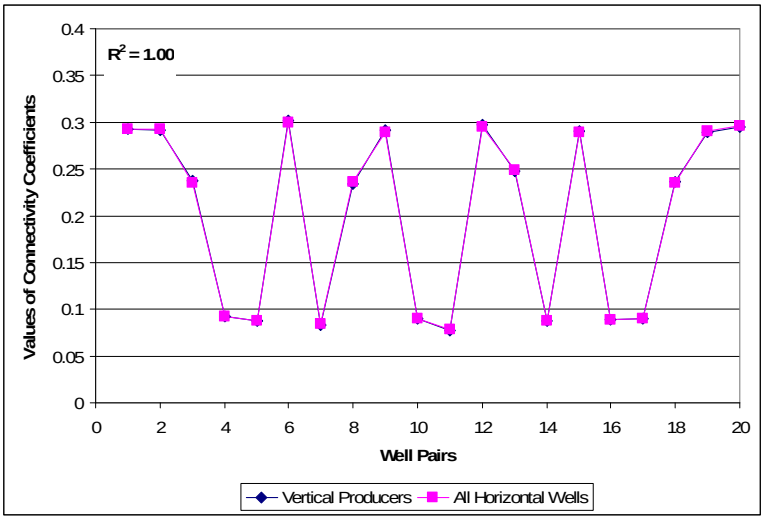


Figure 8.10. Comparison of the interwell connectivity coefficient results for the case Horizontal injectors and vertical producers vs. All horizontal wells in 5x4 Homogeneous Synthetic Reservoir.

8.4. Mixed case of fully penetrating vertical wells and horizontal wells

Fig. 8.11 shows the top view of the permeability distribution for this case. As shown on the figure, wells I01, P01, I03, P03 and I05 are horizontal wells and all the other wells are vertical wells. Fig. 8.12 shows the cross section through wells I04, P04 and I05. Wells I04 and P04 are fully penetrating vertical wells and similar to other horizontal wells, horizontal well I05 is completed in the middle layer.

Table 8.5 and Fig. 8.13 present the interwell connectivity coefficient results for this case. It is obvious that horizontal injectors have better connectivity with the producers than the vertical injector. Table 8.6 and Fig. 8.14 show the corresponding relative interwell permeability results for this reservoir. The relative permeabilities for the pairs of vertical injectors are slightly lower than those of horizontal injectors. This could be due to numerical errors and analytical assumptions. However, the calculated relative interwell permeability is in good agreement with the input permeability for the model of 100 mD. Fig. 8.15 shows the comparison of the interwell connectivity coefficients results obtained from simulation data and by calculation using influence functions. The coefficient results are in good agreement with $R^2 = 0.9681$.

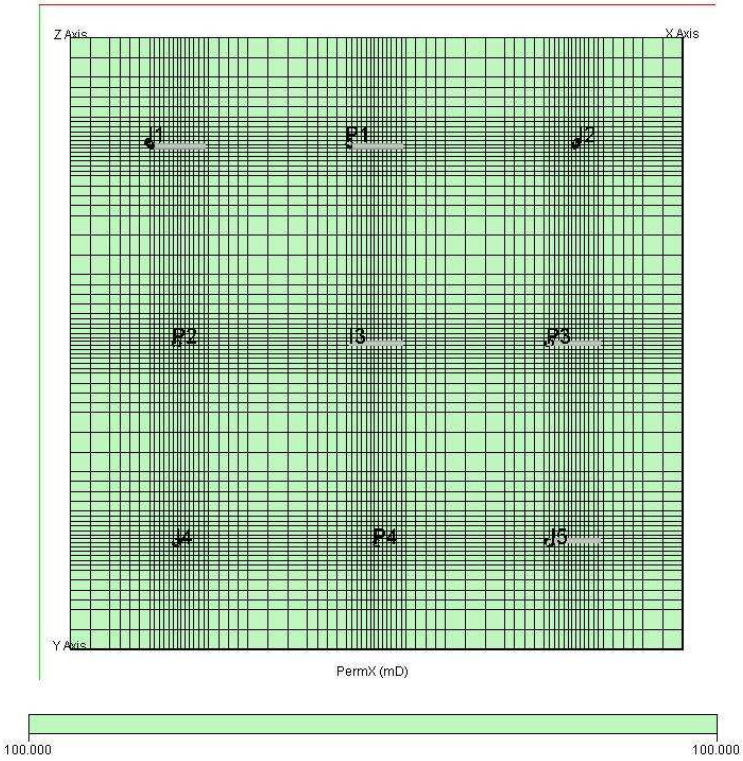


Figure 8.11. Top view of the simulation model showing the x direction permeability for the 5x4 Homogeneous Synthetic field– Mixed horizontal and vertical wells .

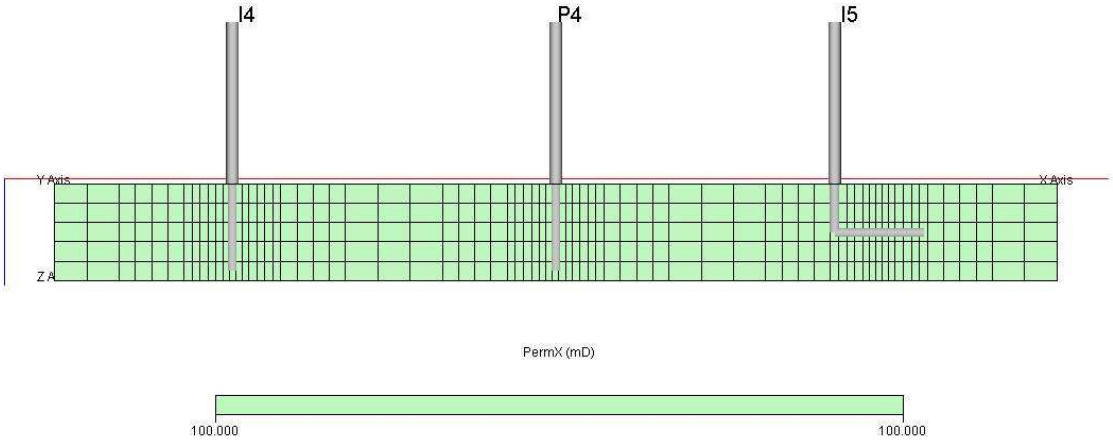


Figure 8.12. Cross sectional view showing three wells of the 5x4 Homogeneous Synthetic field– Mixed horizontal and vertical wells..

Table 8.5: Interwell Connectivity Coefficient results from simulation data for the 5x4 Homogeneous Synthetic field – Mixed horizontal and vertical wells.

	P1	P2	P3	P4	Sum
β_{0j} (psia)	-349.3	-540.1	-350.7	-540.5	-1781
I1	0.34	0.35	0.12	0.14	0.94
I2	0.17	0.06	0.17	0.06	0.47
I3	0.30	0.29	0.31	0.30	1.20
I4	0.06	0.17	0.06	0.17	0.46
I5	0.13	0.13	0.33	0.34	0.93
Sum	1.00	1.00	1.00	1.00	

Table 8.6: Relative interwell permeability results for the 5x4 Homogeneous Synthetic Field– Mixed horizontal and vertical wells (k_{ref}=100mD, Δt_{eq} = 7.33 days)

	P1	P2	P3	P4	Ave.
I1	117	122	96	102	109
I2	80	80	82	83	81
I3	107	104	111	106	107
I4	83	79	82	78	81
I5	100	100	116	118	108
Ave.	97	97	97	97	

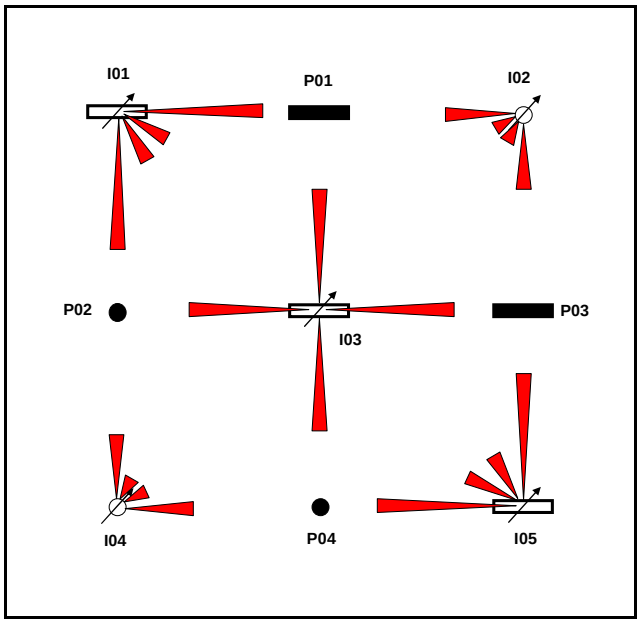


Figure 8.13. Representation of the connectivity coefficients for the 5x4 Homogeneous Synthetic field – Mixed horizontal and vertical wells.

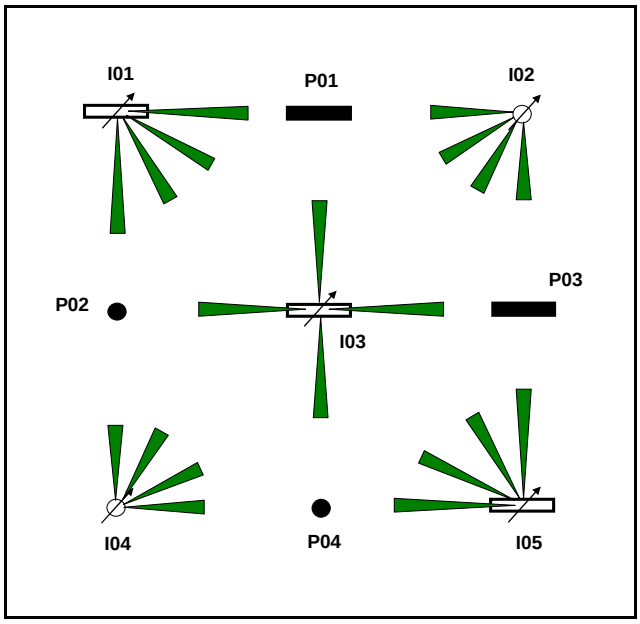


Figure 8.14. Representation of relative interwell permeability for the 5x4 Homogeneous Synthetic field – Mixed horizontal and vertical wells.

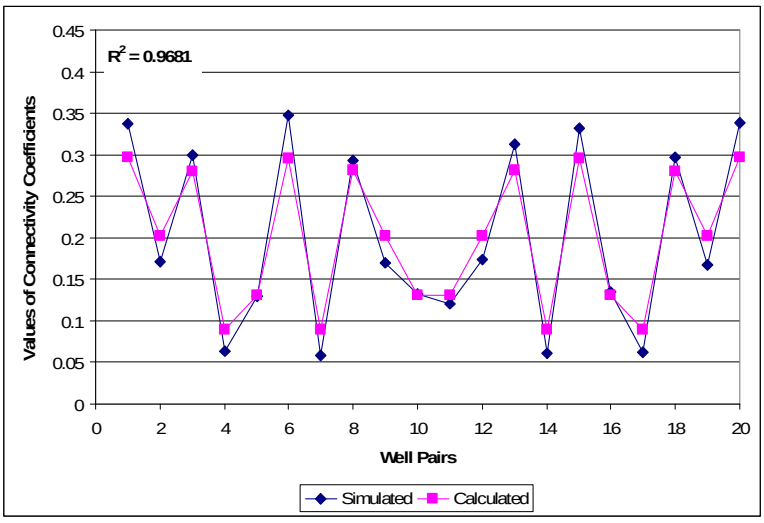


Figure 8.15. Comparison of the simulated and calculated interwell connectivity coefficient results for the 5x4 Homogeneous Synthetic field – Mixed horizontal and vertical wells.

8.5. Reservoir with Vertical Wells, Hydraulically Fractured Wells and Horizontal Wells

In this case, all three well types are present in the 5x4 homogeneous synthetic field. Fig. 8.16 shows the top view of the permeability distribution for this case. As shown on the figure, wells I02, I03 and P04 are horizontal wells, wells I01, P01 and I05 are hydraulically fractured wells and the other wells are vertical wells. The horizontal well lengths are 300 ft, the fracture half-lengths are 145 ft and all vertical wells are fully penetrating the formation. Fig. 8.17 shows the cross section through wells I04, P04 and I05. Well I04 are fully penetrating vertical well, well I05 is hydraulically fractured well and the horizontal well I05 is completed in the middle layer.

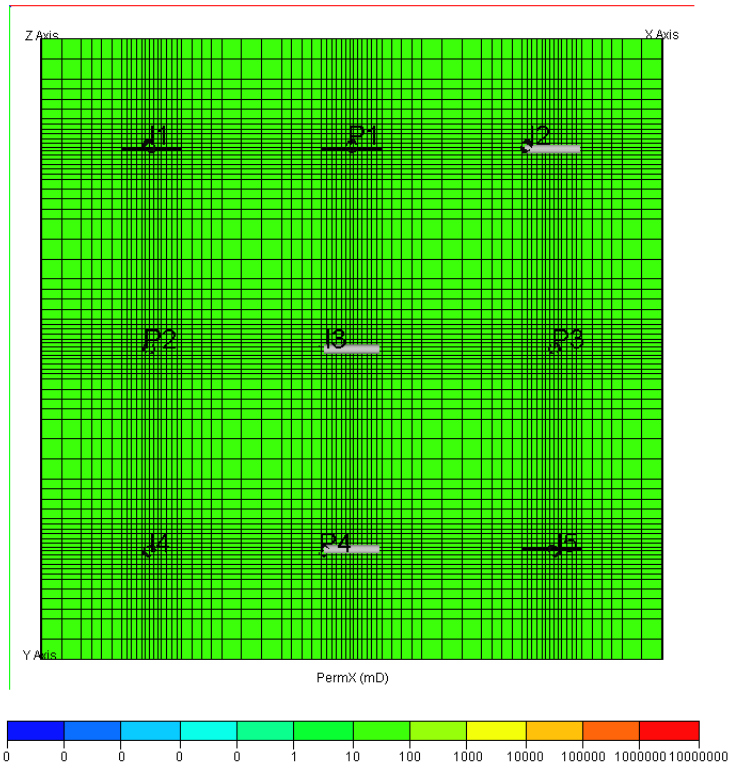


Figure 8.16. Top view of the simulation model showing the x direction permeability for the 5x4 Homogeneous Synthetic field– Mixed horizontal, hydraulically fractured and vertical wells .

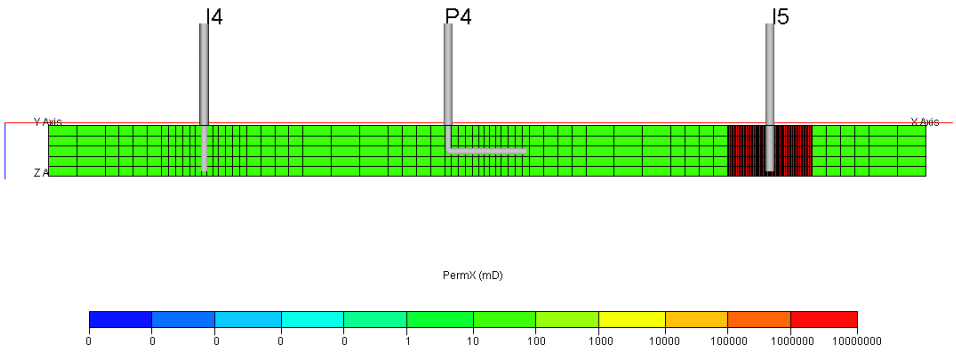


Figure 8.17. Cross sectional view showing three wells of the 5x4 Homogeneous Synthetic field– Mixed horizontal, hydraulically fractured and vertical wells.

Table 8.7 and Fig. 8.18 present the interwell connectivity coefficient results for this case. It is obvious that horizontal and hydraulically fractured injectors have better connectivity with the nearby producers than the vertical injector. The vertically fractured injectors have better connectivity with the nearby producer than the horizontal well have. This is reasonable because the pressure drop along a fractured well is higher than that of a horizontal well of the same half-length. Table 8.8 and Fig. 8.19 show the corresponding relative interwell permeability results for this reservoir.

The relative permeabilities for the pairs of hydraulically fractured injectors are higher than those of horizontal injectors and vertical injectors. This could be due to numerical error and analytical assumptions. Another reason could be the cross flow effect that altered the properties of fluid flow. However, the average relative interwell permeability is in good agreement with the input permeability of the model of 100 mD. Fig. 8.20 shows the comparison of the interwell connectivity coefficients results obtained from simulation data and by calculation using influence functions. Even though the match is not as good as in previous cases, the coefficient results are well proportional with $R^2 = 0.7846$.

Table 8.7: Interwell Connectivity Coefficient results from simulation data for the 5x4 Homogeneous Synthetic field – Mixed horizontal, hydraulically fractured and vertical wells.

	P1	P2	P3	P4	Sum
β_{0j} (psia)	-301.7	-538.9	-524.9	-404.2	-1770
I1	0.39	0.40	0.13	0.14	1.06
I2	0.25	0.08	0.25	0.08	0.65
I3	0.18	0.20	0.19	0.20	0.77
I4	0.05	0.18	0.05	0.18	0.47
I5	0.13	0.14	0.38	0.40	1.06
Sum	1.00	1.00	1.00	1.00	

Table 8.8: Relative interwell permeability results for the 5x4 Homogeneous Synthetic Field– Mixed horizontal, hydraulically fractured and vertical wells (k_{ref}=100mD, Δt_{eq} = 7.33 days)

	P1	P2	P3	P4	Ave.
I1	138	145	110	118	128
I2	86	91	87	91	89
I3	73	78	75	78	76
I4	92	99	92	98	96
I5	110	118	137	146	128
Ave.	100	106	100	106	

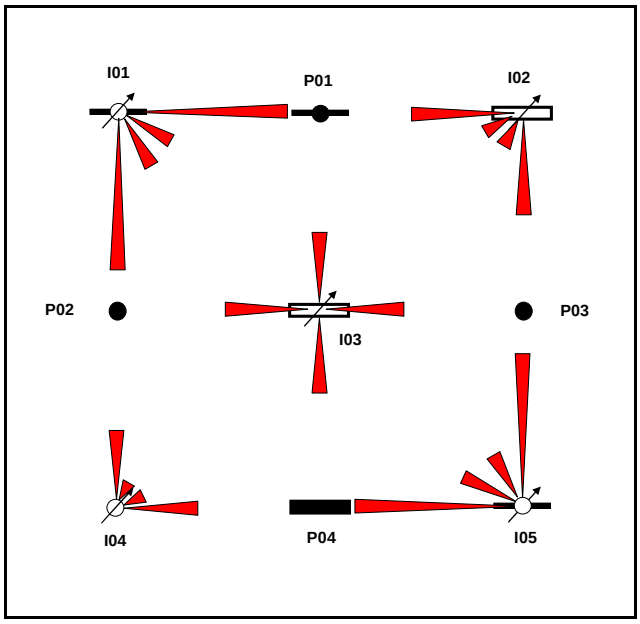


Figure 8.18. Representation of the connectivity coefficients for the 5x4 Homogeneous Synthetic field – Mixed horizontal, hydraulically fractured and vertical wells.

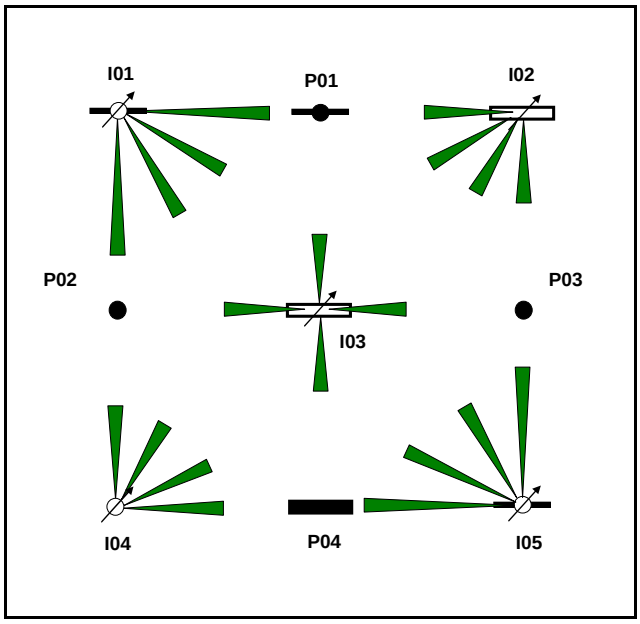


Figure 8.19. Representation of relative interwell permeability for the 5x4 Homogeneous Synthetic field – Mixed horizontal, hydraulically fractured and vertical wells.

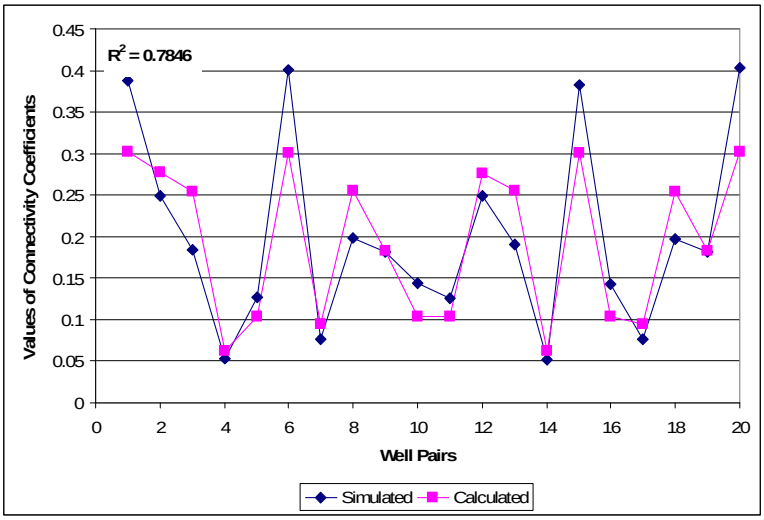


Figure 8.20. Comparison of the simulated and calculated interwell connectivity coefficient results for the 5x4 Homogeneous Synthetic field – Mixed horizontal, hydraulically fractured and vertical wells.

CHAPTER 9 – ANALYSIS OF PRODUCTION DATA OF A WATERFLOOD UNDER THE STEADY STATE FLOW CONDITION

This chapter presents a new analytical model for flow rates data in a waterflood system to provide an in-depth understanding of the MLR technique for production data and the relationships between the interwell connectivity coefficients calculated from production data and other reservoir parameters. The model is based on an analytical solution for bottom hole pressure responses of fully penetrating vertical injectors and producers in a closed rectangular reservoir. The assumption for this model is that the field is under steady-state flow condition. Similar to the case of pressure data, the interwell connectivity coefficient results are used to calculate relative interwell permeability.

Different synthetic reservoir models were analyzed including: homogeneous, anisotropic reservoirs, reservoirs with high permeability channel and transmissibility barriers. Comparisons are made with results obtained from previous studies from both production data and bottom hole pressure data.

9.1. Overview

Production data is one of the most abundant well data in waterfloods. As mentioned before, there are numerous studies concerning interwell connectivity calculation from production data. Albertoni and Lake (2003) used multivariate linear regression analysis of the flow rates in a waterflood to infer interwell connectivity. The advantages of this technique include simplified one-step calculation and availability of the production data. Diffusivity filters are required to account for the time lag and attenuation of the flow rate signals. The method proposed by Albertoni and Lake, however, did not take into account the effect of the flow rates of other producers.

A capacitance model based on the Albertoni and Lake model was developed to account for the shut-in periods and the changes in bottom-hole pressures at the producers (Yousef et al., 2006). The approach still requires subjective judgments.

The analytical model proposed in this chapter is able to take into account the effects of both injectors and producers on the investigated producer or observation well. It also provides a relationship between the interwell connectivity coefficients calculated from production data and other reservoir parameters via the influence functions defined in previous chapters.

9.2. Analytical Model for Reservoir Flowing in Steady State with Injection Wells

9.2.1. MLR method

The main assumption for this analytical model is that the reservoir is flowing under steady state condition. Thus, the producers are under pressure control and the total injection rate is equal to the total production rate at the end of every rate interval. Different from Albertoni and Lake's solution (2003) which assumed all flow rates at the producers are caused by the rates at the injectors and used balanced multivariate regression (BMLR) for the case, the solution presented in this section uses only the MLR method. In the MLR method, a constant term is included in the equations for the response well flow rates; while in the BMLR method, this term is equal to zero. In our case, the term was included in the flow rates of response wells to account for the effect of other response wells. Further explanation can be found in the following section.

Similar to the pressure model, the estimated flow rate at a producer *j* (observation well) is given by:

$$\hat{q}_j(t) = \lambda_{0j} + \sum_{i=1}^{I} \lambda_{ij} q_i(t) \qquad (j = 1, 2, \ldots N) \tag{9.1}$$

where N is the total number of producers and I is the number of injectors. This equation states that at any time the total flow rate at producer j is a linear combination of the flow rate portion of every injector corresponding to that producer plus a constant term, λ_{0j}. The factors λ_{ij} are the weighting factors or interwell connectivity coefficients and the constant term λ_{0j} accounts for the unbalance. If the flow rates of producers and injectors are known, the coefficients λ_{ij} and the term λ_{0j} need to be determined.

Again, the minimization of the errors leads to the following set of I linear equations:

$$\begin{pmatrix} \sigma_{11}^2 & \sigma_{12}^2 & \cdots & \sigma_{1I}^2 \\ \sigma_{21}^2 & \sigma_{22}^2 & \cdots & \sigma_{2I}^2 \\ \vdots & \vdots & \ddots & \vdots \\ \sigma_{I,1}^2 & \sigma_{I2}^2 & \cdots & \sigma_{II}^2 \end{pmatrix} \times \begin{pmatrix} \lambda_{1j} \\ \lambda_{2j} \\ \vdots \\ \lambda_{Ij} \end{pmatrix} = \begin{pmatrix} \sigma_{1j}^2 \\ \sigma_{2j}^2 \\ \vdots \\ \sigma_{Ij}^2 \end{pmatrix} \tag{9.2}$$

which can be solved by standard means. The constant term β_{0j} is given by:

$$\lambda_{0j} = \bar{q}_j - \sum_{i=1}^{I} \lambda_{ij} \bar{q}_i \tag{9.3}$$

where σ^2_{ii} and σ^2_{ij} are injector-injector and injector-producer covariances respectively.

Thus, a set of I+1 equations and I+1 unknowns must be solved for each producer (Equations 9.2 and 9.3). The interwell connectivity coefficients λ_{ij} obtained from the solution of the N systems of equations provide a quantitative expression of the influence of each injector i on each producer j; the larger the λ_{ij}, the greater the influence. The assumption for this test is that the bottom hole pressure at the producers is kept constant.

9.2.2. Analytical Model for Production Data

From Eqs. 4.19 and 4.21, we can write the pressure equation for the producer j as

$$p_{ave}(t) - p_{wf,j}(x_{wDj}, y_{wDj}, t) = \frac{141.2B\mu}{kh}\left[q_j\left(a_{jj} - 2\pi t_{DA}\right)\right] \tag{9.4}$$

Or

$$q_j = \frac{\left[p_{ave}(t) - p_{wf,j}(x_{wDj}, y_{wDj}, t)\right]}{\frac{141.2B\mu}{kh}\left[\left(a_{jj} - 2\pi t_{DA}\right)\right]} \tag{9.5}$$

Substituting Eq. 9.5 to Eq. 4.8 for producer j', we obtain

$$\begin{aligned} &p_{ini} - p_{wf,j'}(x_{wDj'}, y_{wDj'}) = \\ &\frac{141.2B\mu}{kh}\left\{\sum_{j=1}^{n_{pr}} \frac{a_{jj'}\left[x_{wDj'}, y_{wDj'}, x_{wDj}, y_{wDj}, x_{eD}, y_{eD}, t_{AD}\right]\left[p_{ave}(t) - p_{wf,j}(x_{wDj}, y_{wDj}, t)\right]}{\frac{141.2B\mu}{kh}\left[\left(a_{jj} - 2\pi t_{DA}\right)\right]}\right. \\ &\left. - \sum_{i=1}^{n_{inj}} a_{ij'}\left[x_{wDj'}, y_{wDj'}, x_{wDi}, y_{wDi}, x_{eD}, y_{eD}, t_{AD}\right] q_i\right\} \end{aligned} \tag{9.6}$$

Substituting the right hand side of Eq. 9.6 with Eq. 4.19, we have

$$\begin{aligned} &\frac{141.2B\mu}{kh}\left[q_{j'}\left(a_{j'j'} - 2\pi t_{DA}\right) + 2\pi\Delta q_{tot} t_{DA}\right] = \\ &\frac{141.2B\mu}{kh}\left\{\sum_{j=1}^{n_{pr}} \frac{a_{jj'}\left[x_{wDj'}, y_{wDj'}, x_{wDj}, y_{wDj}, x_{eD}, y_{eD}, t_{AD}\right]\left[p_{ave}(t) - p_{wf,j}(x_{wDj}, y_{wDj}, t)\right]}{\frac{141.2B\mu}{kh}\left[\left(a_{jj} - 2\pi t_{DA}\right)\right]} - \right. \\ &\left. - \sum_{i=1}^{n_{inj}} a_{ij'}\left[x_{wDj'}, y_{wDj'}, x_{wDi}, y_{wDi}, x_{eD}, y_{eD}, t_{AD}\right] q_i\right\} \end{aligned} \tag{9.7}$$

Since $\Delta q_{tot} \approx 0$, Eq. 9.7 becomes

$$\left[q_{j'}\left(a_{j'j'}-2\pi t_{DA}\right)\right]=\left\{\sum_{j=1}^{n_{pr}}\frac{a_{jj'}\left[x_{wDj'},y_{wDj'},x_{wDj},y_{wDj},x_{eD},y_{eD},t_{AD}\right]\left[p_{ave}(t)-p_{wf,j}\left(x_{wDj},y_{wDj},t\right)\right]}{\frac{141.2B\mu}{kh}\left[\left(a_{jj}-2\pi t_{DA}\right)\right]}-\right.$$
$$\left.-\sum_{i=1}^{n_{inj}}a_{ij'}\left[x_{wDj'},y_{wDj'},x_{wDi},y_{wDi},x_{eD},y_{eD},t_{AD}\right]q_i\right\} \tag{9.8}$$

Or

$$q_{j'}=-\sum_{i=1}^{n_{inj}}\frac{a_{ij'}}{\left(a_{j'j'}-2\pi t_{DA}\right)}q_i+\Delta q_{sp} \tag{9.9}$$

Where Δq_{sp} is a constant due to constant average reservoir pressure (p_{ave}) and constant bottom hole pressure at the producers ($p_{wf,j}$). Δq_{sp} is defined as

$$\Delta q_{sp}=\sum_{j=1}^{n_{pr}}\frac{a_{jj'}\left[p_{ave}(t)-p_{wf,j}\left(x_{wDj},y_{wDj},t\right)\right]}{\frac{141.2B\mu}{kh}\left(a_{jj}-2\pi t_{DA}\right)\left(a_{j'j'}-2\pi t_{DA}\right)} \tag{9.10}$$

Eq. 9.9 should be equivalent to Eq. 9.1 if we have

$$\lambda_{ij'}=\frac{a_{ij'}}{\left(a_{j'j'}-2\pi t_{DA}\right)} \tag{9.11}$$

and $\lambda_{0j'}=\Delta q_{sp}$ (9.12)

Again, since Eq. 9.9 should be true at any time during the steady state flow, we can adjust the time in t_{DA} term so that Eq. 9.11 is satisfied (the equivalent time). Eq. 9.12, however, is a constant term and depends on the length of the time intervals.

Note that if we assume the flow at every well itself is under pseudo-steady state condition, thus Eq. 5.1 applies, then the term $2\pi t_{DA}$ in the influence functions of the denominators of both Eqs. 9.10 and 9.11 are canceled out. Thus, the denominators do not depend on time. Hence, the interwell connectivity coefficients, $\lambda_{ij'}$, for the producer j',

only depend on the location of producer j' and the influence functions between injectors, i, and the producer j'.

Since p_{ave} stay constant for every time interval and the bottom hole pressures at the producers are equal and constant, we should be able to calculate the p_{ave} from Eq. 9.10:

$$p_{ave,j'}(t) = \frac{\Delta q_{sp}}{\sum_{j=1}^{n_{pr}} \frac{a_{jj'}}{\frac{141.2B\mu}{kh}\left[\left(a_{jj} - 2\pi t_{DA}\right)\left(a_{j'j'} - 2\pi t_{DA}\right)\right]}} + p_{wf,j}\left(x_{wDj}, y_{wDj}, t\right) \tag{9.13}$$

However, since Δp_{sp} is not perfectly constant at every time step and the permeability may vary due to the reservoir heterogeneity, Eq. 9.13 can only be used to calculate the approximate value of p_{ave} with an assumed average permeability. The time involved in Eq. 9.13 should be the total time of each time interval.

9.3. Simulation Results

9.3.1. Model Description

The basic model for this case is the same as in chapter 4 except that the producers are controlled by bottom hole pressures. All wells are vertical wells and the injection rates were generated randomly between 100 and 400 rbbl/day (see Fig. 9.1). The time interval was increased from 30 days to 300 days to guarantee the steady state flow condition. The bottom hole pressure at every producer was kept constant at 300 psia.

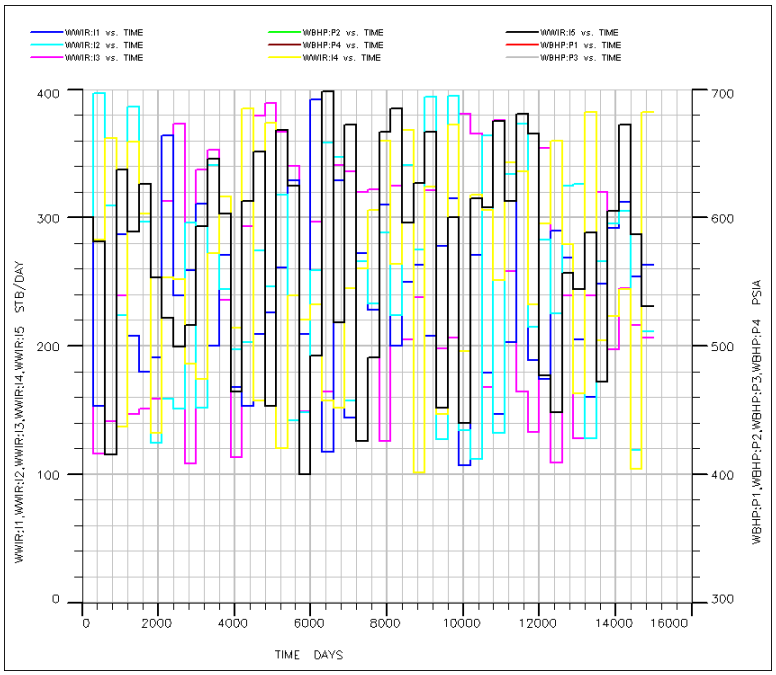


Figure 9.1. Input flow rate data for the injectors, 5x4 homogeneous synthetic field-Production data.

9.3.2. Homogeneous Reservoir

Similar to the homogeneous case of 5x4 Synthetic field in Chapter 4, the permeability for both x and y direction was set to 100 mD for this case. 50 data points were obtained. Fig. 9.2 shows a plot of the cumulative water injection and production for the whole field versus time. At any time, the two values are about equal. Fig. 9.3 presents the total field injection rate versus production rate. The two rates are approximately equal at every time step. Thus, the steady state condition assumption can be considered as satisfied.

Table 9.1 and Fig. 9.4 present the interwell connectivity coefficient results for this case. The results are in good symmetry with the asymmetry coefficient (A_s) of 0.007343 indicating good results. Table 9.2 and Fig. 9.5 show the corresponding relative interwell permeability results for this reservoir. Eq. 4.6 was used through out this chapter to calculate influence function as it is applicable for both early time and late time. Since

the summations of the coefficients for the producers are not constant when bottom-hole pressures are used, we may assume a permeability for one well pair is known, and then adjust the Δt_{eq} so that the calculated interwell connectivity for that pair is equal to the corresponding coefficient obtained from MLR method using simulation data. In our case, the reference pair was I05-P04 with a reference permeability of 100 mD as colored in red in Table 9.2. The resulted relative interwell permeabilities are in very good agreement with the input permeability of 100 mD for the model.

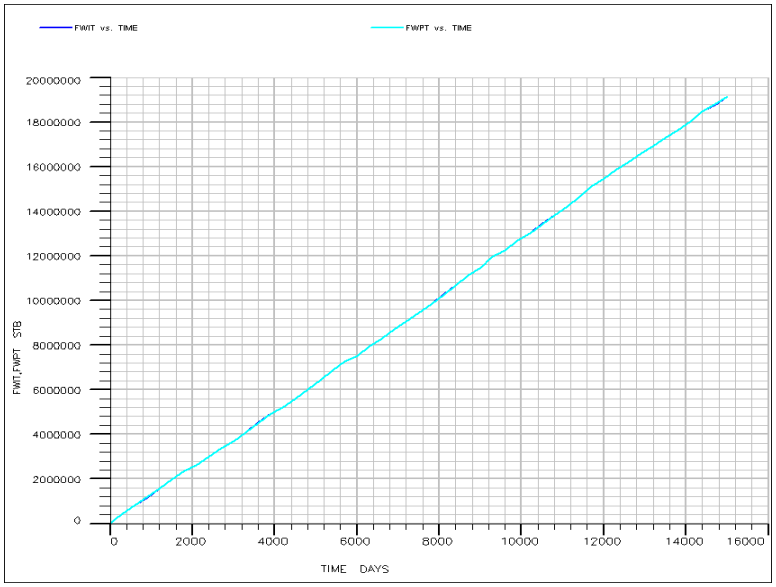


Figure 9.2. Water injection and production total for the 5x4 homogeneous synthetic field-Production data.

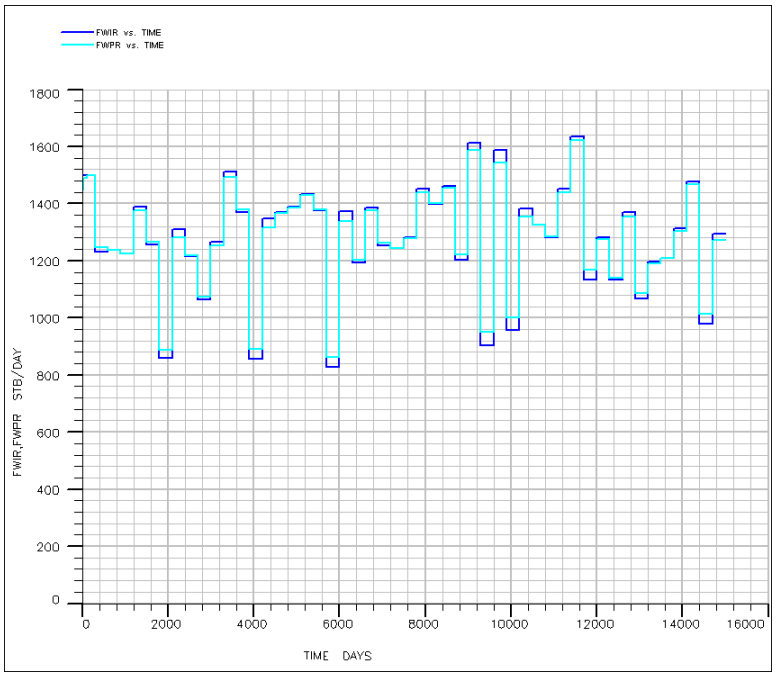


Figure 9.3. Water injection and production rates for the 5x4 homogeneous synthetic field-Production data.

Table 9.1: Interwell Connectivity Coefficient results from MLR for the 5x4 homogeneous synthetic field-Production data (A_s = 0.00734)

	P1	P2	P3	P4	Sum
λ_{0j} (psia)	29.9	30.1	29.9	30.1	120
I1	0.29	0.29	0.14	0.14	0.87
I2	0.31	0.16	0.31	0.16	0.93
I3	0.23	0.23	0.23	0.23	0.90
I4	0.14	0.30	0.14	0.30	0.88
I5	0.16	0.16	0.31	0.31	0.94
Sum	1.13	1.13	1.13	1.13	

Table 9.2: Relative interwell permeability results for the 5x4 Homogeneous Synthetic Field– Production data (k_{ref}=100mD, Δt_{eq} = 7.57 days)

	P1	P2	P3	P4	Ave.
I1	94	94	103	103	98
I2	99	110	99	110	105
I3	94	94	95	95	94
I4	104	94	104	95	99
I5	111	111	100	100	106
Ave.	100	101	100	100	

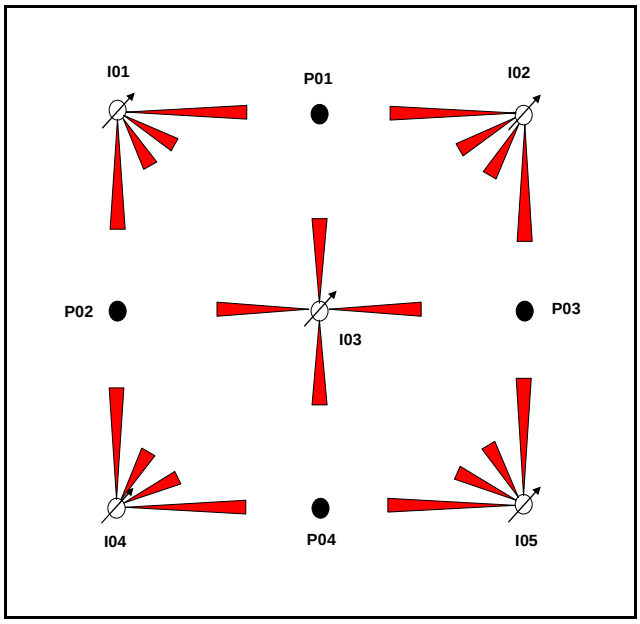


Figure 9.4. Representation of the connectivity coefficients for the 5x4 Homogeneous Synthetic fields – Production data.

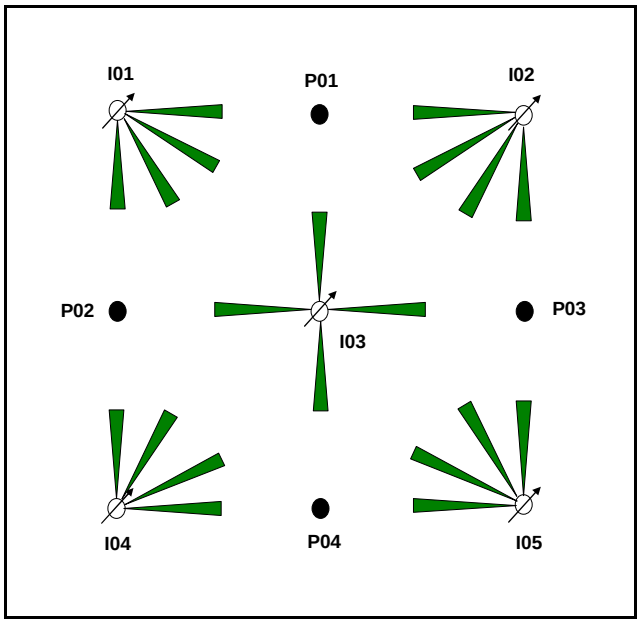


Figure 9.5. Representation of relative interwell permeability for the 5x4 Homogeneous Synthetic field – Production data.

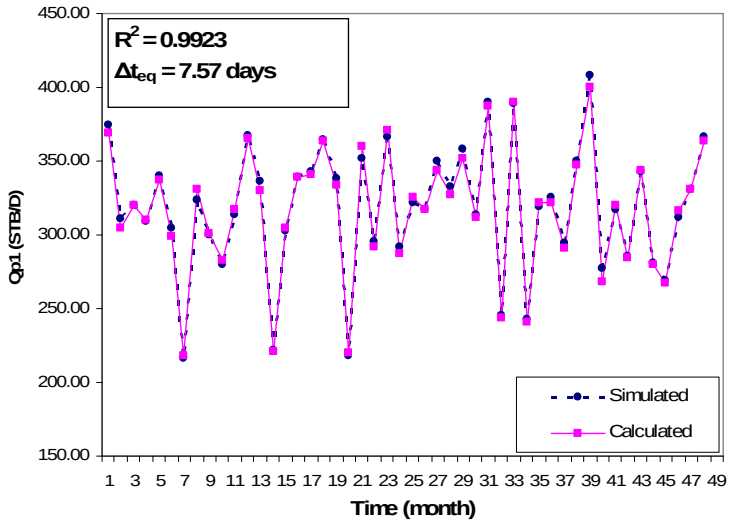


Figure 9.6. Flow rate from Eq.9.9 (t_{eq}=7.57 days) and from simulation results for Well P-01, 5x4 homogeneous synthetic field.

Fig. 9.6 shows the flow rate results for well P-01 obtained from Eqs. 9.9 and 9.10 in comparison with the simulation data. The coefficient of determination (R^2) shown on Fig. 9.6 does not depend on λ_{0j}. Excellent match is observed on Fig. 9.6 with R^2 = 0.9923. The average pressure was calculated to be 727 psi using Eq. 9.13 with the time equal the total length for each time interval of 300 days and λ_{0j} equal 29.9 psia obtained from Table 9.1. The actual value was 650 psia, which is close to the calculated value.

Fig. 9.7 shows the comparison of the interwell connectivity coefficients results obtained from simulation data and from calculations using influence functions. The coefficients are in good agreement with R^2 = 0.9822.

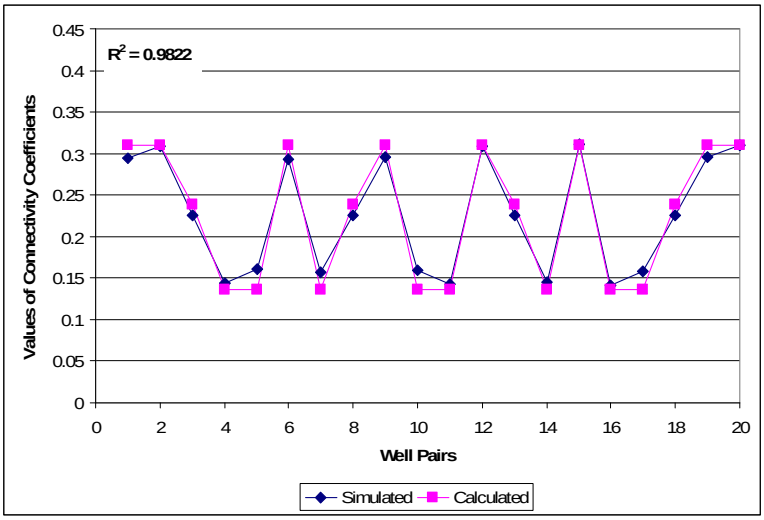


Figure 9.7. Comparison of the simulated and calculated interwell connectivity coefficient results for the 5x4 Homogeneous Synthetic field – Production data.

The input data for the analytical calculation were changed to match the input data the corresponding simulation model in Albertoni's study (the horizontal permeability was changed to 40 mD). The connectivity coefficient results from the analytical model proposed in this study were compared with the results obtained by Albertoni (2002) using MLR with diffusivity filters as shown in Fig. 9.8. The plot indicate a good match between Albertoni's results and the analytical calculation results with $R^2 = 0.9800$. Thus, the final interwell connectivity coefficients obtained from MLR technique with diffusivity filters match well with the steady state analytical solutions.

These results confirm the validity of the analytical model proposed in this chapter. The results also indicate that the diffusivity filters eventually lead the interwell connectivity coefficient results from total injection-production unbalanced flow rate data to the results from steady state data where total injection rates approximately equal to the total production rates.

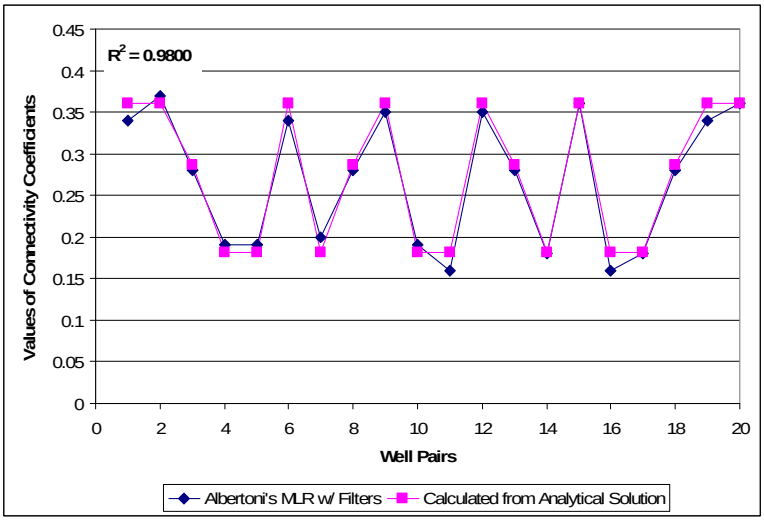


Figure 9.8. Comparison of the interwell connectivity coefficient results for the 5x4 Homogeneous Synthetic field obtained from simulation data using MLR technique with diffusivity filters in the Albertoni and Lake study and the results obtained from analytical model in this study – Production data.

9.3.3. Anisotropic Reservoir

In this case, the effective permeability in the x direction (1000 mD) is tenfold the permeability in the y direction (100 mD). Table 9.3 and Fig. 9.9 show the results for the interwell connectivity coefficients. As expected, the results are well indications of the anisotropy with large coefficients for well pairs in the direction of high permeability. Table 9.4 and Fig. 9.10 present the corresponding relative interwell permeabilities with I01-P01 as reference well pair and with the reference permeability of 316 mD.

Table 9.3: Interwell Connectivity Coefficient results from simulation data for the 5x4 Anisotropic Synthetic field– Production data

	P1	P2	P3	P4	Sum
λ_{0j} (psia)	10.9	8.6	8.6	11.2	39
I1	0.53	0.18	0.17	0.08	0.96
I2	0.53	0.17	0.19	0.08	0.98
I3	0.18	0.31	0.31	0.18	0.97
I4	0.08	0.19	0.17	0.53	0.96
I5	0.08	0.18	0.19	0.53	0.98
Sum	1.39	1.03	1.03	1.39	

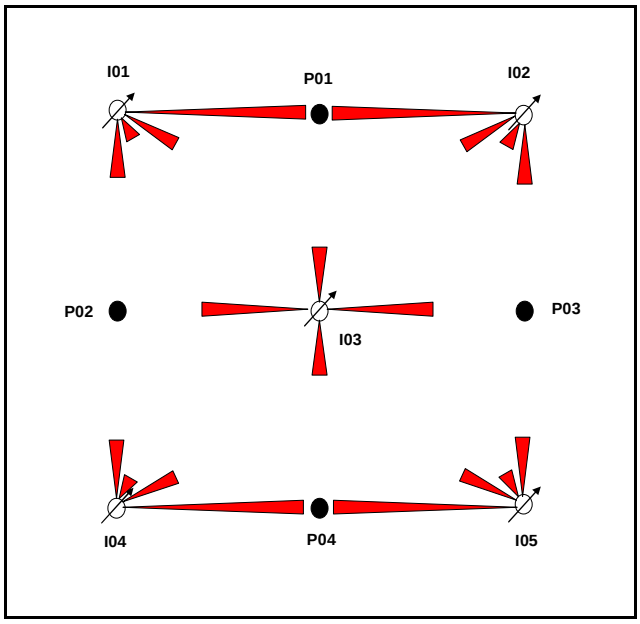


Figure 9.9. Representation of the interwell connectivity coefficients for the case of 5x4 Anisotropic Reservoir – Production data.

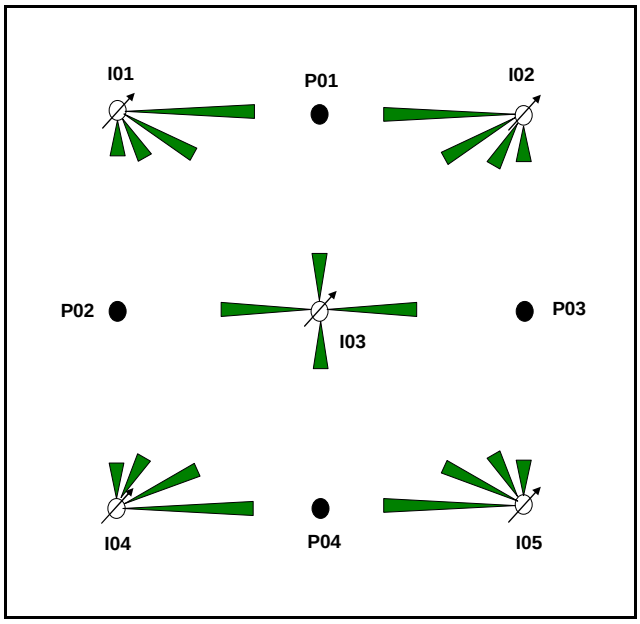


Figure 9.10. Representation of the relative interwell permeabilities for the case of 5x4 Synthetic Reservoir– Production data.

Table 9.4: Relative interwell permeability results for the 5x4 Anisotropic Synthetic Field – Production data (k_{ref}=316 mD, Δt_{eq} = 7.57 days)

	P1	P2	P3	P4	Ave.
I1	**316**	92	194	121	181
I2	319	197	95	127	185
I3	125	217	217	126	171
I4	121	93	194	316	181
I5	128	198	95	320	185
Ave.	202	159	159	202	

9.3.4. Reservoir with high permeability channel

Similar to the high permeability channel cases in previous chapters, the permeability of the channel was ten-fold (1000 mD) of that in other areas of the reservoir (100 mD). Again, all wells are fully penetrating vertical wells. Table 9.5 and Fig. 9.11 show the results for the interwell connectivity coefficients. The results reflect accurately the presence of the channel.

Table 9.5: Interwell Connectivity Coefficient results from simulation data for the 5x4 Synthetic field with high permeability channel – Production data.

	P1	P2	P3	P4	Sum
λ_{0j} (psia)	6.8	6.1	7.0	32.9	53
I1	0.13	0.16	0.06	0.59	0.95
I2	0.20	0.09	0.21	0.46	0.96
I3	0.09	0.12	0.07	0.67	0.96
I4	0.06	0.12	0.05	0.71	0.95
I5	0.06	0.07	0.14	0.71	0.98
Sum	0.54	0.56	0.53	3.15	

Table 9.6: Relative interwell permeability results for the 5x4 Synthetic Field with high permeability channel – Production data (k_{ref}=1000mD, Δt_{eq} = 7.57 days)

	P1	P2	P3	P4	Ave.
I1	128	163	223	**1000**	378
I2	199	264	215	818	374
I3	131	179	106	959	344
I4	225	122	197	904	362
I5	217	231	139	908	374
Ave.	180	192	176	918	

Table 9.6 and Fig. 9.12 present the corresponding relative interwell permeabilities with I01-P04 as the reference well pair and the reference permeability of 1000 mD.

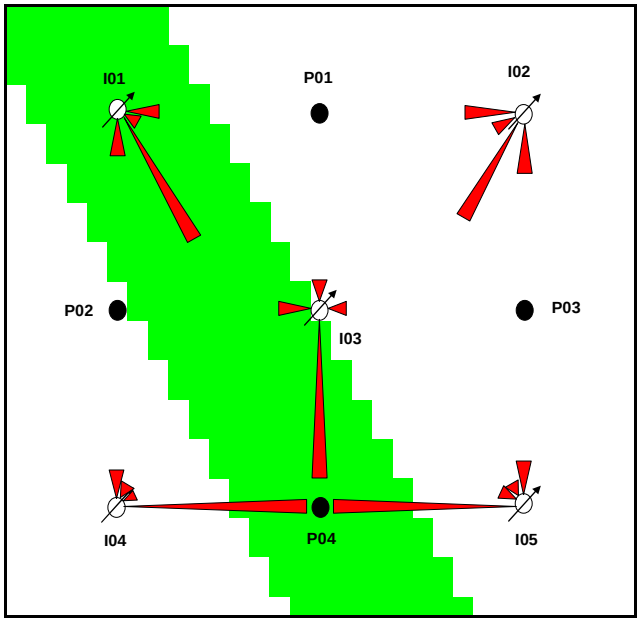


Figure 9.11. Representation of the connectivity coefficients for the case of 5x4 Synthetic Reservoir with high permeability channel – Production data

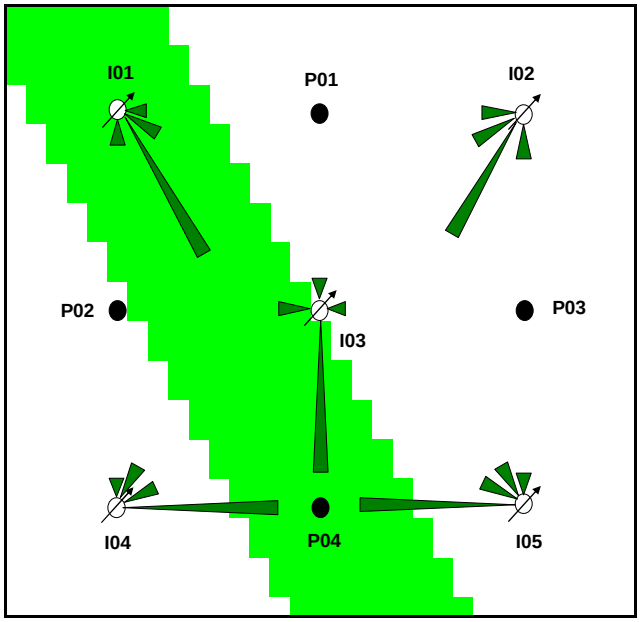


Figure 9.12. Representation of relative interwell permeability for the case of 5x4 Synthetic Reservoir with high permeability channel – Production data.

9.3.5. Reservoir with a partially sealing barrier

Table 9.7 and Fig. 9.13 show the results for the interwell connectivity coefficients for this case. The presence of the partially sealing barrier is well established based on the results. Table 9.8 and Fig. 9.14 present the corresponding relative interwell permeabilities with I04-P02 as a reference well pair and with the reference permeability of 100 mD. A cut-off value of 0.05 was applied to eliminate small coefficients. Thus, the relative interwell permeability for well pairs with interwell connectivity coefficient of less than 0.05 were set to zero. The cut-off value was required because the influence functions were not defined for small coefficients.

Table 9.7: Interwell Connectivity Coefficient results from simulation data for the 5x4 Synthetic field with partially sealing barrier– Production data.

	P1	P2	P3	P4	Sum
λ_{0j} (psia)	18.0	44.9	27.3	37.6	128
I1	0.03	0.51	0.08	0.23	0.85
I2	0.41	0.06	0.37	0.11	0.94
I3	0.05	0.40	0.12	0.32	0.89
I4	0.04	0.39	0.10	0.34	0.87
I5	0.13	0.17	0.32	0.32	0.94
Sum	0.66	1.53	0.99	1.32	

Table 9.8: Relative interwell permeability results for the 5x4 Synthetic field with partially sealing barrier– Production data (k_{ref}=100mD, Δt_{eq} = 7.57 days)

	P1	P2	P3	P4	Ave.
I1	0	141	55	108	76
I2	107	50	94	68	80
I3	0	129	39	103	68
I4	0	**100**	65	87	63
I5	76	88	80	80	81
Ave.	36	101	67	89	

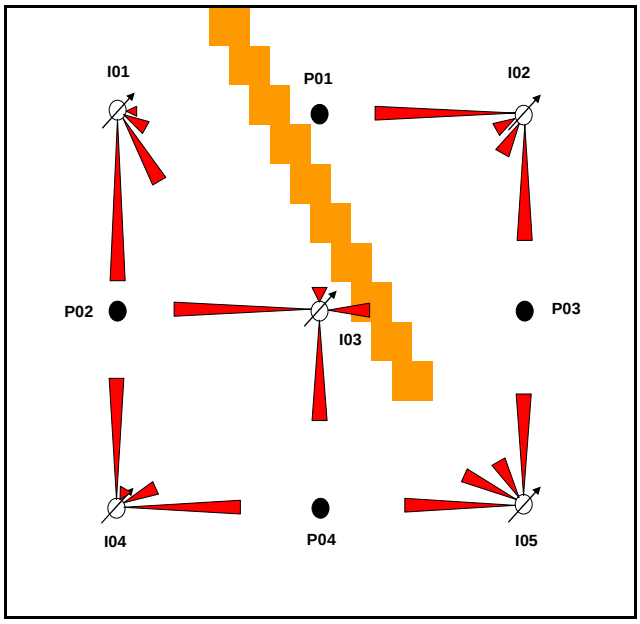


Figure 9.13. Representation of the connectivity coefficients for the case of 5x4 homogeneous reservoir with a partially sealing barrier– Production data.

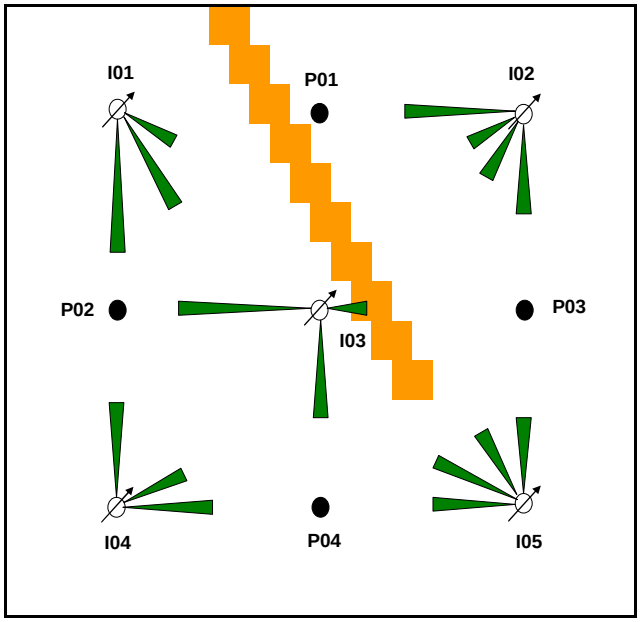


Figure 9.14. Representation of relative interwell permeability for the case of 5x4 dual-porosity reservoir with a partially sealing barrier– Production data.

9.3.6. Reservoir with a sealing barrier

The simulation model for this case is the same as for the corresponding case in Chapter 4. Thus, the only differences are the flow rates and the producer well controls as explained before. Table 9.9 and Fig. 9.15 show the results for the interwell connectivity coefficients. Similar to previous cases, the results clearly reflect the presence of the sealing barrier. Some connectivity coefficients are very small and even negative. They indicate poor connectivity or no connectivity at all.

Table 9.9: Interwell Connectivity Coefficient results from simulation data for the 5x4 Synthetic field with a sealing barrier – Production data.

	P1	P2	P3	P4	Sum
λ_{0j} (psia)	18.5	43.5	27.2	36.6	126
I1	-0.01	0.56	-0.01	0.31	0.85
I2	0.45	0.01	0.48	0.01	0.95
I3	0.00	0.47	-0.01	0.43	0.89
I4	-0.01	0.44	-0.01	0.44	0.87
I5	0.27	0.01	0.66	0.00	0.94
Sum	0.71	1.48	1.12	1.20	

Table 9.10: Relative interwell permeability results for the 5x4 Synthetic Field with a sealing barrier – Production data (k_{ref}=100mD, Δt_{eq} = 5.66 days)

	P1	P2	P3	P4	Ave.
I1	0.00	132.60	0.00	115.08	62
I2	103.67	0.00	110.69	0.00	54
I3	0.00	127.52	0.00	119.04	62
I4	0.00	**100.00**	0.00	100.94	50
I5	103.95	0.00	160.99	0.00	66
Ave.	42	72	54	67	

Table 9.10 and Fig. 9.16 present the corresponding relative interwell permeabilities with I04-P02 as a reference well pair and with the reference permeability of 100 mD. A cut-off coefficient of 0.06 was applied to eliminate the low connectivity coefficients. Thus, the relative interwell permeability corresponding to the coefficients

lower than 0.06 were set to zeros. The resulted relative interwell permeabilities show a clear presence of the sealing barrier.

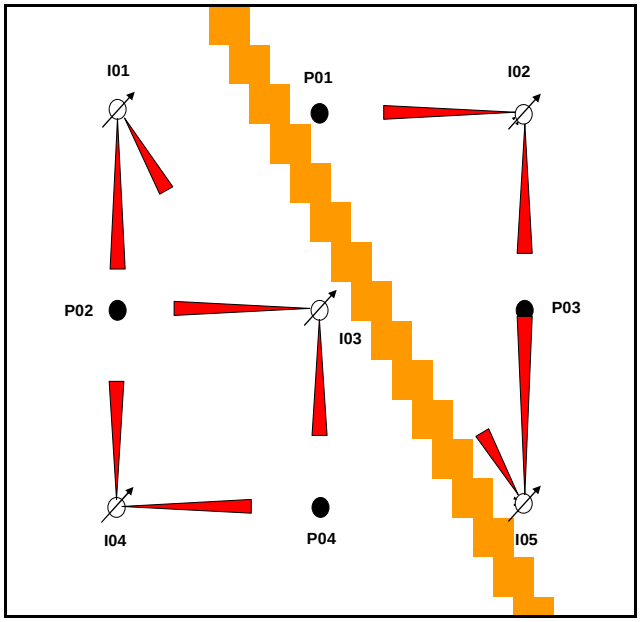


Figure 9.15. Representation of the connectivity coefficients for the 5x4 Synthetic Field with a sealing barrier – Production data.

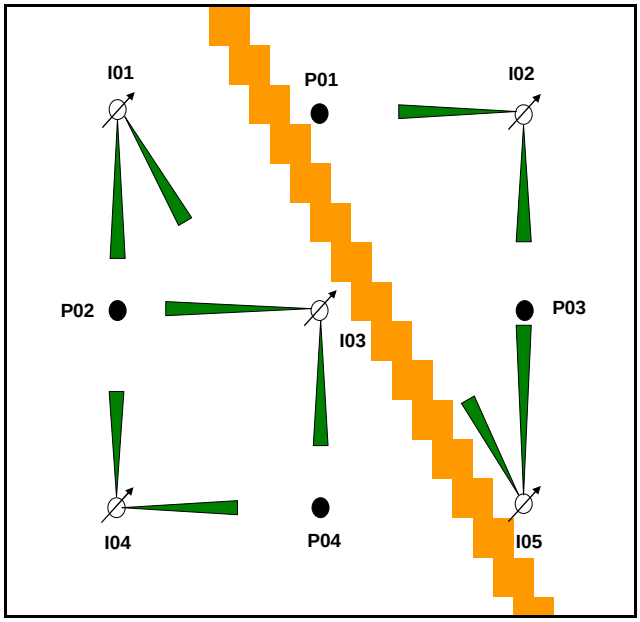


Figure 9.16. Representation of relative interwell permeability for the 5x4 Synthetic Field with a sealing barrier – Production data.

9.3.7. 25x16 Synthetic Field

Similar to the homogeneous case of 25x16 Synthetic field in Chapter 4, the permeability for both x and y direction was set to 100 mD for this case. However, the producers were put on the bottom hole pressure control instead of the flow rate control as in Chapter 4. The injectors were put on flow rate control with the rates randomly generated between 200 and 600 STBD. The time interval between rate changes was 300 days. 130 data points were collected. Fig. 9.17 shows a plot of the cumulative water injection and production for the whole field versus time. At any time, the two values are about equal. Fig. 9.18 presents the total field injection rate versus production rate. The two rates are approximately equal at every time step. Thus, the steady state condition assumption can be considered as satisfied.

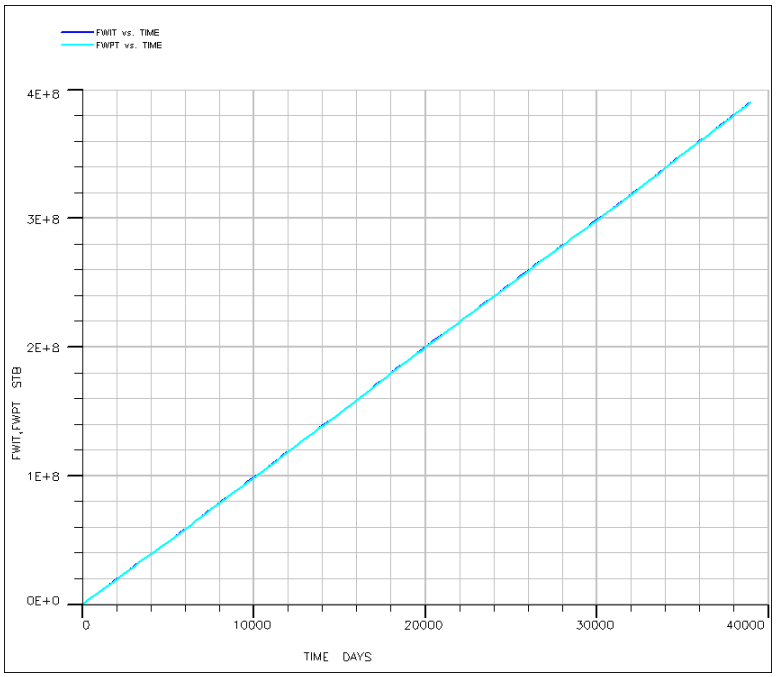


Figure 9.17. Cumulative total water injection and production rates for the 25x16 homogeneous synthetic field-Production data.

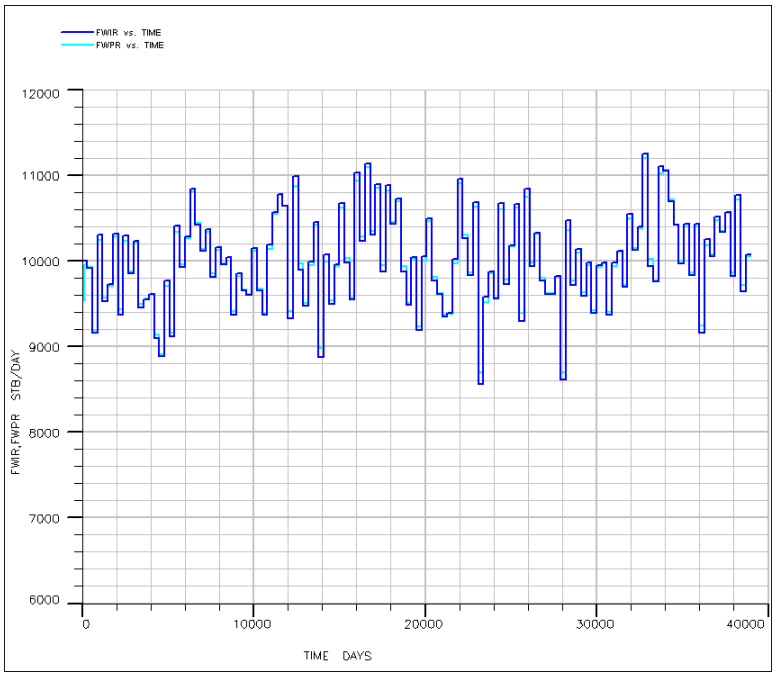


Figure 9.18. Water injection and production rates for the 25x16 homogeneous synthetic field-Production data.

Table 9.11 presents the results for the interwell connectivity coefficients. Good results were obtained for the interwell connectivity coefficients with asymmetry coefficient (A_s) of 0.00588. Table 9.12 and Fig. 9.19 present the corresponding relative interwell permeabilities with I01-P01 as a reference well pair with the reference permeability of 100 mD and the equivalent time of 5.87 days. The reference permeability is marked in red in Table 9.12. A cut-off coefficient of 0.04 was applied to eliminate the low connectivity coefficients. Thus, the relative interwell permeability corresponding to the coefficients lower than 0.04 were set to zeros. Fig. 9.20 shows the plot of all relative interwell permeability values. The results are close to the input value of 100 mD with a few exceptions. More relative interwell permeability values were obtained for this case compared to the naturally fractured reservoir case. The reason is the equation used to calculate influence functions for this case is applicable for both early time and late time and thus better represents the actual field occurrence.

Fig. 9.21 shows the comparison of the interwell connectivity coefficients results obtained from simulation data and by calculation using influence functions. The coefficients are in good agreement with $R^2 = 0.9753$.

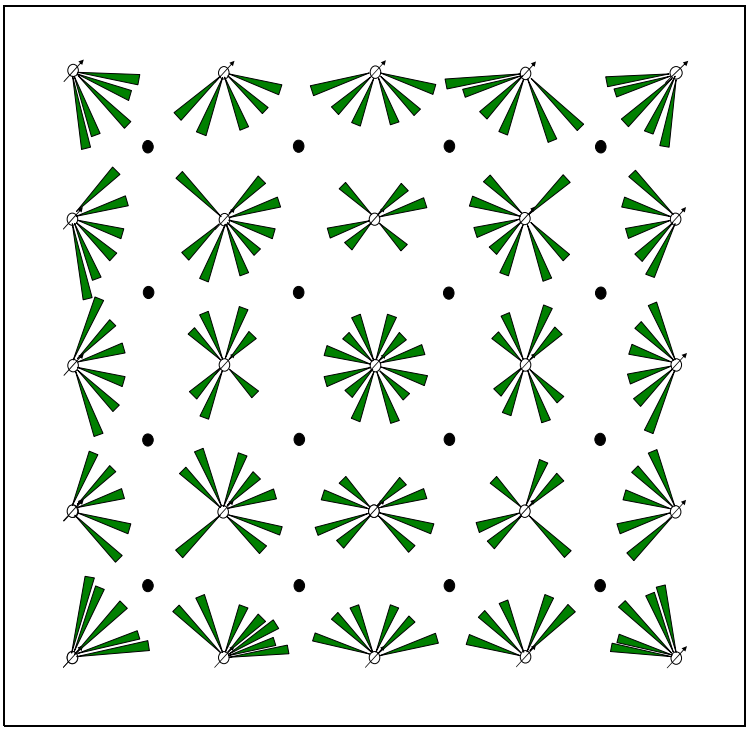


Figure 9.19. Representation of relative interwell permeability for the case of 25x16 Homogeneous Reservoir- Production data.

Table 9.11: Interwell Connectivity Coefficient results from simulation data for the isotropic dual-porosity 25x16 Synthetic field (A_s =0.00588)

	P1	P2	P3	P4	P5	P6	P7	P8	P9	P10	P11	P12	P13	P14	P15	P16	Sum
λ_{0j} (psia)	98.3	93.1	97.4	111.7	82.2	74.0	77.1	92.4	78.0	69.7	72.5	86.1	87.4	82.9	85.7	96.4	1384.7
I1	0.28	0.11	0.04	0.02	0.11	0.05	0.02	0.01	0.05	0.03	0.01	0.00	0.03	0.02	0.01	0.00	0.79
I2	0.22	0.18	0.08	0.03	0.08	0.06	0.04	0.02	0.04	0.03	0.02	0.02	0.02	0.02	0.01	0.01	0.89
I3	0.09	0.18	0.17	0.08	0.04	0.06	0.05	0.04	0.02	0.02	0.02	0.02	0.01	0.01	0.01	0.01	0.81
I4	0.05	0.09	0.20	0.23	0.02	0.04	0.07	0.09	0.01	0.02	0.03	0.04	0.01	0.01	0.02	0.02	0.94
I5	0.02	0.04	0.11	0.28	0.01	0.02	0.05	0.11	0.01	0.01	0.02	0.04	0.00	0.00	0.01	0.02	0.78
I6	0.21	0.08	0.03	0.01	0.18	0.06	0.02	0.00	0.08	0.03	0.01	0.00	0.04	0.02	0.01	0.00	0.79
I7	0.16	0.14	0.06	0.03	0.14	0.12	0.05	0.03	0.06	0.05	0.03	0.02	0.04	0.03	0.02	0.01	0.99
I8	0.05	0.12	0.12	0.05	0.04	0.11	0.11	0.04	0.02	0.03	0.03	0.02	0.01	0.01	0.01	0.01	0.79
I9	0.03	0.06	0.14	0.16	0.03	0.05	0.12	0.14	0.02	0.03	0.05	0.06	0.02	0.02	0.03	0.04	0.99
I10	0.01	0.02	0.07	0.20	0.01	0.02	0.06	0.18	0.01	0.01	0.03	0.08	0.01	0.01	0.02	0.04	0.78
I11	0.09	0.04	0.02	0.01	0.18	0.06	0.02	0.01	0.18	0.06	0.02	0.01	0.09	0.05	0.02	0.01	0.88
I12	0.05	0.04	0.02	0.02	0.12	0.11	0.04	0.02	0.12	0.11	0.03	0.02	0.05	0.04	0.02	0.01	0.82
I13	0.03	0.04	0.04	0.03	0.05	0.11	0.11	0.04	0.05	0.11	0.11	0.05	0.03	0.04	0.05	0.04	0.93
I14	0.01	0.02	0.04	0.06	0.01	0.03	0.11	0.13	0.02	0.03	0.11	0.13	0.01	0.02	0.04	0.05	0.84
I15	0.01	0.02	0.04	0.08	0.01	0.02	0.05	0.17	0.01	0.02	0.05	0.17	0.01	0.02	0.04	0.09	0.81
I16	0.03	0.02	0.01	0.00	0.07	0.03	0.02	0.01	0.18	0.06	0.02	0.01	0.21	0.08	0.03	0.02	0.82
I17	0.04	0.03	0.02	0.02	0.06	0.05	0.03	0.02	0.15	0.13	0.05	0.03	0.17	0.15	0.06	0.03	1.03
I18	0.02	0.02	0.01	0.01	0.03	0.04	0.04	0.03	0.05	0.11	0.11	0.05	0.06	0.13	0.13	0.06	0.90
I19	0.00	0.01	0.01	0.02	0.01	0.02	0.04	0.05	0.01	0.04	0.11	0.13	0.02	0.05	0.13	0.16	0.80
I20	0.01	0.02	0.02	0.04	0.01	0.02	0.04	0.08	0.02	0.03	0.06	0.18	0.02	0.03	0.08	0.21	0.87
I21	0.03	0.02	0.01	0.01	0.05	0.03	0.02	0.01	0.12	0.06	0.03	0.02	0.30	0.12	0.06	0.03	0.93
I22	0.02	0.02	0.01	0.01	0.04	0.03	0.02	0.02	0.08	0.06	0.04	0.02	0.22	0.19	0.08	0.04	0.90
I23	0.01	0.01	0.01	0.01	0.02	0.02	0.02	0.02	0.04	0.06	0.06	0.04	0.09	0.17	0.18	0.09	0.83
I24	0.01	0.01	0.01	0.01	0.01	0.02	0.02	0.03	0.02	0.04	0.06	0.08	0.04	0.08	0.19	0.22	0.86
I25	0.00	0.01	0.01	0.02	0.01	0.01	0.02	0.04	0.01	0.02	0.05	0.11	0.02	0.04	0.11	0.28	0.77
Sum	1.49	1.33	1.32	1.46	1.36	1.19	1.18	1.33	1.37	1.20	1.19	1.35	1.52	1.36	1.35	1.50	

Table 9.12: Relative interwell permeability results for the 25x16 Isotropic Dual-porosity Synthetic Field (k_{ref}=100mD, Δt_{eq} = 5.87 days)

	P01	P02	P03	P04	P05	P06	P07	P08	P09	P10	P11	P12	P13	P14	P15	P16
I01	100	90	97	0	92	87	0	0	106	0	0	0	0	0	0	0
I02	93	80	84	0	88	78	0	0	0	0	0	0	0	0	0	0
I03	95	77	75	89	89	72	70	0	0	0	0	0	0	0	0	0
I04	118	94	88	103	0	89	83	95	0	0	0	0	0	0	0	0
I05	0	99	91	102	0	0	87	91	0	0	0	100	0	0	0	0
I06	90	83	0	0	79	74	0	0	86	0	0	0	109	0	0	0
I07	85	74	82	0	74	63	74	0	86	76	0	0	0	0	0	0
I08	73	60	60	76	67	51	50	0	0	0	0	0	0	0	0	0
I09	0	81	72	82	0	73	62	73	0	0	75	84	0	0	0	0
I10	0	0	78	86	0	0	71	77	0	0	0	83	0	0	0	0
I11	95	91	0	0	79	75	0	0	80	76	0	0	97	93	0	0
I12	73	66	0	0	61	53	0	0	60	52	0	0	73	0	0	0
I13	0	69	68	0	74	53	53	71	75	54	54	74	0	73	75	0
I14	0	0	70	80	0	0	54	65	0	0	53	64	0	0	67	77
I15	0	0	0	87	0	0	68	74	0	0	70	76	0	0	89	96
I16	0	0	0	0	81	0	0	0	79	75	0	0	91	85	0	0
I17	0	0	0	0	88	79	0	0	78	67	78	0	89	77	86	0
I18	0	0	0	0	0	0	0	0	76	56	56	76	86	67	68	88
I19	0	0	0	0	0	0	0	69	0	0	56	67	0	70	67	80
I20	0	0	0	0	0	0	0	85	0	0	76	79	0	0	84	90
I21	0	0	0	0	110	0	0	0	99	95	0	0	110	100	115	0
I22	0	0	0	0	0	0	0	0	89	78	0	0	94	81	85	0
I23	0	0	0	0	0	0	0	0	88	72	72	89	92	76	76	94
I24	0	0	0	0	0	0	0	0	0	0	77	86	0	86	81	94
I25	0	0	0	0	0	0	0	98	0	0	86	91	0	96	90	101

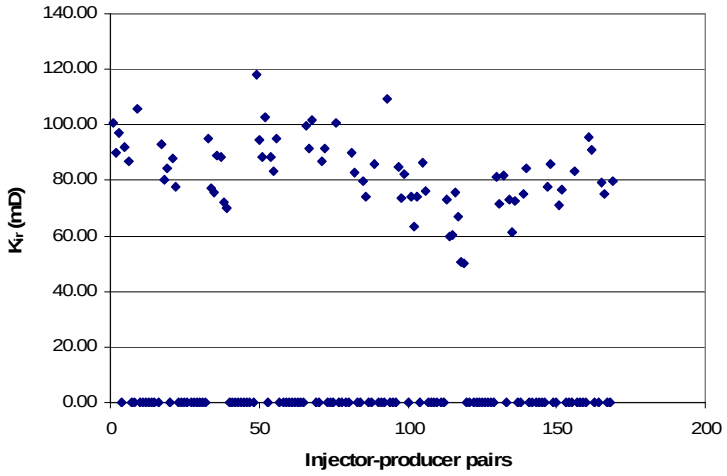


Figure 9.20. Relative interwell permeability results for the case of 25x16 Homogeneous Reservoir- Production data.

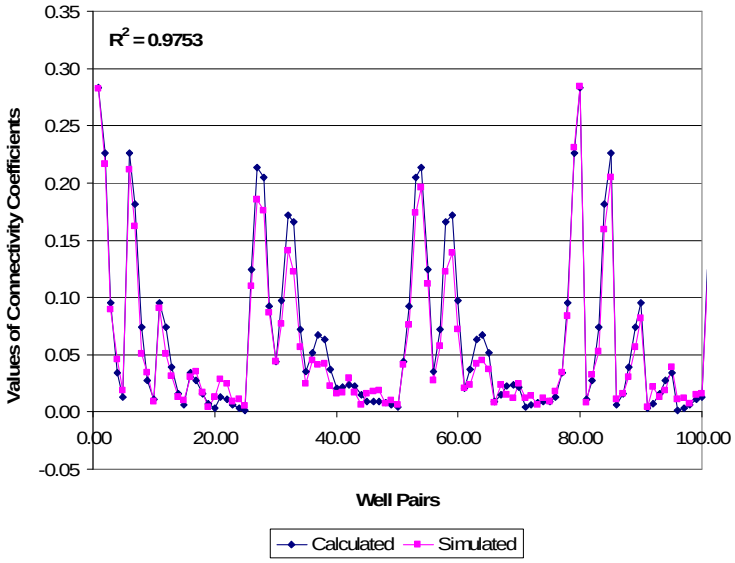


Figure 9.21. Representation of relative interwell permeability for the case of 25x16 Homogeneous Reservoir - Production data.

9.4. Conclusions

Some of the conclusions drawn from this chapter are:

- The mathematical model results accurately match the interwell connectivity coefficients calculated from flow rate data;

- The proposed approach provides better understanding of interwell connectivity determination from flow rate data and an alternative mean to evaluate interwell connectivity from production data;

- Results for relative interwell permeability from flow rate data are in good agreement with the actual input data for the simulation model.

- Even though the reservoir is under steady-state condition or the total injection rate equals total production rate, to account for the effect of the response wells (producers), MLR technique should be used. The constant term represents the effects of all the response wells on the investigated response well.

9.5. Recommended Application

The interwell connectivity coefficients (λ_{ij}) in Eq. 9.1 can be used to predict production rates given injection rates. Fig. 9.22 shows a flowchart of general recommended procedure for a field production forecast and development plan. The flowchart consists of three blocks: the input, calculation and output. The calculation will be based on material balance to keep track of the amount of fluids flowing in and out and remaining. Following step-by-step procedure is recommended:

Step 1: In this step, necessary data are input and the geological model is built. As shown in the input block, data such as net pay thickness map, porosity, fluid saturation, compressibilities, formation volume factors are required. Other required data are the well information, production and pressure history data.

Step 2: If the steady state condition is satisfied, MLR can be used to calculate the interwell connectivity coefficients as shown in calculation block. Since production data

are used in this case, available techniques can be used (Albertoni and Lake, 2003 and Yousef et. al., 2006).

Step 3: The coefficient results can be used to calculate the future production rates for field production forecast using Eq. 9.1. By changing the injection rates, the optimized injection rates that give the highest overall production can be found. Thus, the field production can be optimized.

Step 4: Using material balance, the amount of oil left in the field can be calculated from the oil production data and the approximate drainage area shape of each producer. The drainage area shape can be estimated based on the interwell connectivity coefficients. The higher is the connectivity coefficient of a well pair, the more oil is swept between that well pair. A mathematical technique should be developed to calculate the drainage area shape based on this criteria. Based on the amount of oil left in the field, which is represented by the net pay thickness map, after a certain production period, infill well locations can be identified by locating the places with the most un-swept oil.

Step 5: In order to forecast the production of the field with new wells, either injectors or producers, the interwell connectivity coefficients for each of the new wells need to be calculated. First, the shape factor for all the wells in the field including new wells need to be estimated. Since the reservoir is in irregular shape, the shape factor may need to be calculated numerically. Thus, the geological model of the reservoir can be imported into a reservoir simulator. Then, simulation run for each well can be performed until the well reach pseudo-steady state. The reservoir should be homogeneous for these runs. Reasonable flow rate can be used as well as the reservoir properties. However, the input are not necessarily reflecting actual field data, because the shape factors are

independent on these properties accept the shape of the reservoir. The shape factor can be calculated using Eq. 5.21.

Step 6: Knowing the shape factors, the influence functions can be formulated using Eq. 5.20. Thus, following the procedure to calculate relative interwell permeability, we can estimate the relative interwell permeabilities between existing wells from available production data. Again, these relative interwell permeabilities reflect the actual permeability between the wells.

Step 7: Since there are no production data for the new well, the relative interwell connectivities for well pairs involving new well need to be estimated from available relative interwell permeabilities calculated in Step 5. A new mathematical algorithm similar to geostatistics is required for this step. Different from geostatistics, this algorithm estimate directional permeability instead of permeability at a point. These relative interwell permeabilities can also be estimated using actual data from the field.

Step 8: Once the relative interwell permeabilities and the shape factor of each well are known, the influence function can be formulated as shown in Eq. 5.20. In this recommended procedure, we assume that t_{DA} only depends on the permeabilities and the time. Other parameters are constant.

Step 9: In this step, the interwell connectivity coefficients and the constant term in Eq. 9.1 will be calculated for both existing well and new well. A separate study is required to develop the procedure for this step. Basically, the interwell connectivity coefficients for the existing wells, the relative interwell permeabilities and the shape factor for both old and new wells and the influence function formulation are known, we

need to find the equivalent time to calculate the interwell connectivity coefficients that would give the best estimation of the predicted production rates.

Step 10: Once all the interwell connectivity coefficients for both existing and new wells are available, we can repeat Step 3 to forecast or optimize the field production.

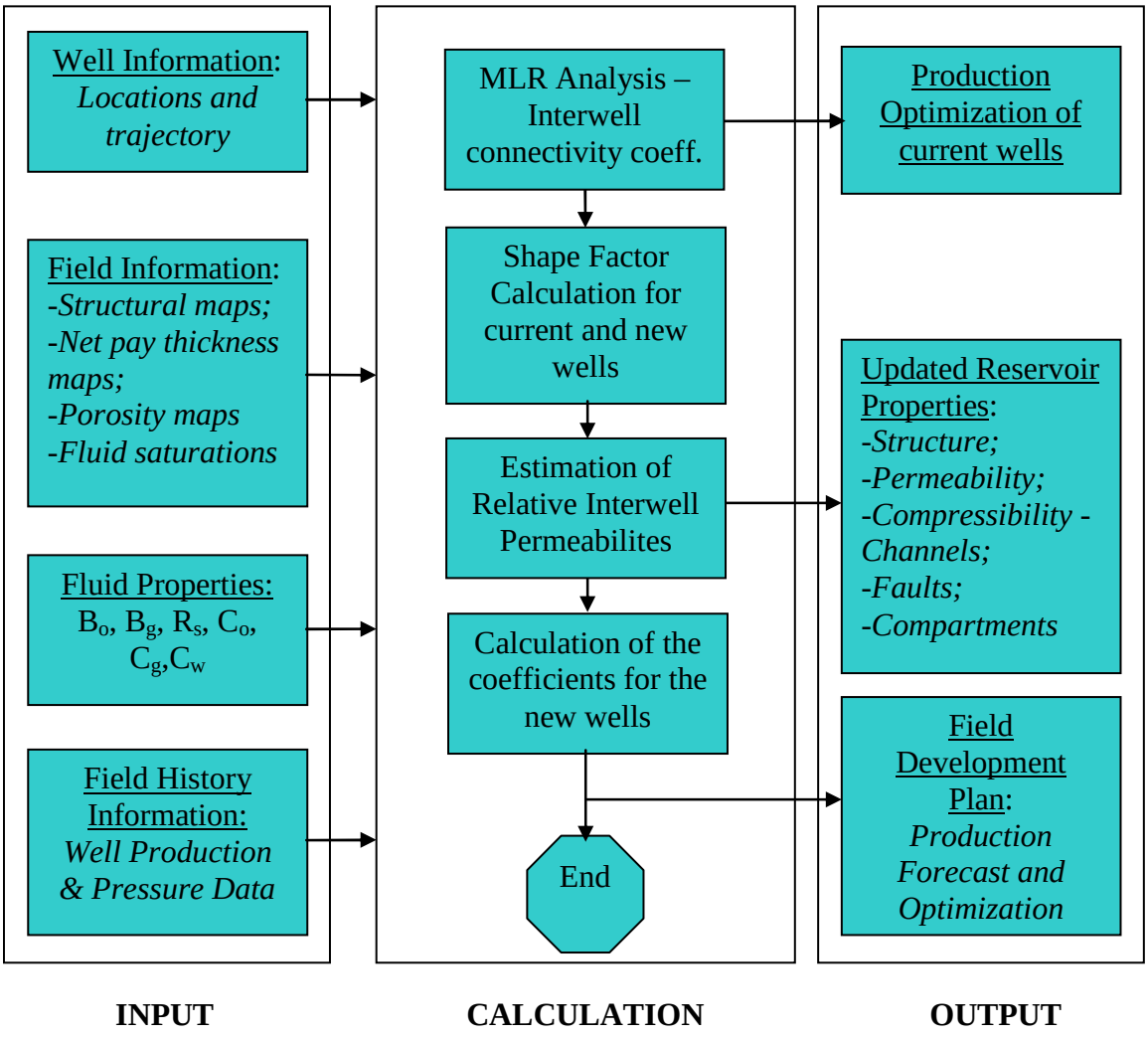


Figure 9.22. Flowchart showing a recommended application for the analytical model for production data in a waterflood.

CHAPTER 10 – CONCLUSIONS AND RECOMMENDATIONS

10.1. Summary and Conclusions

10.1.1. Summary

A new method of determining interwell connectivity by constraint multivariate linear regression using multi-well test pressure data was developed. Communication between injectors and producers is represented by interwell connectivity coefficients, which depend on wellbore conditions at the signal wells, distance between wells and the properties of the reservoir. The quality of the resulting weighting coefficients or interwell connectivity coefficients obtained by this new method is excellent in terms of asymmetry coefficient values (A_s) and determination coefficient (R^2). The results can be used to detect permeability barriers, permeability trends, anisotropic media and relative effect of injectors on producers in a waterflood.

A pseudo-steady state flow solution for a well in a multi well system was used to model the interwell connectivity test. The model was verified using two synthetic reservoir models, one with 5 injector and 4 producers and the other with 25 injectors and 16 producers. Results obtained from the model fit well with the simulation results. Average reservoir pressure change can be calculated and the total reservoir porosity can be estimated. By defining a reference permeability, the interwell connectivity can be presented in terms of relative interwell permeability.

Application of the technique to naturally fractured reservoir represented by dual porosity system was also presented with different cases of reservoir heterogeneities. Results for reservoirs with the presence of hydraulically fractured wells, horizontal wells were also analyzed. Five reservoir cases were considered: (1) hydraulically fractured

wells only, (2) horizontal wells only, (3) hydraulically fractured wells and vertical wells, (4) horizontal wells and vertical wells and (5) all three types of wells.

An analytical model was developed for the existing technique to infer interwell connectivity using production data. The model show excellent agreement with the available results obtained from simulation data. Thus, the model provides better understanding of the technique and opens the door for further developments concerning production data.

10.1.2. Conclusions

Main conclusions drawn from this study are

1. The proposed technique based on bottom hole pressure data is more robust than the existing technique that uses production data. The new technique yields better results without the need of diffusivity filters or subjective judgments while requiring less data points.
2. The new technique can be applied to different wellbore conditions such as vertical wells, vertically fractured wells and horizontal wells.
3. Only the wellbore conditions at the signal wells affect the interwell connectivity coefficients. The wellbore conditions at the response wells are independent of the coefficients.
4. Based on the proposed analytical models for both bottom hole pressure and production data, when production data from a reservoir under steady state condition are used, the interwell connectivity coefficients only depend on the positions of the response wells and the signal well-response well influence functions. Thus, they are not affected by the average reservoir properties or the

influence functions of the signal wells themselves as in the case when pressure data are used.

5. When bottom-hole pressures are used to calculate the relative interwell permeabilities by matching the summation of the interwell connectivity coefficients calculated from the analytical solutions, which is equal to unity, with the summation of the coefficients obtained from simulation data, the relative interwell permeabilities can be estimated. Another way to calculate the relative interwell permeabilities is to assume a permeability for a reference well pair and then calculate the rest of the relative interwell permeabilities according to the reference relative interwell permeability as in the process described in the case where production data are used.

10.2. Recommendations for Future Studies

Many future studies can be based on the results of this work. Following are some suggested research topics:

1. Characteristics of relative interwell permeability and the effects of cross flow on the interwell permeability.
2. Interwell connectivity tests with varied test time interval and multi-phase flow.
3. Extensions of the study to infinite reservoirs and closed reservoirs of different shapes are also recommended.
4. Investigation on inferring interwell connectivity using production data for reservoirs with hydraulically fractured wells, horizontal wells or other well-bore conditions should be conducted.

5. Investigation of interwell connectivity tests for different geological features such as leaking faults.
6. Production optimization techniques should be considered based on the results of the analytical models developed in this study.

NOMENCLATURE

$\bar{P}$	=	average pressure
$\hat{p}_j$	=	modeled pressure change (psia)
p_i	=	pressure at the active well (psia)
p_j	=	pressure at the observation well (psia)
ϕ	=	porosity, fraction
λ_{0j}	=	additive constant term in MLR for pressure data
λ_{ij}	=	interwell connectivity coefficient in MLR for pressure data
ϕ_{tot}	=	total field porosity, fraction
a	=	influence function
A	=	area, ft^2
A_s	=	asymmetry coefficient
B	=	formation volume factor, rbbl/STB
c	=	formation compressibility (psi^{-1})
C	=	shape factor
c_o	=	oil compressibility, psi^{-1}
c_r	=	rock compressibility, psi^{-1}
c_t	=	total compressibility, psi^{-1}
c_w	=	water compressibility, psi^{-1}
E_1	=	Exponential integral function one
GOR	=	gas oil ratio
h	=	formation thickness, ft

I = total number of signal or active wells (injectors) or injector indicator in well names

J = total number of response wells(producers), producer indicator or productivity index, (STB/day)/psi

k = permeability, mD

k_{ir} = relative interwell permeability, mD

k_{ref} = reference permeability, mD

L = reference length

$LSLR$ = Least Square Linear Regression

M = coefficients in average pressure change calculation

m,n = numbers of calculation terms

MLR = Multivariate Linear Regression

n_{inj} = total number of injectors

n_{pr} = total number of producers

n_{well} = total number of wells

O_d = overdetermination coefficient

p = pressure, psia

p_{ave} = average pressure, psia

p_{ini} = initial pressure, psia

p_j = pressure at the observation well, psia

p_{wf} = bottom-hole flowing pressure, psia

q = flow rate (STB/day)

q_{ref} = reference flow rate, STB/day

r = Distance between active and observation wells (ft)

R^2 = coefficient of determination

r_w = wellbore radius, ft

s = skin factor, dimensionless

S_t = Storativity (ft/psi)

t = time, hours

T_r = Transmissibility (mD-ft/cp)

t_s = starting time, hours

V_b = reservoir bulk volume, ft^3

V_p = pore volume, ft^3

x = coordinate or dimension in x-direction, ft

x_e = dimension of study area in the x-direction, ft

x_w = individual well x-coordinate, ft

y = coordinate or dimension in y direction, ft

y_e = dimension of study area in the y direction, ft

y_w = individual well y-coordinate, ft

β_{0j} = additive constant term in MLR for pressure data

β_{ij} = interwell connectivity coefficient in MLR for pressure data

γ = Euler's constant

Δp = pressure change/difference, psi

Δp_{ave} = average pressure change, psi

Δp_{pr} = pressure change corresponding to influence of response wells and change in average reservoir pressure assuming pseudo-steady state flow, psi

Δq_{tot} = field total flow rate, STB/day

Δq_{sp} = a constant account for the effect of producers on flow rate at observation wells assuming steady state flow, STB/day.

Δt = time interval

Δt_{eq} = equivalent pseudo-steady state time interval

μ = fluid viscosity (cp)

P'_m = time rate of change of pressure (psia)

t_m = time to reach the maximum value of time rate of change of pressure (hours)

σ^2_{ii} = injector-injector covariance

σ^2_{ij} = injector-producer covariance

Subscripts

ave = average

D = dimensionless quantity

DA = dimensionless corresponding to area

e = boundary value

eq = equivalent

i' = investigated signal/active well (injector)

i = signal or active well (injector) index

ini = initial value

j = response/observation well (producer) index

j' = investigated response/observation well (producer)

m	=	observed data point or maximum
tot	=	total
w	=	well
wf	=	flowing conditions
xf	=	fracture half length
h	=	horizontal well
v	=	vertical well
f	=	fractured well

Superscripts

l	=	order of data point
L	=	total number of data points
T	=	transposed

REFERENCES

Albertoni, A. and Lake, L.W. 2003. Inferring Interwell Connectivity Only from Well-rate Fluctuations in Waterfloods. *SPE Reservoir Evaluation and Engineering Journal* **6**, Feb. 2003: 6-16.

Albertoni, A. 2002. *Inferring Interwell connectivity From Well-Rate Fluctuations in Waterfloods*. M.S. Thesis, The University of Texas at Austin, 2002.

Bleecker, D. and Csordas, G. 1992. *Basic Partial Differential Equation*. Van Nostrand Reinhold, New York.

Boast98 and EdBoast Software, Department of Energy (DOE), Tulsa, OK, 1998. Online, Dec. 17, 2002. Available at: http://www.npto.doe.gov/Software/simindx.html/

Chapra, S. C. & Canale, R. P. 1988. *Numerical Methods for Engineers*, 2nd Edition. McGraw-Hill, Inc Pub., USA.

Cinco-Ley, H. & Samaniego. 1981. Transient Pressure Analysis for Fractured Wells. *JPT* (Sept. 1981). P. 1479-1766.

De Sant'Anna Pizarro, J.O. 1998. *Estimating infectivity and lateral autocorrelation in heterogeneous media*. Ph.D. Thesis, The University of Texas at Austin, 1998.

DeSwaan-O, A.1976. Analytical Solutions for Determining Naturally Fractured Reservoir Properties by Well Testing. *SPEJ*, June 1976, 117-122.

Dietz, D. N. 1965. Determination of Average Reservoir Pressure From Buildup Survey. *JPT*, Aug. 1965: 955-959; *Trans., AIME*: Vol. 234.

Dinh A. and Tiab D. 2007. Inferring Interwell Connectivity from Well Bottom Hole Pressure Fluctuations in Waterfloods. Paper SPE 106881 presented at the 2007

SPE Production and Operations Symposium, Oklahoma city, OK, 31 March-3 April.

Dinh A. and Tiab D. 2008. Inferring Interwell Connectivity using Bottom Hole Pressure Fluctuations. *SPEREE* 11 (5): 874-881. DOI: 10.2118/106881-PA.

Dinh A. and Tiab D. 2008. Interpretation of Interwell Connectivity Tests in a Waterflood System. Paper SPE 116144 to be presented at the 2008 SPE Annual Technical Conference and Exhibition, Denver, CO, USA, 21-24 Sept.

Dinh, A. 2003. *Reservoir Characterization for the Delaware Childers Field Based on Flow Rates Analysis.* M.S. Thesis, The University of Oklahoma, Norman, May, 2003.

ECLIPSE 100 Black Oil Simulator . 2006. Schlumberger Corp. Version 2006.1.

Engler, T and Tiab, D. 1996. Analysis of Pressure and Pressure Derivative without Type Curve Matching, 4. Naturally Fractured Reservoirs. Journal of Petroleum Science and Engineering, 1996: Vol. 15, 127-138.

Engler, T. W. and Tiab, D., 1996. Analysis of pressure and pressure derivatives without type-curve matching. 6. Horizontal well tests in anisotropic reservoirs. Journal of Petroleum Science and Engineering, Vol.15:pp.153-168.

Goode, P.A., Thambynayagam, R.K.M., 1987. Pressure Drawdown and Buildup Analysis of Horizontal Wells in Anisotropic Media. Paper SPE 14250.

Gringarten, A. C., and Ramey, H. J., Jr. 1973. The Use of the Point Source Solution and Green's Functions for Solving Unsteady Flow Problems in Reservoirs. *Soc. Pet. Eng. J.*, Oct. 1973: 285-296; Trans., AIME, Vol. 255.

Gringarten, A. C., Ramey, H. J., Jr., and Raghavan, R. 1974. Unsteady-State Pressure Distributions Created by a Well With a Single Infinite-Conductivity Vertical Fracture. *Soc. Pet. Eng. J.* (Aug. 1974), pp. 347-360.

Heffer, K.J., Fox, R.J., and McGill, C.A. 1995. Novel techniques show links between reservoir flow directionality, earth stress, fault structure and geomechanical changes in mature waterfloods, Society of Petroleum Engineers, paper SPE 30711, 1995

Jensen, J.L., Lake, L.W., Corbett, P.W.M. and Goggin, D.J. 1997. *Statistics for Petroleum Engineers and Geoscientists*. Upper Saddle River, New Jersey: Prentice-Hall Inc.

Joshi, S.D.1991. *Horizontal Well Technology*. PennWell Publishing Company, Tulsa, OK .

Kazemi, H. 1969. Pressure Transient Analysis of Naturally Fractured Reservoirs. Trans. AIME, 1969: Vol. 246, 451-461.

Lee, J., Rollins, J.B. and Spivey, J.P. 2003. *Pressure Transient Testing*. SPE Textbook Series, SPE, Richardson, TX.

Lin, J. and Yang, H.. 2007. Analysis of Well-Test Data in a Multiwell Reservoir With Water Injection. Paper SPE 110349 presented at the 2007 SPE Annual Technical Conference and Exhibition, Anaheim, CA, Nov. 11-14.

Marhaendrajana, T. 1999. *Modeling and Analysis of Flow Behavior in Single and Multiwell Bounded Reservoirs*, PhD dissertation, Texas A&M U., Texas, Dec.1999.

Marhaendrajana, T., Kaczorowski, N. J., and Blasingame, T. A. 1999. Analysis and Interpretation of Well Test Performance at Arun Field, Indonesia. Paper SPE 56487 presented at the 1999 SPE Annual Technical Conference and Exhibition, Houston, TX, Oct. 3-7.

Onur,M., Serra, K. V., and Reynolds, A. C. 1991. Analysis of Pressure Buildup Data from a Well in a Multiwell System. *SPEFE,* March 1991: 101-110.

Ozkan, E. and Raghavan, R. 1988. Performance of Horizontal Wells Subject to Bottom Water Drive. Paper SPE 18559, SPE, Richardson, TX.

Raghavan, R.: Well test Analysis, Prentice Hall Petr. Engr., Englewood, New Jersey, 1993, p. 56-58.

Refunjol, B.T. 1996. *Reservoir characterization of Northuck Draw field based on tracer response and production/injection analysis,* M.S. Thesis, The University of Texas at Austin.

Tiab, D and Donaldson, E. 2004. *Petrophysics*. 2nd Edition, Gulf Professional Publishing, MA, USA.

Tiab, D. 2005. Analysis of Pressure Derivative Data of Hydraulic Fractured Wells by the Tiab's Direct Synthesis Technique. *J. of Pet. Sci. and Eng.* 49 (2005), p. 1-21.

Tiab, D. and A. Kumar. 1980. Application of PD' function to Interference Analysis Advanced Oil Test Analysis. *JPT,* Aug. 1980, 1465 – 1470.

Tiab, D. and Puthigai, S.K., 1987. Pressure Derivative Type-Curves for a Vertically Fractured Well. *SPEFE,* Oct. 1987: 156-158.

Tiab, D. 1993. Analysis of Pressure Derivative without Type-Curve Matching: Vertically Fractured Wells in Closed Systems. *Journal of Petroleum Science and*

Engineering 11 (1994) 323-333. This paper was originally presented as SPE 26138 at the 1993 SPE Western Regional Meeting, held May 26-28, Anchorage, Alaska.

Umnuayponwiwat S., Ozkan E. and Raghavan R. 2000. Pressure Transient Behavior and Inflow Performance of Multiple Wells in Closed Systems. Paper SPE 62988 presented at the 2000 SPE Annual Technical Conference and Exhibition, Dallas, Texas, 1-4 October.

Umnuayponwiwat, S. and Ozkan, E. 2000. Evaluation of Inflow Performance of Multiple Horizontal Wells in Closed Systems. *Trans. ASME*, March 2000, Vol. 122: 8-13.

Valko P., Doublet L., and Blasingame T.A. 2000. Development and Application of the Multiwell Productivity Index (MPI). *SPEJ*, March 2000: 21-31.

Warren J. E., P. J. Root. 1963. The Behavior of Naturally Fractured Reservoir. *SPEJ*, Sept. 1963: 245-255.

Yousef, A. A. 2006. *Investigating Statistical Techniques to Infer Interwell Connectivity from Production and Injection Rate Fluctuations*, PhD dissertation. University of Texas at Austin, Austin, Texas, May 2006.

Yousef, A. A., Gentil, P., Jensen, J. L., and Lake, Larry W. 2005. A capacitance Model to Infer Interwell Connectivity from Production and Injection Rate Fluctuations. Paper SPE 95322, presented at the SPE Annual Technical Conference and Exhibition held in Dallas, Texas, October 9-12.

APPENDIX A – DERIVATION OF PRESSURE DISTRIBUTION FOR A VERTICAL WELL IN A CLOSED RECTANGULAR RESERVOIR

Let us consider a vertical well in a closed rectangular reservoir. The main assumptions are homogeneous reservoir, isotropic reservoir, fully penetrating vertical well at an arbitrary position. The well produces at constant rate and is considered as a line source as its diameter is small compared to the reservoir. Single-phase flow is assumed with a slightly compressible fluid (Marhaendrajana, 1999).

The diffusivity equation for this well is

$$\frac{\partial^2 p}{\partial x^2}+\frac{\partial^2 p}{\partial y^2}-\frac{q(t)B\mu}{Ahk}\delta(x-x_w, y-y_w)=\frac{\phi\mu c_t}{k}\frac{\partial p}{\partial t} \tag{A.1}$$

With initial and boundary conditions:

$$p(x, y, t=0)=p_i \tag{A.2}$$

$$\left.\frac{\partial p}{\partial x}\right|_{x=0}=\left.\frac{\partial p}{\partial x}\right|_{x=x_e}=0 \tag{A.3}$$

$$\left.\frac{\partial p}{\partial y}\right|_{y=0}=\left.\frac{\partial p}{\partial x}\right|_{y=x_e}=0 \tag{A.4}$$

Define the dimensionless quantities as follows:

$$x_D=\frac{x}{\sqrt{A}} \tag{A.5}$$

$$y_D=\frac{y}{\sqrt{A}} \tag{A.6}$$

$$p_D=\frac{2\pi kh}{q_{ref}B\mu}(p_{ini}-p(x, y, t)) \tag{A.7}$$

$$t_{DA} = \frac{kt}{\phi c_t \mu A} \tag{10.8}$$

Substituting the dimensionless quantities to Eqs. A.1 to A.4, we obtain:

$$\frac{\partial^2 p_D}{\partial x_D^2} + \frac{\partial^2 p_D}{\partial y_D^2} + 2\pi \frac{q(t)}{q_{ref}} \delta(x_D - x_{wD}, y_D - y_{wD}) = \frac{\partial p_D}{\partial t_{DA}} \tag{A.9}$$

$$p_D(x_D, y_D, t_{DA} = 0) = 0 \tag{A.10}$$

$$\left.\frac{\partial p_D}{\partial x_D}\right|_{x_D=0} = \left.\frac{\partial p_D}{\partial x_D}\right|_{x_D=x_{eD}} = 0 \tag{A.11}$$

$$\left.\frac{\partial p_D}{\partial y_D}\right|_{y_D=0} = \left.\frac{\partial p_D}{\partial y_D}\right|_{y_D=y_{eD}} = 0 \tag{A.12}$$

Using Duhamel's principle, we have (Bleecker and Csordas, 1992):

$$p_D(x_D, y_D, x_{wD}, y_{wD}, x_{eD}, y_{eD}, t_{DA}) = 2\pi \int_0^{t_{DA}} \frac{q(\tau)}{q_{ref}} \psi(x_D, y_D, x_{wD}, y_{wD}, x_{eD}, y_{eD}, [t_{DA} - \tau]) d\tau \tag{A.13}$$

Where $\psi(x_D, y_D, t_{DA})$ is the instantaneous line source solution of the following partial differential equations:

$$\frac{\partial^2 \psi}{\partial x_D^2} + \frac{\partial^2 \psi}{\partial y_D^2} = \frac{\partial \psi}{\partial t_{DA}} \tag{A.14}$$

$$\psi(x_D, y_D, t_{DA} = 0) = \delta(x_D - x_{wD}) \delta(y_D - y_{wD}) \tag{A.15}$$

$$\left.\frac{\partial \psi}{\partial x_D}\right|_{x_D=0} = \left.\frac{\partial \psi}{\partial x_D}\right|_{x_D=x_{eD}} = 0 \tag{A.16}$$

$$\left.\frac{\partial \psi}{\partial y_D}\right|_{y_D=0} = \left.\frac{\partial \psi}{\partial y_D}\right|_{y_D=y_{eD}} = 0 \tag{A.17}$$

The delta function term $\delta(x_D - x_{wD})\delta(y_D - y_{wD})$ in the initial condition is a product of two functions (functions of x_D and y_D). Thus, the function $\psi(x_D, y_D, x_{wD}, y_{wD}, x_{eD}, y_{eD}, t_{DA})$ can be rewritten as a product of two one-dimensional initial boundary value functions:

$$\psi(x_D, y_D, x_{wD}, y_{wD}, x_{eD}, y_{eD}, t_{DA}) = \psi_1(x_D, x_{wD}, x_{eD}, t_{DA}) \times \psi_2(y_D, y_{wD}, y_{eD}, t_{DA}) \quad \text{(A.18)}$$

Where $\psi_1(x_D, x_{wD}, x_{eD}, t_{DA})$ and $\psi_2(y_D, y_{wD}, y_{eD}, t_{DA})$ satisfy

$$\frac{\partial^2 \psi_1}{\partial x_D^2} = \frac{\partial \psi_1}{\partial t_{DA}} \quad \text{(A.19)}$$

$$\psi_1(x_D, t_{DA} = 0) = \delta(x_D - x_{wD}) \quad \text{(A.20)}$$

$$\left.\frac{\partial \psi_1}{\partial x_D}\right|_{x_D = 0} = \left.\frac{\partial \psi_1}{\partial x_D}\right|_{x_D = x_{eD}} = 0 \quad \text{(A.21)}$$

and $$\frac{\partial^2 \psi_2}{\partial y_D^2} = \frac{\partial \psi_2}{\partial t_{DA}} \quad \text{(A.22)}$$

$$\psi_2(y_D, t_{DA} = 0) = \delta(y_D - y_{wD}) \quad \text{(A.23)}$$

$$\left.\frac{\partial \psi_2}{\partial y_D}\right|_{y_D = 0} = \left.\frac{\partial \psi_2}{\partial y_D}\right|_{y_D = y_{eD}} = 0 \quad \text{(A.24)}$$

ψ_1 and ψ_2 can be solved using the method of separation of variables. After some mathematical manipulations (Marhaendrajana et al., 1999), the solution for p_D or the influence function for a vertical well in a closed rectangular reservoir can be found as (Eq. 4.6):

$$p_D\left(x_D, y_D, x_{wD,i}, y_{wD,i}, x_{eD}, y_{eD}, t_{DA}\right) = \frac{1}{2}\sum_{m=-\infty}^{\infty}\sum_{n=-\infty}^{\infty} E_1\left[\frac{\left(x_D + x_{wD,i} + 2nx_{eD}\right)^2 + \left(y_D + y_{wD,i} + 2my_{eD}\right)^2}{4t_{DA}}\right] + E_1\left[\frac{\left(x_D - x_{wD,i} + 2nx_{eD}\right)^2 + \left(y_D + y_{wD,i} + 2my_{eD}\right)^2}{4t_{DA}}\right] + E_1\left[\frac{\left(x_D + x_{wD,i} + 2nx_{eD}\right)^2 + \left(y_D - y_{wD,i} + 2my_{eD}\right)^2}{4t_{DA}}\right] + E_1\left[\frac{\left(x_D - x_{wD,i} + 2nx_{eD}\right)^2 + \left(y_D - y_{wD,i} + 2my_{eD}\right)^2}{4t_{DA}}\right] \quad \text{(A.25)}$$

APPENDIX B – DERIVATION OF THE PRESSURE DISTRIBUTION CAUSED BY AN INJECTOR OR A PRODUCER IN A WATERFLOOD

For a producer in a field with both injectors and producers, taking into account the regional pressure decline, the pressure behavior of the producer can be written as:

$$\frac{\partial^2 p_D}{\partial x_D^2}+\frac{\partial^2 p_D}{\partial y_D^2}+2\pi q_{D,j'}\delta\left(x_D-x_{Dj'},y_D-y_{Dj'}\right)-\frac{\partial p_D}{\partial t_{DA}}=2\pi t_{DA}\sum_{j=2}^{n_{pr}}q_{D,j}-2\pi t_{DA}\sum_{i=1}^{n_{inj}}q_{D,i} \quad \text{(B.1)}$$

Solution for Eq. B.1 is

$$p_D\left(x_D,y_D,t_{DA}\right)=a_{j'}\left(x_D,y_D,x_{wDj'},y_{wDj'},t_{AD}\right)+2\pi t_{DA}\sum_{j=2}^{n_{pr}}q_{D,j}-2\pi t_{DA}\sum_{i=1}^{n_{inj}}q_{D,i} \quad \text{(B.2)}$$

Where the flow rate of focus well is $q_{Dj'} = q_{D,j=1}$

Eq. B.2 can be rewritten as

$$p_D\left(x_D,y_D,t_{DA}\right)=a_{j'}\left(x_D,y_D,x_{wDj'},y_{wDj'},t_{AD}\right)+2\pi t_{DA}\left(\sum_{j=1}^{n_{pr}}q_{D,j}-\sum_{i=1}^{n_{inj}}q_{D,i}-q_{D,j'}\right) \quad \text{(B.3)}$$

or $$p_D\left(x_D,y_D,t_{DA}\right)=a_{j'}\left(x_D,y_D,x_{wDj'},y_{wDj'},t_{AD}\right)+2\pi t_{DA}\Delta q_{D,tot}-2\pi t_{DA}q_{D,j'} \quad \text{(B.4)}$$

Where $\Delta q_{D,tot}=\sum_{j=1}^{n_{pr}}q_{D,j}-\sum_{i=1}^{n_{inj}}q_{D,i}$

At the wellbore, substituting $x_D = x_{wDj'} + \frac{r_{wD}}{\sqrt{2}}$, $y_D = y_{wDj'} + \frac{r_{wD}}{\sqrt{2}}$ with $r_{wD}=\frac{r_w}{\sqrt{A}}=\frac{r_w}{x_e}$ into Eq.B.4, we have the dimensionless pressure drop equation for producer j':

$$p_{Dj'}\left(x_{wDj'}+\frac{r_{wD}}{\sqrt{2}},y_{wDj'}+\frac{r_{wD}}{\sqrt{2}},t_{DA}\right)=a_{j'j'}\left(x_{wDj'}+\frac{r_{wD}}{\sqrt{2}},y_{wDj'}+\frac{r_{wD}}{\sqrt{2}},x_{wDj'},y_{wDj'},t_{AD}\right)+ \\ +2\pi t_{DA}\Delta q_{D,tot}-2\pi t_{DA}q_{D,j'} \quad \text{(B.5)}$$

Let $q_{ref}=q_{j'}$ and substitute the definitions of dimensionless quantities to Eq. B.5 we obtain the equation for pressure drop at producer j' in a water flood system as shown in Eq. 4.19. Similarly, for an injector i' in a waterflood system under pseudo-steady state flow, we have

$$p_D(x_D,y_D,t_{DA})=a_{i'}(x_D,y_D,x_{wDi'},y_{wDi'},t_{AD})+2\pi t_{DA}\sum_{j=1}^{n_{pr}}q_{D,j}-2\pi t_{DA}\sum_{i=2}^{n_{inj}}q_{D,i} \quad \text{(B.6)}$$

Where the flow rate of focus well is $q_{Di'}=q_{D,i=1}$

Eq. B.6 can be rewritten as

$$p_D(x_D,y_D,t_{DA})=a_{i'}(x_D,y_D,x_{wDi'},y_{wDi'},t_{AD})+2\pi t_{DA}\left(\sum_{j=1}^{n_{pr}}q_{D,j}-\sum_{i=2}^{n_{inj}}q_{D,i}+q_{D,i'}\right) \quad \text{(B.7)}$$

or $$p_D(x_D,y_D,t_{DA})=a_{i'}(x_D,y_D,x_{wDi'},y_{wDi'},t_{AD})+2\pi t_{DA}\Delta q_{D,tot}+2\pi t_{DA}q_{D,i'} \quad \text{(B.8)}$$

Where $\Delta q_{D,tot}=\sum_{j=1}^{n_{pr}}q_{D,j}-\sum_{i=1}^{n_{inj}}q_{D,i}$

At the wellbore, substituting $x_D=x_{wDj'}+\frac{r_{wD}}{\sqrt{2}}$, $y_D=y_{wDj'}+\frac{r_{wD}}{\sqrt{2}}$ with $r_{wD}=\frac{r_w}{\sqrt{A}}=\frac{r_w}{x_e}$ into Eq.B.4, we have the dimensionless pressure drop equation for injector i':

$$p_{Di'}\left(x_{wDi'}+\frac{r_{wD}}{\sqrt{2}},y_{wDi'}+\frac{r_{wD}}{\sqrt{2}},t_{DA}\right)=a_{i'i'}\left(x_{wDi'}+\frac{r_{wD}}{\sqrt{2}},y_{wDi'}+\frac{r_{wD}}{\sqrt{2}},x_{wDi'},y_{wDi'},t_{AD}\right)+ \\ +2\pi t_{DA}\Delta q_{D,tot}+2\pi t_{DA}q_{D,i'} \quad \text{(B.9)}$$

Let $q_{ref} = q_{i'}$ and substitute the definitions of dimensionless quantities to Eq. B.5 we obtain the equation for pressure drop at injector i' in a water flood system as shown in Eq. 4.20. Notice that the injection flow rates are negative and the production flow rates are positive in the influence function and pressure terms.

APPENDIX C – DERIVATION OF THE LATE TIME PRESSURE DISTRIBUTION FOR A WELL IN A NATURALLY FRACTURED RESERVOIR

Consider an infinite naturally fractured reservoir that consists of two separate media – the matrix system and the fracture system. The matrix system is assumed to have very high storativity and negligible permeability while the fracture system has negligible storativity and distributes to all the permeability of the formation. Assuming slightly compressible single-phase fluid in the fracture system, we have the governing equation based on the law of mass conservation and Darcy's law (Ozkan, 1988):

$$\nabla.\left(\frac{\tilde{k}_f}{\mu}\nabla\Delta p_f\right) = \left(V\phi c_t\right)_f \frac{\partial\Delta p_f}{\partial t} + q_{mf} \tag{C.1}$$

Where the subscript f denotes to fracture system, Δp_f is the pressure drop, $\left(V\phi c_t\right)_f$ is the storativity of the fracture system and q_{mf} is the volumetric flow rate from the matrix system to the fracture system and $\tilde{k}_f$ is the permeability tensor for the fracture system.

For the matrix system, we have

$$q_{mf} = \left(V\phi c_t\right)_m \frac{\partial\Delta p_m}{\partial t} \tag{C.2}$$

Where the subscript m denotes the matrix system.

Assuming the pseudo-steady state flow from the matrix system to fracture system (Warren and Root, 1963), following equation can be obtained

$$q_{mf} = -\alpha\frac{k_m}{\mu}\left(\Delta p_m - \Delta p_f\right) \tag{C.3}$$

Where α is the interporosity shape factor and k_m is the permeability of the matrix system.

Substituting Eq. C.2 to Eqs.C.1 and C.3, we have the following equations:

$$\nabla.\left(\tilde{k}_f \nabla \Delta p_f\right) = \mu\left(V\phi c_t\right)_f \frac{\partial \Delta p_f}{\partial t} + \mu\left(V\phi c_t\right)_m \frac{\partial \Delta p_m}{\partial t} \tag{C.4}$$

$$\alpha k_m \left(\Delta p_m - \Delta p_f\right) = -\mu\left(V\phi c_t\right)_m \frac{\partial \Delta p_m}{\partial t} \tag{C.5}$$

Let us define the dimensionless distance

$$x_{Dj} = \frac{x_j}{L}\sqrt{\frac{k_f}{k_{fi}}} \tag{C.6}$$

where k_{fi} is the principle permeability of the fracture system in j direction, and k_f is an arbitrary constant that may be chosen to be the permeability of an equivalent isotropic system.

Assuming isotropic media, then Eq. C.6 becomes

$$x_{Dj} = \frac{x_j}{L} \tag{C.7}$$

Thus, we can write

$$\nabla_D^2 = \sum_{j=1}^{3} \frac{\partial^2}{\partial x_{Dj}^2} \tag{C.8}$$

The dimensionless time can be defined as

$$t_D = \frac{\eta t}{L^2} \tag{C.9}$$

Where

$$\eta = \frac{k_f}{\left[\left(V\phi c_t\right)_f + \left(V\phi c_t\right)_m\right]\mu} \tag{C.10}$$

The dimensionless storativity and the dimensionless transfer coefficient can be defined respectively as follows

$$\omega = \frac{(V\phi c_t)_f}{\left[(V\phi c_t)_f + (V\phi c_t)_m\right]\mu} \tag{C.11}$$

and

$$\lambda = \alpha \frac{k_m}{k_f} L^2 \tag{C.12}$$

Thus Eqs. C.4 and C.5 can be written as

$$\nabla_D^2 . (\Delta p_f) = \omega \frac{\partial \Delta p_f}{\partial t} + (1-\omega) \frac{\partial \Delta p_m}{\partial t} \tag{C.13}$$

$$\lambda (\Delta p_m - \Delta p_f) = -(1-\omega) \frac{\partial \Delta p_m}{\partial t} \tag{C.14}$$

Considering the radial coordinate r_D,

$$r_D = \sqrt{x_D^2 + y_D^2 + z_D^2} \tag{C.15}$$

we have,

$$\frac{1}{r_D^2} \frac{\partial}{\partial r_D} \left(r_D^2 \frac{\partial \Delta p_f}{\partial r_D} \right) = \omega \frac{\partial \Delta p_f}{\partial t} + (1-\omega) \frac{\partial \Delta p_m}{\partial t} \tag{C.16}$$

Consider a point source at time t = 0, a volume of liquid $\tilde{q}$ is removed from this point source instantaneously. The cumulative flux through the surface of the sphere of radius r_D around the source should be equal to $\tilde{q}$. The mass balance can be written as

$$\lim_{\varepsilon \to 0} \frac{4\pi k_f}{\mu} L \left(r_D^2 \frac{\partial \Delta p_f}{\partial r_D} \right)_{r_D = \varepsilon} = -\tilde{q}\, \delta(t) \tag{C.17}$$

Where the delta function δ is defined as

$$\int_a^b \delta(t)dt = \begin{cases} 1 & if\ [a,b]\ contains\ the\ origin \\ 0 & otherwise \end{cases} \tag{C.18}$$

Taken Laplace transform of Eqs. C.14 and C.16 with respect to t_D, the following equations are obtained respectively:

$$\frac{1}{r_D^2}\frac{d}{dr_D}\left(r_D^2\frac{d\overline{\Delta p_f}}{dr_D}\right) = \omega s\overline{\Delta p_f} + (1-\omega)s\overline{\Delta p_m} \tag{C.19}$$

$$\overline{\Delta p_m} = \frac{\lambda}{\lambda + (1-\omega)s}\overline{\Delta p_f} \tag{C.20}$$

where $\overline{\Delta p}$ denotes the Laplace transform of Δp and s is the Laplace transform variable. Substituting the definition of $\overline{\Delta p_m}$ in Eq. C.20 into Eq. C.19 we have

$$\frac{1}{r_D^2}\frac{d}{dr_D}\left(r_D^2\frac{d\overline{\Delta p_f}}{dr_D}\right) - sf(s)\overline{\Delta p_f} = 0 \tag{C.21}$$

Where

$$f(s) = \frac{sw(1-w)+\lambda}{s(1-w)+\lambda} \tag{C.22}$$

Solving for $\overline{\Delta p_f}$, we obtained the pressure distribution due to a instantaneous point source at some arbitrary location x_{wD}, y_{wD} and z_{wD}

$$\overline{\Delta p_f} = \frac{\tilde{q}}{(V\phi c_t)_f + (V\phi c_t)_m}\left\{\frac{\exp\left[-\sqrt{sf(s)}\right]}{4\pi L^3 R_D}\right\} \tag{C.23}$$

Where

$$R_D = \sqrt{(x_D - x_{wD})^2 + (y_D - y_{wD})^2 + (z_D - z_{wD})^2} \tag{C.24}$$

The Laplace solution for a point source with continuous withdrawal of fluid can then be derived:

$$\overline{\Delta p} = \frac{\bar{\bar{q}}\mu}{4\pi kL} \frac{\exp\left[-\sqrt{u}\sqrt{(x_D - x_{wD})^2 + (y_D - y_{wD})^2 + (z_D - z_{wD})^2}\right]}{\sqrt{(x_D - x_{wD})^2 + (y_D - y_{wD})^2 + (z_D - z_{wD})^2}} \tag{C.25}$$

Where

$$u = sf(s) \tag{C.26}$$

For the naturally fractured reservoir model suggested by Kazemi (1969) and deSwaan-O (1976), f(s) should be redefined as

$$f(s) = 1 + \sqrt{\frac{\lambda'\omega'}{3s}} \tanh\left(\sqrt{\frac{3\omega' s}{\lambda'}}\right) \tag{C.27}$$

Where λ' and ω' are defined as

$$\omega' = \frac{(\phi c_t h)_m}{(\phi c_t h)_f} \tag{C.28}$$

and $$\lambda' = \frac{12L^2}{h_m^2} \frac{(kh)_m}{(kh)_f} \tag{C.29}$$

where h_m and h_f are the thickness of the individual matrix and fracture elements, respectively. The dimensionless time is redefined as

$$t_D = \frac{k_f t}{(\phi c_t)_f \mu L^2} \tag{C.30}$$

Eq. C.25 is the Laplace space solution for the pressure distribution due to a continuous point source located at x_{wD}, y_{wD} and z_{wD} in a infinite reservoir.

Late time solutions in closed rectangular reservoir

The method of images was used to derive the continuous point source solution in a closed rectangular reservoir where all surfaces were impermeable (Ozkan, 1988). For convenience, the following quantity was defined:

$$S_{i,j,l} = \frac{\exp\left[-\sqrt{u}\sqrt{\left(\tilde{x}_{Di} - 2kx_{eD}\right)^2 + \left(\tilde{y}_{Dj} - 2my_{eD}\right)^2 + \left(\tilde{z}_{Dl} - 2nh_D\right)^2}\right]}{\sqrt{\left(\tilde{x}_{Di} - 2kx_{eD}\right)^2 + \left(\tilde{y}_{Dj} - 2my_{eD}\right)^2 + \left(\tilde{z}_{Dl} - 2nh_D\right)^2}} \tag{C.31}$$

For i, j, l = 1 or 2 where

$$\tilde{x}_{D1} = x_D - x_{wD} \tag{C.32}$$

$$\tilde{x}_{D2} = x_D + x_{wD} \tag{C.33}$$

$$\tilde{y}_{D1} = y_D - y_{wD} \tag{C.34}$$

$$\tilde{y}_{D2} = y_D + y_{wD} \tag{C.35}$$

$$\tilde{z}_{D1} = z_D - z_{wD} \tag{C.36}$$

$$\tilde{z}_{D2} = z_D + z_{wD} \tag{C.37}$$

$S_{i,j,l}$ defines the effect of every well including infinite arrays of image wells representing the influence of the boundaries

Thus, the point source solution for this case can be written as

$$\overline{\Delta p} = \frac{\overline{\overline{q}}\mu}{4\pi kLs} \sum_{k=-\infty}^{+\infty} \sum_{m=-\infty}^{+\infty} \sum_{n=-\infty}^{+\infty} \left(S_{1,1,1} + S_{2,1,1} + S_{1,2,1} + S_{2,2,1} + S_{1,1,2} + S_{2,1,2} + S_{1,2,2} + S_{2,2,2}\right) \tag{C.38}$$

After applying a triple summation formula (Ozkan, 1988), we can obtain

$$\overline{\Delta p} = \frac{\tilde{q}\mu}{2kLx_{eD}s}\left\{\frac{\cosh\sqrt{u}\left(y_{eD}-\left|y_D-y_{wD}\right|\right)+\cosh\sqrt{u}\left[y_{eD}-\left(y_D+y_{wD}\right)\right]}{\sqrt{u}\sinh\sqrt{u}y_{eD}}+\right.$$
$$+2\sum_{k=1}^{\infty}\cos k\pi\frac{x_D}{x_{eD}}\cos k\pi\frac{x_{wD}}{x_{eD}}\frac{\cosh\sqrt{u+a}\left(y_{eD}-\left|y_D-y_{wD}\right|\right)+\cosh\sqrt{u+a}\left[y_{eD}-\left(y_D+y_{wD}\right)\right]}{\sqrt{u+a}\sinh\sqrt{u+a}y_{eD}}+$$
$$+2\sum_{k=1}^{\infty}\cos k\pi\frac{x_D}{x_{eD}}\cos k\pi\frac{x_{wD}}{x_{eD}}\frac{\cosh\sqrt{u+b}\left(y_{eD}-\left|y_D-y_{wD}\right|\right)+\cosh\sqrt{u+b}\left[y_{eD}-\left(y_D+y_{wD}\right)\right]}{\sqrt{u+b}\sinh\sqrt{u+b}y_{eD}}+$$
$$\left.+2\sum_{k=1}^{\infty}\cos k\pi\frac{x_D}{x_{eD}}\cos k\pi\frac{x_{wD}}{x_{eD}}\frac{\cosh\sqrt{u+c}\left(y_{eD}-\left|y_D-y_{wD}\right|\right)+\cosh\sqrt{u+c}\left[y_{eD}-\left(y_D+y_{wD}\right)\right]}{\sqrt{u+c}\sinh\sqrt{u+c}y_{eD}}\right. \quad \text{(C.39)}$$

Where $a=\frac{k^2\pi^2}{x_{eD}^2}$; $b=\frac{n^2\pi^2}{h_D^2}$ and $c=\frac{n^2\pi^2}{h_D^2}+\frac{k^2\pi^2}{x_{eD}^2}$

Defining the dimensionless pressure as

$$\overline{p_D}=\frac{2\pi kh}{q\mu}\overline{\Delta p} \quad \text{(C.40)}$$

The solution for a fully penetrating vertical well can be obtained by integrating Eq. C.39 with respect to z'_w over the interval 0 to h, $L = r_w$.

Similarly, the solution for a fully penetrating vertically fractured well can be obtained by integrating Eq. C.39 with respect to z'_w over the interval 0 to h and then with respect to x'_w over the interval x_w-L_{xf} to x_w+L_{xf}, Where L_{xf} is the fracture half length and $L = L_{xf}$..

The solution for a horizontal well can be obtained by integrating Eq. C.39 with respect to x'_w over the interval x_w-$L_h/2$ to x_w+$L_h/2$,. Where $L_h/2$ is the fracture half length and $L = L_h/2$.

Details about the Laplace space solutions for all three types of wells above are provided in details by Ozkan (1988).

Now in order to obtain the late time approximations of the above solutions that are used in this study, we let u becomes s (as time become large, s becomes small and

f(s) approaches 1). The late time solutions in Laplace space can then be inverted to time space to obtain the late time solutions for vertical wells, hydraulically fractured wells and horizontal wells, which are Eqs. 5.1, 6.1 and 7.1 respectively. Since f(s) approaches unity at late time, the naturally fractured reservoir behave the same as a homogeneous single porosity reservoir at late time.